The Function of Ascorbate Oxidase in *Arabidopsis thaliana*

Submitted by Choon Kiat Lim to the University of Exeter

as a thesis for the degree of

Doctor of Philosophy in Biological Sciences

In October, 2012

I certify that all material in this thesis which is not my own work has been identified and that no material has previously been submitted and approved for the award of a degree by this or any other University.

Signature: ……..

Acknowledgements

I would like to first thank my primary supervisor, Prof. Nick Smirnoff for the opportunity to study at Exeter University and also for his patience, guidance and advice throughout the period of this PhD degree. This also goes to my co-supervisor, Dr. Ozgur Akman for his training and close supervision on the dry bench (computational modelling) project.

My deepest gratitude to my postdoc, Dr. Mike Page for his training and extensive advice in various aspects, from experimental techniques, forward planning skills, scientific writing and career planning.

I would like to acknowledge Prof. Murray Grant for his encouragement and valuable feedback.

Special thanks go to the Mezzanine lab members, colleagues in the School of Biosciences and the Systems Biology group for their kindness, warmth and providing a pleasant working atmosphere.

Last but not least, my grateful acknowledgements to the PhD funding provided by the Systems Biology Initiative of Exeter University and the Society for Experimental Biology, Biochemical Society and the Gatsby charitable foundation for providing travel grants to attend various meetings and workshops.

Finally, I would like to thank all of my family members and friends for their support and encouragement during my study.

Abstract

The apoplastic enzyme, ascorbate oxidase (AO), is a blue copper oxidase that catalyses oxidation of ascorbate (AsA) to monodehydroascorbate (MDHA). In *Arabidopsis thaliana*, AO is encoded by three genes (At4g39830, At5g21105 and At5g21100) designated *AO1*, *AO2*, and *AO3* respectively. Since AsA is the most abundant antioxidant in the apoplast and AO is active in this compartment, the regulation of apoplastic AsA redox status by AO and its role in development and environmental perturbations has become a subject of interest.

Phylogenetic analysis showed that AO is present in higher plants, pteridophytes, mosses and green algae. Amino acid sequence analysis showed that AO2 and AO3 shared higher sequence identity than AO1. *In silico* analyses found that AO1 had a distinct expression pattern and subcellular localisation compared to AO2 and AO3, suggesting AO1 might be involved in alternative functions.

Consistent with previous studies, AO activity was high in actively growing tissue of wild-type (WT) *A. thaliana*, supporting a possible role of AO in cell expansion. *ao1*, *ao3* and *ao1ao3* T-DNA insertion mutants were characterised. *ao1* had similar level of AO activity to WT, while *ao3* and *ao1ao3* had 10-20% of WT AO activity. Compared with WT, these T-DNA insertion mutants did not show any phenotypic differences under unstressed or stressed (high light and drought) growth conditions.

An artificial microRNA construct (*amiR-AO*) to silence all three *AO* genes was developed. Also, an overexpression plasmid (*35S::AO3*) harbouring *AO3* gene was constructed. These constructs were used to transform *A. thaliana*. AO activity was undetectable in the *amiR-AO* line, while the *35S::AO3* line had 3-

fold higher AO activity than the WT. Under unstressed normal growth conditions, the *amiR-AO* line had bigger rosette size, whereas the *35S::AO3* line exhibited early flowering and smaller number of rosette leaves. The *amiR-AO* line accumulated more anthocyanin and AsA than WT when acclimated to high light, whereas the *35S::AO3* line accumulated less anthocyanin than WT. In response to drought, the *amiR-AO* line did not show phenotypic differences compared to WT, while the *35::AO3* line had higher rate of leaf water loss and appeared to have greater sensitivity to drought. These results suggest that AO perturbation could, to some extent, affect the growth and stress response of *A. thaliana* although the effect is small.

List of contents

List of figures

List of tables

List of abbreviations

ABA	Abscisic acid
ABRC	*Arabidopsis* Biological Resource Center
AER	Absolute expansion rate
AGI	*Arabidopsis* gene identifier
ATLA	Absolute total leaf area
amiRNA	Artificial microRNA
AO	Ascorbate oxidase
APX	Ascorbate peroxidase
AsA	Ascorbate
bp	Base pairs
cTP	Chloroplast transit peptide
CW	Cell wall
DAS	Day after sowing
DHA	Dehydroascorbate
DW	Dry weight
FW	Fresh weight
gDNA	Genomic DNA
H_2O_2	Hydrogen peroxide
HL	High light
LL	Low light
MDHA	Monodehydroascorbate
MeJa	Methyl jasmonate
miRNAs	MicroRNAs
MS	Murashige and Skoog
mTP	Mitochondrial targeting peptide
NASC	Nottingham *Arabidopsis* Stock Center
nt	Nucleotide
$^1O_2$	Singlet oxygen
O_2^-	Superoxide radical
$^{\cdot}OH$	Hydroxyl radical
PCR	Polymerase chain reaction
PPFD	Photosynthetic photon flux density

Prx	Peroxidase
Redox	Reduction oxidation
ROS	Reactive oxygen species
RWC	Relative water content
SDW	Sterile distilled water
SEM	Standard error of the mean
siRNAs	Short interfering RNAs
SP	Signal peptide
sq RT-PCR	Semi-quantitative reverse transcription PCR
TAIR	The *Arabidopsis* information resource
T-DNA	Transfer-DNA
WMD	Web microRNA designer
WT	Wild-type

Chapter 1. Introduction

1.1. General introduction

As sessile organisms, plants encounter various challenges such as unfavourable weather conditions and pathogen infections. The apoplast region, as the first barrier of plant cells, is therefore a crucial contact point between the plant and external perturbations. The apoplast is defined as the cell wall and intercellular space. Upon contact with external perturbations, changes in metabolites, proteins and ions in the apoplastic region, followed by the signalling events relayed to the cytosolic region and subsequent plant responses (i.e. changes in antioxidant defence systems and growth signals) are crucial to plant growth and survival.

Ascorbate (AsA, also known as vitamin C or ascorbic acid) is present in all compartments and is involved in plant growth and development by regulating its redox state (defined as the ratio of reduced AsA to total AsA). In the apoplast, the AsA redox state is regulated by ascorbate oxidase (AO). Although previous studies reported possible roles of AO, its exact function is unknown. This introduction will give an overview of the function of AO in plants and also present research strategies to study this enigmatic enzyme.

1.2. Ascorbate (AsA) − the multifunctional molecule

AsA is synthesised by some animals and plants but not by prokaryotes. AsA (Figure 1-1) is the most abundant antioxidant in plants. Genetic and biochemical evidence showed that the $_{D}$-mannose/$_{L}$-galactose (Smirnoff-Wheeler) pathway is the major AsA biosynthetic route in plants (Wheeler *et al.*, 1998). In this pathway, $_{D}$-fructose 6-P is converted to AsA through the following intermediates: $_{D}$-mannose 6-P, $_{D}$-mannose 1-P, GDP-$_{D}$-mannose, GDP-$_{L}$-galactose, $_{L}$-galactose 1-P, $_{L}$-galactose, $_{L}$-galactono-1,4-lactone (for review, see Smirnoff, 2011).

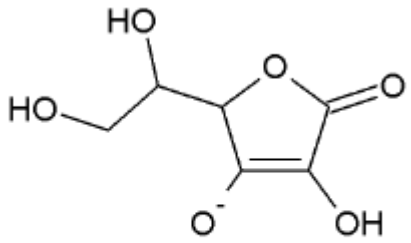

Figure 1-1: Structure of ascorbate. Diagram adapted from Smirnoff (2011).

AsA is found in all sub cellular compartments (e.g. apoplast, chloroplasts, vacuoles, cytosol, mitochondria and peroxisomes). It has an average concentration of 2-25 mM or more in the chloroplast stroma, whereas less AsA is detected in the apoplast (~ 1 mM) (Rautenkranz *et al.*, 1994; Foyer and Lelandais, 1996; Jimenez *et al.*, 1997; Pignocchi *et al.*, 2003; Sanmartin *et al.*, 2003). Recently, the subcellular localisation of AsA in *A. thaliana* and tobacco leaves was studied using immunogold labelling approach and visualised by transmission electron microscope (Zechmann *et al.*, 2011). The accuracy and specificity of this approach is supported by the expected decrease in gold

particle density in *A. thaliana vtc1* and *vtc2* mutants (AsA-deficient mutants) compared with WT. In *A. thaliana*, the highest AsA concentrations were found in the cytosol and peroxisomes and high light stress increased AsA in the cytosol, chloroplasts and vacuoles. AsA was not detected in the apoplast using the immunogold approach although AsA is readily extracted and quantified from apoplastic fluid. Probably apoplastic AsA concentration is below the detection limit of the immunogold approach or the presence of apoplastic AsA could caused by intracellular contamination during the extraction of apoplastic fluid.

In healthy tissues, more than 90% of the intracellular AsA is in the reduced form, whereas in the apoplast, a significant amount of the AsA is in the oxidised form. AsA concentrations are high in photosynthetic tissues, where younger tissues tend to have higher AsA concentrations than the older tissues (Horemans *et al.*, 2000b; Smirnoff, 2011).

During oxidative stress, ascorbate is readily oxidised to the monodehydroascorbate (MDHA) radical, which then rapidly disproportionates to form dehydroascorbate (DHA) and AsA. The oxidised (MDHA or DHA) and reduced forms of AsA are reported to play major roles in plant growth and survival apart from its role in antioxidant defences. For example, they have roles in growth regulation (i.e. cell signalling, cell division and cell expansion), photosynthesis and pathogen defence (Smirnoff, 2000a).

The roles of AsA in plant growth and development are further supported by the discovery of *vitamin c* (*vtc*) mutants in *Arabidopsis thaliana*, where *vtc1* and *vtc2* mutants that have ~30% AsA level than that of wild-type (WT) show a slow growth phenotype (Conklin *et al.*, 1999; Veljovic-Jovanovic *et al.*, 2001; Pastori

et al., 2003). However, recently it has been shown that a *VTC2* T-DNA insertion mutant did not show the slow growth phenotype as exhibited by the *vtc2-1* mutant isolated by Conklin *et al.* (2000) through EMS mutagenesis. In addition, backcrossing of *vtc2-1* to WT rescues the slow growth phenotype (Dr. C. Cobbett, Melbourne, Australia, personal communication). This discovery suggests that altered morphology in the *vtc2-1* mutant was caused by other mutations. In fact, next generation sequencing of *vtc2-1* revealed more than seventy mutation sites in the *vtc2-1* transcriptome (Mike Page, unpublished). Consequently, data based on the *vtc2-1* mutant should be evaluated with care. Nevertheless, the essential function of AsA in plant growth is reinforced by the finding of Dowdle *et al.* (2007), in which the *vtc2 vtc5* double mutant that is unable to synthesize AsA shows growth arrest and bleaching after cotyledon opening.

Recently, it has become clear that the importance of AsA is not restricted to the cytosol and chloroplast. The AsA redox state of the apoplast is a study of great interest. As the first contact of external environment, changes in the apoplastic AsA pool and redox status could provide a sensing mechanism for the external environment (Pignocchi and Foyer, 2003).

1.3. The redox reactions (metabolism) and degradation of AsA

The biological function of AsA results from its ability to act as reducing agent and free radical scavenger because of two attributes. First, AsA readily donates one or two electrons or hydrogen atoms to free radicals. Upon oxidation, AsA produces its first oxidised intermediate, the MDHA radical. Further oxidation of MDHA radicals produces DHA. The second attribute that makes AsA an effective reducing agent is the relatively high stability of MDHA radicals and the presence of enzymes that reduce MDHA and DHA back to AsA (Smirnoff, 2011). The redox reactions of AsA and the regeneration of AsA collectively are part of the ascorbate-glutathione (AsA-GSH) cycle, otherwise known as the Foyer-Halliwell-Asada cycle (Noctor and Foyer, 1998). These reactions have been shown to be present in the chloroplast, cytosol, mitochondria and peroxisomes of plant cells. The AsA-GSH cycle contains a series of enzymatic and non-enzymatic reactions important in alleviating oxidative stress and regulating hydrogen peroxide (H_2O_2) signalling in plants (Asada, 1999; Foyer and Noctor, 2011).

The redox reactions involved in the AsA-GSH cycle are given in Figure 1-2 and described in the following paragraph (see Foyer and Noctor, 2011; Smirnoff, 2011 for review). For clarity, only reactions in the cytosol are shown.

Hydrogen peroxide (H_2O_2) generated in response to oxidative stress (e.g. photosynthesis, photorespiration and oxidative burst) is reduced by cytosolic ascorbate peroxidase (cAPX) using two AsA molecules as substrate, giving rise to two water (H_2O) molecules and the concomitant generation of two molecules of MDHA (Figure 1-2a). Two molecules of MDHA are reduced to AsA *via* NAD(P)H-dependent MDHA reductase (MDHAR) (Figure 1-2b). Alternatively, two MDHA molecules can disproportionate to DHA and AsA (Figure 1-2c). DHA is reduced to AsA by DHA reductase (DHAR) in a GSH-dependent reaction. The oxidised GSH, known as glutathione disulphide (GSSG) is in turn reduced by GSH reductase (GR) at the expense of NAD(P)H (Figure 1-2 d). AsA and DHA are also present in the apoplast. DHA is transported from the cell wall into the cytosol in exchange for AsA *via* a plasma membrane transporter (Figure 1.2e). AO (Figure 1.2f), the apoplastic enzyme studied in this project (see section 1.6.), catalyses the oxidation of AsA in the cell wall to produce MDHA. MDHA is probably reduced by a plasma membrane-bound cytochrome b (Cyt *b*) (Figure 1.2g) or it is likely that cytosolic AsA is used as the electron donor for plasma membrane-bound MDHAR to regenerate AsA at the cell wall (Figure 1.2h).

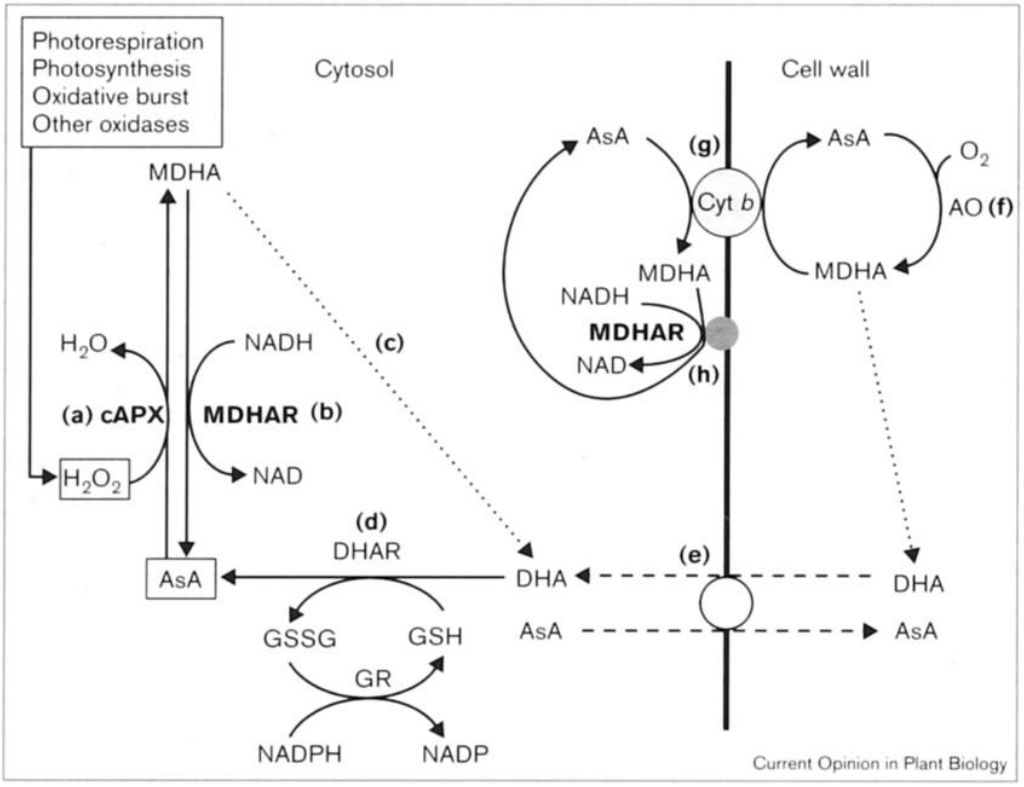

Figure 1-2: Redox reactions of AsA in the plant cell. The reactions are not depicted stoichiometrically. See text on the previous page for descriptions. Figure reproduced from Smirnoff (2000a).

AsA is catabolised to produce $_{L}$-threonate, oxalate and $_{L}$-tartrate. In some plants (members of the grape family, Vitaceae), AsA is degraded to $_{L}$-tartrate *via* C4/C5 cleavage of the AsA carbon skeleton, while in other plants, AsA is degraded to oxalate and $_{L}$-threonate through the C2/C3 cleavage of the AsA carbon skeleton, the latter sometimes being oxidised to $_{L}$-tartrate (Loewus, 1999). A pathway for the degradation of AsA to produce oxalate and $_{L}$-threonate in the apoplast of cultured rose cells has been proposed (Green and Fry, 2005). The proposed pathway involves oxidations and intramolecular rearrangement of the precursor, DHA to produce a novel intermediate, 4-*O*-oxalyl-$_{L}$-threonate. Hydrolysis of 4-*O*-oxalyl-$_{L}$-threonate catalysed by an extracellular esterase gives rise to oxalate and $_{L}$-threonate. The pathway can also occur non-enzymatically. Several steps in the pathway can produce hydrogen peroxide that could contribute to the role of apoplastic AsA as a pro-oxidant, which potentially could induce cell wall loosening (see section 1.5.).

Recently, a more detailed study was performed on the fate of DHA in the AsA degradation pathway. After AsA oxidation to DHA, DHA was first oxidised to a highly reactive intermediate, cyclic-2,3-*O*-oxalyl-$_{L}$-threonolactone (Parsons *et al.*, 2011) then only proceed to subsequent pathways described by Green and Fry (2005). Using high-voltage paper electrophoresis (HVPE), a number of intermediates following DHA degradation were correctly identified (see Parsons and Fry, 2012). Novel intermediates identified in the AsA degradation pathway could play important roles in plant growth and development that is worth future investigation.

1.4. Apoplast – the plant cell frontier

The apoplast is important in various functions such as maintaining cell shape, growth regulation, defence, nutrient transport and signal transduction. As the frontier of plant cells to the external environment, the apoplast plays a crucial role in plant performance by changing cell wall components, ions fluxes, metabolites and proteins in response to altered environmental conditions (Sakurai, 1998). The apoplast contains various components including proteins (e.g. peroxidases, chitinase, extensins and pathogenesis-related proteins), ions (K^+, Ca^{2+} and H^+), metabolites (sugars and polyphenols) and cell wall components (glycoproteins and polysaccharides) (Sattelmacher, 2001; Ge *et al.*, 2011). AsA is presumed to be the main antioxidant in the apoplast and its redox state is regulated by ascorbate oxidase (AO), a cell wall localised enzyme (Pignocchi and Foyer, 2003). The function of AO is described in section 1.6.

1.5. The role of apoplastic AsA in the growth of the cell wall

Apoplastic AsA and DHA are proposed to contribute in cell wall loosening (see below).

A few mechanisms for DHA-mediated cell wall loosening were proposed by Lin and Varner (1991) based on the chemical properties of DHA. Firstly, DHA was presumed to react with the lysine side chain of cell wall proteins, preventing Schiff's base formation with the reducing ends of polysaccharides, thereby reducing cell wall cross-linking. Secondly, DHA was proposed to interact with lysine and arginine residues of cell wall proteins, preventing interaction of cell wall protein and pectin. Thirdly, production of oxalate from cell wall DHA

followed by the formation of calcium oxalate crystals that could reduce cell wall calcium concentration from the calcium-pectin complex. Consequently, pectin cross-linking is reduced, causing cell wall loosening. However, the hypotheses proposed by Lin and Varner have not been followed up.

Another proposed mechanism of AsA involvement in cell wall dynamics has also been proposed. AsA-mediated hydroxyl radical ($^{\cdot}OH$) formation in the apoplast is reported to be involved in non-enzymic scission (backbone cleavage of structural polysaccharides) of cell wall polysaccharides such as pectin and xyloglucan (Fry, 1998; Fry *et al.*, 2001; Tabbì *et al.*, 2001; Dumville and Fry, 2003). AsA, copper ions (Cu^{2+}) and O_2 in the apoplast are required for the generation of $^{\cdot}OH$, which occurs *via* reaction I to III (Fry *et al.*, 2002; Dumville and Fry, 2003):

I) Cu^{2+}-mediated AsA oxidation

$$Cu^{2+} + ½AH_2 \rightarrow Cu^{+} + ½A + H^{+}$$

II) Non-enzymatic oxidation of AsA

$$O_2 + AH_2 \rightarrow H_2O_2 + A$$

III) Production of $^{\cdot}OH$ by Fenton reaction, i.e. the reduction of H_2O_2 by a transition metal ion

$$Cu^{+} + H_2O_2 \rightarrow Cu^{2+} + {}^{\cdot}OH + OH^{-}$$

where AH_2 = AsA, A = DHA

In addition, H_2O_2 produced during apoplastic AsA degradation (see section 1.3.) can also generate $^{\cdot}OH$ (Green and Fry, 2005; Kärkönen and Fry, 2006).

1.6. Ascorbate oxidase (AO) and its function − current state of knowledge

1.6.1. AO − brief history

Formerly known as “hexoxidase”, AO was first isolated from cabbage leaf by Szent-Györgyi (1931) who believed it functioned in the respiration of cabbage with the presence of oxygen and oxidised “hexuronic acid”, which was later renamed as AsA (De Tullio *et al.*, 2004). AO, together with laccase (present in plants and fungi) and ceruloplasmin (present in animal blood serum) belong to the blue copper oxidases, a group of enzymes that contain 4 to 10 atoms of copper in their active site and give a characteristic blue colour in solution form (Dawson *et al.*, 1975). Blue copper oxidases are multi-copper enzymes which catalyse the four-electron reduction of oxygen to water with a concomitant one-electron oxidation of the substrate (Messerschmidt and Huber, 1990). AO oxidises AsA to MDHA, producing four electrons that are used to reduce four Cu^{2+} bound to AO. These four electrons are then passed to oxygen and coupled with 4 protons to form 2 water molecules (De Tullio *et al.*, 2004). Meanwhile, MDHA radicals also tend to disproportionate to AsA and DHA (Figure 1-3). In higher plants, the proposed extracellular localisation of AO is support by the presence of a signal peptide and *N*-glycosylation sites in the AO of cucumber, pumpkin, tobacco and melon (Ohkawa *et al.*, 1989; Esaka *et al.*, 1990; Diallinas *et al.*, 1997; Kisu *et al.*, 1997; Sanmartin *et al.*, 2007). Besides, immunohistochemical experiments also showed that AO in cucurbit plants is mainly localised in cell walls (Chichiricco *et al.*, 1989; Liso *et al.*, 2004).

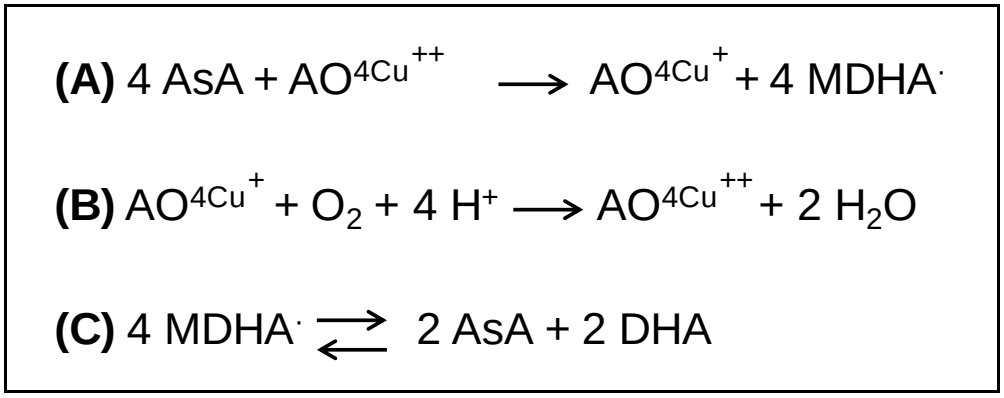

Figure 1-3: AO reaction mechanism. **(A)** AO oxidised four AsA to produce four MDHA radicals and releasing four electrons to reduce four Cu^{2+} that bound to AO. **(B)** Four electrons are transferred from four Cu^{+} to oxygen and coupled with four protons to produce two water molecules. **(C)** Four MDHA radicals can disproportionate to two AsA and two DHA.

1.6.2. AO and its function in ascorbate metabolism

The role of AO and its effects on the apoplastic AsA concentrations were studied in tobacco and tomato using a transgenic approach, by overexpressing or underexpressing the *AO* gene (Pignocchi *et al.*, 2003; Sanmartin *et al.*, 2003; Yamamoto *et al.*, 2005; Garchery *et al.*, 2012). Similarly, the apoplastic AsA concentrations in the *AO3* T-DNA insertion mutant of *A. thaliana* were determined by Yamamoto *et al.* (2005). In general, these studies showed that total apoplastic AsA concentrations of the sense, antisense and T-DNA knockout lines were similar to the WT. AsA redox state is defined as the ratio of reduced AsA to total AsA. Compared with WT, the sense lines showed lower apoplastic AsA redox state whereas the antisense lines showed higher apoplastic redox state, supporting the function of AO in oxidising apoplastic AsA. It should be noted that AO perturbation did not affect the whole tissue (symplast) AsA concentration or its redox state.

1.6.3. AO in development

High AO activity along with low AsA is found in quiescent centres (QC) of maize and squash (*Cucurbita maxima*) roots (Kerk and Feldman, 1995; Jiang *et al.*, 2003; Liso *et al.*, 2004), suggesting the oxidation of AsA gives rise to an oxidising environment which prevents cell division in the QC. Cell division is halted by adding DHA to tobacco cell cultures. On the contrary, DHA increases auxin induced cell elongation (Potters *et al.*, 2010). DHA content is increased in elongated fava bean (Arrigoni, 1994) and MDHA induced cell elongation in onion root meristems (Hidalgo *et al.*, 1989). These observations showed that AsA oxidation, along with high AO activity, occur in rapidly expanding tissue supporting a role for AO in plant growth and development.

A number of studies reported that AO activity is abundant in growing tissue of melon (Diallinas *et al.*, 1997), tobacco (Kato and Esaka, 1996), pumpkin (Esaka *et al.*, 1992) and zucchini (Lin and Varner, 1991). It is reported to be involved in cell wall loosening and reorganisation which contributes to tissue expansion (Lin and Varner, 1991; Diallinas *et al.*, 1997). Kato and Esaka (2000) showed that protoplasts of transgenic tobacco overexpressing pumpkin *AO* expanded more rapidly than WT. In both 5-week-old WT and overexpressing tobacco plants, the youngest leaf had higher AO activity than older leaves (Yamamoto *et al.*, 2005). *AO* transcripts are highly expressed in young and growing tissues of tobacco (Kato and Esaka, 1996). Several mechanisms were proposed by Lin and Varner (1991) regarding the role of DHA in cell wall loosening (see section 1.5.). Transgenic plants overexpressing or underexpressing *AO* were developed to study the role of AO in plant growth. Pignocchi *et al.* (2003) showed that *AO* overexpressing tobacco had an increased stem length compared to WT. By

contrast, Yamamoto *et al.* (2005) and Sanmartin *et al.* (2003) did not observe any plant growth changes in *AO* overexpressing tobacco. Meanwhile Garchery *et al.* (2012) did not observe any phenotypic differences in transgenic tomato plants with decreased AO activity.

1.6.4. AO in response to environmental perturbations

De Tullio *et al.* (2007) showed that AO activity of zucchini (*Cucurbita pepo*) leaves increased in the light, but that the AO activity reversed and remained low when transferred to the dark. Dark-treated plants had higher AO activity when supplied with oxygen, while low oxygen treatment (hypoxia) decreased AO activity. This suggested that AO could be involved in tissue oxygen management, i.e. low AO activity increases oxygen availability (De Tullio *et al.*, 2004; De Tullio *et al.*, 2007).

AO transcripts were strongly suppressed in melon after 6 to 24 hrs of wounding. Endogenous ethylene produced during wounding was proposed to repress *AO* expression (Diallinas *et al.*, 1997). By contrast, García-Pineda *et al.* (2004) showed that pepper (*Capsicum annuum*) *AO* was expressed rapidly in the first hour of wounding.

Garchery *et al.* (2012) showed that decreasing AO activity by an RNA interference (RNAi) approach increased stomatal conductance, fruit yield and sugar content in tomato under water-deficit. Increased stomatal conductance could enhance CO_2 uptake, improve carbon fixation and increase sugar levels in the photosynthetic tissues. Besides, Garchery *et al.* (2012) also proposed that low apoplastic sucrose concentrations in the *AO* RNAi tomato fruit could

draw sucrose from phloem more effectively because the level of sucrose in fruits is negatively correlated with the rate of sucrose import. The imported sucrose is converted to hexoses rapidly in ripening fruit thus increased the sugar content of *AO* RNAi tomato fruit. It is possible that the altered sugar content observed in *AO* RNAi tomato is caused by higher apoplastic AsA redox state compared to WT, although the mechanisms controlling carbon allocation remain to be elucidated.

Other studies reported that *AO*-deficient mutants (antisense) are more tolerant to salt and oxidative stresses (hydrogen peroxide, methyl viologen and ozone) compared with WT while overexpressing plants are susceptible to these treatments (Sanmartin *et al.*, 2003; Yamamoto *et al.*, 2005; Fotopoulos *et al.*, 2006). Additionally, tobacco overexpressing *AO* showed an increase in sensitivity to the necrotrophic fungus, *Botrytis cinerea* (Fotopoulos *et al.*, 2006) and the biotrophic bacteria, *Pseudomonas syringae* (Pignocchi *et al.*, 2006). However, only a phenotypic effect (lesion size) was reported in the *P. syringae* treatment, although extensive analysis was not carried out. Nevertheless, the findings above suggest that AO, probably *via* regulation of apoplastic AsA redox state, affects stress responses.

Intriguingly, a high level of AsA concentrations and AsA redox state (ratio of reduced AsA to total AsA, %) in the apoplast does not contribute to ozone resistance in two cultivars of clover (*Trifolium repens* L. cv Regal) with different levels of sensitivity. The sensitive line had 72% more apoplastic AsA and also a higher AsA redox state (80%) than the resistant clover (AsA redox state = 25%) (D'Haese *et al.*, 2005). Similarly, Ranieri *et al.* (1999) showed that an ozone sensitive Poplar clone had 81% higher reduced apoplastic AsA than a resistant

clone. The findings above propose that factors other than apoplastic AsA were involved for the genotype differences in these plants during ozone treatment. Moreover, an ozone sensitive *A. thaliana* mutant was shown to have a similar AsA pool size as WT (Kanna *et al.*, 2003). These contradictory results suggest that the ability of apoplastic AsA to counteract oxidative stress (with particular reference to ozone) is still a matter of debate. Recently, Balestrini *et al.* (2012) showed that lotus (*Lotus japonicus*) *AO* gene expression is induced by symbiotic interactions with both nitrogen-fixing bacteria and arbuscular mycorrhizal (AM) fungi. The authors proposed that high *AO* expression is required to decrease oxygen concentration during root nodule formation.

1.6.5. AO and its response to hormones

Promoter analysis showed that the pumpkin *AO* gene has an auxin responsive element (Kisu *et al.*, 1997). Furthermore, previous studies reported that auxin treatment increased AO activity and mRNA levels in *Zea mays* root QC and cultured pumpkin fruit (Esaka *et al.*, 1992; Kerk and Feldman, 1995). High auxin was found in the QC *via* polar transport from shoot to root, which in turn caused high AO activity which oxidised AsA to DHA (Jiang *et al.*, 2003). Kerk *et al.* (2000) suggested that AO regulated auxin levels in the root tip through oxidative decarboxylation. In addition, Pignocchi *et al.* (2003) showed that auxin treatment up-regulated *AO* transcript levels and enhanced tobacco growth. By contrast the growth suppressor, salicylic acid (SA) decreased *AO* transcript levels and caused growth inhibition in tobacco. Intriguingly, Pignocchi and co-workers (2006) also showed that auxin enhanced growth promotion is only observed in WT tobacco plants, and the effects of auxin mediated growth

enlargement seemed to lost in overexpressing lines of tobacco plants. Furthermore, Sanmartin *et al.* (2007) showed that jasmonic acid (JA) induced *AO* expression while abscisic acid (ABA) and SA repressed *AO* expression in melon. The studies reported above on the induction of *AO* by hormones further supports the role of AO in growth.

1.6.6. AO and post-transcriptional control

Previous studies showed that *AO* transcript levels did not correlate with its activity. AO is a copper-containing enzyme. Copper treatment enhanced AO activity but not mRNA levels in pumpkin fruit tissue (Esaka *et al.*, 1992). In addition, Kerk and Feldman (1995) showed that a 4-day auxin treatment in maize roots continued to increase AO activity, even though the mRNA level only peaked at day 2 and then decreased before day 4 of the treatment. These findings suggest translation/post-translational regulation is involved in controlling AO activity.

1.7. The model plant *Arabidopsis thaliana*

For the last few decades, *A. thaliana* has been the organism of choice for many researchers in various fields of plant science. The complete genome sequence of *A. thaliana* (The Arabidopsis Genome Initiative, 2000) has enhanced our understanding of plant growth, development and its response to stress. *A. thaliana* is relatively small compared to other plants and therefore it can be easily grown and maintained in the laboratory. It has a short life cycle (about 10 weeks), and self-fertilises to produce many seeds.

To facilitate research in *A. thaliana*, a centralised database − TAIR (Rhee *et al.*, 2003) has been set up to pool various resources on plant materials, genome information and protocols in one place (see TAIR website, http://www.arabidopsis.org/). Also, various databases are available for *A. thaliana* researchers to perform *in silico* analysis on gene expression, metabolic pathways and so on. In addition, seed banks (e.g. NASC, ABRC) have been established to distribute various mutants of *A. thaliana*. All these advantages have made *A. thaliana* an ideal system to study the function of plant.

In this project, *A. thaliana* WT plant and various *AO* mutants were used to study the function of AO (detailed in the following chapters).

1.8. AO in *A. thaliana*

A TAIR database search suggests that *A. thaliana* has three putative *AO* genes: At4g39830, At5g21105 and At5g21100, designated *AO1*, *AO2*, and *AO3* respectively in this thesis. Previous studies showed that an *ao3* T-DNA insertion mutant had about 13% AO activity and a higher apoplastic redox state than WT under unstressed normal growth conditions, but no phenotypic difference was observed between the *ao3* mutant and WT. Interestingly, *ao3* had enhanced seed yield under salinity treatment (Yamamoto *et al.*, 2005). Lee *et al.* (2011) observed that the *ao1ao2* double mutant exhibited smaller rosette size, late flowering, higher total AsA concentrations and higher AsA redox state in whole seedlings compared to the WT. However the AO activity, apoplastic AsA concentrations and *AO* gene expression of this mutant were not reported. Lee *et al.* (2011) also showed that *AO2* expression increased upon gravistimulation, and the *ao1ao2* double mutant had a reduced gravitropic response (root

curvature) and reduced root elongation. Nevertheless, the difference in terms of curvature (angle) and primary root length between WT and the double mutant is minor, in which only 5 degree curvature difference and 2 mm primary root length difference were observed. It appears that more extensive studies are needed to elucidate the function of AO in *A. thaliana*. This could be done by complete suppression of AO activity by producing double or triple knockout mutants. *A. thaliana* transgenic plants that overexpress *AO* genes could be developed as well to complement studies using the *AO* knockout mutants. The strategy to establish these *A. thaliana* lines is described in Chapter 3.

1.9. Research aim and objectives

There is a reasonably large literature reported on the function of AO in growth regulation and stress response. These studies, as reviewed in Chapter 1, have not produced conclusive evidence regarding the role of AO in plants. The findings reported on the AO in the model plant *A. thaliana* are limited in amount and incomplete. By using various AO mutants, this project aims to elucidate the role of AO during development and stress in *A. thaliana*. The objectives of this project were to:

- To develop a series of *A. thaliana* mutants for functional analyses of AO.
- To predict the function of AO during development and stress in *A. thaliana* through data mining from bioinformatic resources.
- To investigate the role of AO during development in *A. thaliana*.

- To study the function of AO in *A. thaliana* during high light and drought stress.

Chapter 2. Materials and methods

2.1. Materials

2.1.1. Chemicals

Unless otherwise mentioned, all chemicals were purchased from Sigma-Aldrich (St Louis, Dorset, UK) or Thermo Fisher Scientific (Loughborough, UK).

2.1.2. Bacterial strains

Escherichia coli strain DH5α (Invitrogen™) was transformed with various plasmid constructs for subcloning. *Arabidopsis thaliana* was transformed with *Agrobacterium tumefaciens* (also known as *Rhizobium radiobacter*) strain GV3101.

2.1.3. Plasmids

The pGEM-T® easy (Promega) vector was used for TA cloning of A-tailed PCR products. This plasmid harboured the ampicillin resistance gene for selection of plasmid-transformed colonies, and the lacZ region for blue/white screening of recombinants.

For Gateway® cloning, pDONR™221 vector (Invitrogen™) was used to recombine *att*B site-containing PCR products to generate entry clones, known as pENTR™ plasmids. Gateway® destination vector harbouring 35S Cauliflower Mosaic Virus (35SCaMV) promoter, pGWB502 was used to overexpress genes of interest and an artificial microRNA (amiRNA) fragment. The features of these plasmids are described in Chapter 3. The pRS300 plasmid (Schwab *et al.*, 2006)

was used as a template to generate amiRNA. The features of this plasmid are described in Chapter 3.

2.1.4. Antibiotics

The antibiotics used for the selection of positive bacterial colonies and plant lines are given below (Table 2-1) and stored at −20°C.

Table 2-1: List of antibiotics used.

Antibiotic	Solvent	Stock concentration	Working concentration
Ampicillin	Sterile distilled water (SDW)	100 mg/ml	100 µg/ml
Kanamycin	SDW	50 mg/ml	50 µg/ml
Tetracycline	SDW	10 mg/ml	10 µg/ml
Spectinomycin	SDW	100 mg/ml	100 µg/ml
Rifampicin	100% methanol	50 mg/ml	25 µg/ml
Gentamycin	SDW	30 mg/ml	30 µg/ml
Hygromycin B	Phosphate buffered saline (PBS) solution	50 mg/ml	20 µg/ml

2.2. Image capture

Images of various *A. thaliana* plant lines under unstressed and stressed growth conditions were captured using a digital camera (E7900, Nikon).

2.3. Plant materials and growth conditions

2.3.1. *A.thaliana* seed stocks

Wild-type (WT) *A. thaliana* ecotype Columbia (Col-0) seeds were obtained from the laboratory. Salk T-DNA insertion *ascorbate oxidase* (*ao*) mutants in the Col-0 background were purchased from the Nottingham *Arabidopsis* Stock Centre (NASC, Nottingham, UK).

2.3.2. Surface sterilisation of seeds

A. thaliana seed surface sterilisation was carried out in a sterile flow hood. The seeds were soaked with 1 ml 70% ethanol for 5 mins at room temperature, with occasional mixing by gentle inversion. The ethanol was removed and seeds were resuspended in 1 ml sterilising solution (10% bleach and 0.05% Tween 20) for 5 mins with occasional shaking. Sterilising solution was then removed and seeds were rinsed five times with 1 ml SDW. After washing with SDW, seeds were incubated in 1 ml 0.1% agar and placed in darkness at 4°C for a stratification period of 2 to 3 days prior to sowing.

2.3.3. Growth of *A. thaliana* on soil

After stratification, seeds were grown on trays containing soil: a mixture of compost (Levington®, Scotts, UK) and vermiculite (Sinclair, UK) in a 3:1 ratio,

pre-treated with 0.02% Intercept solution (Scotts, UK) and covered with a propagator lid for two weeks after germination. Plants were watered twice a week and grown in a controlled environment growth chamber (Reftech, Netherlands) under a short day light regime (photoperiod: 8 hrs light, 16 hrs dark) at photosynthetic photon flux density (PPFD) of 100 µmol m^{-2} s^{-1}, 65% relative humidity (RH), and 23°C to obtain plants with large rosettes. Plants were also grown in a long day (photoperiod: 16 hrs light, 8 hrs dark) controlled environment growth chamber (23°C, 65% RH, PPFD 100 µmol m^{-2} s^{-1}) to induce flowering.

2.3.4. Growth of *A. thaliana* on agar plates

After stratification, surface sterilised seeds were sown in Petri dishes supplemented with half-strength (2.2 g/L) sterile MS media (Murashige and Skoog salts with Gamborg's vitamins, Duchefa Biochemie, Netherland), adjusted to pH 5.8 with 1 M KOH and containing 0.5% phytogel (w/v). Petri dishes were sealed with surgical tape (Micropore™, 3M, USA) and placed horizontally in short day (photoperiod: 8 hrs light, 16 hrs dark) and long day (photoperiod: 16 hrs light, 8 hrs dark) growth chambers (23°C, 65% RH, PPFD 100 µmol m^{-2} s^{-1}) for 2 to 4 weeks. Petri dishes were regularly shifted randomly to prevent positional effects.

2.3.5. Cross pollination of *A. thaliana*

For crossing, long day grown flowering *A. thaliana* plants, typically between 6 and 7-week-old, were used. Mother plants were selected at a stage when they

have developed 5-6 inflorescences, and father plants were chosen from that have started to form siliques. Fine forceps (type 4s, TAAB Laboratories, UK) were used to remove siliques, flower buds with white tips/petals and open flowers which were not used for crossing from mother plants. For one plant, 3-10 unopened flower buds were kept for crossing.

Without damaging the mother plant, a flower bud was fixed gently under a binocular dissecting microscope (Carl Zeiss 47/5022, Jena, Germany) at 10-20x magnification using sticky tape. Two pairs of fine forceps were used to open petals and sepals and then expose immature anthers. These were removed carefully (emasculation) without touching the stigma or style. Forceps were cleaned in between flower buds by dipping them in 95% ethanol followed by SDW. The emasculation process was repeated for all remaining flower buds. Emasculated flower buds were labelled and kept in growth room for 2-3 days to enable the stigma to become receptive for pollination.

Emasculated flower buds were then fixed under dissecting microscope and fertilised with pollen from an open flower of a father plant by rubbing an anther onto the stigma (pollination) of emasculated plants. The pollinated inflorescence were marked with a colour thread and the cross was documented, i.e. mother (♀), father (♂), and date. The plants were then returned to long day growth conditions. Successful crosses were indicated by obvious elongation of siliques.

2.3.6. *A. thaliana* seeds collection

Seeds from self-pollinated and crossed *A. thaliana* were harvested when siliques began to turn yellowish. They were collected by cutting them into a

paper bag and sealed with sticky tape. After one week, dried plant materials can be gently hand-pressed from outside of the bag, and seeds were sieved to separate them from other plant debris. The cleaned and sieved seeds were kept in a labelled microfuge tube and stored in dark at 4°C.

2.4. Transformation of *E. coli* competent cells

Transformation was carried out using the heat-shock method as described in the manufacturer's protocol (Invitrogen^{TM}). Cells were plated out onto LB agar plates supplemented with the appropriate antibiotic and incubated at 37°C overnight.

2.5. RNA and DNA methods

2.5.1. *A. thaliana* RNA extraction and quantification

Frozen tissue was ground in liquid nitrogen with a pre-cooled mortar and pestle. Total RNA was extracted in 600 µl Z6 buffer (8 M guanidinium hydrochloride, 20 mM morpholinoethane sulphonic acid pH 7.0 and 20 mM EDTA), transferred to a cold, sterile 1.5 ml microfuge tube. 600 µl of phenol:chloroform:isoamyl alcohol (25:24:1, v/v/v) was then added and mixed vigorously. The mixture was centrifuged at 16,000 × g at 4°C for 5 mins in a bench-top centrifuge (Eppendorf 5415R). The upper aqueous phase was transferred to a new sterile pre-cooled 1.5 ml microfuge tube, and precipitated with 1/20 volumes 1 M acetic acid and 0.7 volumes 100% ethanol. The samples were mixed by inversion, left to precipitate on ice for 30 mins, and centrifuged at 16,000 × g at 4°C for 20 mins. The resulting pellet was resuspended in 1 ml 70% ethanol and then centrifuged for 5 mins, 4°C at 16,000 × g. The supernatant was discarded, the pellet

allowed to air-dry and dissolved in 100 µl RNase-treated water. The quantity and quality of the RNA was assessed using a NanoDrop™ 1000 UV-Vis spectrophotometer (Thermo Fisher Scientific, Loughborough, UK). The concentration of RNA was quantified using the following equation:

$$\text{RNA (ng/µl)} = A_{260} \times 40$$

The A_{260}/A_{280} ratio was used to assess protein contamination and should ideally be greater than 1.8. The A_{260}/A_{230} ratio assessed RNA sample contamination that caused by guanidine salts used in the RNA extraction procedure and should be greater than 2.0.

2.5.2. cDNA synthesis

Reverse transcription of 1 µg RNA was performed using the RevertAid™ First Strand cDNA Synthesis Kit (Fermentas, Thermo Fisher Scientific, Loughborough, UK) according to the manufacturer's protocol.

2.5.3. Genomic DNA extraction from *A. thaliana*

Genomic DNA (gDNA) extraction was carried out as described by Edwards *et al.* (1991) with modification.

Two to three small *A. thaliana* leaves were placed in a sterile 1.5 ml microfuge tube with 450 µl extraction buffer (200 mM Tris-HCl, pH 7.5, 250 mM sodium chloride and 25 mM EDTA) and ground using a micropestle. The resulting homogenate was centrifuged for 15 mins at 16,000 × g in a bench top centrifuge (Eppendorf 5415R). 400 µl of supernatant was transferred to a sterile microfuge tube and spun as before. 350 µl supernatant was carefully transferred to a new, sterile microfuge tube containing 350 µl 100% isopropanol. The samples were mixed by inversion, left to precipitate at room temperature for 15 mins, then the centrifugation step was repeated and the supernatant discarded. The remaining pellet was washed three times with 70% ethanol. Cleaned pellets were allowed to air dry for 10 mins and then resuspended in 100 µl SDW. gDNA samples were stored at 4°C.

2.5.4. Primer design and synthesis

Primers for subcloning, Gateway® cloning and semi-quantitative reverse transcriptase PCR (sq RT-PCR) were designed using a web-based NetPrimer software (Premier Biosoft, http://www.premierbiosoft.com/netprimer/index.html). Typically primer pairs were designed to be 18-25 bp in length with a similar melting temperature of about 55-60°C and approximately 40-60% GC content. Whenever possible, the 3'end of each primer contained GC or at least a single G or C. Target specificity of the primers designed was assessed by submitting primers sequence to BLAST (NCBI, http://blast.ncbi.nlm.nih.gov/Blast.cgi) and

searched against the entire *A. thaliana* genome for highly related nucleotide sequences.

For genotyping of T-DNA insertion mutants, gene-specific primers flanking left border (LP) and right border (RP) regions of the genomic sequence of the T-DNA insertion site were designed using a web-based T-DNA Primer Design tool (SIGnAL, http://signal.salk.edu/tdnaprimers.2.html). LBb (Left border primer of the T-DNA insertion) was a universal primer (sequence provided by SIGnAL) coupled with RP used to amplify the T-DNA insertion region. Meanwhile, primers for amiRNA were designed using the Web MicroRNA Designer (WMD, http://wmd3.weigelworld.org/) according to the guideline provided.

Primers were synthesised by MWG and provided as 100 µM stocks. Ten-fold diluted sub-stocks (10 µM) were prepared for PCRs.

2.5.5. Polymerase chain reaction (PCR)

PCRs were set up in sterile, thin-walled 0.2 ml PCR tubes and thermal cycling reactions were performed using a G-Storm GS1 thermal cycler (G-Storm Ltd, UK). *Taq* DNA polymerase and Phusion® High-Fidelity DNA polymerase were purchased from New England Biosciences (Hertfordshire, UK) while *Pfu* DNA polymerase and dNTPs were supplied by Promega (Southampton, UK).

2.5.5.1. PCR genotyping of *A. thaliana* T-DNA insertion mutants

Two separate PCRs were carried out for each mutant. The first reaction with LP and RP primers was used to genotype WT plant, while the second reaction with LBb and RP primers was used to genotype T-DNA insertion (Figure 2-1). Each PCR was set up in a 20 µl reaction mixture, contained 2 µl 10x *Taq* DNA polymerase buffer, 4 µl dNTPs (each at 1.25 mM), 2 µl 10 µM forward primer, 2 µl 10 µM reverse primer, 1 µl template (gDNA), 0.25 µl *Taq* DNA polymerase (5 units/µl) and 8.75 µl SDW. The PCR cycles were carried out as follows: initial activation step at 94°C (3 mins), followed by 35 cycles of denaturing, annealing and amplification (94°C for 30 secs, 55°C for 30 secs, 72°C for 1 min per kbp of DNA template) and a final extension step at 72°C for 10 mins. LBb primer, gene specific LP and RP primers (designated as XF and XR respectively, where X is gene name) used in genotyping are given in Table 2-2.

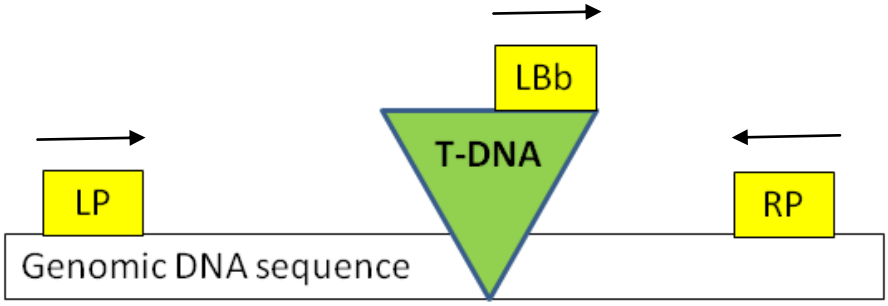

Figure 2-1: Genotyping of T-DNA insertion mutant. Two separate PCRs were carried out: the first reaction with LBb forward (T-DNA specific) and RP reverse primers, and the second reaction with LP forward and RP reverse primers.

Table 2-2: List of primers used for genotyping (SALK T-DNA insertion mutants).

Name	Sequence (5' → 3')	Tm (°C)
LBb	GCGTGGACCGCTTGCTGCAACT	71.24
ao1F	CGGATAAGGGGTATGAACATG	57.22
ao1R	AAGGGTATGGATGCTAAACCG	58.71
ao2F	AACTACATAACGCCGTTCACG	58.19
ao2R	CACGATGAAGCTCTATCCACC	57.18
ao3F	ATCCACGTCGTCAACAAACTC	57.27
ao3R	AGCAAGAGCAGTTGTGCTAGC	57.70

2.5.5.2. Semi-quantitative reverse transcriptase PCR (sq RT-PCR) on cDNA

cDNA samples were 5x diluted and used as a template for the RT-PCR. Amplification of the housekeeping gene *ACTIN2* was performed to normalise the expression level and to ensure equal loading of cDNA samples. RT-PCR was repeated for genes of interest with the amount of cDNA and cycling conditions optimised for the respective primer sets. RT-PCR products were separated by electrophoresis in a 1% (w/v) agarose gel containing 0.5 µg/ml ethidium bromide. Band intensity was quantified from the gel using the histogram function in the ImageJ software (version 1.41o, NIH, USA). Relative gene expression was calculated by normalising the band intensity of the gene of interest to *ACTIN2*.

Primers used in RT-PCR were designed to distinguish between amplification from gDNA and cDNA templates. Primers were designed either to bridge exon-exon junctions so that amplification from gDNA was impossible or to span introns so that significantly larger PCR products from gDNA were obtained than that from cDNA. Primers for RT-PCR are given in Table 2-3. The PCR cycles were carried out as follows: initial activation step at 94°C (3 mins), followed by denaturing, annealing and amplification (94°C for 30 secs, X°C for 30 secs, 72°C for Y secs) and then a final extension for 10 mins at 72°C. The annealing temperature (X°C) depended on the sequence and length of the primer, while the extension time (Y secs) was dependent on the expected product size. Specific PCR conditions for each primer pairs are given in Table 2-4.

Table 2-3: List of primers used in semi quantitative RT-PCR.

Name	Sequence (5' → 3')	Tm (°C)
Actin2F	GCAGGAGATGGAAACCTCAAAG	60.54
Actin2R	GAGATCCACATCTGCTGGAATG	59.38
sqAO1F	GAATCCGACAGATTGGGACTC	58.29
sqAO1R	CGGACGGCTAACTATGCTTG	58.67
sqAO2F	GCTGTTCAGGGACACAAGC	55.78
sqAO2R	CCTGTAGTGGTGTTAGGAAACG	56.90
sqAO3F	GGCTGTTCAAGGACACC	50.02
sqAO3R	GACCATGAATATGCCACGG	56.49

Table 2-4: PCR conditions in semi quantitative RT-PCR.

Reaction Name	Primer pair (Forward & Reverse)	Annealing temperature (X°C)	Extension time (Y secs)	Fragment size (bp)
1	Actin2F & Actin2R	57	28	402
2	sqAO1F & sqAO1R	60	41	777
3	sqAO2F & sqAO2R	57	35	557
4	sqAO3F & sqAO3R	56	42	668

2.5.5.3. Colony PCR

Colony PCR was carried out in a similar way to the PCR for genotyping of T-DNA insertion mutants (section 2.5.5.1.), except that the template used was a bacterial colony picked up using a sterile pipette tip and mixed gently in 20 µl PCR reaction mix. PCR cycling was carried out as follows: initial activation step at 94°C (6 mins), followed by 35 cycles of denaturion, annealing and amplification (94°C for 30 secs, 55°C for 30 secs, 72°C for 1 min per kbp of DNA template) and then a final extension step at 72°C for 10 mins.

2.5.5.4. Overlapping PCR to generate amiRNA

The pRS300 plasmid was used as a template to generate amiRNA by four overlapping PCRs according to the protocol described by Schwab *et al.* (2006). The amiRNA fragment was then recovered from gel extraction then cloned into the overexpression plasmid, pGWB502. Detailed strategies in producing the amiRNA constructs are described in Chapter 3.

Phusion® High-Fidelity DNA polymerase was used in all PCRs to prevent PCR-induced errors in the amplification of the amiRNA sequence. 50 µl reactions were set up, which contained 10 µl 5x Phusion® HF buffer, 8 µl dNTPs (1.25 mM), 4 µl 10 µM forward primer, 4 µl 10 µM reverse primer, 2 µl template (100x diluted pRS300 DNA), 0.5 µl Phusion® DNA polymerase (100 units/µl) and 21.5 µl SDW.

The PCR cycle was initial denaturation: 98°C for 30 secs, 24 cycles: [98°C for 10 secs, X°C for 30 secs, 72°C for Y secs], and final extension: 72°C for 10 mins. The annealing temperature (X°C) depended on the sequence and length

of the primer, while the extension time (Y secs) was dependent on the expected product size. The primers used in all PCRs are given in Table 2-5. The annealing temperature and extension time specific for each PCR are given in Table 2-6.

Table 2-5: List of primers used for amiRNA synthesis.

Name	Sequence (5' → 3')	Tm (°C)
Primer I: miR-s	gaTAATGCGGTTCAATGTGACAAtctctcttttgtattcc	76.43
Primer II: miR-a	gaTTGTCACATTGAACCGCATTAtcaaagagaatcaatga	77.88
Primer III: miR*s	gaTTATCACATTGAAGCGCATTTtcacaggtcgtgatatg	79.26
Primer IV: miR*a	gaAAATGCGCTTCAATGTGATAAtctacatatatattcct	71.82
OligoA	CTG CAA GGC GAT TAA GTT GGG TAA C	65.61
OligoB	GCG GAT AAC AAT TTC ACA CAG GAA ACA G	68.34

Table 2-6: PCR conditions in amiRNA synthesis.

Reaction Name	Primer pair (Forward & Reverse)	Annealing temperature (X°C)	Extension time (Y secs)	Fragment size (bp)
1	Oligo A & Primer IV	55	5	274
2	Primer III & Primer II	51	3	176
3	Primer I & Oligo B	55	5	301
4	Oligo A & Oligo B	55	11	701

2.5.5.5. Amplification of *AO* coding sequence

Coding sequences of *AO1*, *AO2* and *AO3* were amplified to create overexpression constructs. Total RNA was extracted from leaves of 6-week-old WT plants and converted to cDNA. Primers (Table 2-7) were designed to flank the coding sequence of individual *AO* genes and PCR was carried out using the proofreading enzyme *Pfu* DNA polymerase in a 50 µl reaction mixture containing 2 µl template (100 ng/µl), 5 µl 10x *Pfu* DNA polymerase buffer, 8 µl 1.25 mM dNTPs, 5 µl 10 µM forward primer, 5 µl 10 µM reverse primer, 0.35 µl *Pfu* DNA polymerase and SDW to 50 µl. Cycling conditions were: 95°C for 3 mins, 35 cycles [95°C for 1 min, 58°C for 30 secs, 72°C for 3 mins 30 secs], 72°C for 10 mins. Since the expected product size for all three genes was similar, cycling conditions were identical for all three reactions.

PCR products were purified using the QIAquick PCR Purification Kit (Qiagen) to remove the proofreading enzyme and excess nucleotides/primer-dimers from the reaction, and the products were verified on an agarose gel. Purified PCR products containing *AO* coding sequences were subjected to TA cloning.

Table 2-7: List of primers used for amplification of *AO* coding sequences.

Name	Sequence (5' → 3')	Tm (°C)
AO1F	CTTTGATTCTTGGAGACACGA	55.24
AO1R	AAACAGGTGTCTCATTGGCT	54.30
AO2F	TGCCCACTATCTCTTCCTCTC	55.99
AO2R	CTCAAATGCCGTCATACCTT	55.24
AO3F	GCCTATTTCATACACTCACCAG	54.41
AO3R	TTAAGAGATCCTGTTGCACC	52.52

2.5.5.6. PCR to generate *att*B products for Gateway® cloning

Gateway® cloning is a universal technology based on site-specific recombination mediated by bacteriophage lambda. By adding attachment (*att*B) sites to genes of interest, this technique facilitates transfer of the gene of interest to an *att*P-containing intermediate plasmid (Hartley *et al.*, 2000) through BP reaction (see Chapter 3 for more information).

Primers containing *att*B sites were used to amplify the respective templates (pGEM-T® easy vector harbouring either cDNA of *AO* genes or amiRNA, see section 2.5.12.) in two sets PCR by a proofreading enzyme, Phusion® DNA polymerase, produced *att*B flanked PCR products.

The first PCR was used to amplify the sequence of interest with the following primers (see Table 2-8): **Forward primer** containing the following was designed: 1) part of the *att*B1 site (AAA AAA GCA GGC T) followed by 2) two nucleotides from template-specific sequence to maintain the proper reading frame and followed by 3) 15 to 18 bp of template-specific sequence. **Reverse primer** containing the following were also designed 1) part of the *att*B2 site (CAA GAA

AGC TGG GT) followed by 2) one nucleotide from template-specific sequence to maintain proper reading frame and followed by 3) 15 to 18 bp of template-specific sequence. The first PCR was set up in a reaction mixture consisting of: 10 ng DNA template, 4 µl 5x Phusion® HF buffer, 4 µl 1.25 mM dNTPs, 2 µl 10 µM forward primer, 2 µl 10 µM reverse primer, 0.25 µl Phusion® DNA polymerase and SDW to 20 µl. For PCR with all three *AO* coding sequences, the reaction was initial denaturation: 98°C for 30 secs, 15 cycles: [98°C for 10 secs, 57°C for 30 secs, 72°C for 28 secs], and final extension: 72°C for 10 mins. The PCR conditions were identical as the products (*AO1*, *AO2* and *AO3* coding sequences) shared similar size. For PCR to amplify amiRNA, the condition was initial denaturation: 98°C for 30 secs, 15 cycles: [98°C for 10 secs, 55°C for 30 secs, 72°C for 7 secs], and final extension: 72°C for 10 mins.

The second set of PCR was used to introduce the complete *att*B sites to the PCR product with *att*B1 and *att*B2 adapter primers (Table 2-8). The 50 µl reaction mixture contained 2 µl template (obtained from first PCR), 10 µl 5x Phusion® HF buffer, 8 µl 1.25 mM dNTPs, 4 µl 10 µM forward primer, 4 µl 10 µM reverse primer, 0.5 µl Phusion® DNA polymerase and SDW to 50 µl. The PCR cycle for *AO* coding sequences was initial denaturation: 98°C for 30 secs, 20 cycles: [98°C for 10 secs, 59°C for 30 secs, 72°C for 28 secs], and final extension: 72°C for 10 mins. The PCR condition was identical as the products (*AO1*, *AO2* and *AO3* coding sequences) shared similar size. For PCR to amplify amiRNA, the condition was initial denaturation: 98°C for 30 secs, 20 cycles: [98°C for 10 secs, 55°C for 30 secs, 72°C for 7 secs], and final extension: 72°C for 10 mins.

The *attB* flanked PCR products were then used for Gateway® cloning as described in section 2.5.13.

Table 2-8: List of primers used to generate *att*B products for Gateway® cloning.

Name	Sequence (5' → 3')	Tm (°C)
attB1	G GGG ACA AGT TTG TAC AAA AAA GCA GGC T	70.95
attB2	GGG GAC CAC TTT GTA CAA GAA AGC TGG GT	72.43
AO1F-gateway	AAA AAA GCA GGC TCG AAA ATG ATG AGA CCG	74.05
AO1R-gateway	CAA GAA AGC TGG GTA TCA GCG TTT AGT CTG	69.99
AO2F-gateway	AAA AAA GCA GGC TTA TAT ATG TCT TAT GAT GAG	65.58
AO2R-gateway	CAA GAA AGC TGG GTA TCA ATT GCG GTT CC	73.39
AO3F-gateway	AAA AAA GCA GGC TAT TCC ATG GCG GTA ATT GTG	76.20
AO3R-gateway	CAA GAA AGC TGG GTT TTA AGG GCG TCC CCG G	80.72
amiRNA-F-GW	AAA AAA GCA GGC TCA AAC ACA CGC TCG GAC GCA	82.38
amiRNA-R-GW	CAA GAA AGC TGG GTC ATG GCG ATG CCT TAA ATA	77.07

Red = Gateway® sequence, Blue =Additional nucleotides (from gene specific sequence) to maintain the proper reading frame, underlined = gene specific sequence

2.5.6. Restriction Endonuclease digest of DNA

Restriction enzymes were obtained from Promega or NEB. Plasmid DNA was digested with restriction enzyme to linearise plasmid, to verify the presence of the insert, or to release gene of interest from the plasmid for cloning. A typical

20 µl reaction contained 200-500 ng/µl DNA (~1−3 µl), 10x buffer, 10 mg/ml BSA and 1 unit restriction enzyme. Reaction mixtures were incubated at 37°C for 2-3 hrs, and were stopped by heat inactivation at 65°C for 20 mins. Plasmid DNA was then separated on agarose gel by electrophoresis.

2.5.7. DNA ligation

DNA obtained from PCR or restriction enzyme digest was ligated into a vector in a 10 µl reaction mixture. Typical vector concentration for ligation was about 50-100 ng/µl and a 3:1 molar ratio of insert:vector was used. Insert and vector DNAs were mixed with 5x ligase buffer (Promega), 1 unit of T4 DNA ligase (Promega) and SDW to final volume of 10 µl. The reaction was incubated overnight at 4°C and 1-2 µl ligation mix was used for transformation.

2.5.8. Agarose gel electrophoresis

Agarose gel was prepared by melting 1-2% (w/v) agarose in 1x TAE buffer (40 mM Tris-Acetate, 1 mM EDTA). Smaller PCR products (~200 bp) were electrophoresed on a higher percentage (i.e. 2%) agarose gel, whereas larger PCR products were electrophoresed on a lower percentage (i.e. 1%) agarose gel. DNA samples were mixed with 6x loading buffer [0.25% (w/v) bromophenol blue, 0.25% (w/v) xylene cyanol FF, and 30% (v/v) glycerol]. Depending on the product size, either a 1 kb DNA ladder (Fermentas) or 100 bp DNA ladder (NEB) was loaded next to the sample as DNA size marker. DNA ladder and samples were separated by gel electrophoresis in 1x TAE buffer at 100-125 V.

2.5.9. Gel extraction and purification of DNA

DNA bands were visualised under a UV trans-illuminator and expected bands were excised with clean razor blade. DNA was extracted and purified using QIAquick Gel Extraction Kit (Qiagen) according to the manufacturer's protocol. DNA was eluted in 40 µl SDW and the quality and concentration of the purified DNA was determined by NanoDrop analysis. Purified DNA was stored at −20°C.

2.5.10. Quantification of DNA

The purified DNA was quantified using a NanoDrop^{TM} 1000 UV-Vis spectrophotometer (Thermo Fisher Scientific, Loughborough, UK) with the following equation for double-stranded DNA:

$$\text{DNA (ng/µl)} = A_{260} \times 50$$

The ratio of A_{260}/A_{280} was used to assess DNA purity and should be between 1.8 and 2.0.

2.5.11. DNA sequencing

Purified plasmid DNA or PCR products were submitted to Eurofins MWG Operon or Source Bioscience for sequencing in accordance with their instructions. The sequencing result was then viewed and analysed by aligning the actual sequence (result obtained) to the theoretical sequence (sourced from database) using ApE software.

2.5.12. A-tailing and TA cloning

Since blunt-end PCR products were obtained using proofreading DNA polymerase (e.g. Phusion® and *Pfu*), A-tailing was carried out to create single 3'deoxyadenosine overhangs in PCR fragment before cloning into the pGEM-T® easy vector containing single 3'deoxythymidine overhangs. Reactions were set up by adding 15 µl of purified PCR product, 2 µl 10x *Taq* DNA polymerase buffer, 2 µl dATP (2 µM) and 1 µl *Taq* DNA polymerase (5 units/µl) followed by 20-30 mins incubation at 72°C. For TA cloning, 1 µl of A-tailed PCR product was ligated into the pGEM-T® easy vector according to the procedure described in section 2.5.7.

2.5.13. Gateway® cloning

Two major steps involved in Gateway® cloning: BP and LR reactions. In BP reaction, *att*B-flanked PCR product (see section 2.5.5.6.) recombined with *att*P-containing donor vector to create an *att*L-flanked entry clone in a reaction catalysed by BP Clonase™ II enzyme mix. In LR reaction, the *att*L-containing entry clone recombined with an *att*R flanked destination vector to produce *att*B-flanked expression clone in the presence of LR Clonase™ II enzyme mix. The BP and LR cloning steps and reaction setup were all carried out according to the manufacturer's instructions (Invitrogen™). Recombined DNA from BP and LR reactions were transformed with *E. coli* DH5α™ competent cell. Colonies were picked and genotyped by PCR to confirm the present of the insert. Primers used in PCR are given in Table 2-9. Detailed strategies to produce various expression clones are described in Chapter 3**.**

Table 2-9: List of primers used in PCR to genotype colonies produced from Gateway® BP and LR cloning steps.

Name	Sequence (5' → 3')	Tm (°C)
pGWB-F	GACGCACAATCCCACTATCCTTC	62.55
M13F	GTAAAACGACGGCCAG	49.01
AO1Ri	CTGTAGATTCCATCGCTCGTC	57.36
AO2Ri	CTGTAGTGGTGTTAGGAAACG	52.69
AO3Ri	CGTCTTCTCATCAATCCCCG	60.15
Primer II: miR-a	gaTTGTCACATTGAACCGCATTAtcaaagagaatcaatga	77.88

2.5.14. Plasmid DNA extraction from *E. coli*

Plasmid DNA was extracted using the GeneJET™ Plasmid Miniprep Kit (Fermentas). A single bacterial colony was picked, inoculated into 5 ml LB liquid media with the appropriate antibiotic and shaken (200 rpm) for 16 hrs at 37°C. Bacterial cultures were pelleted by centrifugation at 16,000 × g for 2 mins and the supernatant discarded. Cell lysis and plasmid DNA was extracted according to the manufacturer's protocol. Plasmid DNA was eluted in 40 µl SDW and the quality and concentration of the purified plasmid DNA was determined by NanoDrop analysis. Plasmid DNA was stored at −20°C.

2.6. Generation of *A. thaliana* transgenic lines

2.6.1. Preparation of competent *Agrobacterium tumefaciens* cells

A. tumefaciens competent cells were provided by Dr. George Littlejohn (Exeter University). The protocol is described as follows:

A single colony of *A. tumefaciens* strain GV3101 was selected and inoculated into a 5 ml of 2YT liquid media containing rifampicin (25 µg/ml) and gentamycin (30 µg/ml), then shaken overnight at 180 rpm at 37°C. 2 ml of overnight culture was added into 50 ml of fresh 2YT media in a 250 ml flask and grown at 28°C until the OD_{600} reached 0.5 – 1.0. The culture was chilled on ice and pelleted by centrifugation at 3000 × g for 5 mins at 4°C. The supernatant was discarded and cells were resuspended in 1 ml of ice cold 20 mM $CaCl_2$. Resuspended cells were then dispensed into 50 µl aliquots in pre-chilled 1.5 ml microfuge tube and snap-frozen in liquid nitrogen. The frozen competent cells were stored at −80°C.

2.6.2. Transformation of *A. tumefaciens* cells by freeze-thaw method

An aliquot of competent cells were thawed on ice. 1 µg of plasmid DNA was added to the cells followed by snap-freezing in liquid nitrogen. The cells containing plasmid DNA were thawed at 37°C for 5 mins. 1 ml 2YT liquid media was then added to the cells and incubated at 28°C with constant shaking (200 rpm) for 3 hrs to allow expression of the antibiotic resistance genes. Cells were then pelleted at 16,000 × g for 30 secs, and resuspended with 100 µl 2YT liquid media. 100 µl of transformed cells were spread onto LB agar plates (+ antibiotics) and incubated at 28°C for two to three days until colonies developed. A single colony was selected and inoculated in a 50 ml 2YT liquid culture (+ antibiotics), shaken overnight (200 rpm) at 28°C. A glycerol stock containing 700 µl of the overnight culture and 300 µl of 50% glycerol was prepared in a 1.5 ml microfuge tube, and stored at −80°C. 2 µl of the overnight culture was used as the template for colony PCR.

2.6.3. *A. tumefaciens* mediated transformation of *A. thaliana* by the floral-dip method

Floral-dip method was adapted from Clough and Bent (1998). *A. thaliana* WT plants (ecotype Col-0, T_0) were grown in the long day growth chamber for 5-6 weeks until flowers developed. Then inflorescences were cut to induce more flowers after one week. About six pots (each containing 12 plants) were used for one transformation.

A 50 ml liquid 2YT starter culture supplemented with antibiotics (100 µg/ml spectinomycin, 25 µg/ml rifampicin and 30 µg/ml gentamycin) was inoculated with 10 µl culture from the glycerol stock and shaken overnight at 200 rpm, 28°C. 10 ml of the starter culture was used to inoculate a 400 ml liquid 2YT (+ antibiotics: 100 µg/ml spectinomycin, 25 µg/ml rifampicin and 30 µg/ml gentamycin) and grown overnight at 200 rpm, 28°C. Cells were harvested by centrifugation at 4750 × g for 15 mins at room temperature. The pellet was resuspended in 5% (w/v) sucrose to a final OD_{600} ~ 0.8-1.0. Silwett L-77 (Lehle seeds, USA) was added to a final concentration of 0.036% (v/v). The *A. tumefaciens* solution was poured in a tray and *A. thaliana* flowers dipped in the solution for 10 secs with agitation. Dipped plants were blotted dry on blue towel to remove excess solution and then covered in a sealed bag and placed in a dark environment overnight. The next day, plants were uncovered, returned to the long day growth chamber and allowed to set seed (T_1).

2.6.4. Selection of transgenic (antibiotic resistance) plants

Screening of transformants was performed according to the method described by Harrison *et al.* (2006).

T_1 seeds were harvested and surface sterilised. Seeds were then sown on half strength (2.2 g/L) MS media containing 0.3% (w/v) phytagel and 20 µg/ml (v/v) hygromycin B. The seeds were stratified at 4°C for two days, then incubated for 6 hrs under continuous white light in order to activate germination. The media plates were then wrapped with aluminum foil and kept at 22°C for three days. Then, the foil was removed and plates were returned to the long day growth chamber and incubated for one week. Transformants were identified by selecting the seedlings which showed elongated hypocotyls compared to non-transformants. 10 transformants were then picked up from media plates and grown in soil. Transformants were genotyped to verify presence of the correct transgene. Positive T_1 plants were allowed to set seed (T_2).

2.6.5. Screening for single-insertion, homozygous lines

Single-insertion lines were selected by plating 100 T_2 seeds of each line on MS media containing hygromycin B. T_2 lines showing 3:1 segregation (75% or roughly 68-77% resistance) on antibiotic selection were assumed to be single-insertion. Approximate 6 to 10 lines of these T_2 plants were selected and allowed to set seed (T_3). About 40 T_3 seeds from each line were plated onto MS media containing hygromycin B, with lines showing 100% resistance assumed to be homozygous. Homozygous T_3 plant lines were used for all downstream experiments.

2.7. Abiotic stress treatments on *A. thaliana*

2.7.1. Drought treatment

Six-week-old plants of similar size were selected prior to the experiment. For drought treatment, water was withheld from plants for 14 days; watered plants were used as control. During the drought period, soil water content (measured by the reduction of pot + soil weight) and relative humidity of the growth chamber were monitored. Samples were harvested for experiments on day 14.

2.7.2. High light treatment

Six-week-old plants were transferred from the short day growth chamber to an environment controlled growth cabinet (Microclima 1000E, Snijders, Tilburg, Netherlands) and acclimated for four days under long day conditions (photoperiod: 16 hrs light, 8 hrs dark, 23°C, 65% RH, PPFD 100 µmol m^{-2} s^{-1}). For high light treatments, these plants were subjected to a PPFD of 550-650 µmol m^{-2} s^{-1}, 16 hrs light period for 7 days. Control (low light) plants were grown in the same cabinet at a PPFD of 100 µmol m^{-2} s^{-1}.

2.8. Growth parameters

2.8.1. Germination rate

Surface sterilised and vernalised seeds were sown on half-strength MS agar media and kept in a growth chamber for two weeks. Germination rate (%) was scored by recording the number of germinated seeds from the total number of seeds sown.

2.8.2. Relative water content (RWC)

RWC was calculated according to the following formula:

$$(FW-DW) / (RW-DW)$$

Weight was measured using an analytical balance. Fresh weight (FW) was obtained from the detached leaves of watered and drought treated plants on day 14; rehydrated weight (RW) was obtained by incubating detached leaves with deionised water in a Petri dish, kept overnight at room temperature in the dark, then blotted dry with paper towel; dry weight (DW) was recorded after putting rehydrated leaves in an oven at 75°C overnight.

2.8.3. Leaf water loss

Fully expanded leaves from well-watered plants were detached, kept at room temperature and fresh weight was measured every 15 mins for a period of 1.5 hrs. Leaf water loss was plotted as the percentage of reduction in fresh weight relative to the initial fresh weight.

2.8.4. Photosynthetic capacity

Chlorophyll fluorescence was measured using a FluorImager imaging system (Technologica, UK) and its software (V2.217). Plants were dark adapted for 20 mins, then subjected to a saturated pulse at PPFD of 6144 μmol m^{-2} s^{-1}. The dark adapted maximum quantum efficiency of photosystem II (F_v/F_m) was recorded.

2.8.5. Measurement of total leaf area and absolute expansion rate

The expansion rates of the experimental plants (unstressed normal growth conditions or stress treatments) were closely monitored by taking pictures of these plants with a digital camera for the indicated period of time (described in result chapters). For each picture captured, a standard 15 cm ruler was placed next to the plants for scaling. ImageJ software (version 1.41o, NIH, USA) was used to draw an outline around the leaf image and total leaf area was measured with a calibrated scale bar. Absolute expansion rate (AER) at day *x* was performed according to the following formula (Goh *et al.*, 2012):

$AER_x = (m_x - m_{x-1}) / (t_x - t_{x-1})$, where m is the total leaf area measurement, t is time (day), m_x is measurements at day *x* and m_{x-1} is measurements at previous time point.

2.8.6. Cell measurements

Fully expanded leaves of 5 to 6-week-old plants were preserved in 100% ethanol overnight and then viewed under a light microscope (Carl Zeiss Primo Star, Germany) at 20x objective magnification. Optical microscopic images of palisade mesophyll cells were obtained with AxioCam MRc 5 digital camera (Carl Zeiss, Germany). Cell area and dimensions were measured using ImageJ software (version 1.41o, NIH, USA).

2.9. Analytical methods

2.9.1. Conversion of tissue fresh weight to tissue dry weight for assays in the drought experiment

Several assays in this project required tissue fresh weight (FW) as a reference (see Results in Chapter 5 and 6). However FW of drought stressed plants is significantly lower than the watered plants due to lower water content in drought tissue. Therefore, FW of watered and drought tissues was calculated for dry weight (DW) to ensure results obtained in drought experiments were not caused by variation in water content between watered and drought tissues. The following formula was used to convert FW to DW:

$$DW = (DW_{RWC} / FW_{RWC}) \times FW_i$$

where DW_{RWC}, FW_{RWC} = DW and FW of tissues from the same plant that used for RWC experiment (see section 2.8.2.). FWi = FW of tissues from the same plant that used for the respective drought experiment.

2.9.2. Ascorbate oxidase (AO) activity

Plant tissue was homogenised in ice-cold extraction buffer (50 mM HEPES and 1 mM Na_2EDTA, pH 7.0). The crude extracts were centrifuged at 16,000 × g for 5 mins, the supernatant (designated as the soluble fraction) was collected. The pellet was washed with the same extraction buffer and centrifuged at 16,000 × g for 5 mins. The supernatant was discarded and the pellet was resuspended in same buffer with the addition of 100 mM $CaCl_2$, vortexed and centrifuged at 16,000 × g for 5 mins. The supernatant (designated as ionically-bound cell wall fraction) was collected.

AO activity was assessed based on a spectrophotometric method (Oberbacher and Vines, 1963) by measuring the oxidation of ascorbate (AsA) by AO in the extracts at 265 nm for 3 mins at room temperature using a UV-Vis Spectrophotometer (Shimadzu, Japan). The 1 ml reaction mixture in a quartz cuvette contained 850 µl assay buffer (25 mM K_2HPO_4, 12.5 mM citric acid and 0.1 mM Na_2EDTA, pH 6.0), 50 µl of 50 µM AsA and 100 µl extracts.

As the same amount of tissue might have different protein concentration, the AO activity was expressed on a tissue weight (µmol AsA oxidised/min/g tissue weight) and protein (µmol AsA oxidised/min/mg protein) basis, after normalising the absorbance reading to tissue weight (g) and total protein content respectively. Total protein was assayed according to the Bradford method (Bradford, 1976) using γ-globulin as a standard. An extinction coefficient for AsA of 14 mM^{-1} cm^{-1} at 265 nm was used in calculations (Pignocchi *et al.*, 2003).

Alternatively, a microplate protocol was used to measure AO activity (Tecan, Switzerland). The assay mixture contained 150 µl of assay buffer (25 mM K_2HPO_4, 12.5 mM citric acid and 0.1 mM Na_2EDTA, pH 6.0), 20 µl of 100 µM AsA and 30 µl extracts.

2.9.3. Peroxidase activity

Peroxidase activity was measured in the same extracts used for AO assay. The assay contained 940 µl assay buffer (50 mM HEPES and 1 mM Na_2EDTA, pH 7.0), 20 µl of 20 mM pyrogallol and 20 µl extract. The reaction started by adding 20 µl 3 mM H_2O_2 to the mixture and followed by 100 secs reaction, measured using a UV-Vis Spectrophotometers (Shimadzu, Japan). The oxidation of

pyrogallol was followed at 430 nm using an extinction coefficient of 2.47 mM^{-1} cm^{-1} (Veljovic-Jovanovic *et al.*, 2001). Total protein was measured according to the Bradford method (Bradford, 1976) using γ-globulin as a standard. Similar to the AO assay, peroxidase activity was expressed on a tissue weight (µmol pyrogallol oxidised/min/g tissue weight) and protein (µmol pyrogallol oxidised/min/mg protein) basis, after normalising the absorbance reading to tissue weight (g) and total protein content respectively.

Alternatively, a microplate protocol was used to measure peroxidase activity (Tecan, Switzerland). The assay mixture contained 220 µl of assay buffer (50 mM HEPES, 1 mM Na_2EDTA, pH 7.0), 5 µl of 20 mM pyrogallol, 20 µl of extract, and 5 µl of 3 mM H_2O_2 in a total volume of 250 µl. An extinction coefficient corrected for path length in the microplate assay (1.953 mM^{-1} cm^{-1}) was used (Sultana, 2011).

2.9.4. Bradford assay on total protein content

Total protein contents of plant extracts were quantified based on the method described by Bradford (1976). Bradford reagent was 5x diluted in deionised water. Protein standards for assay calibration were prepared at 0.04, 0.08, 0.12 and 0.16 mg/ml from stock γ-globulin (2 mg/ml). Reaction mixture contained 20 µl extract or standard added to 230 µl of Bradford reagent in a 96-well plate and incubated at room temperature for 20 mins. The A_{550} was measured against blank of Bradford reagent (no protein added) using a VersaMax microplate reader (Molecular devices, USA). Total protein content of plant extract (mg/g) was estimated based on a standard curve.

2.9.5. Determination of chlorophyll and carotenoid contents

Fully expanded leaves were harvested, weighed and placed in a 1.5 ml microfuge tube containing 600 µl 80% acetone and stored in the dark at 4°C overnight. The supernatant was transferred to a new tube and kept at 4°C in dark. The extraction procedure was repeated on the same leaves and the supernatants pooled and used for analyses. 200 µl supernatant was transferred to a 96-well plate and absorbance at 470 nm, 647 nm and 663 nm was measured using an Infinite M200 plate reader (Tecan, Switzerland). The blank consisted of 200 µl 80% acetone. The following formulae were used to calculate chlorophyll a, chlorophyll b and carotenoid contents (Lichtenthaler and Buschmann, 2001):

Chlorophyll a (chl*a*), (µg/ml) = $12.25\ A_{663} - 2.79\ A_{647}$

Chlorophyll b (chl*b*), (µg/ml) = $21.50\ A_{647} - 5.10\ A_{663}$

Carotenoid (µg/ml) = $(1000\ A_{470} - 1.82$ chl*a* $- 85.02$ chl*b*$) / 198$

2.9.6. Determination of total anthocyanin content

Total anthocyanins were determined as described by Page *et al.* (2012) using 100 µl of the same extract that was prepared for AsA analysis (section 2.10.). Samples were diluted 1:1 with 1% metaphosphoric acid (MPA) and the blank consisted of 200 µl 1% MPA. The absorbance at 530 nm and 657 nm was measured using an Infinite M200 plate reader (Tecan, Switzerland).

2.10. Ascorbate (AsA) analysis

2.10.1. Whole leaf AsA extraction

Fully expanded rosette leaves were harvested from 6 to 8 week old plants, and frozen with liquid nitrogen. Leaf tissues were ground in 1% MPA at a ratio of 0.1 g/ml. The homogenate was centrifuged at 16,000 × g for 5 mins, 4°C. The supernatant was collected and stored at −80°C until AsA analysis.

2.10.2. Apoplast AsA extraction

Apoplastic fluid was prepared using a method described by Sultana (2011). Fresh 6 to 7-week-old leaf tissue was excised, weighed and cut into 3 roughly equal pieces and vacuum infiltrated at -90 kPa, (3 × 1 min) with a chilled phosphate buffer (25 mM K_2HPO_4, 12.5 mM citric acid, pH 3) using a vacuum diaphragm pump system (ILMVAC, UK). Infiltrated leaves were blotted dry, transferred to a syringe tube, then placed in a 15 ml Falcon tube containing 100 µl 3% MPA and centrifuged for 10 mins, 100 × g at 4°C. Apoplastic fluid collected was transferred to a 1.5 ml microfuge tube. The apoplastic fluid was weighed, immediately frozen and stored at −80°C until analysis. An illustration of the apoplastic extraction steps is shown in Figure 2-2.

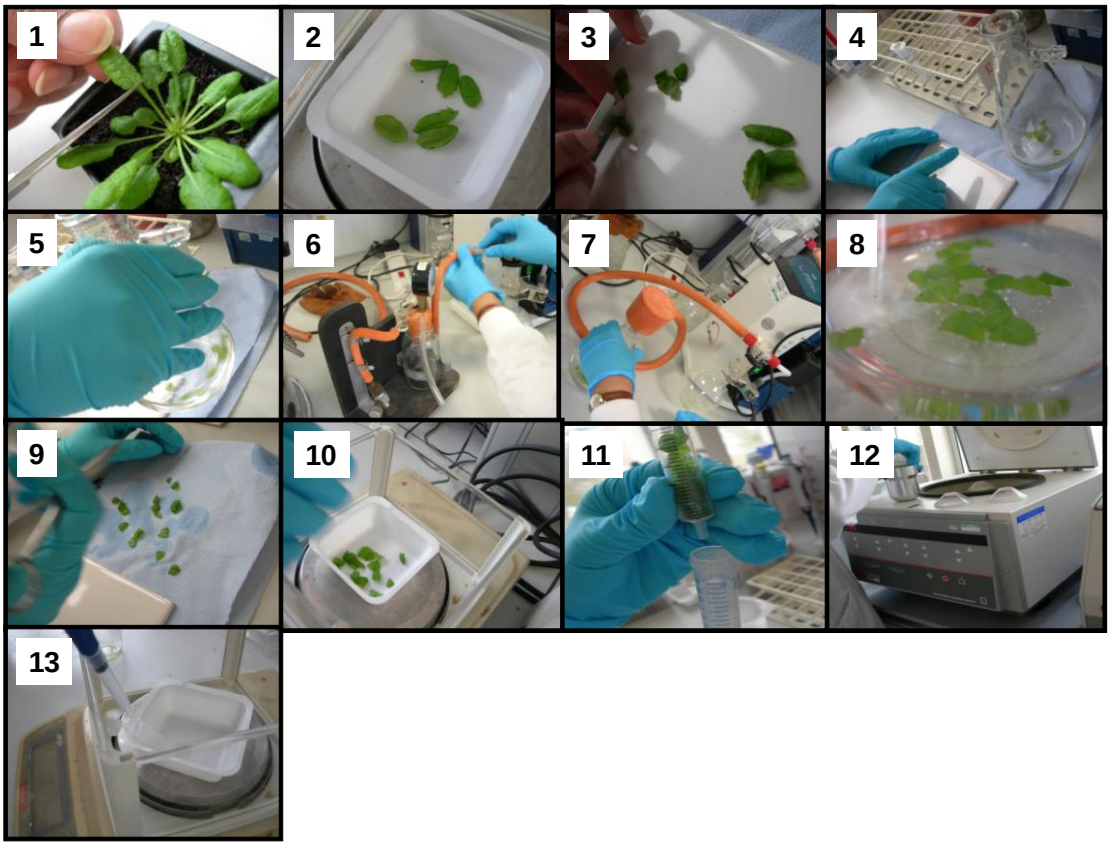

Figure 2-2: Extraction of apoplastic AsA. Fresh leaves were excised **(1)**, weighed **(2)** and cut into three equal portions **(3)**. Cut leaves were transferred to extraction buffer and shaken gently **(4 - 5)**. A vacuum gauge was connected to the vacuum diaphragm pump to ensure correct pressure used prior to the extraction **(6)**. Leaves were vacuum infiltrated with extraction buffer **(7)** with bubbles seen forming around the leaf edge **(8)**. Infiltrated leaves were blotted dry **(9)** and weighed **(10)**. Leaves were then transferred to a 5 ml syringe tube and placed in a 15 ml Falcon tube containing 3% MPA **(11)** and centrifuged **(12)**. The apoplastic fluid collected was transferred to a 1.5 ml microfuge tube and weighed **(13)**. Samples were stored at −80°C until analysis.

2.10.3. Quantification of AsA using HPLC

For AsA measurement, 125 µl of each sample was mixed with an equal volume of 1% MPA to assay reduced AsA. Another 125 µl of each sample was mixed with an equal volume of 20 mM tris(2-carboxyethyl)phosphine hydrochloride

(TCEP, dissolved in 1% MPA) for 20 mins to reduce DHA and quantify total AsA (AsA + DHA). These samples were then loaded into HPLC vials and measured by HPLC as described by Page *et al.* (2012).

Mobile phases contained 95% water, 5% acetonitrile, 0.1% formic acid (A) and 95% acetonitrile, 5% water, 0.1% formic acid (B). 20 µl of sample was injected onto a Phenomenex Luna C18 column (10 µm particle size, 250 × 4.6 mm) and subjected to the following gradient using a Dionex DX500 HPLC system (Dionex, Sunnyvale, USA): 0 min – 0% B; 4 mins – 40% B; 7 mins – 100% B; 9 mins – 100% B; 10 mins – 0% B; 2 mins post time. Flow rate was maintained at 1 ml min^{-1} and the assay was carried out at 21°C. AsA was detected using a SPD-10A dual wavelength detector (Shimadzu, Japan) at 265 nm and 280 nm, and had a retention time of approximately 3.5 mins.

Data were analysed with Chromeleon software (Dionex, Sunnyvale, USA). The peak purity of AsA was determined by monitoring the 265/280 nm signal ratio, which is ~10 for pure AsA. AsA was quantified by comparison with external standards using the peak areas at 265 nm.

Alternatively, AsA was quantified using a 1200 series Rapid Resolution HPLC system (Agilent Technologies, Palo Alto, USA), with identical mobile phases and gradients described for Dionex DX500 HPLC system. The AsA data were acquired using the ChemStation software (Agilent Technologies, Palo Alto, USA) and analysed in a similar way described for Chromeleon software.

2.11. Phylogenetic tree construction

Amino acid sequences encoding AO for several species were retrieved from NCBI (http://www.ncbi.nlm.nih.gov/) by homology searches (BLAST, Altschul *et al.*, 1990) using *A. thaliana* sequences. In addition, amino acid sequence encoding multi-copper oxidase for a green alga (*Volvox carteri*) was retrieved from NCBI (detailed in Chapter 4) and used as the outliner in the phylogenetic tree construction. These amino acid sequences were aligned with the built-in ClustalW (Thompson *et al.*, 1994) programme of the MEGA 5 software (Tamura *et al.*, 2011) using the default parameters. Gaps in the alignment were ignored prior to tree constructions. Phylogenetic trees were drawn with Neighbor-Joining method using the MEGA 5 software. Bootstrap values based on 1000 replicates were calculated to test the reliability of the tree topology.

2.12. Software and bioinformatic tools

In silico gene expression analysis for genes of interest was assessed using the eFP browser microarray database (Winter *et al.*, 2007). *In silico* analysis of promoter elements was performed using PlantCARE (Rombauts *et al.*, 1999). The plasmid map was drawn by BioEdit, version 7.1.3.0 (Hall, 1999). DNA sequence annotation, alignment and virtual restriction digest was performed using ApE (http://biologylabs.utah.edu/jorgensen/wayned/ape/). Phylogenetic trees were drawn using the MEGA 5 software (Tamura *et al.*, 2011). Bioinformatic tools from the Center for Biological Sequence Analysis (CBS), Technical University of Denmark (http://www.cbs.dtu.dk/services/index.php) were used to obtain information on the predicted subcellular localisation and

post-translational modification of AO protein. Descriptions for some of these tools are available in Chapter 4.

2.13. Statistical analyses

Statistical analyses were performed using GraphPad Prism version 6.00 for Windows (GraphPad Software, San Diego California USA). Statistical significance between datasets were performed using one-way analysis of variance (ANOVA) followed by post hoc test (Dunnett or Turkey) or two-tailed *t*-test. Values at $p<0.05$ were considered statistically significant.

Chapter 3. Establishment of plant lines

3.1. General introduction

Various resources have been created for *A. thaliana* researchers (see TAIR website, http://www.arabidopsis.org/). These include a large collection of indexed T-DNA insertion mutants and RNAi lines. These loss-of-function mutants facilitate study of the gene function and save considerable amount of time in developing mutants (Alonso *et al.*, 2003; Hilson *et al.*, 2004).

A previous study in *A. thaliana ao3* T-DNA insertion mutant did not reveal a clear phenotype (Yamamoto *et al.*, 2005). Lee *et al.* (2011) showed that an *ao1ao2* double mutant (crossing of *ao1* and *ao2* T-DNA mutants) had smaller size and late flowering but the AO activity of this double mutant was not assessed. Lack of a clear phenotype in *ao3* may be caused by functional redundancy due to action of other *AO* genes. Therefore, it is essential to develop double or triple mutants of the three *AO* genes in order to resolve the function of this enzyme.

Three homozygous T-DNA mutants for individual *AO* genes: *ao1*, *ao2* and *ao3* were obtained and an *ao1ao3* double mutant was developed in the initial part of this project. However, there are no phenotypic differences in these mutants (see Chapter 5 and Chapter 6). Also, two of the *AO* genes-*AO2* and *AO3* are located next to each other within the same chromosome, which hampers the effort to produce an *ao2ao3* double mutant by crossing. Therefore an artificial microRNA (amiRNA) construct was developed as an attempt to silence all three *AO* genes.

Due to gene redundancy, study of AO function by loss-of-function mutation could be insufficient for complete functional analysis of these *AO* genes. Gain-

of-function mutants were created by producing *AO* overexpressing transgenic plants which carry the *AO* cDNAs driven by a constitutive 35SCaMV promoter. The following sections give background information on the approaches (i.e. T-DNA, amiRNA, and Gateway® cloning) employed to obtain plant lines needed for this project.

3.1.1. T-DNA insertion mutants

Insertional mutagenesis is one of the ways to disrupt gene function by inserting foreign DNA into the gene of interest. The first approach of insertional mutagenesis in *A. thaliana* involved the use of transposons, small mobile DNA elements that can move within the genome. Transposon insertion can be a convenient tool to target mutation of tandem array genes along a chromosome. However, the mobility of this transposable element can lead to instability in successive generations (Krysan *et al.*, 1999).

The capability of *Agrobacterium tumefaciens* to transfer part of its DNA, transfer DNA (T-DNA) into a plant's genome from its Ti plasmid makes it an excellent tool for genetically transforming plants. Apart from being a good tool in plant transformation, by inserting T-DNA into a coding gene, this method not only disrupts gene function but also serves as a marker for identification of the mutation (Azpiroz-Leehan and Feldmann, 1997). The insertion of a piece of T-DNA about 5 to 25 kb in length generally produces a dramatic disruption of gene function due to the small introns and less intergenic materials present in *A. thaliana* as compared with other organisms (Krysan *et al.*, 1999).

Since T-DNA insertion into the *A. thaliana* genome is random, it is impossible to target mutation of a specific gene. A huge collection of T-DNA insertions is needed to saturate the *A. thaliana* genome to the extent that at least one insert is available in each gene so that a catalogue of gene-indexed mutants can be made on a genome-wide scale (Azpiroz-Leehan and Feldmann, 1997; O'Malley *et al.*, 2007). A multi-laboratories collaboration has performed genome-wide T-DNA insertional mutagenesis of *A. thaliana* and has created insertion mutants for about 74% of the predicted *A. thaliana* genes (Alonso *et al.*, 2003). This large collection of T-DNA mutants is distributed *via* seed banks: the Nottingham *Arabidopsis* Stock Centre (NASC) or the *Arabidopsis* Biological Resource Center (ABRC). In this project, T-DNA mutants for all three *AO* genes were sourced from NASC.

3.1.2. amiRNA approach

MicroRNAs (miRNAs) are small 21 to 24 nucleotide (nt) non-coding endogenous single stranded RNA (ssRNA) that play important roles in gene regulation by targeting mRNAs for degradation or translational repression (Baulcombe, 2004). In *A. thaliana*, 15 distinct miRNA families have been reported and they are mainly involved in the control of plant development (Bartel, 2004).

Artificial microRNA (amiRNA) is an approach using a miRNA precursor to generate a synthetic 21-mer miRNA sequence that induces silencing of the target gene(s) (Figure 3-1A) (Ossowski *et al.*, 2008). amiRNA technology was first employed in *A. thaliana* by Parizotto (2004) to target reporter gene silencing.

It was later found that amiRNA can silence endogenous genes of *A. thaliana* as well as other plant species (Alvarez *et al.*, 2006; Schwab *et al.*, 2006).

Compared to the hairpin RNAi approach (Figure 3-1B), amiRNA is a fairly new strategy in gene silencing. Both methods silence genes by producing short interfering RNA (siRNA) that is incorporated into RNA-induced silencing complexes (RISC), bind to the complement target mRNA and lead to its degradation by catalytic subunits of RISC, Argonaute (Ago) proteins. However, the hairpin RNAi precursor is constructed in antisense and sense orientation, forming a long dsRNA and therefore producing many siRNAs after being processed by DICER-like proteins. This may lead to non-target gene silencing. amiRNA technique, by contrast, mainly generates one siRNA that offers high specificity in gene silencing (Ossowski *et al.*, 2008). Another advantage of amiRNA strategy is to silence multiple target genes, especially those present in tandem arrays (i.e. functionally related genes located next to each other on the same chromosome) where currently no convenient tool is available for their knockout. In the *A. thaliana* genome, 20% of the genes are found in tandem arrays (Schwab *et al.*, 2006). *AO2* (At5g21105) and *AO3* (At5g21100) is one of the examples.

A web-based tool known as the Web MicroRNA Designer (WMD) was developed by Weigel and co-workers (Ossowski *et al.*, 2008) to automate amiRNA design from the gene(s) of interest. The detailed protocol is available at the WMD website (http://wmd3.weigelworld.org/). The strategy to design amiRNA for three *AO* genes is described in the Results and Discussion section of this chapter.

Figure 3-1: Gene silencing in plants by small RNA. **(A)** amiRNAs are transcribed from non-coding genes by RNA polymerase II and processed by dsRNA-binding protein (HYL1) and DICER-like protein (DCL1) to 21-nucleotide (nt) miRNA. The miRNA duplex is then methylated by HUA ENHANCER 1 (HEN1). The miRNA is then incorporated into the RNA-induced silencing complex (RISC), guided by Argonaute proteins (AGO1) to induce cleavage of target transcript. **(B)** Hairpin RNAi precursor is constructed in antisense and sense orientation, forming a long dsRNA and processed by DCL4 to 22-, 24- or 21-nt siRNAs duplex. siRNAs duplex also can be generated from ssRNA by RNA-dependent RNA polymerase (RDR6). The 21-nt siRNA is methylated by HEN1, guided by AGO1 to incorporate into RISC and leads to cleavage of target transcript. Figure adapted from Ossowski *et al.* (2008).

3.1.3. Gateway® cloning

Prior to the generation of transgenic plants, a simple and effective cloning system is required to develop all vector constructs. The conventional cloning method by DNA restriction and ligation is tedious and laborious. The introduction of Gateway® system (Invitrogen™) has provided a rapid and efficient way to insert genes of interest into various compatible vectors and thus facilitate studies on gene function and protein expression. Since then, It has become a method of choice and various compatible vectors have been constructed to use in Gateway® cloning (Karimi *et al.*, 2007). The Gateway® technique was first developed by researchers at Life Technologies (Hartley *et al.*, 2000) and now distributed by Invitrogen™. Details of the concept and protocol of Gateway® cloning system is available on Invitrogen website (www.invitrogen.com).

In brief, the Gateway® system is based on site-specific recombination mediated by bateriophage lambda which facilitates the integration of phage into the *E. coli* chromosome. *In vitro* recombination between DNA fragment (gene of interest) flanked by attachment (*att*) sites and vector that contained compatible *att* sites can take place in a mixture of phage and *E.coli* encoded proteins (Clonase™ II enzyme mix). The first reaction of Gateway® cloning is BP reaction (Figure 3-2A), mediated by BP Clonase™ II enzyme mix, which involved the recombination of *att*B flanked DNA fragment (gene of interest) with *att*P flanked donor vector (pDONR) to produce an *att*L containing entry clone (pENTR). This is followed by LR reaction (Figure 3-2B), the second step facilitated by LR Clonase™ II enzyme mix to recombine *att*L containing pENTR with *att*R

containing destination vector (pDEST) to create *att*B flanked expression clone (pEXPR).

Figure 3-2: Gateway® cloning principle. **(A)** BP reaction mediated by BP Clonase™ II, the *att*B-flanked PCR product is combined with *att*P-containing donor vector to create *att*L-flanked entry clone and *att*R-flanked by-product. **(B)** LR reaction mediated by LR Clonase™ II, the entry clone is recombined with *att*R-flanked destination vector to produce the *att*B-flanked expression clone and *att*P-flanked by-product. Reproduced from the Gateway® Technology with Clonase™ II manual, May 2009 version (Invitrogen).

3.1.4. Gateway binary vector

Agrobacterium mediated genetic transformation of plant cells by transferring T-DNA of its Ti plasmid led to the invention of a binary vector. This is because researchers learnt that T-DNA transfer can take place even though the virulence genes and T-DNA required for successful transformation were split into two replicons (Lee and Gelvin, 2008). As a result, a “disarmed” *Agrobacterium* strain which carried a Ti plasmid and a plasmid which carried an artificial T-DNA that can be replicated in both *E. coli* and *Agrobacterium* were

developed. The entire combination (disarmed strain + plasmid) is referred as “binary vector”, but often only the plasmid carries T-DNA is usually called binary vector.

Binary vector (contained gene of interest) has greatly improved functional gene analysis *in planta* by producing transgenic plants from *Agrobacterium* transformation. A typical binary vector contained the right border (RB) and the left border (LB) of the T-DNA sequences, multiple cloning sites, a selectable marker gene for plants (antibiotic or herbicide resistance), a reporter gene, and other genes of interest. The vector backbone contains origin of replication for *E. coli* and *Agrobacterium*, and selectable marker genes (e.g. antibiotic resistance) for the bacteria.

The conventional binary vector construction that involved restriction digest and ligation is time consuming and laborious. By employing the advantages of Gateway® cloning, a series of Gateway-compatible binary vectors for plant science studies were developed by Nakagawa *et al.* (2007). These Gateway binary vectors (pGWBs) allow genes fusion with various kinds of reporter and tag that greatly facilitate the studies in protein subcellular localisation, promoter analysis, recombinant protein expression and protein-protein interaction. The pGWBs are available for non-commercial research and the list of vectors is available at http://shimane-u.org/nakagawa/gbv.htm. In this project, pGWB502 vector was used to develop transgenic plants. The pGWB502 vector contains a constitutive 35S Cauliflower Mosaic Virus (35SCaMV) promoter/terminator, a hygromycin resistance marker for plant selection and a spectinomycin bacterial selectable marker (Figure 3-3).

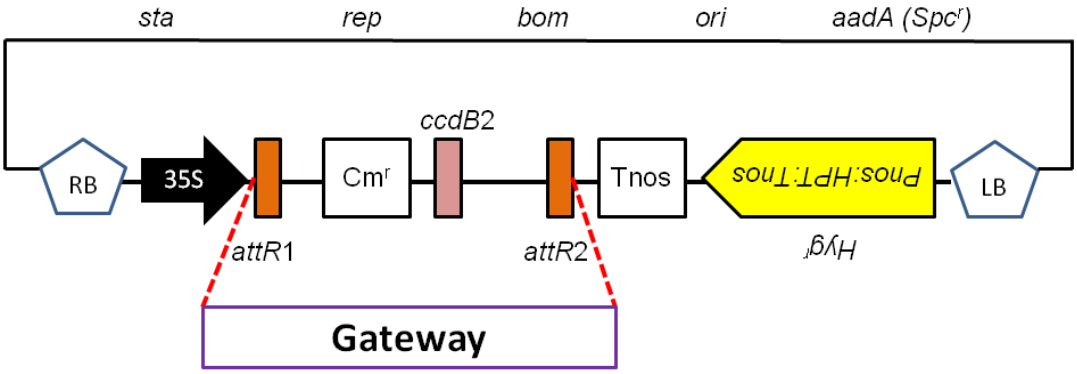

Figure 3-3: Schematic illustration of the pGWB502 vector. It has a hygromycin resistance selectable marker (Hyg^r) for plant that placed in a reverse orientation to the target genes cloned by the Gateway® LR reaction, which is recombined *via attR* sites at the "Gateway" area marked by red dotted lines. The cloned gene is expressed by 35SCaMV promoter. Revised from Nakagawa *et al.* (2007).

RB, right border; *LB*, left border; *sta*, region for stability in *Agrobacterium*; *rep*, broad host-range replication origin; *bom*, *cis*-acting element for conjugational transfer; *ori*, ColE1 replication origin; Cm^r, chloramphenicol resistance marker (chloramphenicol acetyl transferase) used for selection in the bacteria; *aadA*, spectinomycin resistance (Spc^r) marker used for selection in the bacteria; *ccd*B, negative selection marker used in the bacteria and Tnos, nopaline synthase terminator.

3.1.5. Chapter aim

This chapter describes strategies used to establish plant materials required for functional analyses of AO, the lines developed are as follows:

- Homozygous T-DNA insertion mutants for all three *AO* genes were identified by genotyping and backcrossed with WT *A. thaliana* to remove extraneous mutation.

- The *ao1ao3* double mutant was developed by crossing.

- An amiRNA construct to silence all three *AO* genes was developed and named as *amiR-AO* thereafter in this thesis. The *amiR-AO* fragment was placed under the control of the constitutive 35SCaMV promoter by cloning *amiR-AO* into a gateway binary vector (pGWB502). The construct was then transformed to *A. thaliana* by *A. tumefaciens* strain GV3101 to develop *35S::amiR-AO* transgenic plants.

- In order to generate transgenic plants overexpressing the *AO* gene, overexpression constructs, each harboured the coding sequence (cDNAs) of individual *AO* gene (*AO1*, *AO2* and *AO3*) were cloned into pGWB502 then followed by *A. tumefaciens* mediated transformation of *A. thaliana* to produce *35S::AO1*, *35S::AO2* and *35S::AO3* lines.

3.2. Results and Discussion

3.2.1. Selection of T-DNA insertion mutants from seed bank

The availability of T-DNA insertion mutants (developed by Salk, Alonso *et al.*, 2003) for *AO* genes was searched against seed bank, the Nottingham *Arabidopsis* Stock Centre (NASC), by entering the respective *Arabidopsis* Gene

Identifier (AGI) code (i.e. At4g39830 for *AO1*; At5g21105 for *AO2* and At5g21100 for *AO3*). The TAIR nucleotide sequence viewer (http://www.arabidopsis.org/servlets/sv) was used to find out the predicted T-DNA insertion region of these Salk lines in the gDNA sequence of individual *AO* genes. Whenever possible, a T-DNA mutant with the insertion point in an exon or a region close to start codon was selected, whereas those at intron and 3' untranslated region (UTR) were ignored. All these measures were taken into consideration in order to obtain T-DNA mutant lines with effectively knocked down/out *AO* expression. T-DNA lines for each gene were selected and ordered (Table 3-1). The predicted T-DNA inserted location for these mutants is illustrated in Figure 3-4.

Table 3-1: T-DNA lines used in this study.

Gene ID	Gene Name	NASC ID	Salk line	T-DNA insertion
At4g39830	*AO1*	N636041	SALK_136041	Exon
At5g21105	*AO2*	N665814	SALK_039183C	Exon
At5g21100	*AO3*	N608854	SALK_108854	Exon

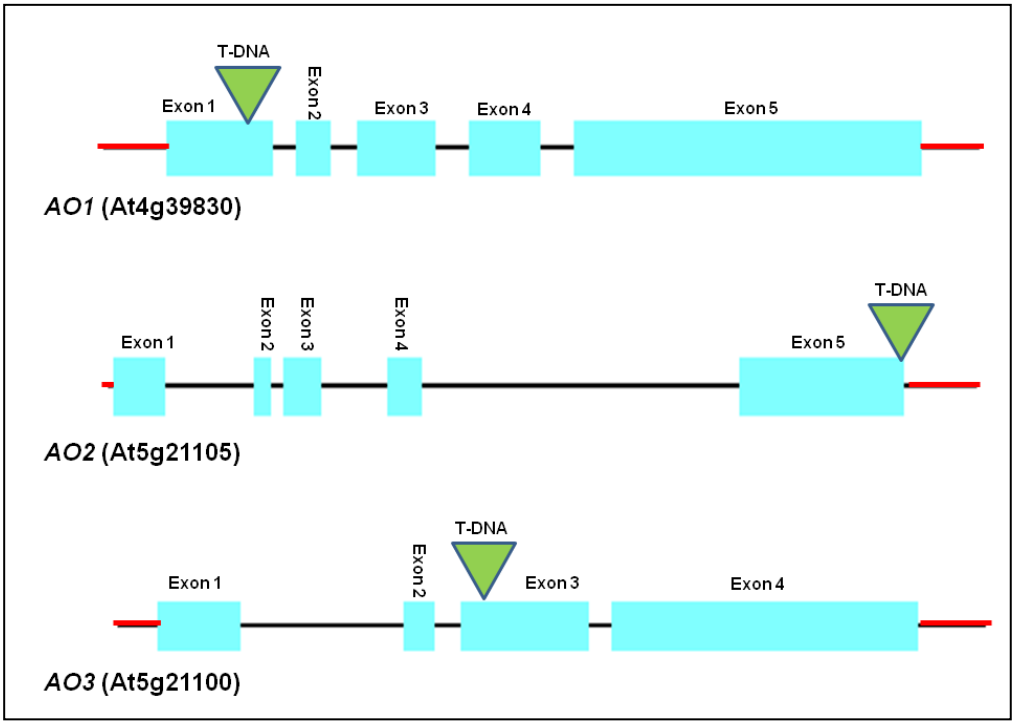

Figure 3-4: Schematic diagram of *AO1*, *AO2* and *AO3* gDNA with predicted T-DNA insertion. The red line indicates untranslated region, dark line indicates intron.

3.2.2. Verification and backcrossed of homozygous *AO* T-DNA insertion mutants

T-DNA lines for *AO1* and *AO3* were in segregating form, so it is possible to get WT, heterozygous (HZ) and homozygous (HM) plants. T-DNA insertion mutants conferred kanamycin resistance, but the antibiotic resistance phenotype may be lost due to gene silencing after several generations of growth. Therefore seeds of the *AO* T-DNA insertion mutants were sown on soil, gDNA was then extracted and genotyped by PCR.

SIGnAL T-DNA Primer Design tool was used to design gene specific forward (LP) and reverse (RP) primers flanking T-DNA insertion region of the genome sequence (see method, section 2.5.4.). Two separate PCRs were carried out (see method, section 2.5.5.1.): first reaction with LBb (T-DNA left border primer) and RP primers; second reaction with LP and RP primers. The PCR with LBb+RP primers pair produced amplicons of about 500 bp in HZ and HM plants but not in WT plant (Figure 3-5A). The PCR with LP+RP primers pair gave product size of about 900-1100 bp on WT and HZ plants but not in HM (Figure 3-5B).

A strategy to backcross HM *ao* mutants and its expected segregation ratio was developed for monogenic inheritance (Figure 3-6). Only 3−4 plants per line were backcrossed to reduce germplasm variation. The numbers of HM/HZ/WT plants scored were in accordance to the segregation ratio for the respective generation. F4 plants were then used in following experiments.

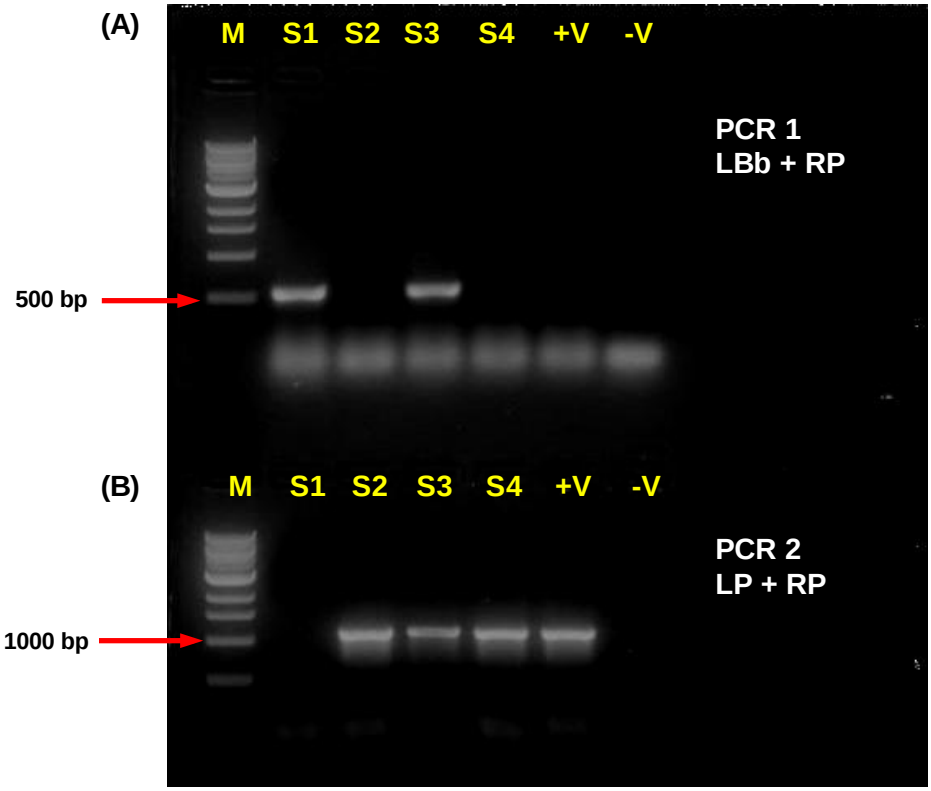

Figure 3-5: Genotyping of *AO* T-DNA insertion mutants. gDNA was extracted from four individual plants and two PCRs were performed for each sample (S1−S4): **(A)** PCR 1 amplified with T-DNA specific LBb forward primer and gene specific reverse (RP) primer; **(B)** PCR 2 amplified with gene specific forward (LP) and reverse (RP) primers. The gel image illustrates typical PCR product size for HM (S1: single band at ~ 500 bp in PCR 1), HZ (S3: dual bands at ~ 500 bp in PCR 1 and ~900-1100 bp in PCR 2) and WT (S2, S4: single band at ~ 900-1100 bp in PCR 2). M lane is loaded with 1000 bp DNA ladder, +V is positive control (gDNA of untransformed WT plant) and –V is negative control (SDW). WT = wild-type, HZ = heterozygous, and HM = homozygous plants respectively.

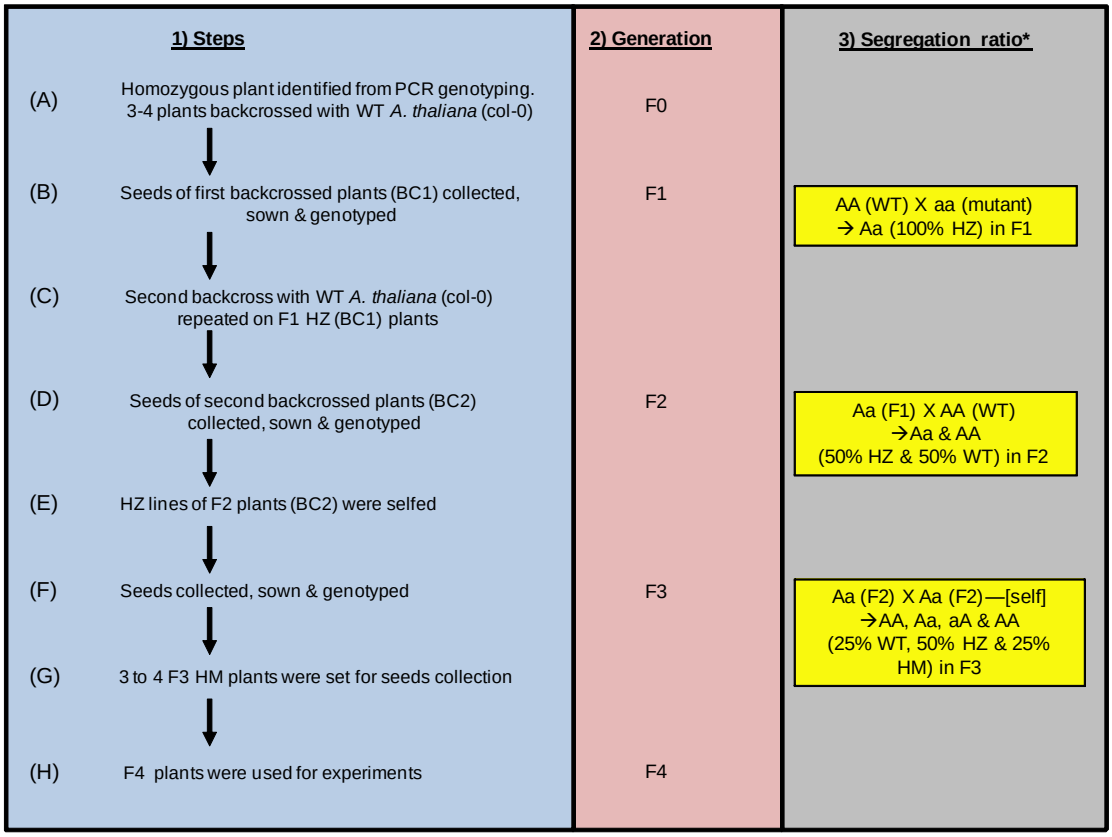

Figure 3-6: Backcrossing strategy of homozygous *AO* T-DNA insertion mutants. **Column 1** describes 8 steps (**A−H**) involved in backcrossing T-DNA insertion *ao* mutants twice to WT *A. thaliana*. The corresponding generation during crossing is given in **column 2**, i.e. F0 = homozygous *ao* mutants prior to backcrossing, F1 = offspring after first backcrossed, F2 = offspring after second backrossed, F3 = offspring of selfed F2 and F4 = offspring of F3 generation. The segregation ratios of F1, F2 and F3 generations are given in **column 3**. *AA and aa denote dominant and recessive genotypes for *AO* gene respectively. WT = wild-type, HZ = heterozygous, and HM = homozygous plants respectively.

3.2.3. Construction of *ao1ao3* double mutant

ao1ao3 double mutant were developed by crossing *ao1* and *ao3* T-DNA mutant. Since *ao1* and *ao3* are recessive mutants, a segregation ratio of 15:1 for F2 generation was proposed for homozygous unlinked recessive genes. Out of 34 F2 plants genotyped, 3 were *ao1ao3* double mutant. Chi-square for goodness

of fit test showed that *ao1ao3* mutants scored were fit to the expected segregation ratio (section 3.2.4.).

3.2.4. Genetic and chi-square test for *ao1ao3* double mutant

Suppose A = *AO1*, a = *ao1*, B = *AO3* and b = *ao3*. The segregation after crossing *ao1* and *ao3* is:

F0: aaBB (*ao1*) X AAbb (*ao3*) = F1: AaBb (heterozygous for *AO1* and *AO3* genes)

F1 plants were selfed (AaBb X AaBb), the segregation for the resulting F2 lines is described in the following Punnett square:

	AB	aB	Ab	ab
AB	AABB	AaBB	AABb	AaBb
aB	AaBB	aaBB	AaBb	aaBb
Ab	AABb	AaBb	AAbb	Aabb
ab	AaBb	aaBb	Aabb	aabb (*ao1ao3*)

The following Chi-square test was conducted to test if *ao1ao3* scored is consistent with the expected 15:1 ratio:

Hypothesis: a 15:1 ratio is proposed for obtaining *ao1ao3*
Total number of plants genotyped = 34;
Observed non *ao1ao3* = 31; observed *ao1ao3* = 3;
Expected non *ao1ao3* = 15/16 × 34 = 31.875; expected *ao1ao3* = 1/16 × 34 = 2.125;
$\chi^2 = (31-31.875)^2 / (31.875) + (3 - 2.125)^2 / (2.125) = 0.024 + 0.360 = 0.384$.
Since 0.384 < critical value of 3.84 at $p<0.05$, so the hypothesis is accepted.

3.2.5. Generation of *amiR-AO* construct

A list of amiRNA sequences (Figure 3-7A) is generated by submitting AGIs for *AO1*, *AO2* and *AO3* to WMD (see section 3.1.2. for background information).

The sequence (“TAATGCGGTTCAATGTGACAA”) that showed the highest target specificity to silence all three *AO* genes was selected. The chosen amiRNA sequence which is intended to silence all three *AO* genes is named as *amiR-AO* in this thesis. The specificity of the *amiR-AO* sequence to silence each *AO* gene is ranked according to the descending order of hybridisation energy (kcal/mol): *AO2 > AO3 > AO1* (Figure 3-7B).

Four primers were retrieved from the “oligo” tool of WMD by submitting the *amiR-AO* sequence. These four primers were used in overlapping PCR to replace endogenous miRNA and miRNA* duplex of the template pRS300 with *amiR-AO* and *amiR-AO** (Figure 3-8). The PCR product was ligated into pGEM-T® easy vector (TA cloning, section 3.2.7.) and sequence verified. *amiR-AO* was then isolated and recombined with 35S overexpression vector (pGWB502) using Gateway® cloning. The resulting overexpression construct was used to transform *A. thaliana*.

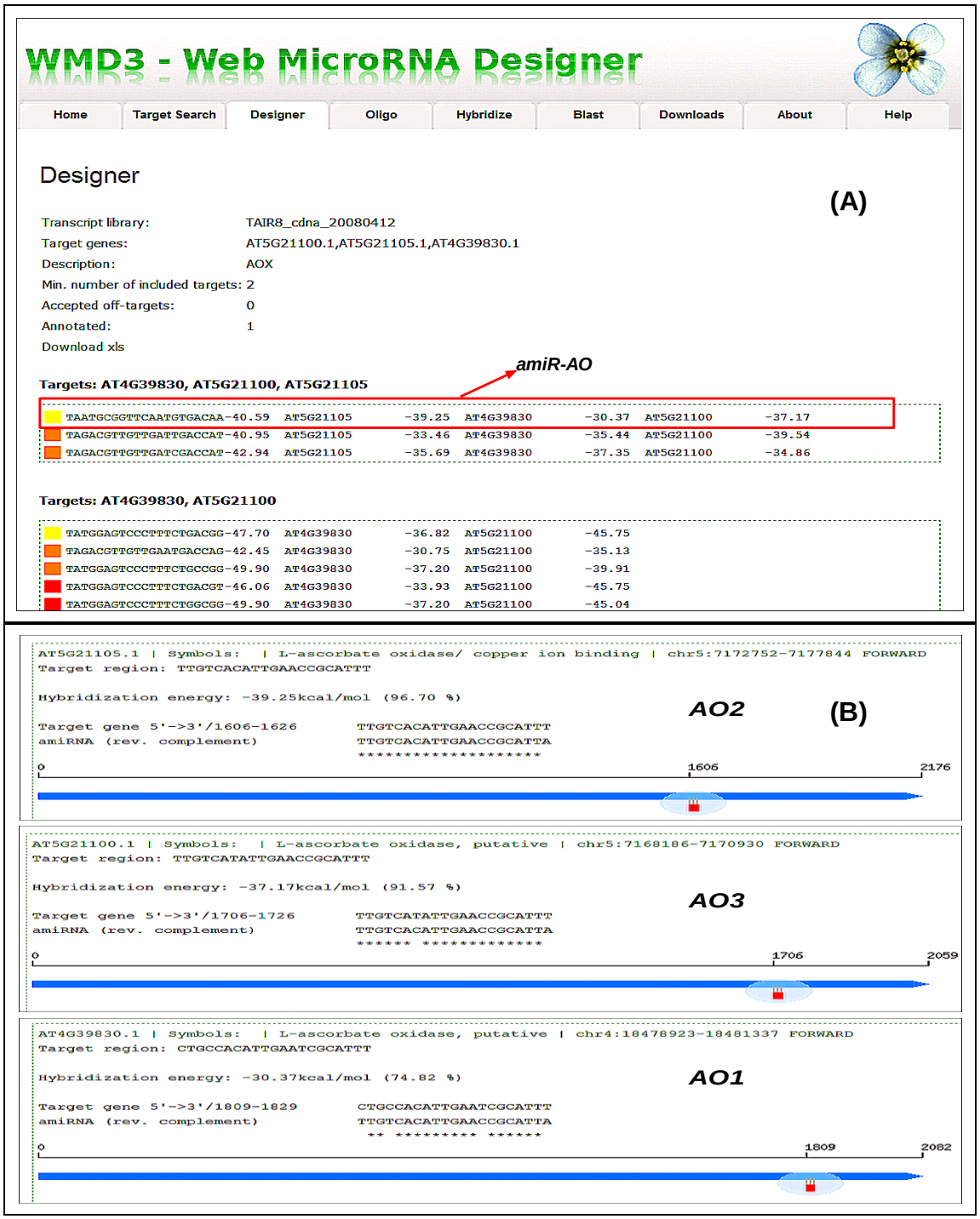

Figure 3-7: Screenshot of Web MicroRNA Designer version 3 (WMD3). AGIs for *AO1*, *AO2* and *AO3*, i.e. At4g39830, At5g21105 and At5g21100 were submitted to WMD. Three amiRNA sequences that are able to target *AO1*, *AO2* and *AO3* were generated. The sequence that ranked in the first place (marked with red box) was selected to generate *amiR-AO* construct **(A)**. Specificity of *amiR-AO* binding to *AO* transcripts are ranked in descending order based on hybridisation energy (kcal/mol) **(B)**.

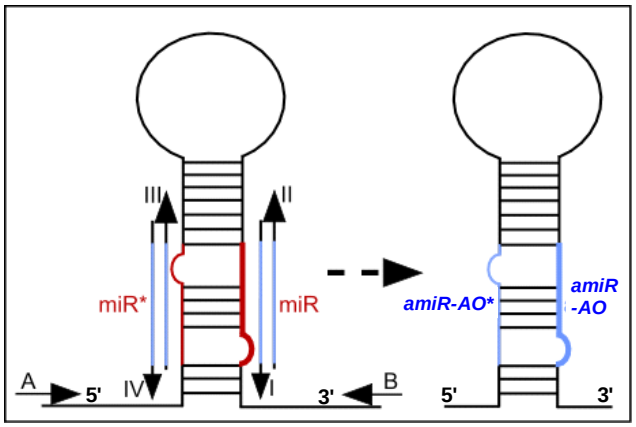

Figure 3-8: Generation of *amiR-AO* by overlapping PCR. The endogenous miRNA-miRNA* duplex (red strands) on template plasmid, pRS300 was replaced with *amiR-AO* and *amiR-AO** duplex (blue strands). Four primers (I to IV) containing *amiR-AO* and *amiR-AO** sequence are retrieved using WMD, while A and B are primers based on the pRS300 sequence. Three independent PCRs were performed to generate three fragments containing: 1) 5' arm to the *amiR-AO** (amplified by primer A and IV), 2) stem loop from *amiR-AO** to *amiR-AO* (amplified by primer III and II), and 3) *amiR-AO* to the 3'arm (amplified by primer I and B). Products from these three PCRs are combined in the last PCR (amplified by primer A and B) to overlap the *amiR-AO**−stem loop−*amiR-AO* region, thereby generates the *amiR-AO* fragement for downstream cloning experiments and plant transformation. See methods for experimental protocol. Figure modified from Schwab *et al.* (2006).

In this study, I have employed a relatively new amiRNA approach for targeted gene silencing of all three *AO* genes. The same approach was used to effectively knockdown a targeted group of expansin genes (*EXPA10*, *EXPA1*, *EXPA5*, and *EXPA3*) in *A. thaliana* (Goh *et al.*, 2012). Although amiRNA is relatively effective in targeted gene silencing, it involved multiple PCR steps. By contrast, a more recent miRNA gene silencing technique, known as MiRNA Induced Gene Silencing (MIGS), introduced by de Felippes *et al.* (2012) only

involved one PCR step. MIGS technique uses miR173 (a 22-nt miRNA of *A. thaliana*), that can trigger production of trans-acting small interfering RNAs (tasiRNAs) to silence endogenous gene. By fusing a gene of interest upstream of the miR173 target site, it is enough for effective target genes silencing. MIGS can be used for knockdown of a single, multiple or functionally unrelated genes in *A. thaliana* or other plant species.

3.2.6. Amplification of *AO* coding sequences

AO1, *AO2*, and *AO3* overexpression constructs were developed by fusing the respective *AO* coding sequence under the expression of constitutive 35SCaMV promoter. The *AO* gene coding sequences were amplified (primers and PCR conditions are detailed in section 2.5.5.5.) from cDNA of WT *A. thaliana*. The coding sequence was ligated into the pGEM-T® easy vector (TA cloning, section 3.2.7.) and sequence verified. *AO* coding sequence was then isolated and recombined with 35S overexpression vector (pGWB502) using Gateway® cloning system. The resulting overexpression construct was used to transform *A. thaliana*.

3.2.7. TA cloning

The *amiR-AO* (section 3.2.5.) and *AO* coding sequences (section 3.2.6.) were amplified from PCRs using proofreading DNA polymerase. 3'-A overhangs were created to these blunt end products, ligated to commercial TA vector, pGEM-T® easy (Figure 3-9). The plasmid constructs were used to transform *E. coli* DH5α™, and then selected on LB agar media with 100 µg/ml ampicillin. Colonies were genotyped *via* PCR followed by plasmid extraction and then

sequenced to confirm target gene sequence integrity. These constructs were used as the template for Gateway® cloning.

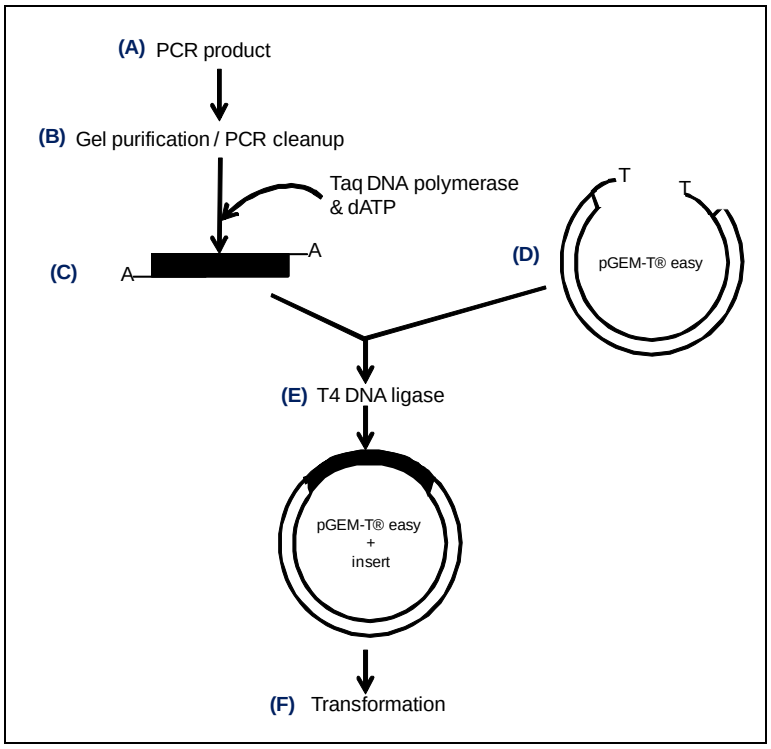

Figure 3-9: TA cloning strategy. **(A)** *amiR-AO* and *AO* coding sequences were amplified by PCRs, **(B)** the PCR products were purified by gel extraction or reaction clean up, **(C)** 3'-A overhangs were created in these PCR products in a reaction containing *Taq* DNA polymerase and dATP. The resulting fragments were mixed with pGEM-T® easy vector **(D)**, ligated with T4 DNA ligase **(E)**. The constructs developed were used to transform *E. coli* DH5α™.

3.2.8. Gateway® cloning: addition of *att*B sites to target genes

A PCR product containing *attB* sites is needed to perform BP recombination reaction with *attP* sites containing donor vector, pDONR™221. The full *attB* sites at 29 bp were considered too long to incorporate onto gene specific primers and so two separate PCRs were carried out. The first PCR used primers containing target gene sequence and part of the *attB* sites; the second PCR used primers containing full *attB* sites (section 2.5.5.6.).

The primers used in first PCR were designed in a way that the *attB1* sites were added at the 5' end of target genes (forward primers) and *attB2* sites were added at the 3' end (reverse primers). An example of the primer design for first PCR is shown (Figure 3-10). In forward primer the *att*B1 sites end with a thymidine (T), so two additional nucleotides are needed to maintain the proper reading frame. These two nucleotides cannot be AA, AG, or GA, because these will introduce a stop codon (TAA, TGA or TAG) and terminate the target gene transcription. In the reverse primer, a single nucleotide was added between the *attB2* sites and the stop codon of the target genes to maintain the proper reading frame.

Target specific primers containing *attB* sites (Table 2-8) were used to amplify the target sequence (*AO* coding sequences and *amiR-AO*) from pGEM-T® easy constructs. This produced target sequence with partial *attB* sites (Figure 3-11). These PCR products were used as templates in a second PCR to add the full *attB* sites (Table 2.8, *att*B1 and *att*B2 primers). The final PCR product was cleaned up or gel purified and used directly in the Gateway® BP reaction.

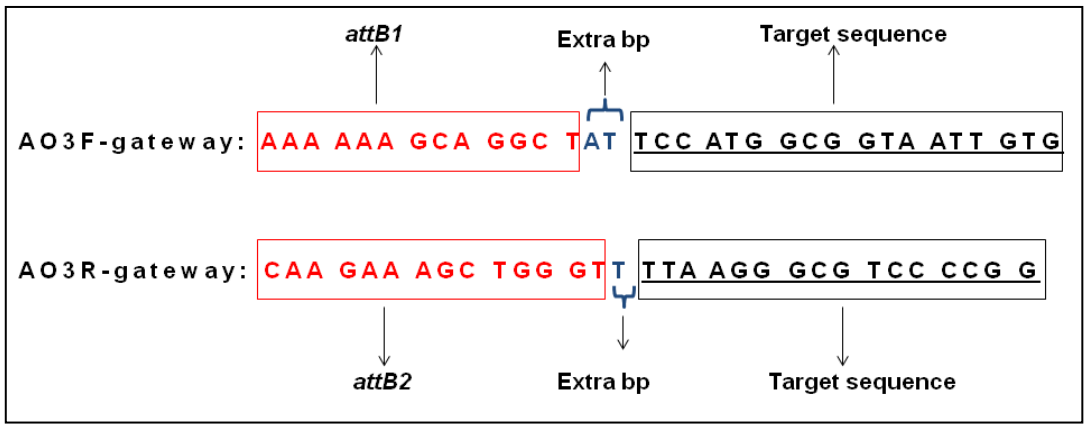

Figure 3-10: Primer design to incorporate *att*B sites to target genes. These primers contained a section of the *att*B1 sites (red font), extra base pairs added to maintain proper reading frame (blue font) and *AO3* gene specific sequence (dark font).

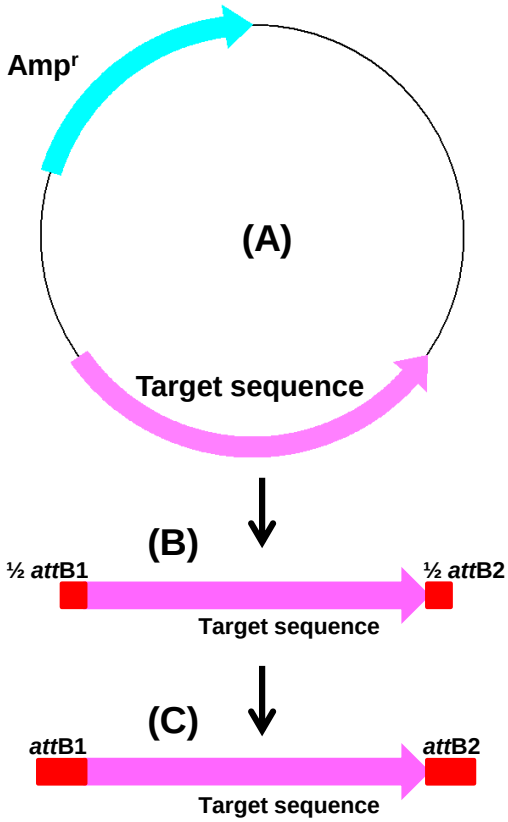

Figure 3-11: Amplification of target gene to add *att*B sites. Target genes were amplified from pGEM-T® easy vector **(A)** *via* PCR to add half length of the *att*B sites **(B)**. A second round of PCR was performed to add the full *att*B sites to the target genes **(C)**.

3.2.9. Gateway® BP reaction

The *att*B-flanked PCR product was recombined with the Gateway® donor vector, pDONR™221 in the BP reaction. This should generate a pENTR™ plasmid containing the target sequence and an unwanted by-product (Figure 3-12).

An equal amount of *att*B-flanked PCR product and pDONR™221 were recombined in BP reaction which was catalysed by BP Clonase™ II. The reaction mix was incubated at 25°C for 3 hrs and then stopped by adding Proteinase K provided. Recombined DNA was used to transform *E. coli* DH5α™ competent cells and were selected on LB agar media with 50 µg/ml kanamycin. 8 to 10 colonies were picked and genotyped by PCR to confirm the presence of insert. It should be noted that the non-recombined pDONR™221 vector should not survive due to the negative selective pressure imposed by *ccd*B gene. A single colony that contained an insert was cultured overnight with LB liquid media containing 50 µg/ml kanamycin. Plasmid DNA was extracted from the culture and verified by restriction analysis to confirm the presence and correct orientation of the construct. Plasmid DNA with the correct banding was sequenced to confirm the integrity of the target sequence. Four entry clones were generated with the BP reaction: *pENTR™::AO1*, *pENTR™::AO2*, *pENTR™::AO3* and *pENTR™::amiR-AO*. These constructs were used in the Gateway® LR reaction.

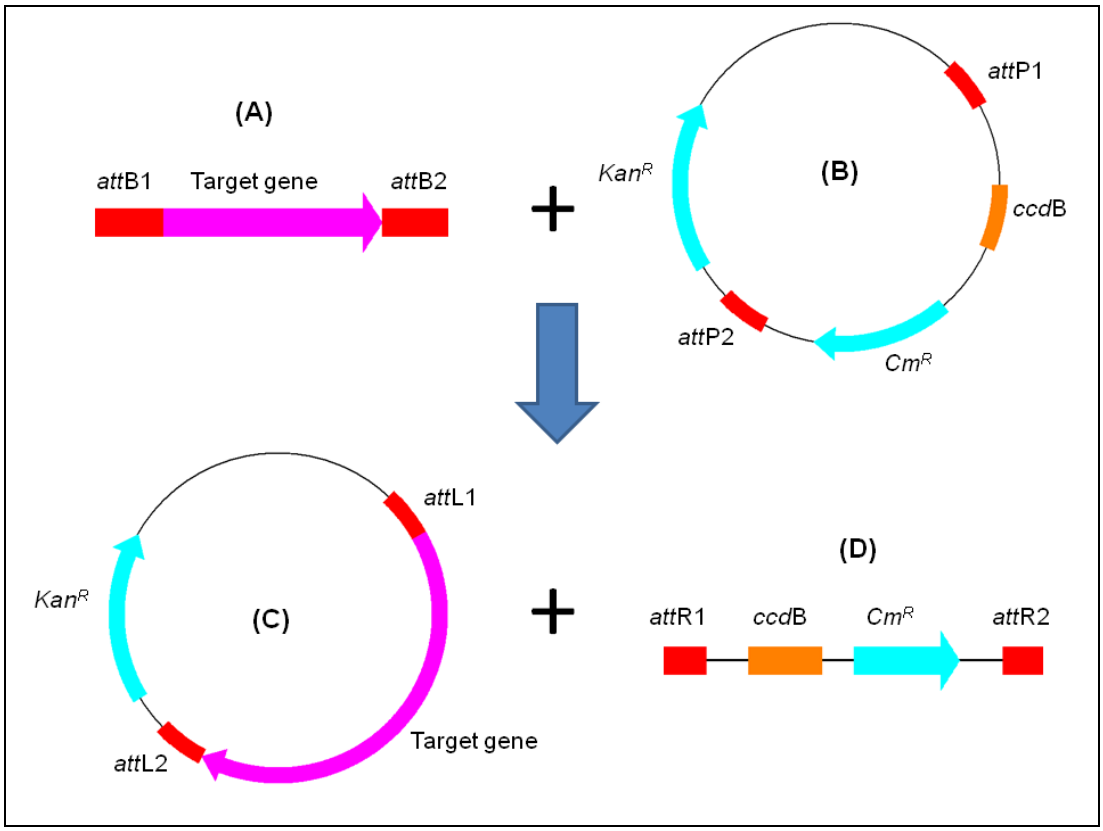

Figure 3-12: The BP reaction – recombination of target genes into the intermediate Gateway® donor vector, pDONR™221. Complementary *att* sites on **(A)** target genes and **(B)** pDONR™221 allow recombination *via* BP Clonase™ II. Recombination creates a **(C)** pENTR™ plasmid harbouring the target gene and **(D)** an unwanted by-product.

3.2.10. Gateway® LR reaction

The entry clone developed (section 3.2.9.) from the BP reaction was recombined with a pGWB502 expression vector under LR reaction. *att*L sites on the entry clone recombined with *att*R sites on pGWB502, allowing directional transfer of the target sequence into the expression vector (Figure 3-13).

An equal amount of entry clone and pGWB502 were recombined in LR reaction which was catalysed by LR Clonase™ II. The reaction mix was incubated at 25°C for 3 hrs and then stopped by adding Proteinase K provided. Recombined DNA was used to transform *E. coli* DH5α™ competent cells and were selected on LB agar media with 100 µg/ml spectinomycin. 8 to 10 colonies were picked and genotyped by PCR to confirm the presence of the insert. As in the BP reaction, the pGWB502 that had not recombined should not survive due to the negative selective pressure imposed by the *ccd*B gene. Additionally, colonies harbouring pDONR™221 should not survive since they confer resistance to kanamycin rather than spectinomycin. A single colony that contained an insert was cultured overnight with LB liquid media containing 100 µg/ml spectinomycin. Plasmid DNA was extracted from the culture and verified by restriction analysis to confirm the presence and correct orientation of the construct. Plasmid DNA with the correct banding pattern was sequenced over the recombination boundaries (pGWB) to confirm successful integration of the target sequence. Four constructs were generated with the LR reaction: pGWB502::*AO1*, pGWB502::*AO2*, pGWB502::*AO3* and pGWB502::*amiR-AO*. These constructs are thereafter renamed as *35S::AO1*, *35S::AO2*, *35S::AO3* and *amiR-AO* in this thesis. These overexpression constructs were used to transform *A. tumefaciens*.

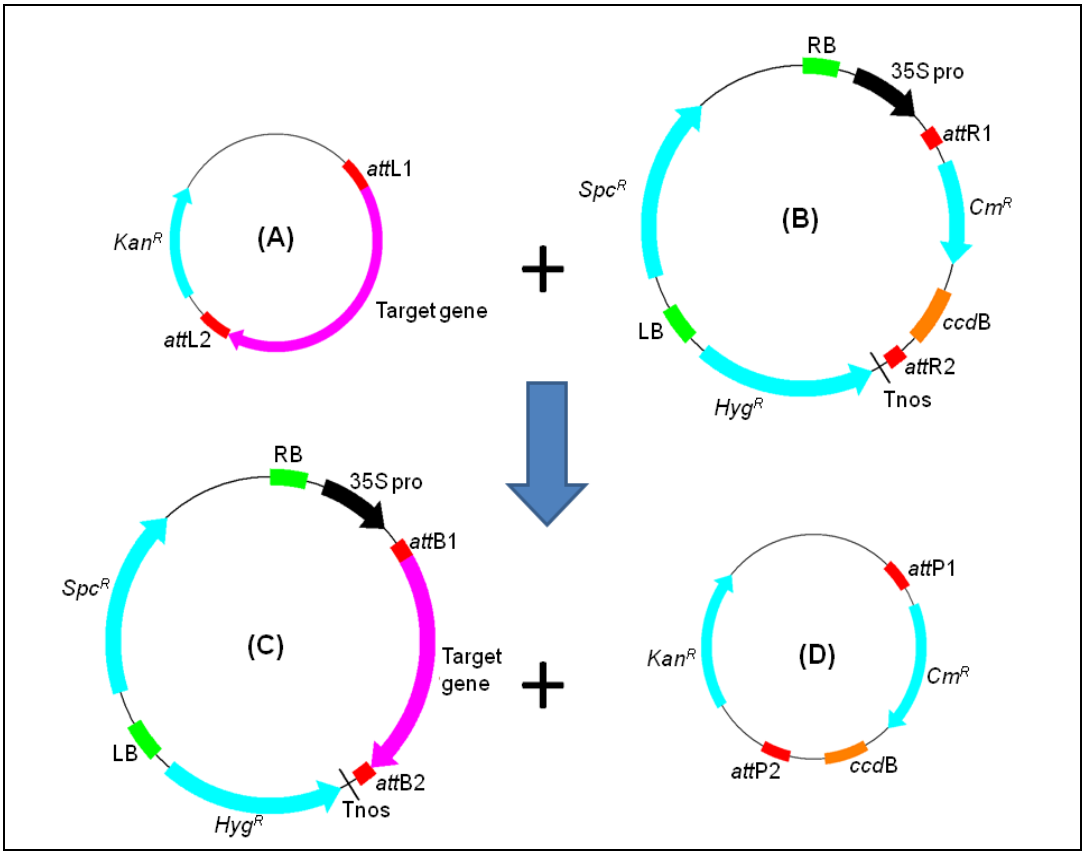

Figure 3-13: The LR reaction – recombination of a pENTR™ plasmid with pGWB502 expression vector. Complementary *att* sites on a **(A)** pENTR™ plasmid harbouring a target gene and **(B)** pGWB502 allow recombination *via* LR Clonase™ II. This results in an **(C)** expression plasmid and **(D)** an unwanted by-product.

3.2.11. Screening of transgenic plants

The plasmid constructed from LR reaction was used to transform *A. tumefaciens* strain GV3101 by the freeze-thaw method (section 2.6.2.). These *A. tumefaciens* constructs were then used to transform WT Col-0 *A. thaliana* (designated as T_0 generation) by the floral-dip method (section 2.6.3.). The pGWB502 plasmid carrying hygromycin phosphotranferase (*hpt*) gene that conferred hygromycin resistance, so transgenic plants should grow under hygromycin pressure.

A rapid and reliable screening method for transformed *A. thaliana* seedlings was employed (Harrison *et al.*, 2006). This method (dark-induced hypocotyl elongation) allows rapid identification of transformed seedlings compared to the normal screening method (looking at the lethality of non-transformants under unstressed normal growth condition). Apart from being time consuming, the lengthy screening period of normal method can lead to fungal contamination. This is because transformed seeds were collected from flowers where high sucrose concentration was used in the *A. tumefaciens* dipping solution. Also, dipped plants were kept in a warm and damp environment before removing to growth room, a condition ideal for fungal growth. Fungal contamination may deplete antibiotic present in the selection medium and hence lead to the selection of false positive seedlings.

T_1 seeds were harvested and sown on half-strength MS solid media with 20 µg/ml hygromycin for selection (section 2.6.4.). The seeds were incubated in the dark condition at room temperature for 3 days and then returned to growth room for one week, to promote cotyledon development before transfer to soil. In the presence of hygromycin, both transformed and non-transformed seedlings

germinated and had green cotyledons. The transformed seedlings, however, had longer hypocotyls than the non-transformed seedlings (Figure 3-14). PCR was carried out to confirm the presence of the transgenes in selected hygromycin resistance seedlings, with a forward primer (pGWB-F, Table 2-9) that amplified from part of the 35S promoter sequence and a reverse primer (Table 2-9: AO1Ri, AO2Ri, AO3Ri and Primer II for *35S::AO1*, *35S::AO2*, *35S::AO3* line and *amiR-AO* respectively) that amplified from part of the target sequence. The following T_1 lines (10 plants per line) were obtained: *35S::AO1*, *35S::AO2*, *35S::AO3* and *amiR-AO*.

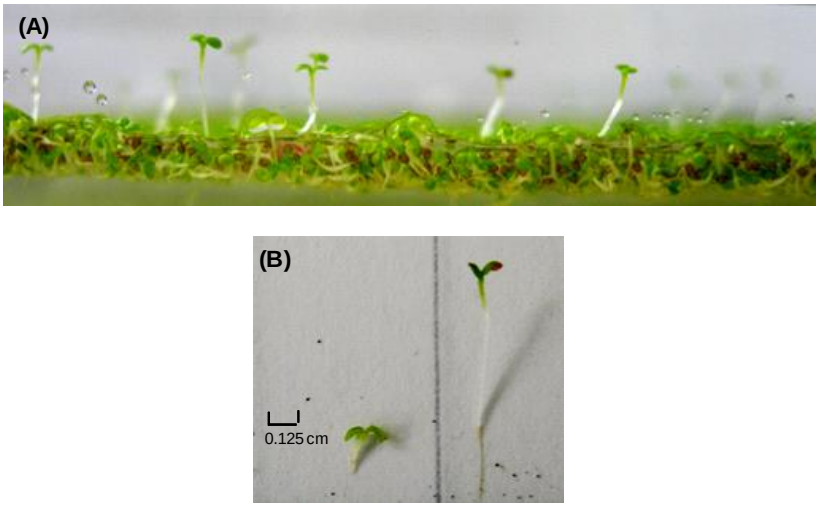

Figure 3-14: Screening of transformed seedlings. T_1 seeds were harvested from transformed *A. thaliana* and sown on half-strength MS solid media with 20 µg/ml hygromycin for selection. The seeds were incubated in dark condition at room temperature for 3 days and then returned to growth room to promote cotyledon development. The transformed seedlings had longer hypocotyls **(A)** and hypocotyl length of the transformed seedlings was 4 times longer than the non-transformed seedlings **(B)**, scale bar = 0.125 cm.

3.2.12. Screening for single-insertion homozygous lines

The establishment of *35S::AO1*, *35S::AO2*, *35S::AO3* and *amiR-AO* lines were only initiated in the final stage of this PhD project after the characterisation of *ao1*, *ao2*, *ao3* and *ao1ao3* T-DNA insertion mutants (detailed in Chapter 5 and Chapter 6). Therefore only *amiR-AO* and *35S::AO3* were screened for single-insertion and homozygousity in order to keep the downstream experiments manageable.

Ten T_1 *amiR-AO* plants (Figure 3-15) and seven T_1 *35S::AO3* plants (Figure 3-16) were identified using PCR genotyping. These genotyped T_1 plants were allowed to self, T_2 seeds were collected and further characterised through segregation analyses. 100 T_2 seeds from each independent plant were sown

onto half-strength MS agar media with 20 µg/ml hygromycin for selection. 75% (or roughly 68-77%) of transformed seedlings should obtain for single-insertion. Plant lines that had more than 80% transformed seedlings implied multi-insertions. Plants with single insertion were selected, selfed and T_3 seeds were collected. About 40 T_3 seeds from each independent plant were sown onto half-strength MS agar media with 20 µg/ml hygromycin for selection. Homozygosity of the transformants is characterised by 100% hygromycin resistance in the segregation analysis of T_3 plants. T_3 and T_4 seeds were used for downstream experiments.

Four T_2 *amiR-AO* lines were scored as carrying a single-insertion. Homozygous lines were found in these single-insertion lines (Table 3-2). Likewise, four *35S::AO3* lines were scored as carrying a single insertion (T_2). Homozygous lines were found in these single insertion lines (Table 3-3).

The characterisations of *amiR-AO* and *35S::AO3* lines are given in Chapter 5 and 6.

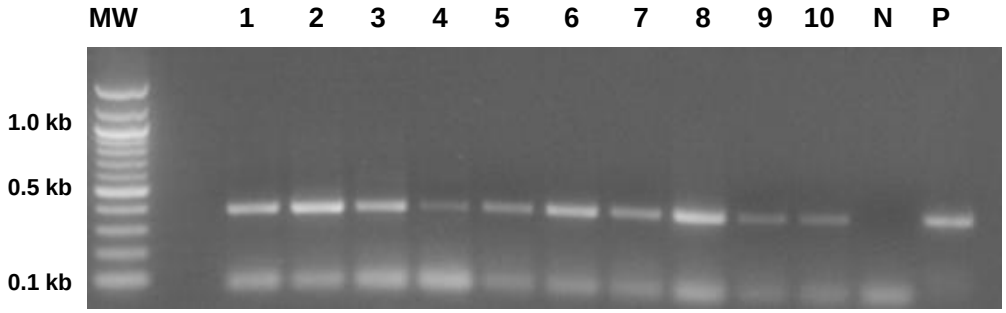

Figure 3-15: PCR genotyping of transgenic *amiR-AO* seedlings. Agarose gel image showing PCR product amplified from gDNA of 10 transformed T_1 lines (labelled 1−10). All lines are confirmed as harbouring the *amiR-AO* construct. MW = molecular weight marker with relevant sizes to the left of the gel image. N = negative control (WT gDNA), P = positive control (pGWB502::*amiR-AO* plasmid DNA as template). Expected product size is 379 bp.

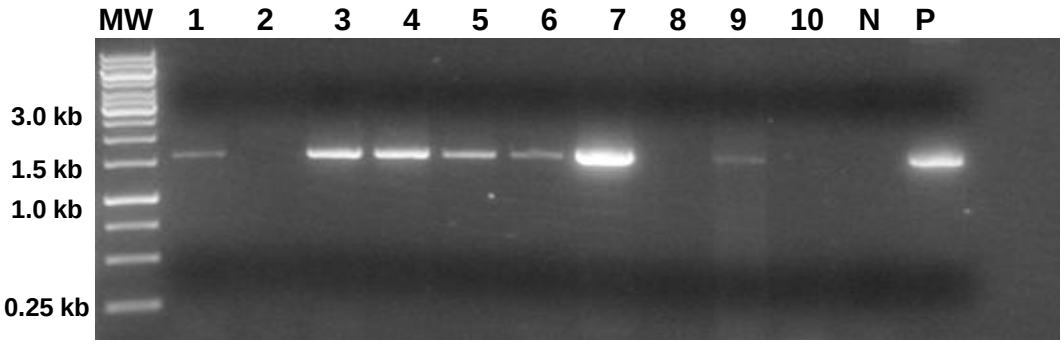

Figure 3-16: PCR genotyping of transgenic *35S::AO3* seedlings. Agarose gel image showing PCR product amplified from gDNA of 10 transformed T_1 lines (labelled 1−10). 7 lines are confirmed as harbouring the *35S::AO3* construct. MW = molecular weight marker with relevant sizes to the left of the gel image. N = negative control (WT gDNA), P = positive control (pGWB502::*AO3* plasmid DNA as template). Expected product size is 1596 bp.

Table 3-2: Segregation analyses of T_2 and T_3 generation of *amiR-AO* transformants for hygromycin resistance.

T_2 line [a]	% transformants	T_3 line [b]	Homozygous line [c]
1	70	11 − 16	1/6
2	64	21 − 26	---
3	77	31 − 36	1/6
4	89	41 − 46	1/6
5	80	51 − 56	---
6	72	61 − 66	1/6
7	86	71 − 76	---
8	93	81 − 86	1/6
9	64	91 − 96	---
10	69	10-1 – 10-6	1/6

[a] Red text denotes lines that carrying single insertion, [b] 6 T_3 plants were sown from each of the T_2 line, [c] number of lines (out of six) that showed 100% hygromycin B resistance. "---"means segregation analyses were not performed for the respective T_3 lines.

Table 3-3: Segregation analyses of T_2 and T_3 generation of *35S::AO3* transformants for hygromycin resistance.

T_2 line [a]	% transformants	T_3 line [b]	Homozygous line [c]
1	90	11 − 16	1/6
2	71	21 − 26	2/6
3	72	31 − 36	2/6
4	60	41 − 46	---
5	71	51 − 56	2/6
6	75	61 − 66	1/6
7	65	71 − 76	---

[a] Red text denotes lines that carrying single insertion, [b] 6 T_3 plants were sown from each of the T_2 line, [c] number of lines (out of six) that showed 100% hygromycin B resistance. "---"means segregation analyses were not performed for the respective T_3 lines.

3.3. Summary

In this chapter, I have described a series of strategies to develop various *A. thaliana* lines that are essential to characterise the role of AO. Functional analyses of these mutants during development are described in Chapter 5. The response of these mutants during stress is described in Chapter 6.

Chapter 4. *In silico* analyses of the function of ascorbate oxidase in *A. thaliana*

4.1. Background

A list of bioinformatic tools used to perform *in silico* analyses is given in Table 4-1. These tools are reviewed in the following sections.

Table 4-1: List of bioinformatic tools used in this project.

Tool	Description	Link	Reference
Arabidopsis eFP browser	Global gene expression database	http://bar.utoronto.ca/efp/cgi-bin/efpWeb.cgi	Winter *et al.* (2007)
Arabidopsis translatome eFP browser	Visualise polysomal mRNAs ("Translatomes") data of *A. thaliana* seedlings subjected to hypoxia stress	http://efp.ucr.edu/	*Mustroph et al.* (2009)
Cell eFP browser	Visualise protein subcellular localisation data of *A. thaliana* from SUBA	http://bar.utoronto.ca/cell_efp/cgi-bin/cell_efp.cgi	Winter *et al.* (2007)
NCBI's Conserved Domain Database (CDD)	Functional annotation of protein sequences with known conserved domains	http://www.ncbi.nlm.nih.gov/Structure/cdd/wrpsb.cgi	Marchler-Bauer *et al.* (2011)
DictyOGlyc	Predicts the presence of *O*-(alpha)-GlcNAc glycosylation sites	http://www.cbs.dtu.dk/services/DictyOGlyc/	Gupta *et al.* (1999)
MEGA 5	Amino acid sequence alignment and phylogeny tools	http://www.megasoftware.net/	Tamura *et al.* (2011)
NetNGlyc	Predicts *N*-Glycosylation sites	http://www.cbs.dtu.dk/services/NetNGlyc/	Blom *et al.* (2004)
PlantCARE	Search known *cis*-acting regulatory element of promoter sequences	http://bioinformatics.psb.ugent.be/webtools/plantcare/html/	Lescot *et al.* (2002)
SignalP	Predicts the presence and location of signal peptide cleavage sites	http://www.cbs.dtu.dk/services/SignalP/	Dyrløv Bendtsen *et al.* (2004)
SUBA	Protein subcellular localisation	http://suba.plantenergy.uwa.edu.au/	Heazlewood *et al.* (2007)
TargetP	Protein subcellular localisation: mitochondrial, chloroplastic, secretory pathway, or other	http://www.cbs.dtu.dk/services/TargetP/	Emanuelsson *et al.* (2000)

4.1.1. Functional prediction of the gene of interest by sequence similarity and phylogenetic analyses

High throughput sequencing has generated numerous datasets and allows researchers to predict the function of the gene of interest, by comparing its sequence to the sequence of the genes with known function using a simple tool like BLAST (Altschul *et al.*, 1990). This is because genes with similar sequences will normally have a similar function. Phylogenetic analysis is a systematic tool of comparative genomics that helps us to discover hierarchical relationships among genes/proteins of interest. Similar to species evolution, the hierarchy of genes/proteins reflects a continuing process of gene duplication and divergence. This technique provides a powerful way to find out the origin of the gene of interest, its relatedness to other species and to infer its possible function by identifying its homologs, i.e. paralogous or orthologous genes (Eisen, 1998; Thornton and DeSalle, 2000). Orthologs are homologous genes that are present in different species as a result of speciation events whereas paralogs are homologous genes that are present in the same species as a result of gene duplication. Orthologs often have the same function but paralogs usually do not retain the same function (Nei, 1996; Thornton and DeSalle, 2000).

Many bioinformatic tools are available for phylogenetic analysis (see Pavlopoulos *et al.*, 2010 for review). MEGA 5 was used in this project. MEGA 5 is a comprehensive open source software that offers a number of useful features such as: multiple sequence alignment on nucleotide or amino acid sequences (e.g. ClustalW, Thompson *et al.*, 1994), various clustering algorithms (maximum parsimony, maximum likelihood, Neighbor-Joining and minimum evolution) for the construction of a phylogenetic tree and options to

present phylogenetic trees in different styles (i.e. radiation, circle) (Kumar *et al.*, 2008; Tamura *et al.*, 2011).

4.1.2. Protein subcellular localisation databases

Most proteins in eukaryotic cells are encoded in the nuclear genome and synthesised in the cytosol. Some of these proteins need to be sorted in the endoplasmic reticulum (ER) and targeted for subsequent transportation to the mitochondria, the chloroplast or the secretion pathway (e.g. cell wall, apoplast). This subcellular localisation sorting is depends on the N-terminal targeting sequence (Emanuelsson *et al.*, 2000). The N-terminal target sequence destined for the mitochondrion, the chloroplast and the secretory pathway, known as mitochondrial targeting peptides (mTPs), chloroplast transit peptides (cTPs) and signal peptides (SPs) respectively, are unique in term of the conserved amino acid residues presence and are different from each other (see Emanuelsson *et al.*, 2000). Knowledge of a protein subcellular localisation is important to gain insight of a protein function, because different subcellular locations often represent different cellular environments and proteins found within this location should in principle play a role that define the function of this compartment. For example, proteins located in cell wall often have a role in cell wall growth and regulation (Heazlewood *et al.*, 2005).

Subcellular location of a protein can be determined *via* experimental approaches (e.g. imaging of fluorescent fusion proteins in intact cells) or predicted through bioinformatic targeting algorithms. Bioinformatic resources provide a simple and rapid way to predict subcellular location of a protein based

on its amino acid sequence before an experiment is conducted (Lu and Last, 2008). A number of bioinformatic tools for the prediction of protein subcellular localisation are hosted at the Center for Biological Sequence Analysis, Technical University of Denmark. For example, SignalP (http://www.cbs.dtu.dk/services/SignalP/) is designed to predict the presence of SPs in proteins, ChloroP (http://www.cbs.dtu.dk/services/ChloroP/) is used to predict cTPs and TargetP (http://www.cbs.dtu.dk/services/TargetP/) is developed as an integrated tool to predict the presence of mTPs, cTPS, or SPs in a query amino acid sequence (Emanuelsson *et al.*, 2007).

The subcellular location database for *Arabidopsis* proteins (SUBA) is an integrated database that hosts a variety of experimental data (e.g. visualisation of fluorescent proteins that attached to proteins of interest, peptide identification *via* mass spectrometry) and bioinformatic resources (e.g. TargetP, Swiss-Prot) for predictions of protein subcellular localisation in *A. thaliana* (Heazlewood *et al.*, 2007) (http://suba.plantenergy.uwa.edu.au/). The subcellular localisation data from SUBA also can be visualised *via* the Cell eFP browser (Winter *et al.*, 2007; http://bar.utoronto.ca/cell_efp/cgi-bin/cell_efp.cgi).

In this project, SignalP, TargetP and SUBA were used to explore the predicted subcellular location of all three AO proteins.

4.1.3. Post-translational modifications

Post-translational modifications (PTMs) involve enzymatic, covalent chemical modifications of proteins after the translation of mRNAs. These modifications

are essential to maintain correct structure, cellular location and function of a protein (Farley and Link, 2009). A list of common PTMs is given in Table 4-2.

Glycosylation is the most common PTM, where oligosaccharide chains are covalently linked to certain amino acid residues. Glycosylation is essential for protein stability, protein localisation, cell adhesion, enzyme activity and protein interactions. Two common type of glycosylation are *N*-glycosylation and *O*-glycosylation. In *N*-glycosylation, an oligosaccharide is transferred to the asparagine (N) residue of the N-X-S/T consensus sequence, where X is any amino acid except proline, S is serine and T is threonine. Unlike *N*-glycosylation, *O*-glycosylation does not have a conserved sequence, the common characteristic is that the oligosaccharide is attached to serine and threonine residues in close proximity to proline residues (see Spiro, 2002; Blom *et al.*, 2004).

It has been shown that *N*-glycosylation sites are present in the AO protein of melon and pumpkin (Esaka *et al.*, 1990; Sanmartin *et al.*, 2007). Two bioinformatic resources (DictyOGlyc and NetNGlyc), listed in Table 4-1 (Blom *et al.*, 1999; Gupta *et al.*, 1999; Blom *et al.*, 2004) were used to predict potential PTMs in the AO proteins of *A. thaliana*.

Table 4-2: Common post-translational modifications (PTMs) of proteins. Adapted from Farley and Link (2009).

PTM	Proposed biological function
Phosphorylation pSer, pThr, pTyr	Cellular signalling processes, enzyme activity, intermolecular interactions
Glycosylation	
O-linked	Regulatory elements
N-linked	Protein secretion, signalling
Proteinaceous	
Ubiquitination	Protein degradation signal
Sumoylation	Protein stability
Nitrosative	
Nitration, nTyr	Oxidative damage
Nitrosylation, nSer, nCys	Cell signalling
Acetylation	Histone regulation, protein stability

4.1.4. *In silico* promoter and gene expression analyses

Cis-acting regulatory elements (CARES) or promoters are short conserved motifs of 5 to 20 nucleotides that are normally located upstream of the start codon of a gene, and are involved in controlling gene expression. Identification and characterisation of CAREs can help us to understand how gene expression is regulated (Rombauts *et al.*, 2003). Two commonly used plant-specific CARE databases are PlantCARE (Lescot *et al.*, 2002) and PLACE (Higo *et al.*, 1999). The user can submit a query promoter sequence to these databases and search against known CAREs for functional prediction of query promoter. The PlantCARE database was used in this project due to its user friendly interface and because the PLACE database is no longer maintained.

The availability of large-scale microarray data allows researchers to explore expression profile of the gene of interest in response to various treatments (abiotic, biotic and hormone) and growth conditions. Several databases were developed to facilitate interpretation and visualisation of these data (see Lu and Last, 2008), in which *Arabidopsis* eFP browser (Winter *et al.*, 2007) is one of the examples. *Arabidopsis* eFP browser displays a series of microarray data (development, abiotic stress, hormone, ecotype, light and pathogen studies) that is sourced from the AtGenExpress project (Schmid *et al.*, 2005; Kilian *et al.*, 2007). Compared with other databases, eFP browser offers simple and user-friendly way of presenting data, whereby the gene expression data can be presented in a bar chart with a table of expression values or visualised *via* pictures of *A. thaliana* that reflect the experimental conditions where the microarray data were obtained. In this project, *AO* gene expression data during development were obtained from the *Arabidopsis* eFP browser microarray database. *AO* gene expression during high light and drought stress were obtained from in-house databases (see Results section).

4.1.5. *Arabidopsis* translatome eFP browser

The *Arabidopsis* translatome eFP browser (http://efp.ucr.edu/) gives graphical representations on the expression of ribosomal-associated mRNAs (translatomes) for the gene of interest in *A. thaliana* seedlings subjected to hypoxia stress. This cell-specific gene expression dataset was obtained by immunoprecipitation of translatomes from specific cell populations of *A. thaliana* seedlings, which were developed by tagging the ribosomal protein with a FLAG tag and expressed with cell specific promoters (see Mustroph *et al.*, 2009).

4.1.6. Chapter aim

This chapter provides a comprehensive overview of the potential role of ascorbate oxidase in *A. thaliana* through data mining from bioinformatic resources. Results in this chapter mainly focus on the evolutionary relationship, protein subcellular localisation, post-translational modifications, *in silico* promoter and gene expression analyses of each *AO* gene and AO protein. The information presented in this chapter could give a useful insight and foundation for future investigators to study the function of AO in *A. thaliana*.

4.2. Results and Discussion

4.2.1. Amino acid sequence analysis of AO in *A. thaliana*

The percent of amino acid sequence identities of three AO in *A. thaliana* were compared (Table 4-3). AO2 and AO3 were closely related to each other, with 73% identity score found in these two sequences. AO1 was found to be less closely related to AO2 and AO3, showed 48% and 50% sequence identity to AO2 and AO3, respectively. AO2 and AO3 are located next to each other in the same chromosome (chromosome 5), so the high identity between AO2 and AO3 could be the result of a gene duplication event.

In order to determine the level of similarity between AO in *A. thaliana* and other dicotyledonous plants, multiple sequence alignment using ClustalW (Thompson *et al.*, 1994) was performed. These plants (cucumber, squash, tobacco, pea and tomato) were selected because their AO activity was reported previously (Ohkawa *et al.*, 1989; Lin and Varner, 1991; Pignocchi *et al.*, 2003; Matamoros *et al.*, 2010; Garchery *et al.*, 2012). Medicago was included because it is the model plant for plant symbiotic study and the role of AO in symbiotic interactions with fungi and bacteria was reported (Balestrini *et al.*, 2012). As shown in Figure 4-1, amino acid sequences of all three *AO* genes were highly conserved, which suggests that AO in *A. thaliana* might play similar function to AO in these plants.

Table 4-3: Amino acid sequence identity (%) of three *AO* genes in *A. thaliana*.

	AO1 (At4g39830)	**AO2 (At5g21105)**	**AO3 (At5g21100)**
AO1 (At4g39830)	-	48	50
AO2 (At5g21105)	48	-	73
AO3 (At5g21100)	50	73	-

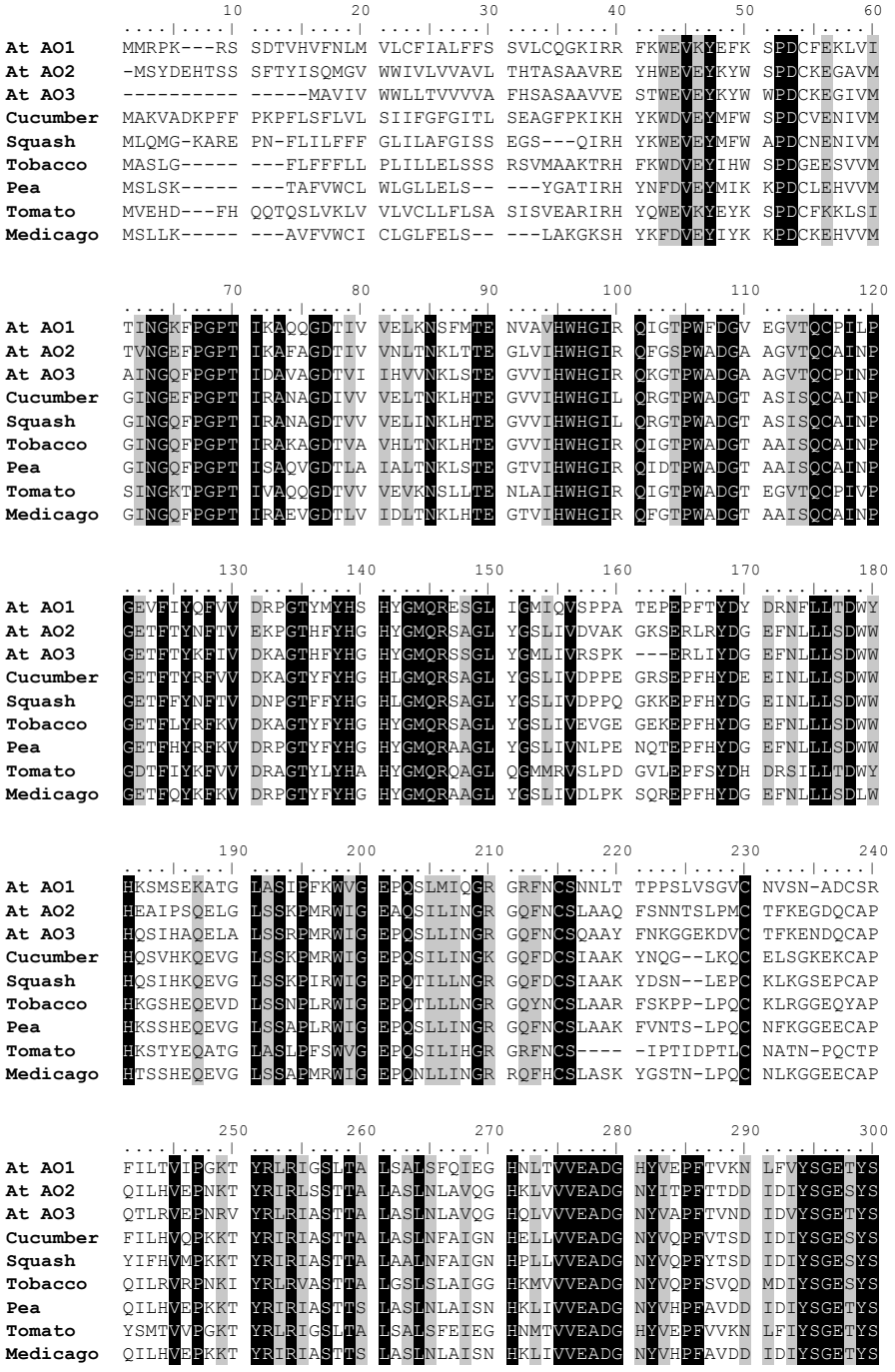

Figure 4-1: Amino acid sequence alignment of *A. thaliana* AO (At AO1, At AO2 and At AO3) with known homologues from other plants. Legends on the following page.

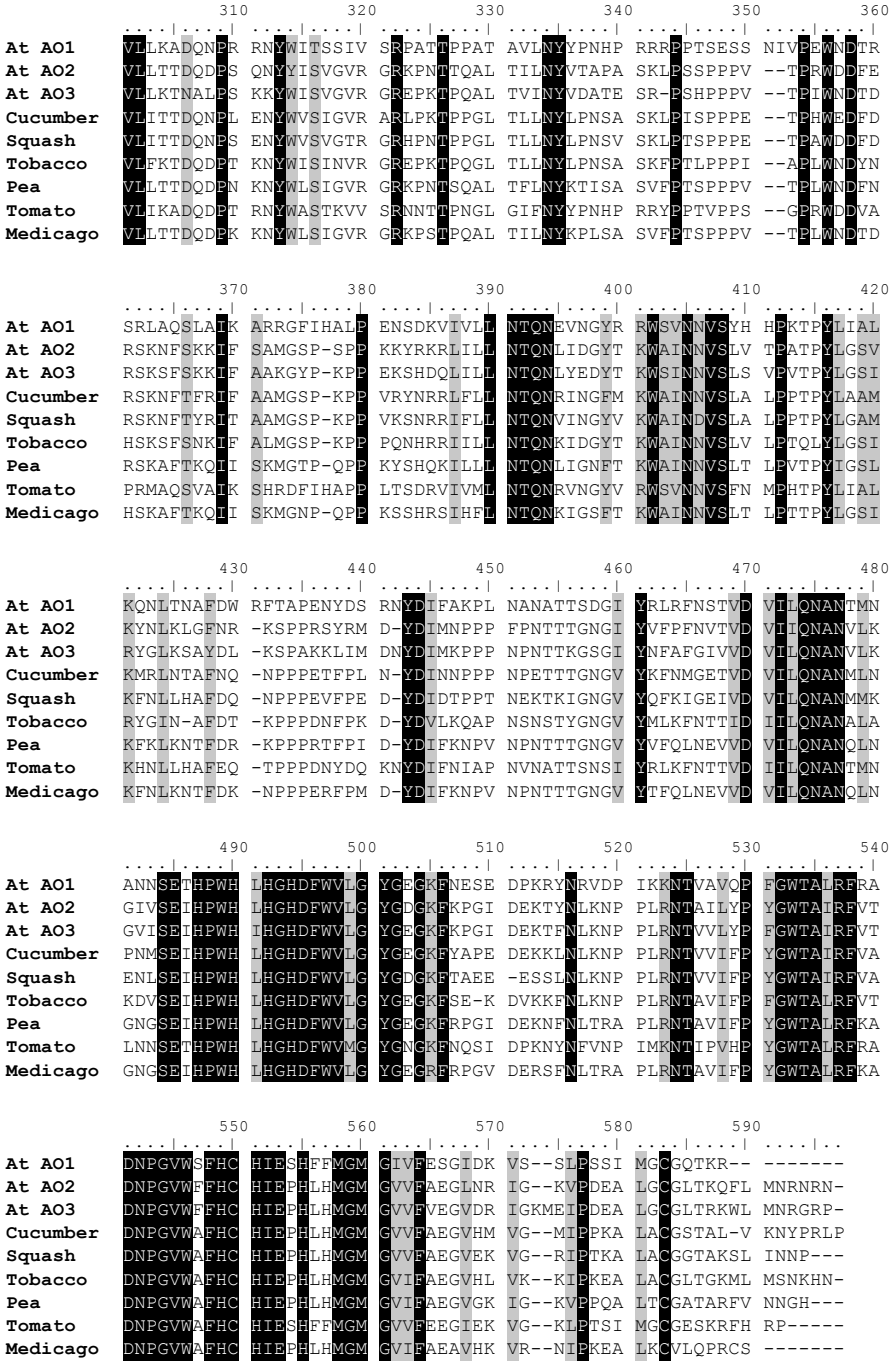

Figure 4-1: Amino acid sequence alignment of *A. thaliana* AO (At AO1, At AO2 and At AO3) with known homologues from other plants. Sequence alignments were performed with ClustalW using the default settings. Identical residues are shaded in black and similar residues, determined by BLOSUM62 similarity matrix are shaded in grey.

Sequences were retrieved from NCBI and the GenBank accession number is shown in square brackets. At AO1 [NP_195693.1], At AO2 [NP_680176.5], At AO3 [NP_197609.1]; cucumber, *Cucumis sativus* [CBY84386.1]; squash, *Cucurbita maxima* [CAA39300.1]; tobacco, *Nicotiana tabacum* [Q40588.1]; pea, *Pisum sativum* [BAH28261.1]; tomato, *Solanum lycopersicum* [NP_001234829.1] and medicago, *Medicago truncatula* [CAA75577.1].

4.2.2. Phylogenetic analysis of AO

To assess the evolutionary relationship among AO in *A. thaliana* and other plant species, amino acid sequences of 24 species were aligned with ClustalW and the aligned sequence was used to construct an unrooted tree using the Neighbor-Joining method of MEGA 5 software (Table 4-1). A bootstrap analysis based on 1000 replicates was performed to test the reliability of the tree topology.

Based on the phylogenetic tree (Figure 4-2), these species were assigned to five groups, namely group A1, A2, B, C, and D. Group A1 composed of AO solely from the dicotyledonous plants, as supported by high bootstrap value (94%). Group A1 was subdivided into few clusters based on their taxonomy. AO from *A. thaliana*, *Arabidopsis lyrata*, mustard and turnip were grouped together to form a Brassicaceae family clade. Despite of high sequence similarity between *A. thaliana* AO2 and AO3, *A. thaliana* AO2 and *A. lyrata* AO were more closely related to each other than *A. thaliana* AO3. Within the Brassicaceae clade, there was a distinct separation between AO from *Arabidopsis* and AO from *Brassica*.

AO from cucumber, melon and squash (Cucurbitaceae) were clustered together. AO in melon is composed of a small family of four proteins. Melon AO4 was clustered with cucumber AO and squash AO independently from melon AO1 and melon AO3. AO from medicago, pea, strawberry, poplar and castor bean, with the exception of tobacco AO, belong to the subclass Rosids were clustered as one clade within group A1, of which medicago and pea belong to the legume family (Fabaceae) were grouped together.

Group B was composed of AO solely from monocotyledon plants. Maize and barley AO were more closely related than the rice AO, suggesting AO from rice evolved independently from that of maize and barley (bootstrap value 78%).

Group C were AO from pteridophytes (lycophyte) and moss. There was a significant divergence between AO in the non-vascular plant (moss) and the vascular plant (lycophyte), indicated by a bootstrap value of 84%. The phylogenetic tree also showed that AO from lycophyte and moss were highly diverged from the monocots/dicots AO, as supported by bootstrap value of 97%.

Group A2 refers to a group of AO from diverse families of dicotyledonous plants such as Fabaceae (soybean), Vitaceae (grape vine), Brassicaceae (*A. thaliana*), Cucurbitaceae (melon), Solanaceae (tomato and pepper) that evolved separately from group A1 and clustered as an independent clade. Intriguingly, AO1 of *A. thaliana* and AO2 of melon were clustered in group A2, separated from their counterparts in group A1. Within group A2, pepper AO and tomato AO from the family of Solanaceae were clustered together. The group A2 clade joined with a cluster of group A1, B and C, suggesting the evolution that gave rise to AO of group A2 occurred independently after the divergence of primitive, monocots and dicots plants, although the bootsrap value is low (41%).

To assess the evolutionary relationship between AO protein in higher plant and the plant ancestor, green algae, amino acid sequences from *Chlamydomonas reinhardtii* and *Volvox carteri* were included in the phylogenetic tree. *C. reinhardtii* contained AO domain in its amino acid sequence whereas amino acid sequence of *V. carteri* contained multi-copper oxidase domain but not AO domain (Figure 4-3). There was a significant divergence between AO in *C.*

reinhardtii and AO in higher plants, indicated by long scale and supported by 100% bootstrap value, therefore assigned as group D. Meanwhile, *V. carteri* that does not have predicted AO domain (Figure 4-3) did not cluster together with *C. reinhardtii* and further diverged from the phylogenetic tree.

Although not conclusive, phylogenetic analysis can give us clues about the possible evolutionary relationship and function of AO in different species. Phylogenetic analysis showed that AO already exists even before the split of monocots and dicots. Phylogenetic analysis also showed that AO is highly conserved across the plant kingdom because AO is present in “ancient plants” (e.g. green alga, mosses) to higher plant (monocots/dicots). However, the significant divergence between monocots/dicots with green alga, lycophyte and moss shows that functional diversity may occur due to evolutionary changes. In fact, a study by Paciolla and Tommasi (2003) showed that AO activity in moss (*Brachythecium velutinum*) and liverwort (*Marchantia polymorpha*) were measured in the cytosolic fraction instead of the cell wall fraction as occurs in the higher plants. This suggests the localisation of the AO in these species is different from higher plants. Besides, Caputo *et al.* (2010) also detected AO in the cytosol, cell wall and chloroplasts of a green alga (*Chaetomorpha linum*) by using a pumpkin AO antibody in immunogold-transmission electron microscopy. Intriguingly, Tommasi *et al.* (1990) showed that AO was absent in the non-photosynthetic parasitic plant, *Cuscuta reflexa*, although other AsA metabolising enzymes such as MDHAR and DHAR were retained. As such, it should be emphasised that this phylogenetic tree is not an exhaustive means to dissect the complete evolutionary history of AO in plants. The topology and the order of

evolutionary distances might change in future with the availability of complete genome sequence information in other plants.

In *A. thaliana*, AO2 and AO3 shared greater amino acid identity than AO1 (Table 4-3). This is also reflected in the phylogenetic analysis (Figure 4-2), which suggests the *A. thaliana* AO1 underwent independent evolution compared to the gene duplication that occurred in the AO2 and AO3. Similar pattern was observed in the melon AO, where melon AO2 was closely related to pepper and tomato AO than its own family member. Sanmartin *et al.* (2007) had performed gene expression analysis on melon *AO1*, *AO2*, *AO3* and *AO4* genes but failed to detect melon *AO2* expression in growing melon tissue, suggesting an alternative function played by melon *AO2* or the possibility of pseudogene. Therefore, the evolutionary divergence between AO1 to AO2 and AO3 in *A. thaliana* may give rise to functional diversity which could be verified *via* gene expression or knockout studies of *AO1* gene.

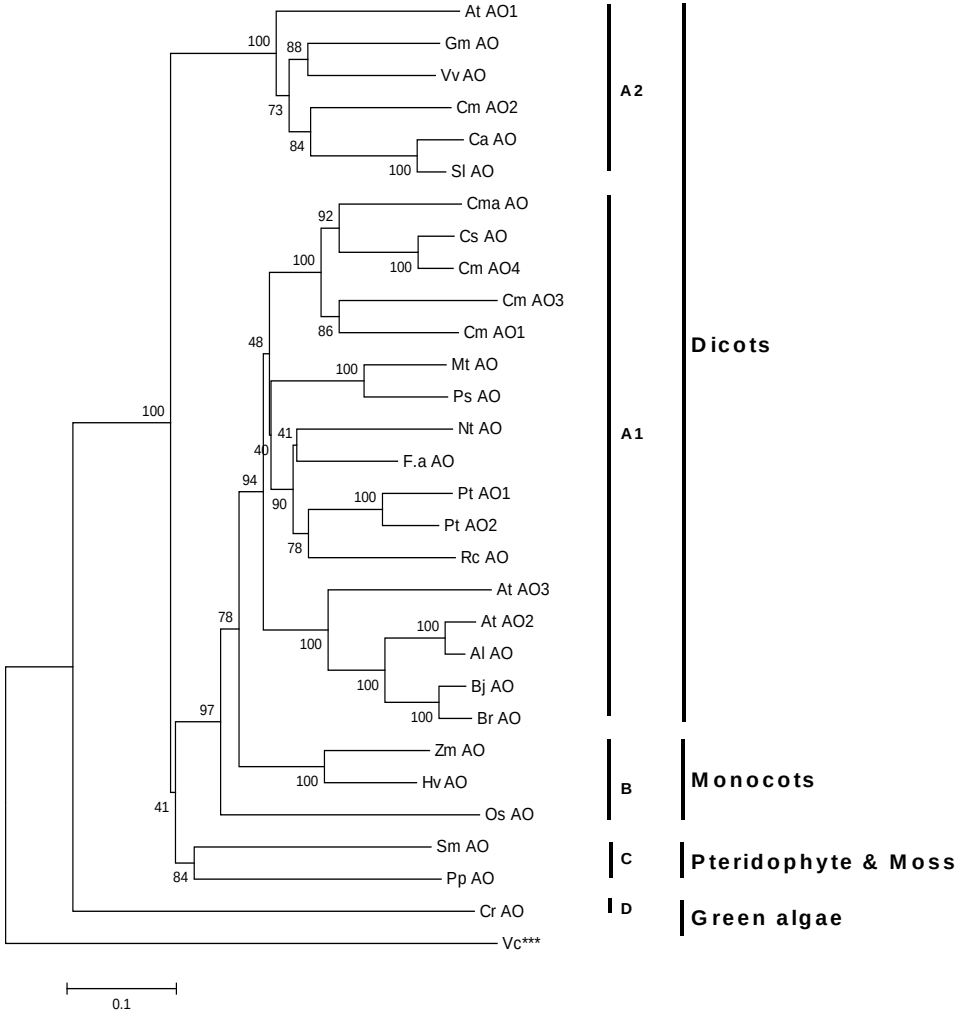

Figure 4-2: Phylogenetic tree of AO from plants. Amino acid sequences were retrieved from NCBI, aligned with ClustalW and used to construct an unrooted tree using the Neighbor-Joining method in MEGA 5. Values (percentages) at the nodes are derived from bootstrap analysis based on 1000 replicates. Scale bar indicates 0.1 amino acid substitution per site.

The common name is shown in parentheses while the GenBank accession number is shown in square brackets. **Al**, *Arabidopsis lyrata* [XP_002871967.1]; **At**, *Arabidopsis thaliana* [AO1: NP_195693.1, AO2: NP_680176.5, AO3: NP_197609.1]; **Bj**, *Brassica juncea* (mustard) [AAF20933.1]; **Br**, *Brassica rapa* (turnip) [BAG50513.1]; **Ca**, *Capsicum annuum* (pepper) [AAF33751.1]; **Cm**, *Cucumis melo* (melon) [AO1: AAF35910.1, AO2: CAA71274.1, AO3: CAA71275.1, AO4: AAF35911.2]; **Cma**, *Cucurbita maxima* (squash) [CAA39300.1]; **Cr**, *Chlamydomonas reinhardtii* (green alga) [XP_001690061.1]; **Cs**, *Cucumis sativus* (cucumber) [CBY84386.1]; **F.a**, *Fragaria x ananassa* (strawberry) [AFF19043.1]; **Gm**, *Glycine max* (soybean) [XP_003524331.1]; **Hv**, *Hordeum vulgare* (barley) [BAJ87129.1]; **Mt**, *Medicago truncatula* (medicago) [CAA75577.1]; **Nt**, *Nicotiana tabacum* (tobacco) [Q40588.1]; **Os**, *Oryza sativa* (rice) [BAA20520.1]; **Pp**, *Physcomitrella patens* (moss) [XP_001751352.1]; **Ps**, *Pisum sativum* (pea) [BAH28261.1]; **Pt**, *Populus trichocarpa* (poplar) [AO1: XP_002312838.1, AO2: XP_002299782.1]; **Rc**, *Ricinus communis* (castor bean) [XP_002530197.1]; **Sl**, *Solanum lycopersicum* (tomato) [NP_001234829.1]; **Sm**, *Selaginella moellendorffii* (lycophyte) [XP_002985774.1]; **Vc**, *Volvox carteri* (green alga) [XP_002954949.1]; **Vv**, *Vitis vinifera* (grape vine) [XP_002281497.2]; **Zm**, *Zea mays* (maize) [ACG30138.1]. *** Amino acid sequence of multi-copper oxidase was retrieved from *V. carteri* to construct the phylogenetic tree.

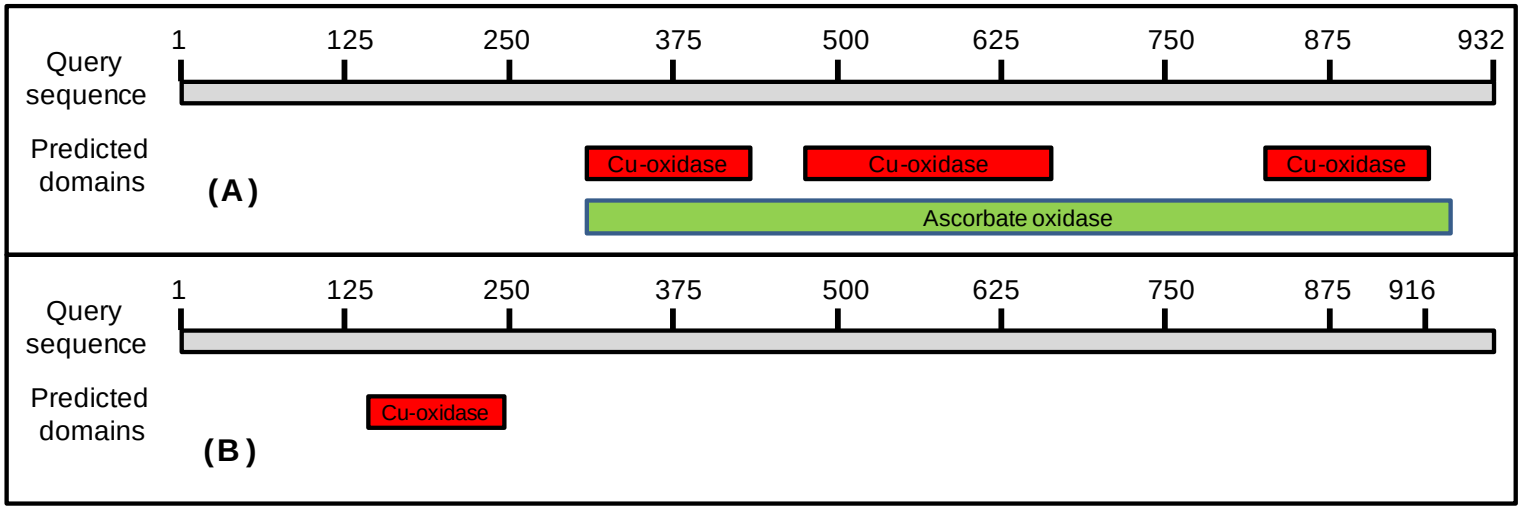

Figure 4-3: Conserved domains identified in the amino acid sequences of **(A)** *C. reinhardtii* and **(B)** *V. carteri*. Amino acid sequences were retrieved from NCBI and conserved domains were annotated using the NCBI's Conserved Domain database (http://www.ncbi.nlm.nih.gov/Structure/cdd/wrpsb.cgi). Cu-oxidase: Multicopper oxidase.

4.2.3. Predicted subcellular localisation and post-translational modifications of AO proteins

Cell eFP browser (Table 4-1) was used to display the subcellular localisations data for all three AO proteins predicted by the SUBA database. All three AO proteins had predicted subcellular localisations in “extracellular” and “endoplasmic reticulum” compartments (Figure 4-4A to C). Interestingly, AO1 was also predicted to be located in the cytosol, mitochondria and peroxisome (Figure 4-4A). The SignalP 3.0 and TargetP 1.1 servers were used to predict potential signal peptides and possible cleavage sites. All AO proteins were predicted to have one signal peptide cleavage site (Table 4-4). The DictyOGlyc and NetNGlyc servers were used to predict glycosylation pattern in AO proteins. All AO proteins were *N*-glycosylated. In addition, AO2 and AO3 were also *O*-glycosylated (Table 4-4).

The presence of signal peptides and predicted extracellular localisation of AO1, AO2 and AO3 proteins is in consistent with AO proteins in other plants (Mertz, 1961; Chichiricco *et al.*, 1989; Esaka *et al.*, 1990; Kato and Esaka, 1996; Diallinas *et al.*, 1997; Kisu *et al.*, 1997; Pignocchi and Foyer, 2003; Liso *et al.*, 2004; Sanmartin *et al.*, 2007). All three AO proteins were also found to be present in endoplasmic reticulum (ER). This is because as a secretory protein, AO contains a signal peptide that targeted it for translocation to ER, then transported through the Golgi apparatus and exported by secretory vesicles to the apoplast (Emanuelsson *et al.*, 2007). Other subcellular locations such as cytosol, mitochondria and peroxisome were predicted for the AO1 protein. The possible reason is due to low sequence identity and evolutionary difference compared with AO2 and AO3 that resulted in the diversity of subcellular

localisation. An experimental approach using fluorescently-tagged protein or immunogold labelling should be employed to determine the exact subcellular location of each AO protein.

In agreement with other AO proteins (Esaka *et al.*, 1990; Sanmartin *et al.*, 2007), AO1, AO2 and AO3 in *A. thaliana* were predicted to have *N*-glycosylation. In addition, AO2 and AO3 are also predicted to be *O*-glycosylated. Glycosylation is a common post-translational modification in plant cell wall proteins that occurs during translocation to ER and Golgi apparatus before secretion to the cell wall (Jamet *et al.*, 2008).

(A)

AO1 (At4g39830)
Cytosol, endoplasmic reticulum, extracellular, mitochondria and peroxisome

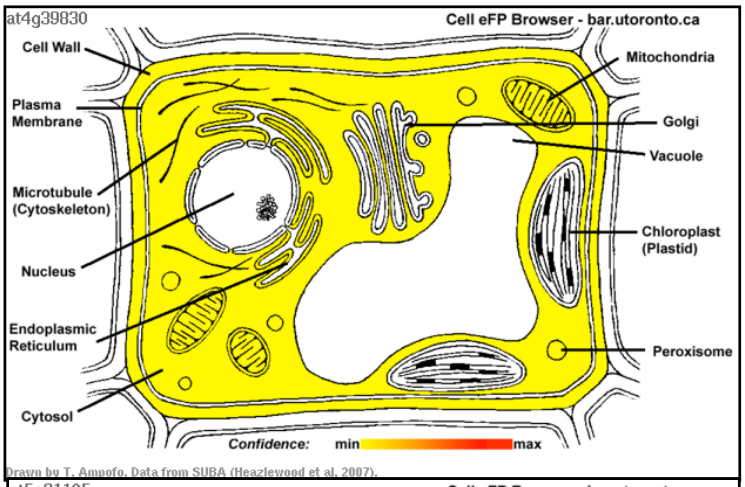

(B)

AO2 (At5g21105)
Endoplasmic reticulum and extracellular

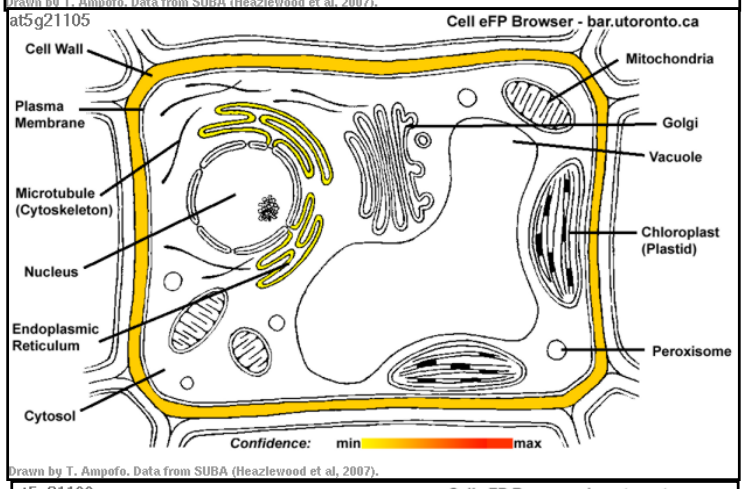

(C)

AO3 (At5g21100)
Endoplasmic reticulum and extracellular

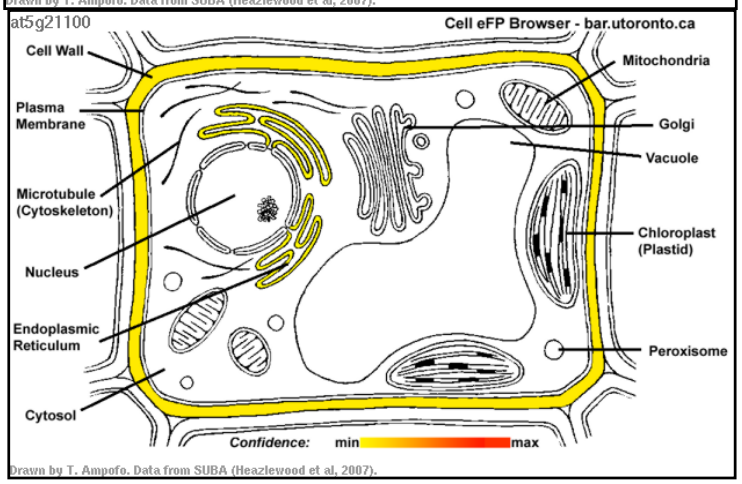

Figure 4-4: Predicted subcellular localisation of AO proteins. Data from SUBA are visualised with cell eFP browser. The subcellular locale for **(A)** AO1, **(B)** AO2 and **(C)** AO3 is coloured in yellow.

Table 4-4: Predicted subcellular localisation, potential signal peptide cleavage site and glycosylation pattern of AO proteins. Analyses were performed using SignalP 3.0, TargetP 1.1, DictyOGlyc and NetNGlyc servers.

Name	Protein length (a.a.)	Signal peptide length (a.a.)	*Predicted cleavage site (a.a.)	Mature protein (a.a.)	**Glycosylation
AO1 (At4g39830)	582	31	Between pos. 31-32 (VLC-QG)	551	*N*-linked (211, 268, 419 and 462)
AO2 (At5g21105)	588	35	Between pos. 35-36 (ASA-AV)	553	*O*-linked (344, 345, 372 and 374) and *N*-linked (81, 126 and 247)
AO3 (At5g21100)	573	21	Between pos. 21-22 (ASA-AV)	552	*O*-linked (143) and *N*-linked (196 and 336)

a.a.: amino acid, pos: position.
*Predicted cleavage site between amino acid pos. X-Y corresponds to that the mature protein starts at (and includes) position Y. The corresponding amino acid (given in single letter code) at the indicated position is shown in parentheses (i.e. letter after the dash "-", refers to the first amino acid of mature protein).
**Position (pos.) for predicted residues is shown in parentheses.

4.2.4. *In silico* promoter and gene expression analyses of *AO* genes in *A. thaliana*

4.2.4.1. Promoter analysis of *AO* genes in *A. thaliana*

To identify c*is*-acting regulatory elements (CARES) present in the promoter of *AO* genes, 1000 bp sequences upstream of the start codon of each *AO1*, *AO2* and *AO3* gene were queried against an online database, PlantCARE (Table 4-1). A large number of common CARES like TATA-box and CAAT-box were identified but were ignored because they were not considered as promoter-specific elements for *AO*. The known CARES obtained for all three *AO* genes were counted and grouped together based on their broad functions: 1) light-responsive element, 2) stress-responsive element, 3) hormone-responsive element and 4) growth and development. The percent occurrence of individual elements, based on the calculated number of element relative to the total CARES found in *AO1*, *AO2* and *AO3* promoters is shown in Figure 4-5. Half of the CARES found in the PlantCARE database were involved in light-responsiveness. A substantial amount of CARES were involved in stress and hormone responses. A small number of CARES were involved in growth and development (Figure 4-5).

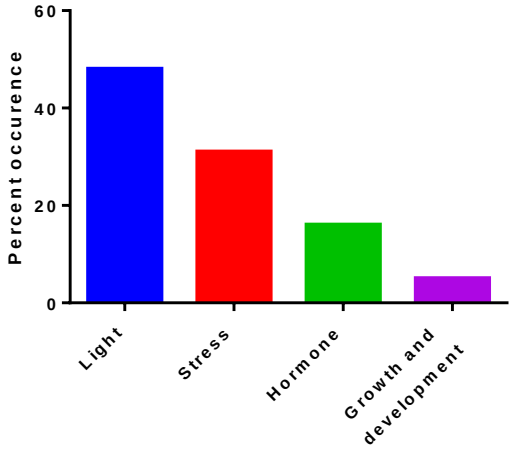

Figure 4-5: Functional categories of the *cis*-acting regulatory elements present in the promoters of all *AO* genes in *A. thaliana*. The promoters of *AO* genes were searched against the PlantCARE database. The percent occurrence was calculated according to the number of elements assigned to each group (light, stress, hormone and growth and development), relative to the total number of elements found.

Specific CARES for *AO1*, *AO2* and *AO3* are listed in Table 4-5, Table 4-6 and Table 4-7 respectively. A significant number of light-responsive motifs were found in the promoter of all three *AO* genes. Stress-responsive elements involved in drought, wound, anaerobic, fungal, low temperature, heat and plant defence responses were generally found in the *AO* promoters. Similarly, a small number of hormone-responsive elements in particular those involved in ABA, auxin, salicylic acid, MeJA, ethylene and gibberellin were also found in the *AO* promoters.

Table 4-5: C*is*-acting regulatory elements in the promoter of the *AO1* gene.

Motif name	Sequence	Function	Number of occurrence
	Light-responsive element		
3-AF1	AAGAGATATTT	Light responsiveness	1
AT1-motif	AATTATTTTTTATT	Light responsiveness	1
Box 4	ATTAAT	Light responsiveness	1
Box II	TGGTAATAA	Light responsiveness	1
I-box	gGATAAGGTG / aAGATAAGA	Light responsiveness	2
TCT-motif	TCTTAC	Light responsiveness	2
	Stress-responsive element		
ARE	TGGTTT	Anaerobic fermentation	1
W box	TTGACC	Wound responsive element	2
HSE	AAAAAATTTC	Heat stress responsiveness	2
LTR	CCGAAA	Low temperature responsiveness	1
TC-rich repeats	ATTTTCTCCA	Defence and stress responsiveness	2
	Hormone-responsive element		
TCA-element	CCATCTTTTT	Salicylic acid responsiveness	1
TGA-element	AACGAC	Auxin responsiveness	1
	Growth and development		
Skn-1_motif	GTCAT	Endosperm expression	3

Table 4-6: C*is*-acting regulatory elements in the promoter of the *AO2* gene.

Motif name	Sequence	Function	Number of occurrence
	Light-responsive element		
ATCT-motif	AATCTGATCG	Light responsiveness	1
Box 4	ATTAAT	Light responsiveness	1
Box I	TTTCAAA	Light responsiveness	1
G-Box	CACGTA / CACGTT / GTACGTG / TACGTG	Light responsiveness	5
TCCC-motif	TCTCCCT	Light responsiveness	1
TGG-motif	GGTTGCCA	Light responsiveness	1
	Stress-responsive element		
ARE	TGGTTT	Anaerobic fermentation	2
W box	TTGACC	Wound responsive element	2
HSE	AAAAAATTTC / AGAAAATTCG	Heat stress responsiveness	2
MBS	TAACTG	MYB binding site involved in drought-inducibility	1
TC-rich repeats	GTTTTCTTAC	Defence and stress responsiveness	1
	Hormone-responsive element		
ABRE	TACGTG	ABA responsiveness	1
CGTCA-motif	CGTCA	MeJA responsiveness	1
ERE	ATTTCAAA	Ethylene responsiveness	1
P-box	CCTTTTG	Gibberellin responsiveness	1
TGACG-motif	TGACG	MeJA responsiveness	1

Table 4-7: C*is*-acting regulatory elements in the promoter of the *AO3* gene.

Motif name	Sequence	Function	Number of occurrence
	Light-responsive element		
AE-box	AGAAACAA	Light responsiveness	1
ATCT-motif	AATCTAATCC	Light responsiveness	1
Box I	TTTCAAA	Light responsiveness	2
G-Box	CACGTG / CACGTA / ACACGTGT / TACGTG	Light responsiveness	6
GT1-motif	AATCCACA	Light responsiveness	1
TCT-motif	TCTTAC	Light responsiveness	1
	Stress-responsive element		
W box	TTGACC	Wound responsive element	2
TC-rich repeats	GTTTTCTTAC	Defence and stress responsiveness	1
	Hormone-responsive element		
ABRE	CACGTG / TACGTG	ABA responsiveness	2
ERE	ATTTCAAA	Ethylene responsiveness	1
	Growth and development		
NON-box	AGATCGACG	Meristem specific activation	1
Skn-1_motif	GTCAT	Endosperm expression	2

4.2.4.2. *AO* expression profile during development

The *AO* expression profile during development has not been reported in *A. thaliana* previously. A web-based microarray database, eFP browser (Table 4-1), was used to obtain a comprehensive view on the expression of *AO* in various tissues. Data of a rosette leaf (equivalent to a fully expanded leaf at the middle rosette of a 6-week-old plant) and its leaf parts (petiole, proximal half and distal half), cauline leaf, primary inflorescence stem, open flowers and floral organ (sepals, petals, stamens and carpels), senescing leaf and roots were mined. The expression profiles of *AO1*, *AO2* and *AO3* are shown in Figure 4-6.

In general, the expression of *AO1* was lower than *AO2* and *AO3* in leaves and flowers except in the distal half of rosette leaves where *AO1* shows similar expression to *AO3*. Except for senescing leaves, the expression of *AO2* was fairly similar across all the tissues examined, although *AO2* expression was slightly higher in stems and flowers than rosette leaves. *AO3* showed a distinct expression pattern during development. *AO3* expression was higher during the reproductive stage; in particular in cauline leaves and flowers. Among three *AO* genes, *AO2* had the highest expression in roots, where *AO3* expression was barely detected. *AO3* was the major gene expressed in cauline leaves and flowers compared to *AO1* and *AO2*. Intriguingly, *AO1* showed a reverse expression pattern in different parts of rosette leaves (petiole < proximal half < distal half), although tissue expansion stops first at the distal half followed by the proximal half and then the petiole. By contrast, *AO2* and *AO3* had higher expression in petioles than the distal half of rosette leaves. Among floral organs examined, *AO2* expression was relatively consistent compared with *AO1* and *AO3*. Low *AO1* expression was observed in petals, stamens and carpels compared to sepals. Meanwhile *AO3* had high expression in petals, intermediate expression in stamens and carpels and low expression in sepals. In senescing leaves, all three *AO* genes showed a same expression level.

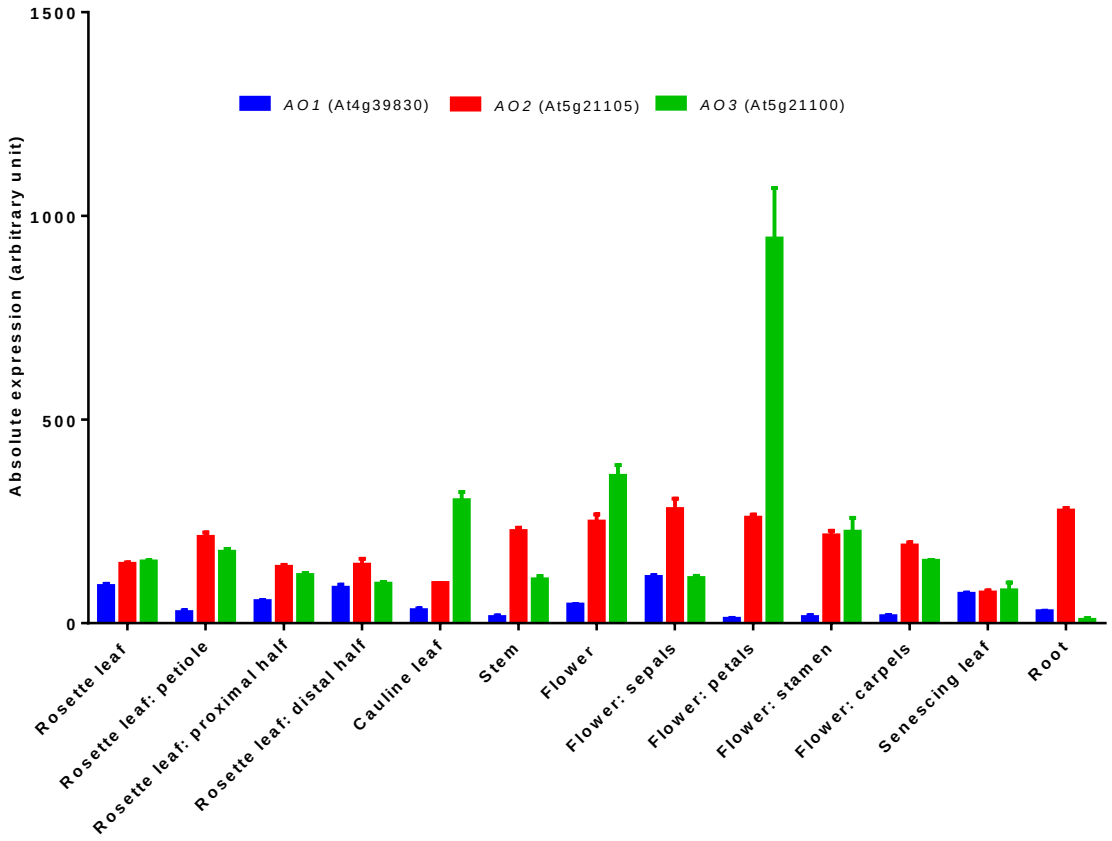

Figure 4-6: Gene expression profile of the *A. thaliana AO* genes during development. Data were mined from the *Arabidopsis* eFP browser (http://bar.utoronto.ca/efp/cgi-bin/efpWeb.cgi). "Absolute" gene expression denotes that the expression level in each tissue is directly compared to the highest signal recorded for the given gene.

4.2.4.3. *AO* gene expression during high light acclimation

The *AO* gene expression of WT *A. thaliana* acclimated to four-day high light (HL, 550-650 µmol m^{-2} s^{-1}) and low light (LL, 100 µmol m^{-2} s^{-1}) treatments were determined from mRNA-Seq data established in my lab (Page *et al.*, unpublished) and is shown in Figure 4-7. The *AO1* expression was significantly down-regulated when acclimated to HL. Meanwhile, there was only a small increase in the expression of *AO2* and *AO3* during HL treatment.

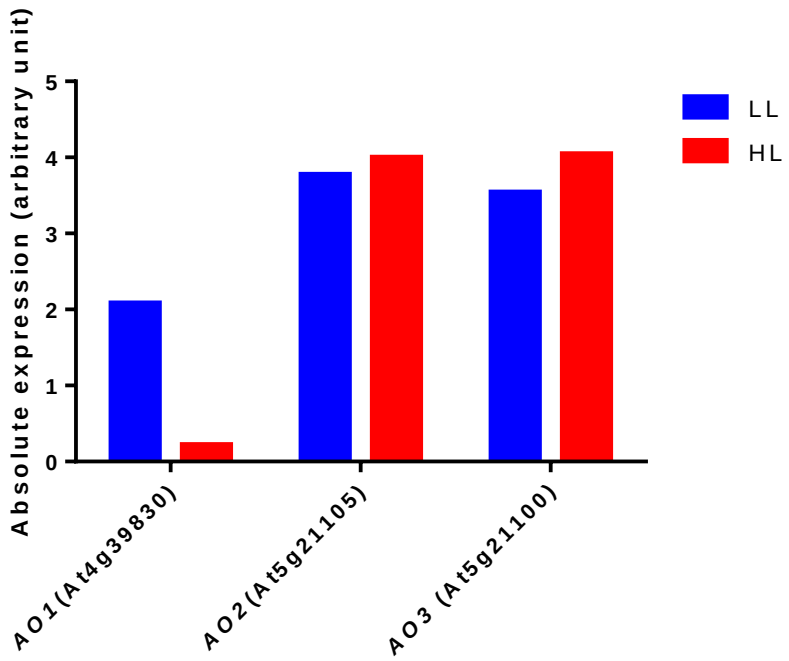

Figure 4-7: *AO* gene expression in WT *A. thaliana* after four days of high light (HL, PPFD = 550-650 µmol m^{-2} s^{-1}) or low light (LL, PPFD = 100 µmol m^{-2} s^{-1}) treatments, determined by mRNA-Seq from our in-house database (unreplicated mRNA-Seq data, Page *et al.*, unpublished). Values are mean absolute expression. The unit of gene expression is presented as fragments per kilobase of exon per million fragments mapped (FPKM).

4.2.4.4. *AO* gene expression in response to drought

The expression of *AO* gene in WT *A. thaliana* during drought was obtained from the *Plant Responses to Environmental STress in Arabidopsis* (PRESTA) microarray database (PRESTA Consortium – Warwick, Essex and Exeter Universities, unpublished). Drought experiment was conducted *via* progressive soil drying approach where water was withheld from plants for 13 days. *AO1* expression was down-regulated after 13 days of drought. The expression of *AO2* and *AO3* was similar on day 0 and day 13 of the drought treatments due to high error bars present in these datasets, although *AO2* and *AO3* expression was up-regulated after 13 days of drought (Figure 4-8).

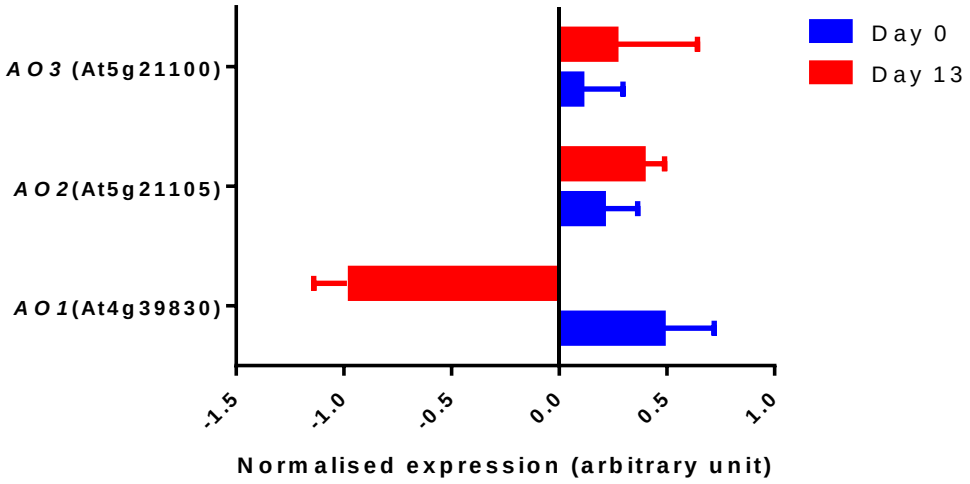

Figure 4-8: *AO* gene expression in WT *A. thaliana* after 13 days of drought treatment. Data on day 0 and day 13 of the treatment were obtained from the *Plant Responses to Environmental STress in Arabidopsis* (PRESTA) microarray database (PRESTA Consortium – Warwick, Essex and Exeter Universities, unpublished). Values are mean ± SEM, n = 4. The expression level was normalised to median gene expression.

4.2.4.5. General discussion: *In silico* promoter and gene expression analyses of *AO* genes in *A. thaliana*

In silico promoter analysis showed that the expression of *AO* genes in *A. thaliana*, generally, might be regulated by light, stress, hormones and growth. Unfortunately, study on the promoter of *AO* in plants is limited compared to *AO* gene expression analysis. Previously, only Kisu *et al.* (1997) showed that an *AO* gene in pumpkin contained a promoter element for auxin regulation. Nevertheless, the gene expression of *AO* in different plants in response to hormones, light and stress treatments was reported in a number of studies (see below).

The light response of *AO* gene were demonstrated by De Tullio *et al.* (2007) and Pignocchi *et al.* (2003) in zucchini and tobacco respectively, in which an *AO* transcript is up-regulated by light compared to the dark-treated plants. AO activity is increased by continuous far red light; far red light/red light reversibility experiments showed a light-mediated response of AO, suggesting phytochrome is involved in the regulation of AO activity (Hayashi and Morohashi, 1993). The effect of ethylene, wound, cold and heat treatments on the expression of three tomato *AO* genes was assessed by Ioannidi *et al.* (2009). Only cold treatment enhanced the transcript level of tomato *AO2*, whereas other treatments (ethylene, wound, cold and heat) did not affect the expression of *AO* genes. Meanwhile, Diallinas *et al.* (1997) showed that *AO* gene expression in melon was suppressed by wounding. By contrast, García-Pineda *et al.* (2004) observed a transient expression (after 1 hr treatment) of pepper *AO* in response to wounding, and proposed a distinct regulation of *AO* between climacteric fruit (melon) and non-climacteric fruit (pepper). Sanmartin *et al.* (2007) showed that the *AO* gene family in melon behaved differently to varied stresses. The expression of melon *AO1*, *AO2* and *AO3* was not affected by wounding and heat stress, but melon *AO4* was up-regulated in response to wounding and heat stress.

In response to hormone treatment, Pignocchi *et al.* (2003) showed that tobacco *AO* gene was up-regulated by auxin but suppressed by salicylic acid (SA). Sanmartin *et al.* (2007) showed that jasmonic acid (JA) induced melon *AO4* expression while abscisic acid (ABA) and SA repressed melon *AO4* expression. JA treatment also induced the expression of *AO* gene in the common bean (*Phaseolus vulgaris*) nodules (Loscos *et al.*, 2008). By contrast, hormone

treatments (ethylene, JA and ABA) did not affect the *AO* gene expression in broccoli florets (Nishikawa *et al.*, 2003).

Expression analysis of *AO* genes during development and in response to high light acclimation and drought were assessed using the *Arabidopsis* eFP browser microarray database and in-house microarray and mRNA-Seq databases. Consistent with the distinct subcellular localisation and phylogenetic pattern observed, *AO1* exhibited unique expression pattern during high light acclimation and drought. These stresses repressed *AO1* expression, whereas *AO2* and *AO3* expression did not vary during drought and high light treatments. Furthermore, low *AO1* gene expression in leaves and flowers might suggest a separate function of *AO1* in plant growth compared to *AO2* and *AO3*. *AO1* knockout mutant and transgenic *A. thaliana* that overexpress *AO1* might give us clue on the role played by *AO1*.

Taken together, data from published literature and *in silico* predictions suggest that the *AO* gene expression in *A. thaliana* might be positively or negatively regulated by light, hormone and stress, and it also appears that each *AO* gene has a distinct expression pattern. Clearly, the interaction of *AO* with hormone and environmental perturbations is complex and should be experimentally verified by looking at the expression of *AO* genes in *A. thaliana* during development and stress. The effects of knocking out or overexpressing *AO* in *A. thaliana* should be investigated.

4.2.5. Translatome data for *AO* genes in *A. thaliana* seedlings

The “shoot-root” translatome data for *AO1*, *AO2* and *AO3* were sourced from the *Arabidopsis* translatome eFP browser (http://efp.ucr.edu/). No apparent difference in the gene expression of *AO1*, *AO2* and *AO3* in the shoot of 7-day-old *A. thaliana* seedlings was observed under control or hypoxic conditions (Figure 4-9 to 4-11), although the *AO2* gene expression in the cotyledon and leaf epidermis appeared to be lower in hypoxic seedlings (Figure 4-10). The gene expression for *AO1* (Figure 4-9) and *AO3* (Figure 4-11) in the root cells of hypoxic seedlings was similar to the control counterparts. The *AO2* gene expression was decreased in the root cells of hypoxic seedlings, indicated by a change of fluorescence intensity in the root image (Figure 4-10).

The translatome data showed that the level of *AO2* gene expression in roots was higher than *AO1* and *AO3* under control conditions, which is in agreement with the *in silico* gene expression result that obtained from the *Arabidopsis* eFP browser (see Figure 4-6), suggesting that the *AO2* gene expression is abundant in roots.

The *AO2* gene expression was decreased under hypoxia stress, suggesting low oxygen condition could repress the expression of *AO* gene. It has been shown that AO activity is positively correlated with O_2 concentration in zucchini (*Cucurbita pepo*) (Arrigoni *et al.*, 2003; De Tullio *et al.*, 2007). Meanwhile, hypoxic conditions decreased the AO activity in maize and zucchini (De Tullio *et al.*, 2007). Several hypotheses for the role of AO in oxygen management were proposed by De Tullio *et al.* (2004): AO suppression is required to increase oxygen availability. For example, low AO activity in wounded melon fruit (Diallinas *et al.*, 1997) could increase O_2 and AsA availability, which is essential

to increase the rate of respiration (wound respiration) and the synthesis of hydroxyproline-containing proteins that are required for wound healing. In addition, AO may be indirectly involved in photosynthesis by regulating O_2 level generated in chloroplasts. During photosynthesis, O_2 is produced in the chloroplast, diffuses to the cytosol, crosses to the apoplast and then releases to external environment *via* stomata. The diffusion of oxygen from chloroplasts to the apoplast is a slow process therefore an effective mechanism is required to increase the O_2 diffusion in order to prevent oxidative damages occurs inside the cells. In this situation, AO as an O_2-consuming enzyme could help to establish a steep O_2 concentration between chloroplasts and the apoplast, thereby increasing the diffusion of O_2 from chloroplast to the apoplast (Arrigoni *et al.*, 2003; De Tullio *et al.*, 2004). Meanwhile, Blokhina and Fagerstedt (2010) proposed that AO could function under hypoxic conditions by controlling O_2 level and AsA redox state. However, there is no evidence reported on the relationship between AO and AsA during hypoxic conditions.

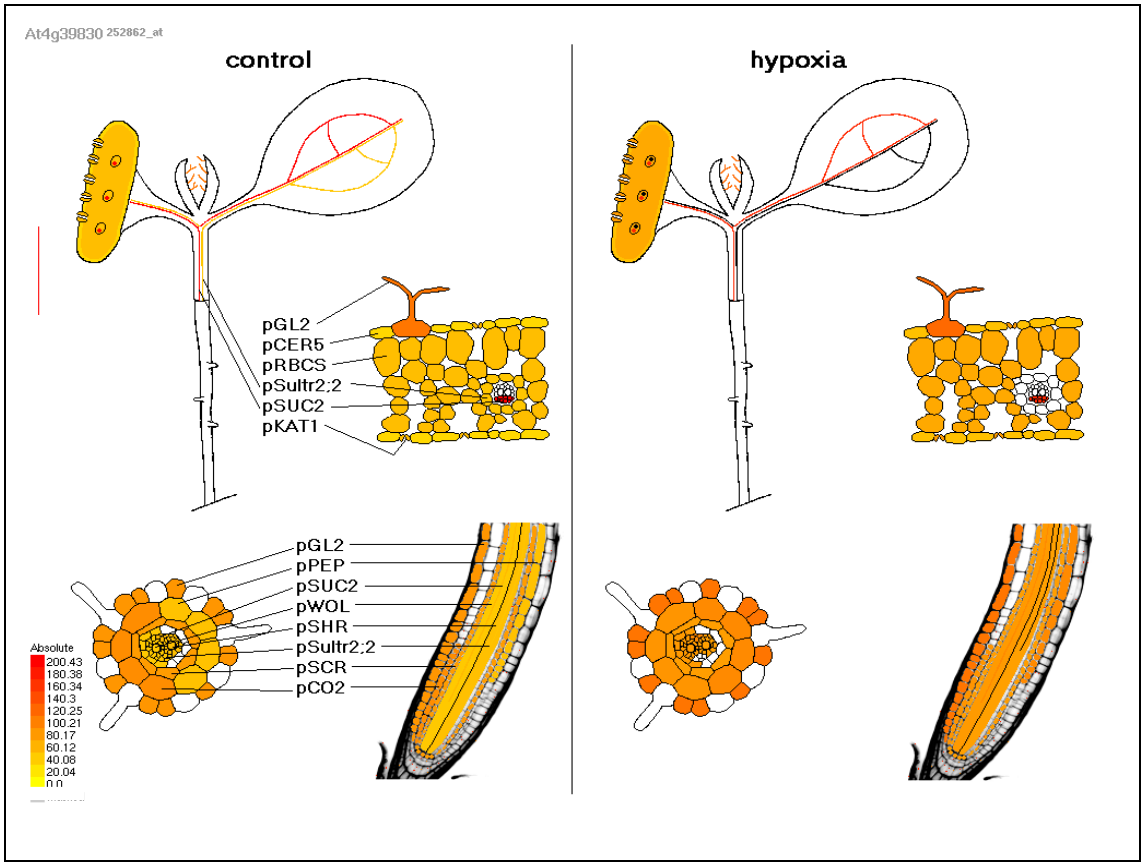

Figure 4-9: Translatome analysis for the *AO1* gene in the shoot and root of 7-day-old *A. thaliana* seedlings subjected to hypoxia stress. Data were mined from the *Arabidopsis* translatome eFP browser. The gene expression is illustrated in the respective fluorescence image, indicated by the false colur code, and regions in white indicate that the gene expression information is not available.

pGL2: GLABRA2 promoter, pCER5: promoter for cuticular wax gene, pRBCS: promoter for rubisco small subunit, pSULTR2;2: promoter for sulfate transporter, pSUC2: promoter for sucrose transporter2, pKAT1: promoter for K^+ channel, pPEP: promoter for endopeptidase, pWOL: WOODENLEG promoter, pSHR: SHORTROOT promoter, pSCR: SCARECROW and pCO2: promoter for cortex specific transcript.

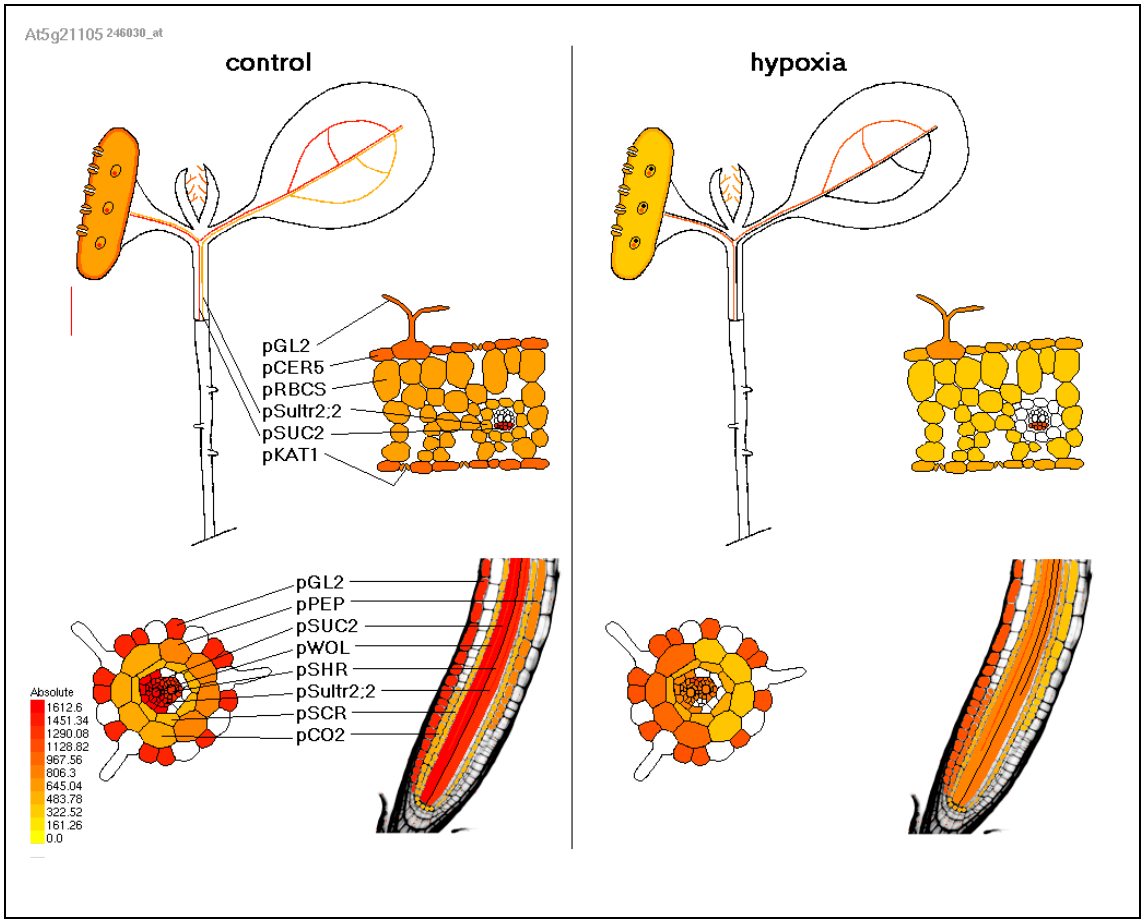

Figure 4-10: Translatome analysis for the *AO2* gene in the shoot and root of 7-day-old *A. thaliana* seedlings subjected to hypoxia stress. Data were mined from the *Arabidopsis* translatome eFP browser. The gene expression is illustrated in the respective fluorescence image, indicated by the false colur code, and regions in white indicate that the gene expression information is not available.

pGL2: GLABRA2 promoter, pCER5: promoter for cuticular wax gene, pRBCS: promoter for rubisco small subunit, pSULTR2;2: promoter for sulfate transporter, pSUC2: promoter for sucrose transporter2, pKAT1: promoter for K^+ channel, pPEP: promoter for endopeptidase, pWOL: WOODENLEG promoter, pSHR: SHORTROOT promoter, pSCR: SCARECROW and pCO2: promoter for cortex specific transcript.

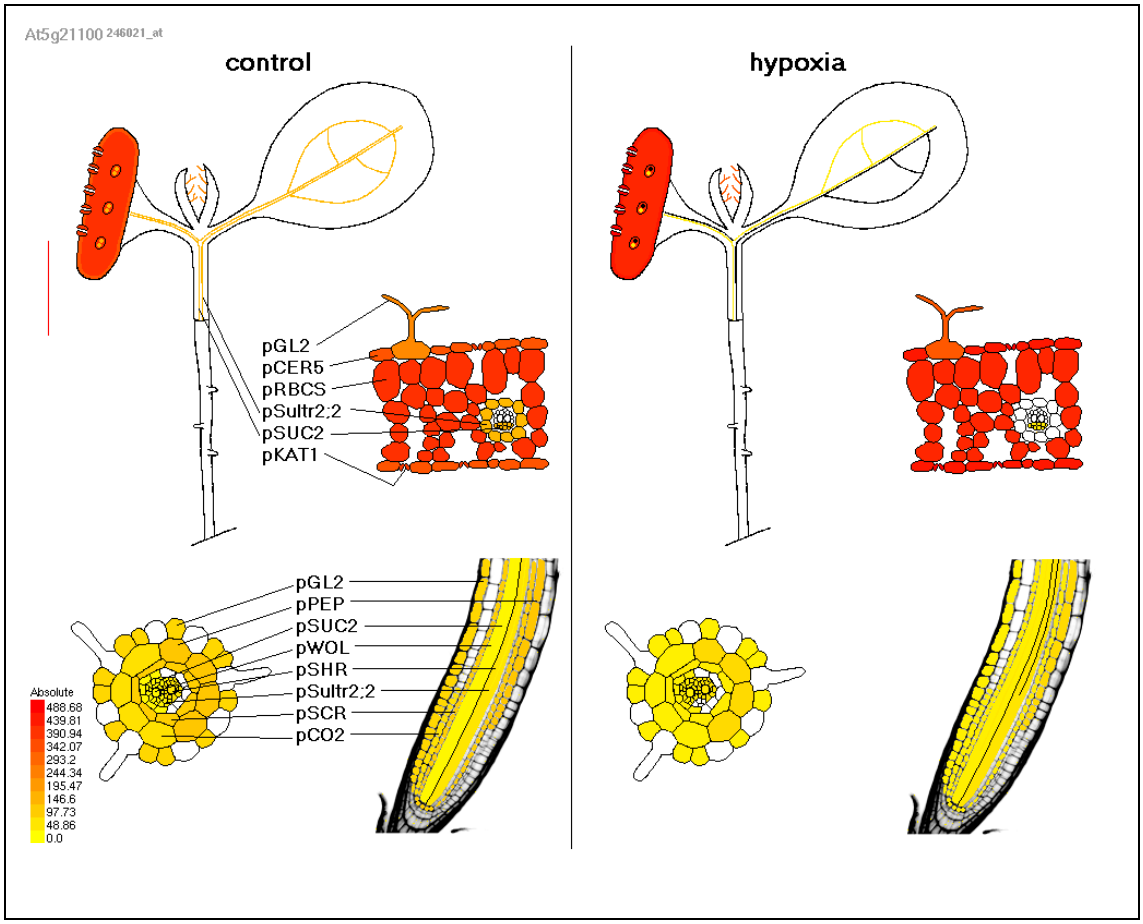

Figure 4-11: Translatome analysis for the *AO3* gene in the shoot and root of 7-day-old *A. thaliana* seedlings subjected to hypoxia stress. Data were mined from the *Arabidopsis* translatome eFP browser. The gene expression is illustrated in the respective fluorescence image, indicated by the false colur code, and regions in white indicate that the gene expression information is not available.

pGL2: GLABRA2 promoter, pCER5: promoter for cuticular wax gene, pRBCS: promoter for rubisco small subunit, pSULTR2;2: promoter for sulfate transporter, pSUC2: promoter for sucrose transporter2, pKAT1: promoter for K^+ channel, pPEP: promoter for endopeptidase, pWOL: WOODENLEG promoter, pSHR: SHORTROOT promoter, pSCR: SCARECROW and pCO2: promoter for cortex specific transcript.

Chapter 5. The function of ascorbate oxidase during development

5.1. General introduction

Previous studies reported high AO activity and *AO* gene expression were positively correlated with cell growth and expansion. Matamoros *et al.* (2010) showed that immature pea fruit had higher AO activity than mature and over-mature fruits. Young tissues and growing region of tobacco had higher AO activity and expression than older tissues (Kato and Esaka, 1996; Yamamoto *et al.*, 2005). Higher AO activity and gene expression were found in both developing fruit and younger leaves of zucchini squash (*Cucurbita pepo*; Lin and Varner, 1991). AO activity was abundant in young fruits of tomato (Garchery *et al.*, 2012), melon (Diallinas *et al.*, 1997) and pumpkin (Esaka *et al.*, 1992). Pallanca and Smirnoff (1999) showed that AO activity is positively correlated with growth of the radicle in pea seedlings. There is also correlation between AO activity and growing zone in pea and maize roots (Mertz, 1961; Suzuki and Ogiso, 1973). Since DHA is the stable product of apoplastic AsA oxidation by AO, it is interesting to note that high DHA is detected in the apoplast of growing hypocotyls of *Vigna angularis* (Takahama and Oniki, 1994; Takahama, 1996). Added DHA in tobacco cell cultures increases auxin-induced cell expansion (Potters *et al.*, 2010). It has been shown that auxin-mediated growth also increases *AO* gene expression and activity in pumpkin, tobacco and *V. angularis* (Esaka *et al.*, 1992; Takahama and Oniki, 1994; Pignocchi *et al.*, 2003). All these examples showed that high AO activity in active growing tissue is well conserved in various plant species, suggesting a possible role of AO and cell wall AsA in cell expansion.

However, the mechanisms involved remain unknown. Several hypotheses involved oxidised apoplastic AsA (MDHA/DHA) and AO were purposed. Lin and Varner (1991) proposed that DHA could interact with cell wall protein to prevent cross-linking of cell wall protein with polysaccharide, resulting in looser walls (see Chapter 1, section 1.5.). However, it should be noted that Lin and Varner (1991) did not measure the cell wall AsA and DHA concentrations in their study. Alternatively, MDHA is proposed to be involved in trans-membrane electron transport. MDHA treatment causes plasma membrane hyperpolarisation and increases H^+-ATPase activity, resulting cell expansion, vacuolation and solute uptake in onion roots (Hidalgo *et al.*, 1989; González-Reyes *et al.*, 1994). However, this claim was only tested on onion roots.

The direct way to examine the function of AO in growth is through genetic manipulations of *AO* gene. Transgenic tobacco plants that overexpress and underexpress *AO* were developed. These transgenic plants showed similar phenotype to the WT under unstressed normal growth conditions despite the alternation in apoplastic AsA redox state (Sanmartin *et al.*, 2003; Yamamoto *et al.*, 2005). By contrast, Pignocchi *et al.* (2003) showed that the tobacco AO overexpressor had increased shoot biomass and stem height under unstressed normal growth conditions in controlled environment growth chambers. Intriguingly, this phenotype was not observed when the overexpressor was cultivated in a greenhouse. Similarly, Garchery *et al.* (2012) showed that *AO* RNAi tomato plants had a similar phenotype to WT under unstressed normal growth conditions.

A previous study in *A. thaliana* showed that the AO-deficient mutant, *ao3* is more tolerant to salinity treatment (Yamamoto *et al.*, 2005), but the role of AO in

the development of *A. thaliana* has remains unknown. Lee *et al.* (2011) found that an *A. thaliana ao1ao2* double mutant exhibited smaller rosette size and late flowering but the AO activity and the apoplastic AsA status was not reported for this mutant.

5.1.1. Peroxidases

If AO is associated with cell expansion then the interaction between AO and other cell wall components such as cell wall peroxidases should not be overlooked. Peroxidases are a diverse group of proteins that are grouped into three different classes. Class I peroxidases are intracellular peroxidases that form three distinct groups − ascorbate peroxidases, cytochrome *c* peroxidases and catalase. Class II peroxidases are found in fungi and are involved in lignin degradation. Class III peroxidases are secreted proteins that form a large multigene family in all land plants (Welinder, 1992; Passardi *et al.*, 2005).

Two catalytic cycles are proposed in peroxidase mode of action: 1) the peroxidative cycle that catalyse the reduction of H_2O_2 by using electrons from various donor molecules such as phenolic compounds, lignin precursors, auxin or secondary metabolites; 2) the hydroxylic cycle, in which can converts peroxidase to oxyferroperoxidase, produces various reactive oxygen species (Passardi *et al.*, 2004; Cosio and Dunand, 2009). These dynamic catalytic cycles mean that class III peroxidases are involved in diverse functions such as cell wall cross-linking, cell elongation, auxin metabolism, and biotic and abiotic stress responses.

In *A. thaliana*, class III peroxidases are encoded by a large family of 73 genes (Cosio and Dunand, 2009). These peroxidases have a distinct expression

pattern in various plant parts like flowers, leaves, stems and roots (Tognolli *et al.*, 2002). The precise function of peroxidase isoforms *in planta* remains elusive due to the large number of genes present in *A. thaliana*, as such functional analyses of peroxidases through reverse genetic is hampered by gene redundancy. A handful of publications have reported on the function of peroxidase in *A. thaliana* development. Passardi *et al.* (2006) showed that *Prx33* and *Prx34* are involved in cell elongation or growth regulation through auxin oxidase activity. The *prx33 prx34* knockdown lines have larger leaves and exhibit delayed senescence compared to WT (Daudi *et al.*, 2012). Pedreira *et al.* (2011) showed that overexpression of *Prx37* led to a dwarf phenotype in plant, caused by increased cross-linking in cell wall due to accumulated amount of phenolic compounds in this overexpressor.

Plasma membrane NADPH oxidases-mediated and class III peroxidases-mediated oxidative burst are required for pathogen resistance in plant (Bolwell and Wojtaszek, 1997). French bean (*Phaseolus vulgaris*) peroxidase cDNA was used to develop *A. thaliana* antisense plants that have successfully knocked down *Prx33* and *Prx34* expression. The antisense plants were impaired in H_2O_2 production and were more susceptible than WT plants to bacterial and fungal pathogens (Bindschedler *et al.*, 2006). Similar to the antisense line, the *Prx33* and *Prx34* T-DNA insertion lines had reduced levels of reactive oxygen species (ROS) and decreased callose deposition when challenged with synthetic peptides Flg22. The *Prx33* T-DNA insertion mutant is more susceptible to *Pseudomonas syringae* infection than WT (Daudi *et al.*, 2012). In addition, knockdown of *Prx33* and *Prx34* in *A. thaliana* cell cultures decreased the expression of genes and production of proteins involved in the microbe-

associated molecular patterns (MAMPs)-elicited responses that are essential for pathogen-triggered immunity (PTI) (O'Brien *et al.*, 2012).

AsA is also implicated in the peroxidase reaction. AsA is able to impair the catalytic reaction of peroxidases by re-reducing the intermediate phenolic radical produced during the peroxidative reaction (De Gara, 2004). Meanwhile, It has been shown that high peroxidase activity is found in AsA-deficient *vtc* mutants (Veljovic-Jovanovic *et al.*, 2001; Colville and Smirnoff, 2008; Sultana, 2011). High peroxidase activity also found in *A. thaliana* plants expressing antisense $_L$-galactose dehydrogenase, an enzyme involved in AsA biosynthesis (Gatzek *et al.*, 2002). An increase in peroxidase activity is proposed to control H_2O_2 concentration in AsA-deficient plants (Gatzek *et al.*, 2002). To date, the relationship between peroxidase activity and the perturbation of apoplastic AsA by AO have not been described.

5.1.2. Chapter aim

Given *A. thaliana* is the model organism in plant science research, it is surprising that the role of AO in plant growth has not been reported in this species. This chapter presents the relationship between AO and the growth of *A. thaliana*, in which a connection between AO and growing tissues of WT *A. thaliana* is described. Using various experimental techniques, the growth of *AO* T-DNA insertion mutants, *amiR-AO* and *35S::AO3* lines isolated (see Chapter 3) were compared with the WT. The finding from *in silico* analyses of AO during development in *A. thaliana* (see Chapter 4) is examined experimentally.

5.2. Results

Unless otherwise specified, all plants used for the following experiments were grown under unstressed normal growth conditions at a short day light regime (8 hrs light, 16 hrs dark).

5.2.1. Ionically-bound cell wall AO activity in various tissues of WT *A. thaliana* during vegetative growth stage

Various leaves of 6-week-old WT *A. thaliana*, grown under short day conditions (8 hrs light, 16 hrs dark) were extracted to assess ionically-bound cell wall AO activity in the vegetative growth stage. These leaves, as illustrated in Figure 5-1D were divided into four groups: I) “young”, defined as newly emerging leaves, II) “intermediate”, defined as expanded young leaves, in which the rosette size is about 50% of the final size (growth stage 3.50, Boyes *et al.*, 2001), III) “mature”, defined as expanded leaves where the growth stage is 75% of final size (growth stage 3.70, Boyes *et al.*, 2001), and IV) “old”, referred to cotyledon or leaves with visible onset of senescence.

The AO activity in various vegetative tissues showed a similar trend when expressed on a FW or protein basis (Figure 5-1A and B). Young leaves had the highest activity compared to intermediate, mature and old leaves. The AO activity between intermediate and mature leaves was not significantly different. The lowest AO activity was found in old leaves. Total protein content as quantified by the Bradford method decreased in the following order: young and intermediate leaves > mature leaves > old leaves (Figure 5-1C).

To assess if different AO activities were present within a single leaf, fully expanded mature leaves (growth stage 3.70, Boyes *et al.*, 2001) of 6-week-old WT *A. thaliana* were separated into three equal portions (Figure 5-2D). The AO activity when expressed in both ways, decreased in the following order: leaf base > mid leaf > leaf tip (Figure 5-2A and B). There was no significant difference in the total protein content of these leaf parts (Figure 5-2C).

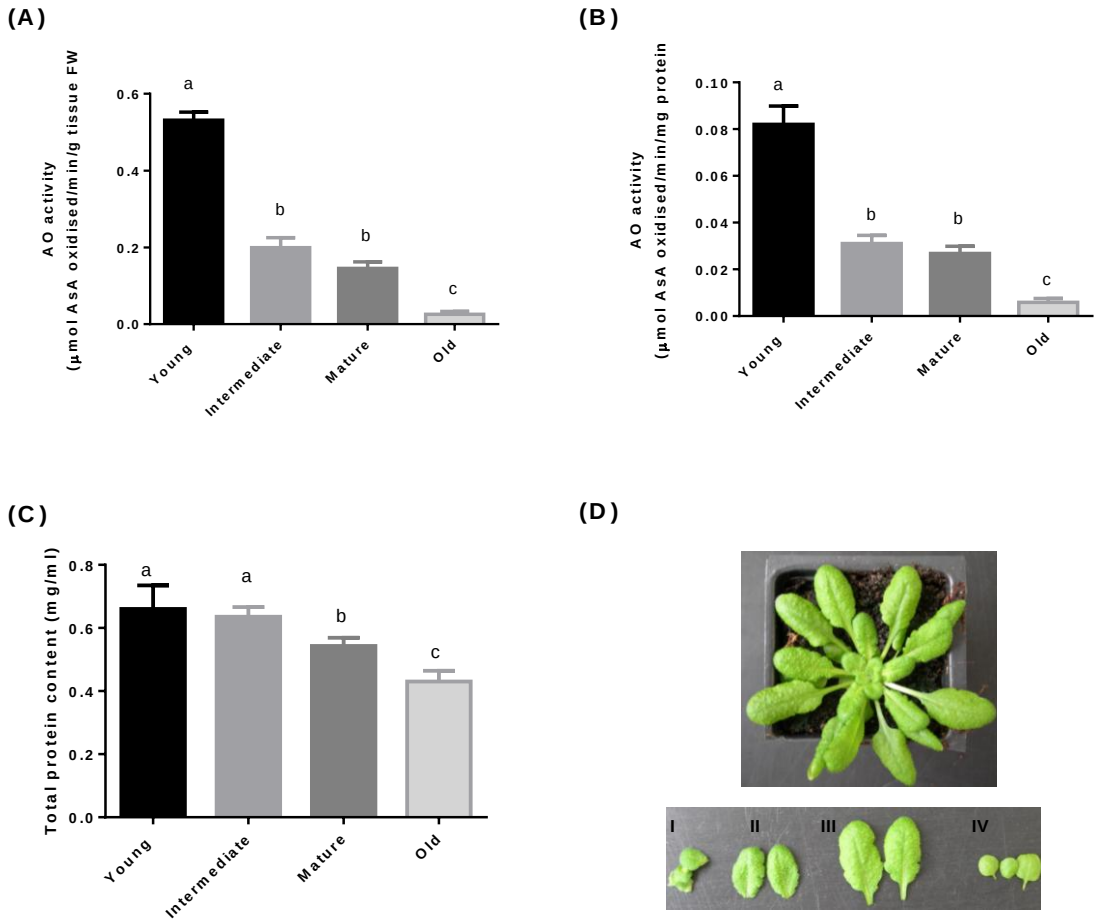

Figure 5-1: Ionically-bound cell wall AO activity in vegetative tissues of 6-week-old WT *A. thaliana*. The activity was expressed on a fresh weight **(A)** and protein **(B)** basis, respectively. **(C)** Protein concentration in tissue extracts (mg ml^{-1}). Due to varying amount of tissue extracted these values cannot be directly compared to enzyme activity data in A and B. **(D)** Picture of a 6-week-old WT plant during vegetative growth stage and the representative leaves for each stage: **(I)** young, **(II)** intermediate, **(III)** mature and **(IV)** old. Values are mean ± SEM, n = 5. Different letters above the bars denote the values are significantly different using one way ANOVA and Tukey tests ($p<0.05$). Values bearing the same letter are not significantly different from each other.

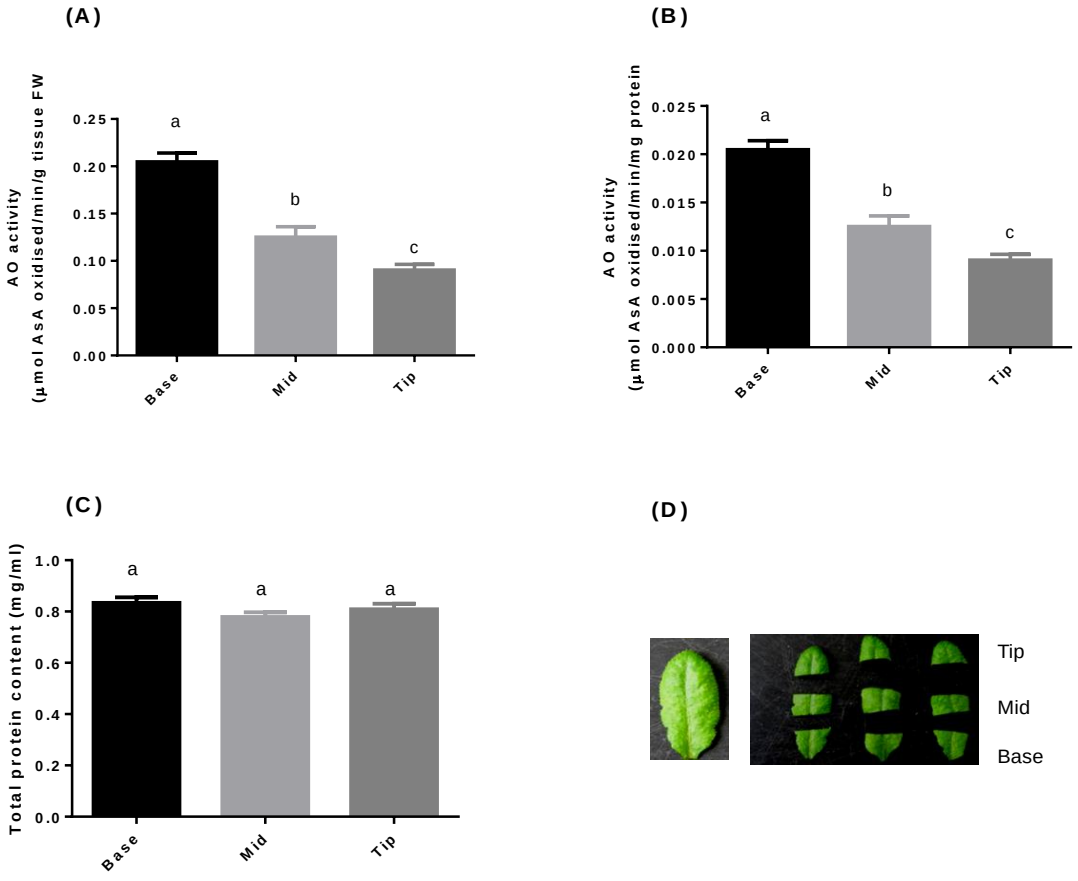

Figure 5-2: Ionically-bound cell wall AO activity in various parts (base, mid and tip) of a mature leaf. The activity was expressed on a fresh weight **(A)** and protein **(B)** basis, respectively. **(C)** Protein concentration in tissue extracts (mg ml^{-1}). Due to varying amount of tissue extracted these values cannot be directly compared to enzyme activity data in A and B. **(D)** Picture of various leaf parts of a mature leaf from 6-week-old WT plants during vegetative growth stage. Values are mean ± SEM, n = 6. Different letters above the bars denote the values are significantly different using one way ANOVA and Tukey tests ($p<0.05$). Values bearing the same letter are not significantly different from each other.

5.2.2. Ionically-bound cell wall AO activity in various tissues of WT *A. thaliana* during reproductive growth stage

At the vegetative stage of *A. thaliana*, the youngest leaf and the actively growing region of mature leaf showed the highest AO activity which decreased during progression to maturity (section 5.2.1.). When rosette growth is complete, *A. thaliana* proceeds to the reproductive stage eventually and so more resources are allocated to reproductive organs. To assess if AO activity corresponds to growing reproductive tissues, various tissues (rosette leaf, cauline leaf, flowers and main inflorescence stem) of 6-week-old WT *A. thaliana* (growth stage 6.50, Boyes *et al.*, 2001), grown under unstressed normal long day light regime (16 hrs light, 8 hrs dark) were harvested to study ionically-bound cell wall AO activity (Figure 5-3D). Flowers had higher activity than rosette leaf, cauline leaf and main inflorescence stem when AO activity expressed on a FW or protein basis (Figure 5-3A and B). Rosette leaf, cauline leaf and flowers shared similar protein content (Figure 5-3C) except inflorescence stem that had lower protein content. AO in flower buds and open flowers were extracted and assayed separately in order to assess the effect of developmental differences in the AO activity of flowers. As shown in Figure 5-4, flower buds had higher AO activity and total protein content than open flowers.

Since flowers had higher AO activity than other tissues at reproductive stage, AO activity of individual floral organs (Figure 5-5D) was assessed to examine which organ contributed to the highest AO activity in flowers. Petals and carpels had higher AO activity (expressed on a FW basis) compared to sepals and stamens (Figure 5-5A). The AO activity between petals and carpels and also between sepals and stamens was not significantly different. When AO activity

was expressed on a protein basis, the activity decreased in the following order: petals > carpels > sepals and stamens (Figure 5-5B). This discrepancy was attributed by the difference in the total protein content of these floral organs, where carpels had the highest protein level, followed by sepals with intermediate protein level; petals and stamens had the lowest and similar protein content (Figure 5-5C).

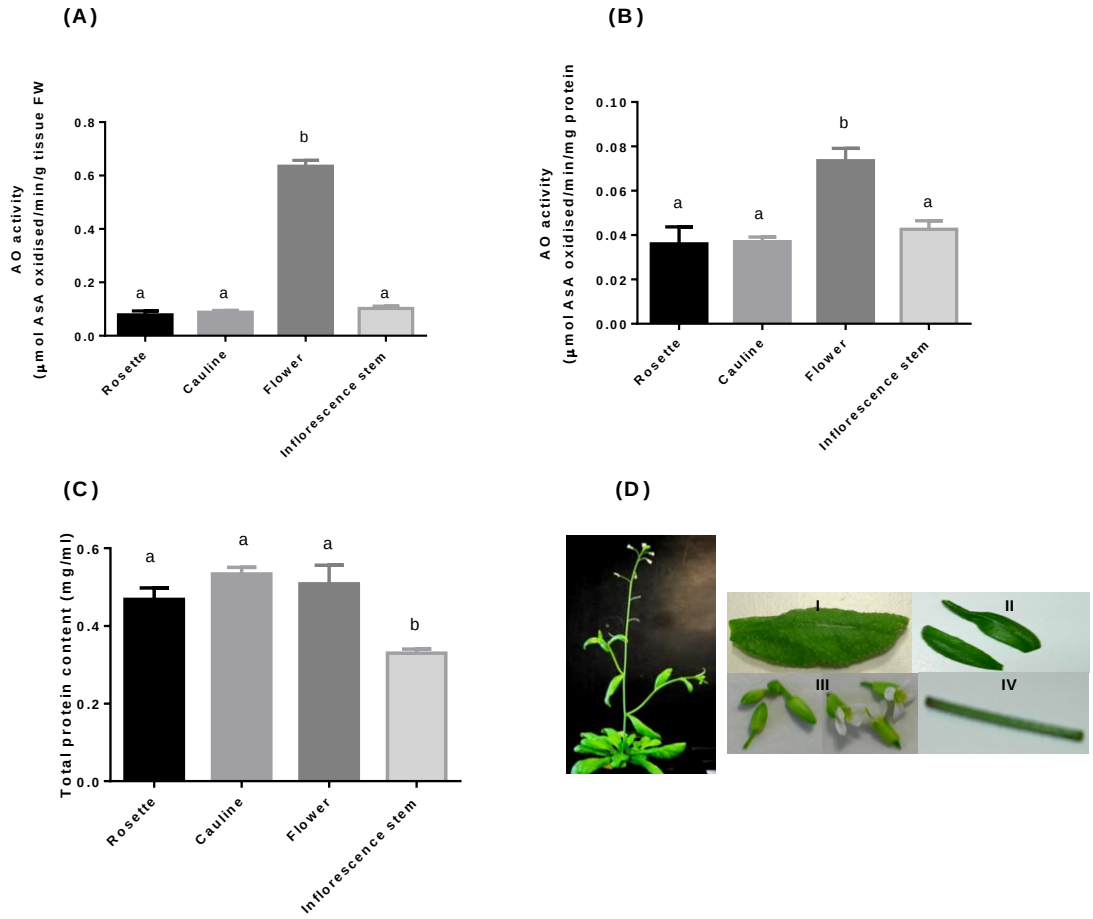

Figure 5-3: Ionically-bound cell wall AO activity in reproductive tissues of 6-week-old WT *A. thaliana*, grown under long day light regime (16 hrs light, 8hrs dark). The activity was expressed on a fresh weight **(A)** and protein **(B)** basis, respectively. **(C)** Protein concentration in tissue extracts (mg ml^{-1}). Due to varying amount of tissue extracted these values cannot be directly compared to enzyme activity data in A and B. **(D)** Picture of a 6-week-old WT plant during reproductive growth stage and the representative image of tissues harvested: **(I)** rosette leaf, **(II)** cauline leaves, **(III)** flowers and **(IV)** inflorescence stem. Values are mean ± SEM, n = 4. Different letters above the bars denote the values are significantly different using one way ANOVA and Tukey tests ($p<0.05$). Values bearing the same letter are not significantly different from each other.

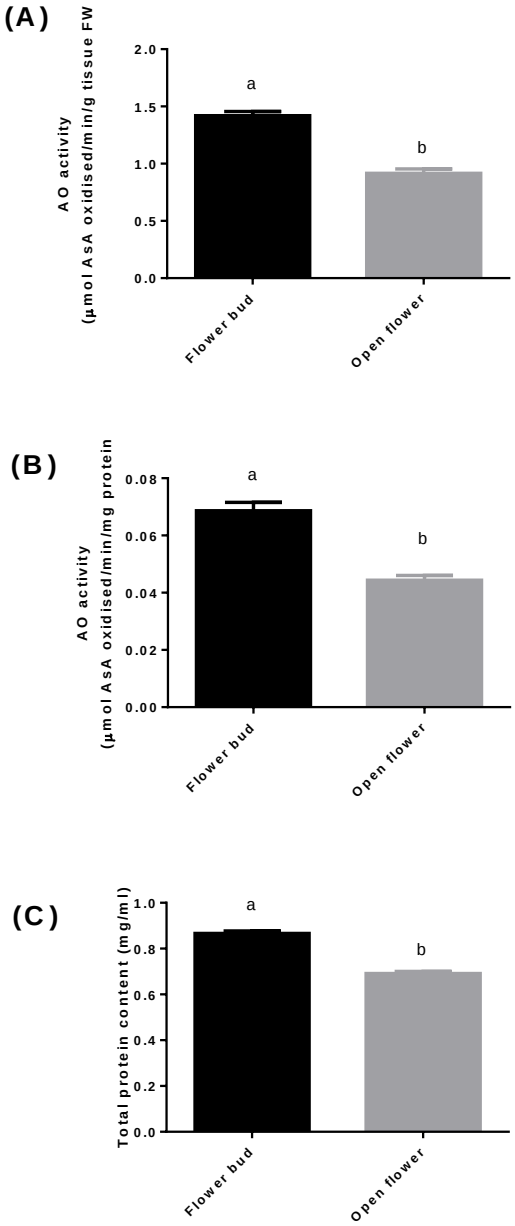

Figure 5-4: Ionically-bound cell wall AO activity between flower buds and open flowers in WT *A. thaliana*. 6-week-old plants grown under long day light regime (16 hrs light, 8 hrs dark) were used. The activity was expressed on a fresh weight **(A)** and protein **(B)** basis, respectively. **(C)** Protein concentration in tissue extracts (mg ml^{-1}). Due to varying amount of tissue extracted these values cannot be directly compared to enzyme activity data in A and B. Values are mean ± SEM, n = 4. Different letters above the bars denote the values are significantly different using a two-tailed *t*-test ($p<0.05$).

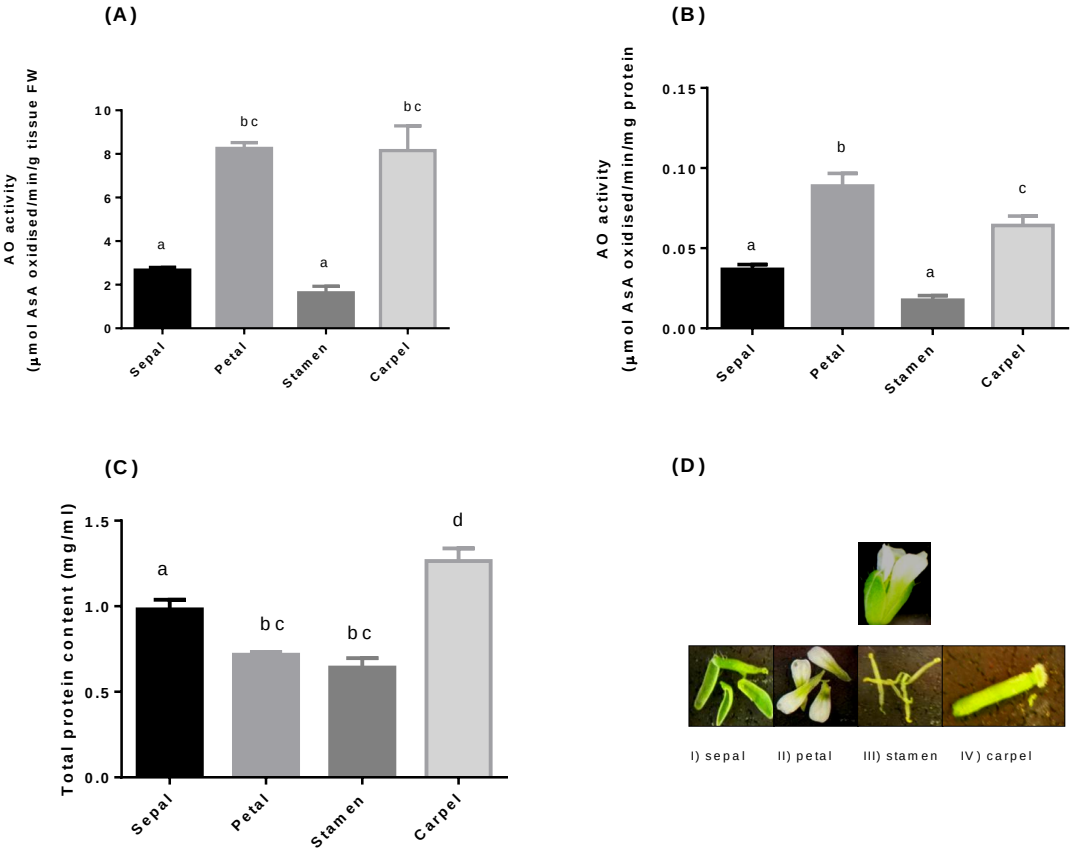

Figure 5-5: Ionically-bound cell wall AO activity in floral organs of WT *A. thaliana*. The activity was expressed on a fresh weight **(A)** and protein **(B)** basis, respectively. **(C)** Protein concentration in tissue extracts (mg ml^{-1}). Due to varying amount of tissue extracted these values cannot be directly compared to enzyme activity data in A and B. **(D)** Picture of a flower from 6-week-old WT plant, grown under long day light regime (16 hrs light, 8 hrs dark) and the representative image of the floral organs harvested: **(I)** sepals, **(II)** petals, **(III)** stamens and **(IV)** carpels. Values are mean ± SEM, n = 4. Different letters above the bars denote the values are significantly different using one way ANOVA and Tukey tests ($p<0.05$). Values bearing the same letter are not significantly different from each other.

5.2.3. *AO* gene expression in various tissues of WT *A. thaliana* during vegetative and reproductive growth stages

RT-PCR was carried out to assess individual *AO* gene expression in various tissues of WT *A. thaliana* during vegetative and reproductive growth stages. The primers and PCR conditions are detailed in section 2.5.5.2. The PCR products were subjected to agarose gel electrophoresis and visualised after ethidium bromide staining. The band intensity of these PCR products was quantified using Image J software to provide a semi-quantitative measurement of gene expression level. The gene expression of these tissues obtained from RT-PCR was compared to the expression level from the microarray database, eFP browser (Winter *et al.*, 2007).

During the vegetative stage, each *AO* gene had a distinct expression pattern in young, intermediate and mature leaves. Increased *AO1* expression was associated with increased leaf age: young < intermediate < mature (Figure 5-6A and 5-6D); *AO2* had the highest expression in young leaves but the expression of intermediate and mature leaves was undifferentiated (Figure 5-6B and 5-6E); *AO3* expression was higher in intermediate leaves and mature leaves than young leaves (Figure 5-6C and 5-6F).

AO gene expression in young, intermediate and mature leaves performed was compared with the expression of rosette leaf 2, rosette leaf 4 and rosette leaf 6 sourced from eFP browser (Figure 5-6G to I). *AO2* expression in rosette leaf 2, rosette leaf 4 and rosette leaf 6 obtained from eFP browser (Figure 5-6H) showed a positive correlation to the *AO2* expression in young, intermediate and mature leaves obtained from RT-PCR (Figure 5-6B and 5-6E). By contrast, *AO1* and *AO3* expressions from eFP browser (Figure 5-6G and I) were partially

correlated to the gene expression obtained in RT-PCR (Figure 5-6A and C). *AO2* gene expression showed a positive correlation with AO activity (i.e. high activity in young leaf and similar activity in intermediate and mature leaf, Figure 5-1) but not *AO1* and *AO3*.

During the reproductive stage, rosette and cauline leaves had higher *AO1* expression than the flowers (Figure 5-7A and 5-7B). *AO2* expression was fairly similar across tissues (Figure 5-7B and 5-7E). Strong expression of the *AO3* gene was found in flowers compared with rosette and cauline leaves (Figure 5-7C and 5-7F). The expression of *AO* gene in rosette leaf, cauline leaf and flowers was compared with the expression of rosette leaf 8, cauline leaf and flower stage 12 sourced from eFP browser. *AO1* (Figure 5-7A and 5-7D) expression obtained from RT-PCR were similar to the expression from eFP browser (Figure 5-7 G). *AO3* expression (Figure 5-7C and 5-7F) showed a positive correlation with AO activity (i.e. high activity in flowers and similar activity in rosette and cauline leaves, Figure 5-3) but not *AO1* and *AO2*.

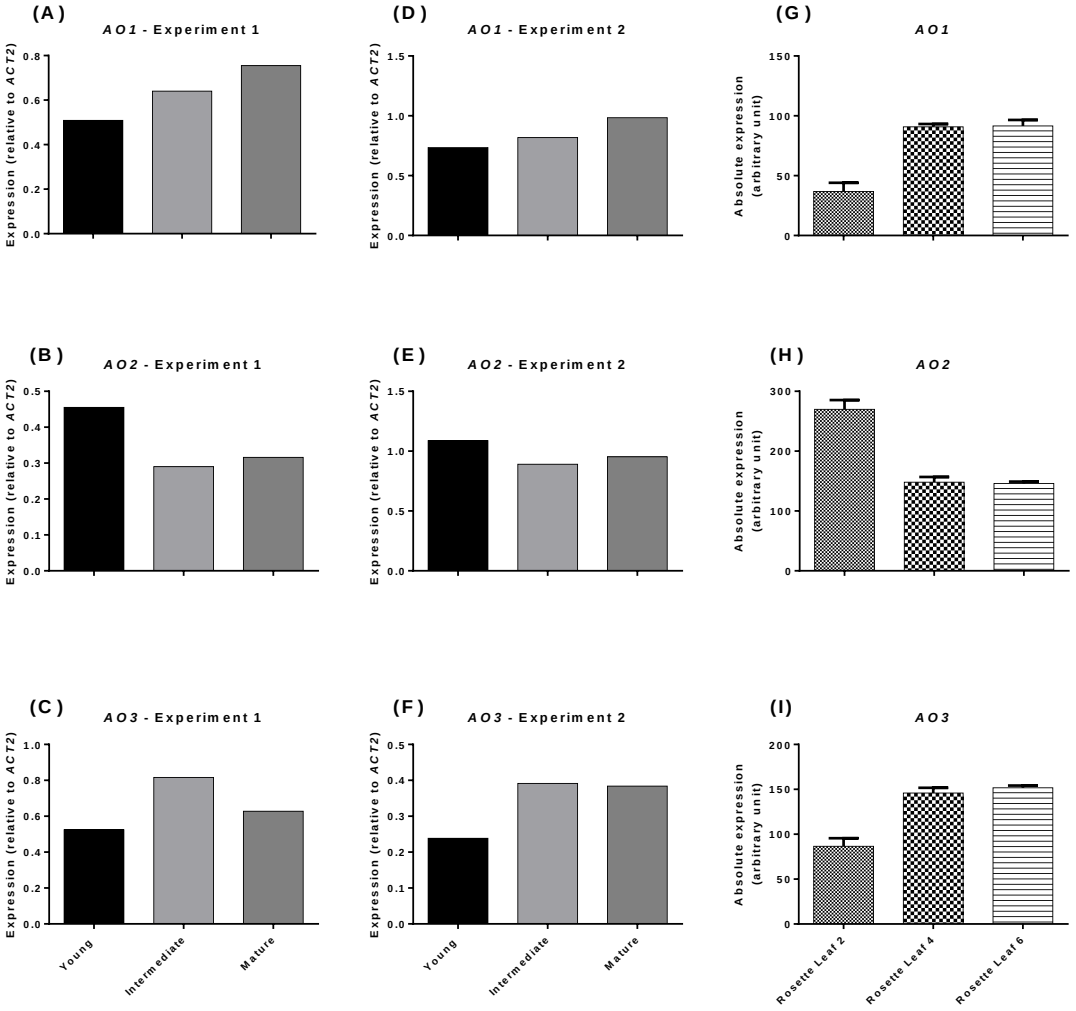

Figure 5-6: Relative transcript levels of *AO* genes in vegetative tissues of WT *A. thaliana*. Vegetative tissues were pooled from four independent 6-week-old plants. The transcript levels were determined by semi-quantitative RT-PCR, where staining intensities of PCR products **(A)** *AO1*, **(B)** *AO2* and **(C)** *AO3* were quantified using Image J software and normalised against *ACT2*. The result for second independent experiment is given **(D−F)**. *AO1*, *AO2* and *AO3* expression in designated vegetative tissues were obtained from the eFP browser microarray database **(G−I)**.

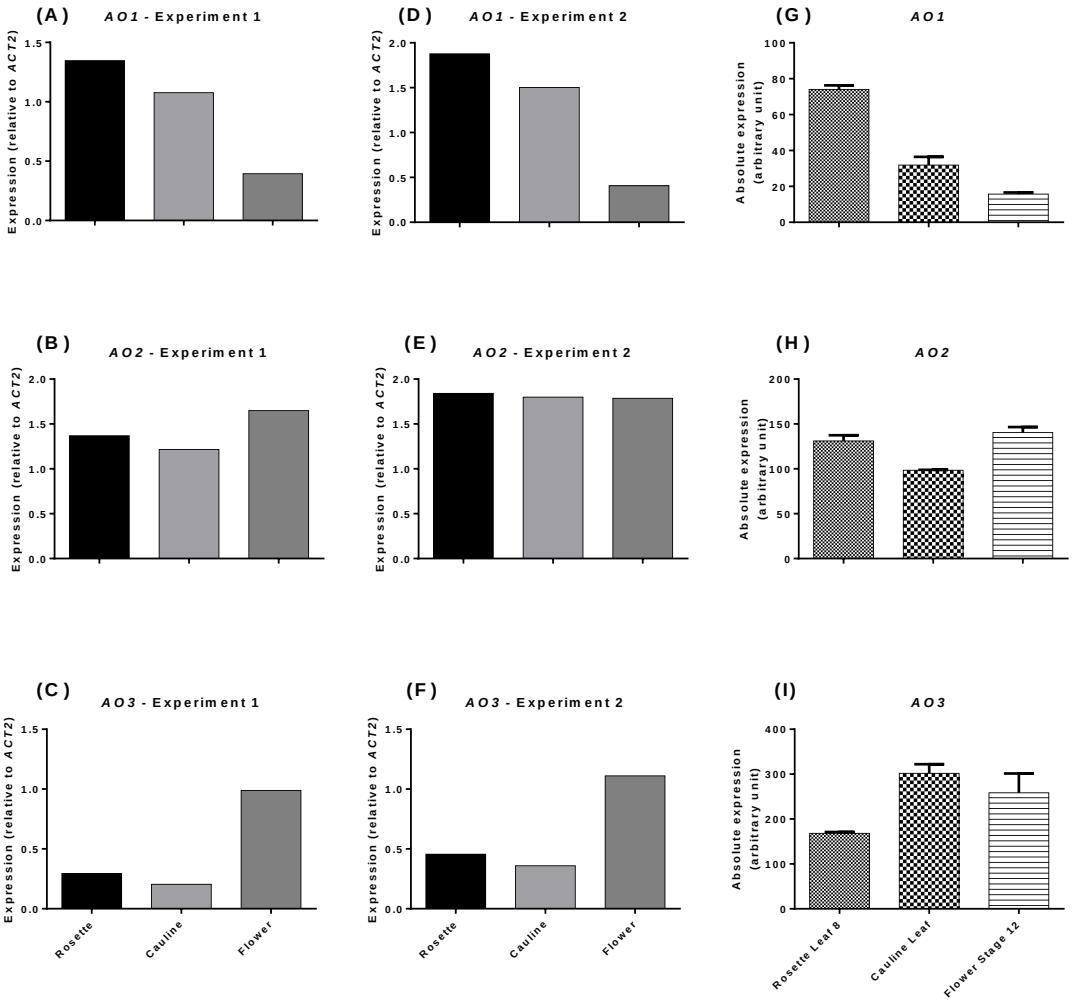

Figure 5-7: Relative transcript levels of *AO* genes in reproductive tissues of WT *A. thaliana*. Reproductive tissues were pooled from four independent 6-week-old plants, grown under long day light regime (16 hrs light, 8 hrs dark). The transcript levels were determined by semi-quantitative RT-PCR, where staining intensities of PCR products **(A)** *AO1*, **(B)** *AO2* and **(C)** *AO3* were quantified using Image J software and normalised against *ACT2*. The result for second independent experiment is given **(D−F)**. *AO1*, *AO2* and *AO3* expression in designated reproductive tissues were obtained from the eFP browser microarray database **(G−I)**.

5.2.4. AsA concentrations in various tissues of WT *A. thaliana* during vegetative and reproductive growth stages

Samples used in the AsA extraction and analyses were similar to those used in the studies of AO activity. Whole leaf AsA was extracted from various leaves of WT *A. thaliana* during the vegetative stage (young, intermediate, mature and old); meanwhile for reproductive stage: rosette leaf, cauline leaf, flowers (open flowers and buds) and main inflorescence stem were extracted and assayed.

During the vegetative stage, young and intermediate leaves had greater concentrations of reduced AsA than mature and old leaves. This contributed to higher total AsA pool (AsA + DHA) in these leaves than the mature and old leaves. The difference in the AsA pool and the reduced AsA concentration of young and intermediate leaves was not statistically significant. Old leaves had the lowest AsA pool and reduced AsA concentration. The levels of DHA were similar among the four types of tissues (Figure 5-8A).

During reproductive stage, flowers had the highest reduced AsA and DHA levels than the rosette leaf, cauline leaf and main inflorescence stem. The total AsA pool in flowers was significantly greater than in rosette leaf, cauline leaf and main inflorescence stem. Similar levels of reduced AsA and DHA were observed in the rosette leaf, cauline leaf and main inflorescence stem (Figure 5-8B).

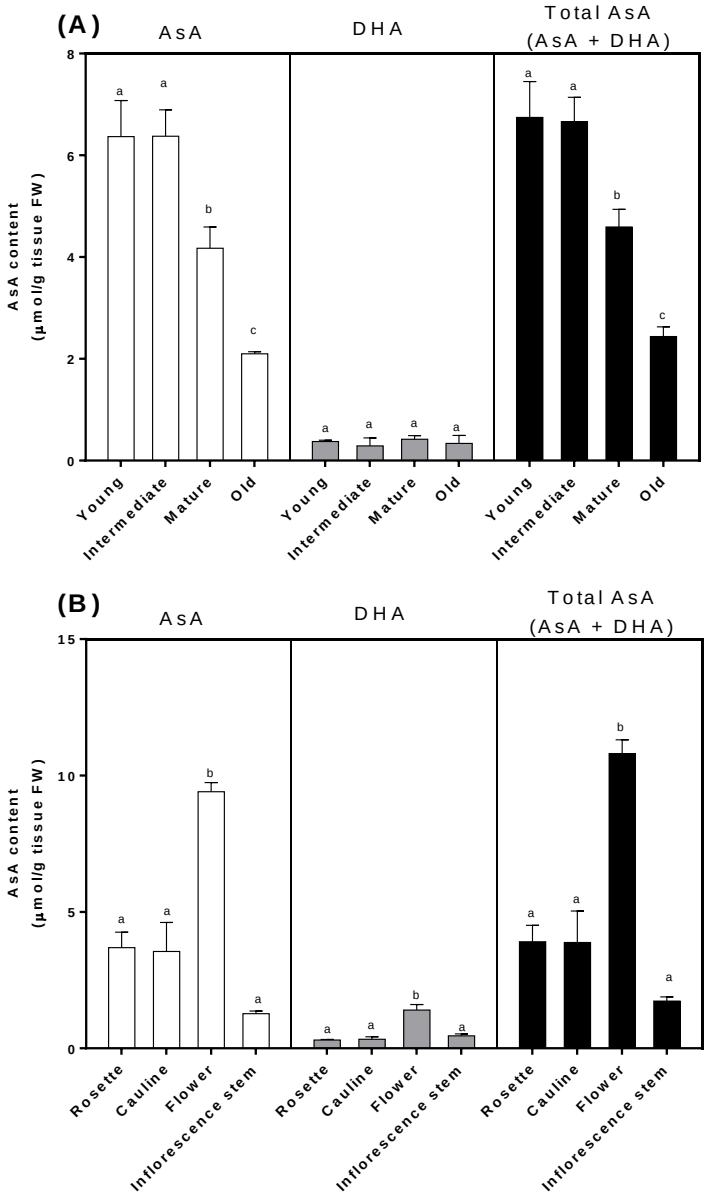

Figure 5-8: AsA concentrations in various tissues of WT *A. thaliana* during vegetative and reproductive growth stages. **(A)** Whole tissue reduced AsA, DHA and total AsA pool from young, intermediate, mature and old leaves of 6-week-old WT plants during the vegetative growth stage. **(B)** Whole tissue reduced AsA, DHA and total AsA pool from rosette leaf, cauline leaf, flowers and inflorescence stem of 6-week-old WT plants during the reproductive growth stage. Values are mean ± SEM, n = 4. Different letters above the bars denote the values are significantly different using one way ANOVA and Tukey tests ($p<0.05$). Values bearing the same letter are not significantly different from each other. Statistical analyses for reduced AsA, DHA and total AsA data were performed separately.

5.2.5. *AO* gene expression in *AO* T-DNA insertion mutants

The results obtained in sections 5.2.1. and 5.2.2. as well as findings reported in the literature (see Introduction) suggest that high AO activity is present in growing tissue. As AO activity is potentially associated with plant growth, *AO* T-DNA insertion mutants were obtained from NASC to assess the effect of *AO*-deficiency in the growth and development of *A. thaliana*. These mutants (*ao1, ao2, ao3, ao1ao3*) were prepared as described in Chapter 3.

The gene expression of the *ao1*, *ao2*, *ao3* and *ao1ao3* T-DNA insertion mutants was assessed by RT-PCR from fully expanded leaves of a pool of 4 plants (Figure 5-9). The primers and PCR conditions are detailed in section 2.5.5.2. All three *AO* genes were detected in WT plants. In the *ao1* mutant, the *AO1* gene expression was undetectable; while in the *ao3* mutant, the *AO3* gene expression was undetectable. The expression of *AO1* and *AO3* genes were undetectable in the *ao1ao3* double mutant (Figure 5-9B). This result suggests that T-DNA insertion effectively disrupted *AO1* and *AO3* expression in *ao1* and *ao3* mutants respectively. An *ao1ao3* double mutant, developed from the crossing of *ao1* and *ao3* had both *AO1* and *AO3* expressions disrupted. Single *AO* gene knockout in *ao1* and *ao3* mutants did not affect expression levels of the other two *AO* genes. *AO2* expression was fairy similar between *ao1ao3* and all other lines, and no compensatory effects were seen from *AO2*, although two copies of the *AO* gene in this double mutant were disrupted (Figure 5-9B). Intriguingly, the *ao2* mutant showed similar transcript abundance to other genotypes, suggesting *ao2* is neither a knockdown nor knockout mutant (Figure 5-9A). As a result, *ao2* was not included for all the following experiments. Two separate gel images are shown in Figure 5-9, because the *ao1ao3* double

mutant was only obtained after the *ao2* mutant was excluded for all the following experiments.

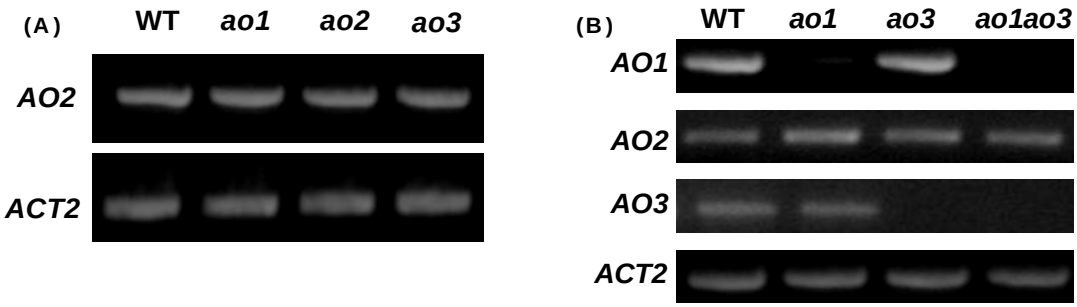

Figure 5-9: Transcript levels of *AO* genes in leaves of WT and *AO* T-DNA insertion mutants. Leaves were pooled from four independent 6-week-old plants. Transcript levels were determined by semi-quantitative RT-PCR. Actin (*ACT2*) was used as the internal control. **(A)** The expression of *AO2* gene in WT, *ao1*, *ao2* and *ao3*. **(B)** The expression of *AO1*, *AO2* and *AO3* in WT, *ao1*, *ao3* and *ao1ao3*. This experiment was repeated two times and similar results were obtained.

5.2.6. Ionically-bound cell wall AO activity in *AO* T-DNA insertion mutants

The AO activity in the leaves and the flowers of *ao1*, *ao3*, and *ao1ao3* mutants under unstressed normal growth conditions were assessed (Figure 5-10). *ao2* was not included for all the following experiments because gene expression analysis (section 5.2.5) showed that it is not a knockout/knockdown mutant. AO activity was expressed on a FW or protein basis. Similar results obtained when AO activity expressed in either way. In leaves, *ao1* had similar activity to the WT, but *ao3* and *ao1ao3* had only 20% of the AO activity of WT and *ao1* (Figure 5-10A and B). Likewise in flowers, *ao1* showed similar AO activity to WT and both *ao3* and *ao1ao3* had very low AO activity, which was about 10% of WT and *ao1* (Figure 5-10D and E). Higher total protein content was found in the flowers (Figure 5-10F) compared to leaves (Figure 5-10C), but there was no significant difference between the total protein content of WT and *ao* mutants.

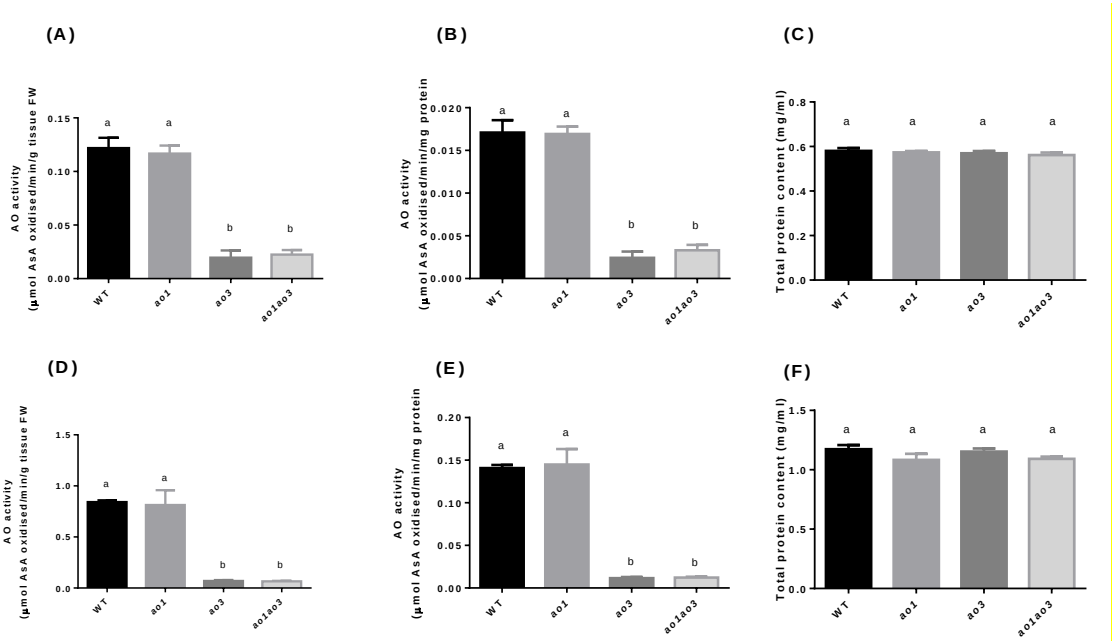

Figure 5-10: Ionically-bound cell wall AO activity in leaves and flowers of WT and *AO* T-DNA insertion mutants. AO activity in the fully expanded leaves of six-week-old *A. thaliana* WT and *ao1*, *ao3*, *ao1ao3* mutants, expressed on a fresh weight **(A)** and protein **(B)** basis, respectively. AO activity in the open flowers of six-week-old *A. thaliana* WT and *ao1*, *ao3*, *ao1ao3* mutants, grown under long day light regime (16 hrs light, 8 hrs dark), expressed on a fresh weight **(D)** and protein **(E)** basis, respectively. Protein concentration in leaves **(C)** and flowers **(F)** extracts (mg ml^{-1}). Due to varying amount of tissue extracted these values cannot be directly compared to enzyme activity data in A, B, D and E. Values are mean ± SEM, n = 4 to 6. Different letters above the bars denote the values are significantly different using one way ANOVA and Tukey tests ($p<0.001$). Values bearing the same letter are not significantly different from each other.

5.2.7. The phenotype of *AO* T-DNA insertion mutants

Phenotypes of *ao1*, *ao3* and *ao1ao3* mutants were compared with the WT to assess the effect of AO-deficiency in *A. thaliana* growth and development. Under unstressed normal growth conditions, there was no clear morphology difference between WT and *ao* mutants at vegetative (Figure 5-11A) and reproductive growth stages (Figure 5-11B). Growth kinetics of *ao* mutants and WT were compared to assess if there is any difference in leaf expansion rate. The absolute leaf expansion rate (AER) and total absolute leaf area (ATLA) were quantified in plants grown in short day light (8 hrs light, 16 hrs dark) under unstressed normal conditions, from 19 days after sowing (DAS) until 29 DAS. The AER and ATLA were similar in all lines (Figure 5-12). Besides, the seed germination rate, total number of rosette leaves, the rate of inflorescence emergence and the rate of flower initiation were similar between *ao* mutants and WT (Table 5-1).

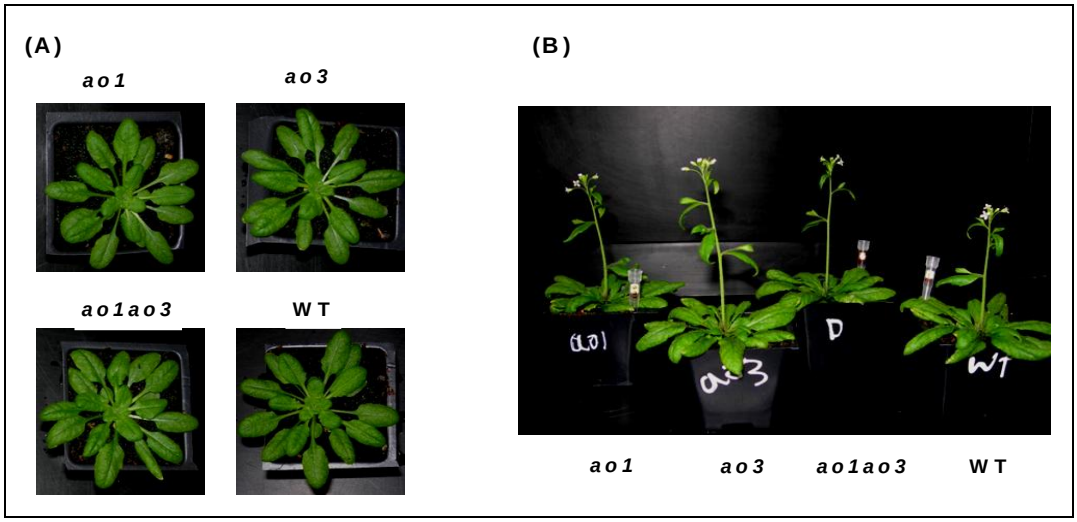

Figure 5-11: Phenotype of WT and *AO* T-DNA insertion mutants. 6-week-old plants during vegetative stage grown under short day light regime (8 hrs light, 16 hrs dark) **(A)** and 6-week-old plants during reproductive stage grown under long day light regime (16 hrs light, 8 hrs dark) **(B)**.

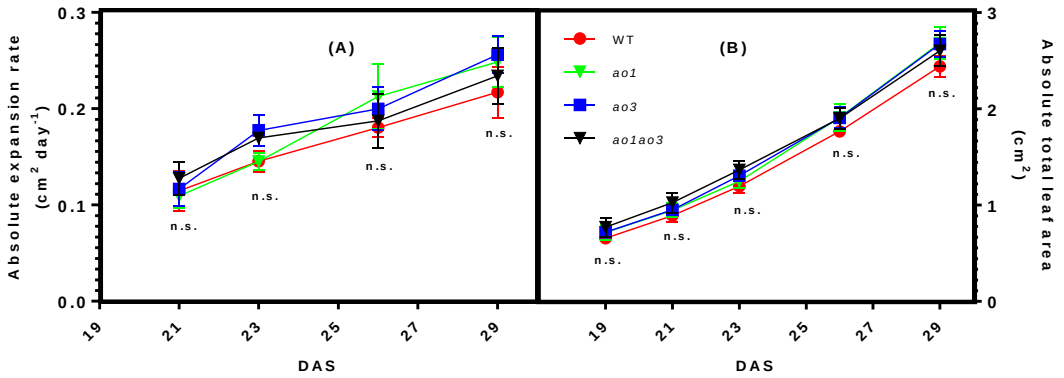

Figure 5-12: Leaf growth of WT and *AO* T-DNA insertion mutants under SD growth conditions (8 hrs light, 16 hrs dark). Absolute leaf expansion rate **(A)** and absolute total leaf area **(B)** were measured from 19 to 29 DAS. Values are mean ± SEM, N = 4, n = 6, where N = number of independent experiments, n = number of biological replicates for each line per independent experiment. Data were analysed with one way ANOVA and Tukey tests, indicated no significant (n.s.) differences between genotypes. SD, short day; DAS, days after sowing.

Table 5-1: Growth parameters of WT and *AO* T-DNA insertion mutants. Values are mean ± SEM (n = 12). Data were analysed with one way ANOVA and Tukey tests, indicated no significant (n.s.) differences between genotypes. DAS, days after sowing.

[1]Phenotype	WT	*ao1*	*ao3*	*ao1ao3*
Germination (%)	96.88 ± 1.88 ^{ns}	92.19 ± 3.00 ^{ns}	96.88 ± 1.80 ^{ns}	95.31 ± 3.00 ^{ns}
Total number of rosette leaves / plant	17.00 ± 0.60 ^{ns}	16.75 ± 0.41 ^{ns}	16.38 ± 0.38 ^{ns}	17.50 ± 0.53 ^{ns}
Inflorescence emergence (DAS)	32.13 ± 1.13 ^{ns}	31.58 ± 0.80 ^{ns}	32.58 ± 1.13 ^{ns}	30.00 ± 0.95 ^{ns}
Flower initiation (DAS)	35.88 ± 1.13 ^{ns}	34.17 ± 0.80 ^{ns}	34.75 ± 1.04 ^{ns}	33.17 ± 0.89 ^{ns}

[1] Germination was percentage of plate grown seeds that showed cotyledons from total seeds sown. Total number of rosette leaves was observed on 6-week-old plants grown in a short day light regime (8 hrs light, 16 hrs dark). Inflorescence emergence and flower initiation were observed on plants grown in a long day light regime (16 hrs light, 8 hrs dark).

5.2.8. AsA concentrations in *AO* T-DNA insertion mutants

AO is a cell wall localised AsA oxidising enzyme, so the effect of AO perturbation on whole leaf AsA and apolastic AsA concentrations were examined in the *ao* mutants. Fully expanded leaves in the middle of the rosette of 6-week-old WT and *ao* mutants were extracted and assayed for whole leaf AsA concentrations. The whole leaf DHA concentration of WT and *ao* mutants was significantly lower than the reduced AsA concentration (Figure 5-13A). This contributed to a high AsA redox state (ratio of reduced AsA to total AsA) in all lines (Figure 5-13B). However, the whole leaf reduced AsA, DHA, total AsA pool (AsA + DHA) and the AsA redox state between WT and *ao* mutants were not significantly different under unstressed normal growth conditions (Figure 5-13).

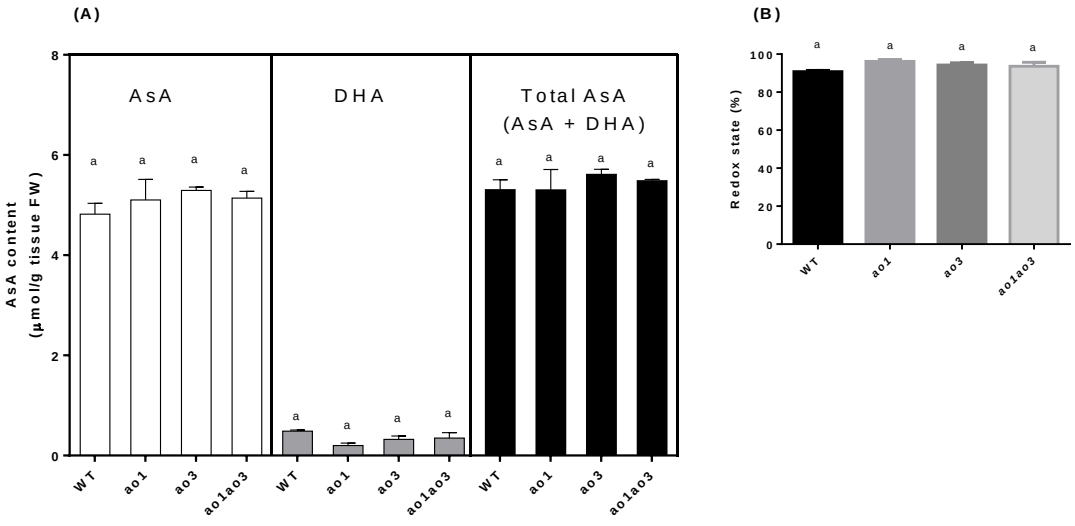

Figure 5-13: Whole leaf AsA concentrations in WT and *AO* T-DNA insertion mutants. Fully expanded leaves from 6-week-old plants were used. **(A)** Reduced AsA, DHA and total AsA pool of WT, *ao1*, *ao3* and *ao1ao3*. **(B)** Percent redox state (ratio of reduced to total AsA) of WT and *ao* mutants. Values are mean ± SEM, n = 4. Different letters above the bars denote the values are significantly different using one way ANOVA and Tukey tests ($p<0.001$). Values bearing the same letter are not significantly different from each other. Statistical analyses for reduced AsA, DHA and total AsA data were performed separately.

Apoplastic AsA concentrations were determined from the same plants as used for whole leaf AsA analysis. Entire rosette leaves from a pool of two plants (6-week-old) were used for each extraction. The apoplastic fluid recovered from vacuum infiltration (known as the yield of apoplastic fluid) was similar across all lines (Figure 5-14C). The total apoplastic AsA pool (AsA + DHA) between WT and *ao* mutants were not significantly different. *ao3* and *ao1ao3* mutants had higher reduced AsA concentration than *ao1* and WT, but the apoplastic DHA concentrations were similar across all lines (Figure 5-14A). As shown in Figure 5-14B, *ao3* and *ao1ao3* mutants had higher AsA redox state (ratio of reduced AsA to total AsA) in comparison with *ao1* and WT.

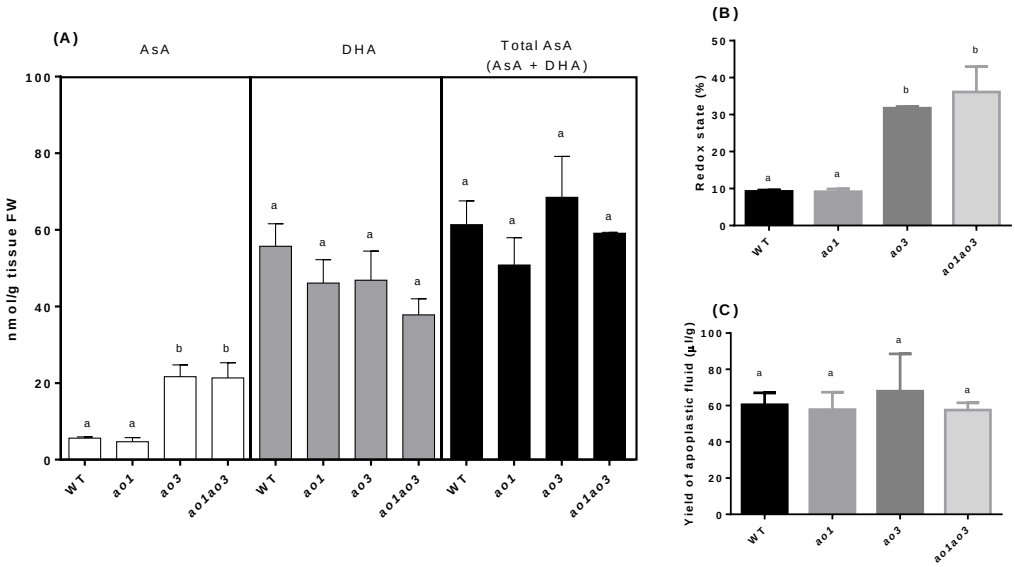

Figure 5-14: Apoplastic AsA concentrations in WT and *AO* T-DNA insertion mutants. All rosette leaves from 6-week-old plants were used. **(A)** Reduced AsA, DHA and total AsA pool of WT, *ao1*, *ao3* and *ao1ao3*. **(B)** Percent redox state (ratio of reduced to total AsA) of WT and *ao* mutants. **(C)** Yield of apoplastic fluid after vacuum infiltration. Values are mean ± SEM, N = 2, n = 2, where N = number of biological replicate; n = pool of plants per biological replicate. Different letters above the bars denote the values are significantly different using one way ANOVA and Tukey tests ($p<0.05$). Values bearing the same letter are not significantly different from each other. Statistical analyses for reduced AsA, DHA and total AsA data were performed separately.

5.2.9. Histological analyses of *AO* T-DNA insertion mutants

Histological characterisation was performed to examine if cell development was affected by AO-deficiency. The representative images of palisade mesophyll cells obtained from fully expanded leaves at the middle rosette of 40 DAS plants are shown in Figure 5-15, and the cell morphology was similar between WT and the *ao* mutants. The cell area, cell width and cell length of *ao* mutants were not statistically different from the WT, although the double mutant, *ao1ao3* showed an increase (14.8%) in cell area compared to WT. The total cell number per leaf between WT and the *ao* mutants were similar (Table 5-2).

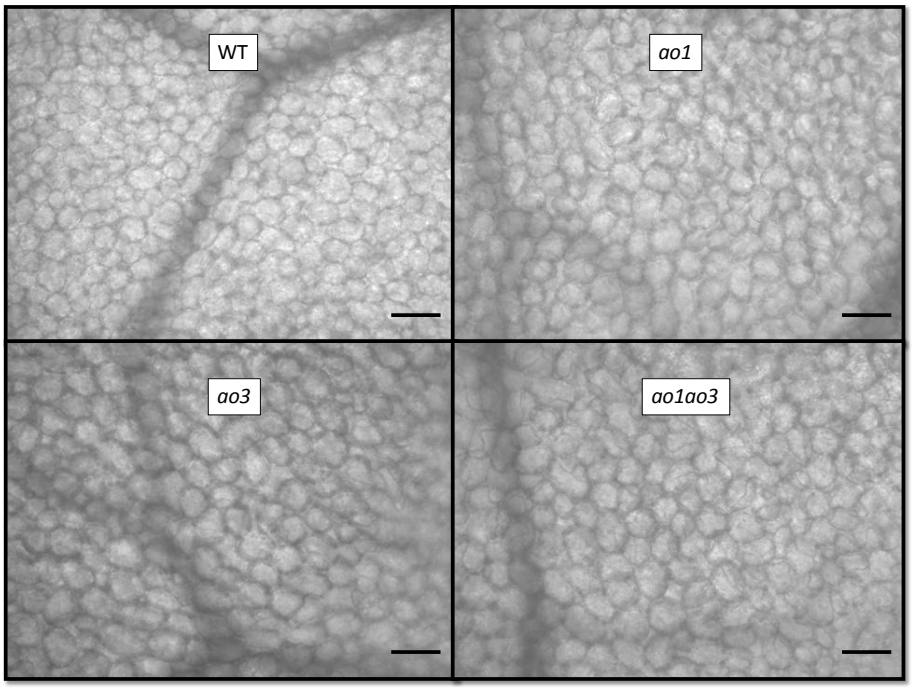

Figure 5-15: Adaxial palisade mesophyll cells from the middle lamina of WT, *ao1*, *ao3* and *ao1ao3* leaves. Fully expanded leaves of the 40 DAS plants grown under long day light regime (16 hrs light, 8 hrs dark) were used. Scale bars = 50 µm. DAS, days after sowing.

Table 5-2: Dimensions of adaxial palisade mesophyll cells in WT and *AO* T-DNA insertion mutants. Fully expanded leaves of the 40 DAS plants grown under long day light regime (16 hrs light, 8 hrs dark) were used. 6 biological replicates were used for each genotype, 40 cells at the middle lamina from a leaf of each replicate were measured and averaged. Values are mean ± SEM, ns denotes the values are not significantly different from WT using one way ANOVA and Tukey tests ($p<0.05$).

Genotype	Cell area (μm^2)	Cell width (µm)	Cell length (µm)	[1]Cell number /unit area (0.09 mm^2)	[2]Estimated cell density (cells/mm^2)	Leaf area (mm^2)	[3]Estimated total number of cells/leaf
WT	1052 ± 44.99	27.66 ± 0.97	41.48 ± 0.94	79 ± 5	874 ± 53	85.55 ± 4.90	74781 ± 4504
ao1	1105 ± 73.71 [ns]	28.61 ± 1.21 [ns]	42.88 ± 1.74 [ns]	76 ± 6 [ns]	845 ± 63 [ns]	85.57 ± 3.86 [ns]	72255 ± 5423 [ns]
ao3	1148 ± 43.60 [ns]	29.07 ± 0.49 [ns]	44.66 ± 0.88 [ns]	79 ± 4 [ns]	872 ± 47 [ns]	88.22 ± 2.12 [ns]	76948 ± 4134 [ns]
ao1ao3	1208 ± 20.04 [ns]	31.02 ± 0.67 [ns]	45.08 ± 1.11 [ns]	78 ± 4 [ns]	870 ± 40 [ns]	83.35 ± 1.78 [ns]	72542 ± 3362 [ns]

[1] Cell number was counted on 300 µm × 300 µm sections (equivalent to 0.09 mm^2) within the microscopic images.
[2] Cell density was estimated by dividing the cell number by 0.09 mm^2.
[3] The total number of cells in a leaf was estimated by multiplying the estimated cell density to the leaf area.

5.2.10. Ionically-bound cell wall peroxidase activity in *AO* T-DNA insertion mutants

The peroxidase activity was measured to assess the effect of AO-deficiency on other cell wall components. The peroxidase from the ionically-bound cell wall fraction was assayed as described in Chapter 2 (section 2.9.3). Unless otherwise mentioned, peroxidase activity mentioned in this thesis refers to ionically-bound cell wall peroxidase activity. As in the AO assay, the peroxidase activity was expressed on a FW or protein basis. The peroxidase activity in *ao* mutants was not significantly different from the WT under unstressed normal growth conditions either expressed on a FW or protein basis (Figure 5-16A and B). Total protein content was similar across all lines (Figure 5-16C).

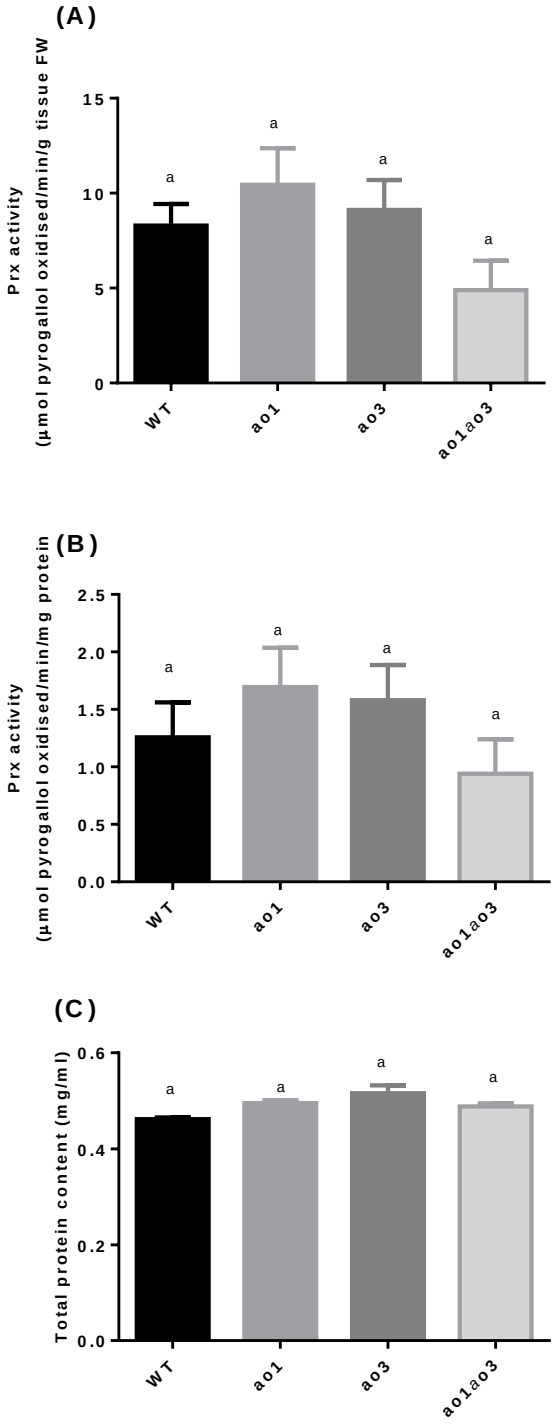

Figure 5-16: Ionically-bound cell wall peroxidase activity in the fully expanded leaves of six-week-old *A. thaliana* WT and *ao1*, *ao3*, *ao1ao3* mutants, expressed on a fresh weight **(A)** and protein **(B)** basis, respectively.

(C) Protein concentration in tissue extracts (mg ml^{-1}). Due to varying amount of tissue extracted these values cannot be directly compared to enzyme activity data in A and B. Values are mean ± SEM, n = 4. Different letters above the bars denote the values are significantly different using one way ANOVA and Tukey tests ($p<0.05$). Values bearing the same letter are not significantly different from each other.

5.2.11. AO activity in *amiR-AO* and *35S::AO3* transgenic lines

Despite the low AO activity present in *ao3* and *ao1ao3* mutants, the lack of growth phenotype had prompted me to develop additional *A. thaliana* transgenic lines, 1) by overexpressing the *AO3* gene and 2) by employing an amiRNA approach to silence all three *AO* genes. The establishment of these lines is described in Chapter 3. Results from the characterisation of *AO* T-DNA insertion mutants (section 5.2.6.) showed that *AO3* is the major contributor of AO activity in the leaves and the flowers of *A. thaliana*, so the *AO3* coding sequence was cloned and constitutively expressed under the control of the 35SCaMV promoter. An amiRNA construct (described in Chapter 3) was constructed (known as *amiR-AO* in this thesis), and was also cloned and placed under the control of the 35SCaMV promoter. Several homozygous T_3 *amiR-AO* and *35S::AO3* lines were isolated as described in Chapter 3. Six *amiR-AO* lines, referred to as lines 1.5, 3.6, 4.2, 6.5, 8.5, and 10.5 were chosen to screen for AO activity. It should be noted that *amiR-AO* line 4.2 and line 8.5 are multi-insertion lines (see Table 3-2). Four *35S::AO3* lines, referred to as lines 2.2, 3.3, 5.1 and 6.6 were chosen to screen for AO activity. As in previous results, the AO activity was expressed on a FW and protein basis.

Of six *amiR-AO* lines screened: lines 1.5, 4.2, and 10.5 showed similar AO activity to the WT when the activity expressed on a FW basis; line 6.5 had 3-fold lower AO activity than WT. Surprisingly, AO activity was not detected in lines 3.6 and 8.5 (Figure 5-17A). When the activity expressed on a protein basis, all *amiR-AO* lines had reduced AO activity and the activity remained undetectable in lines 3.6 and 8.5 (Figure 5-17B). Except line 8.5 that had slightly higher total

protein content, the protein concentration was similar between WT and other *amiR-AO* lines (Figure 5-17C).

Of four *35S::AO3* lines screened: lines 2.2, 3.3 and 5.1 showed similar AO activity to the WT when the activity expressed on a FW basis (Figure 5-18A), while line 6.6 had 3-fold higher AO activity than the WT and similar trend observed when AO activity expressed on a protein basis (Figure 5-18B). There was no significant difference in the total protein content of all lines assessed (Figure 5-18C).

Two *amiR-AO* lines (line 3.6 and 8.5) that showed undetectable AO activity and a *35S::AO3* lines (line 6.6) that showed the highest AO activity were selected for further experiments. Spectrophotometer traces (Figure 5-19) for AO activity are shown to confirm the lack of AO activity in two *amiR-AO* lines (lines 3.6 and 8.5). As shown in Figure 5-19, there was no obvious reduction in the absorbance reading of *amiR-AO* lines (line 3.6 and 8.5) throughout the AO assay period compared to WT. Meanwhile, the overexpressor showed a greater reduction in absorbance reading than WT. These transgenic lines are referred to as *amiR-AO (3.6)*, *amiR-AO (8.5)* and *35S::AO3* in this thesis.

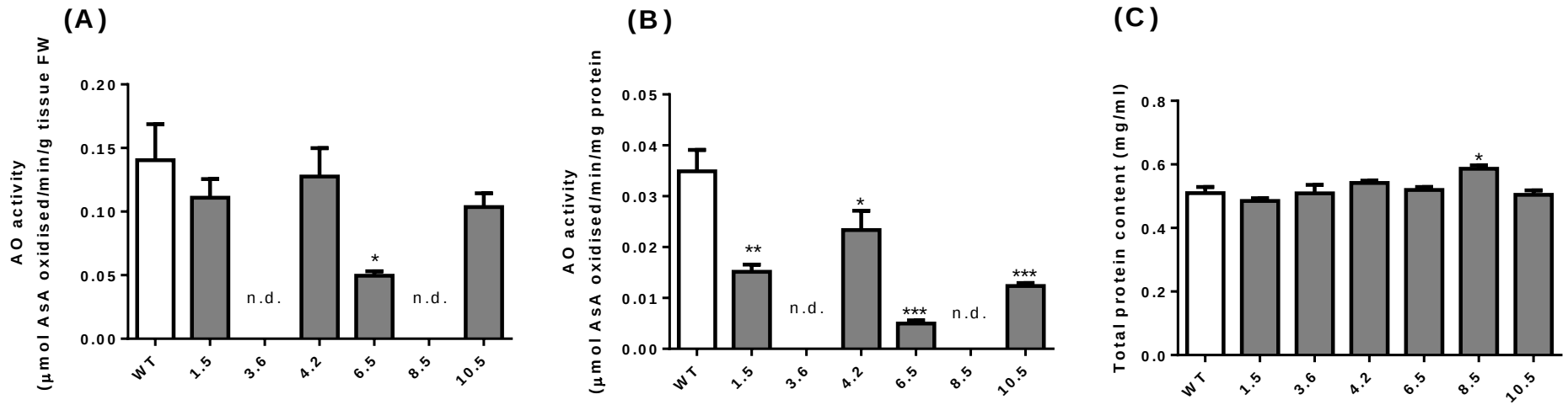

Figure 5-17: Ionically-bound cell wall AO activity of *amiR-AO* transgenic plants. The AO activity was expressed on a fresh weight **(A)** and protein **(B)** basis, respectively. **(C)** Protein concentration in tissue extracts (mg ml^{-1}). Due to varying amount of tissue extracted these values cannot be directly compared to enzyme activity data in A and B. Values are mean ± SEM, n = 3 to 4. Asterisks denote significant differences compared to WT: *p<0.05, **p<0.01 and ***p<0.001 (one way ANOVA and Tukey test). N.d.: AO activity not detected.

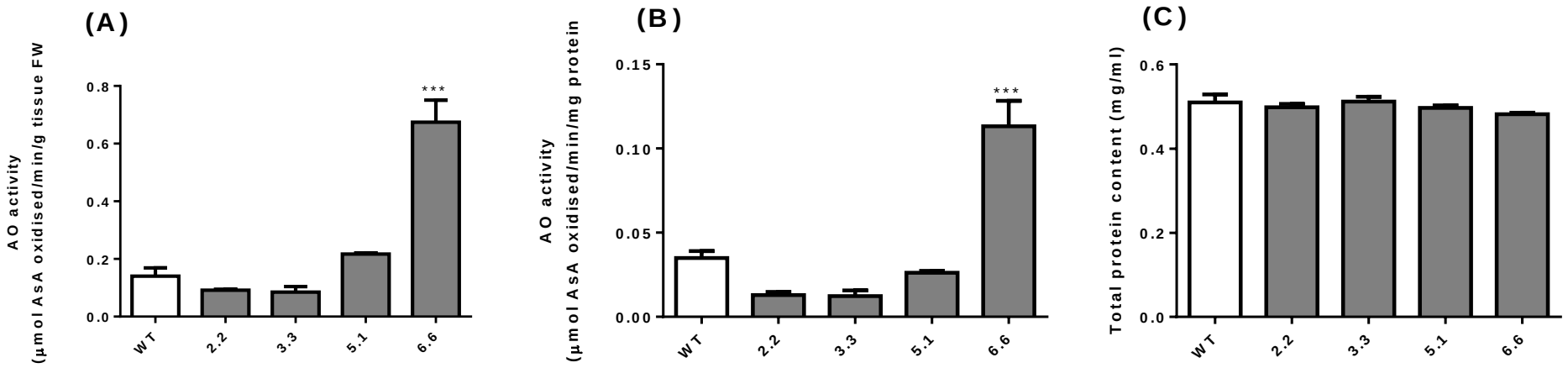

Figure 5-18: Ionically-bound cell wall AO activity of *35S::AO3* transgenic plants. The AO activity was expressed on a fresh weight **(A)** and protein **(B)** basis**,** respectively. **(C)** Protein concentration in tissue extracts (mg ml^{-1}). Due to varying amount of tissue extracted these values cannot be directly compared to enzyme activity data in A and B. Values are mean ± SEM, n = 3 to 4. Asterisks denote significant differences compared to WT: *p<0.05, **p<0.01 and ***p<0.001 (one way ANOVA and Tukey test).

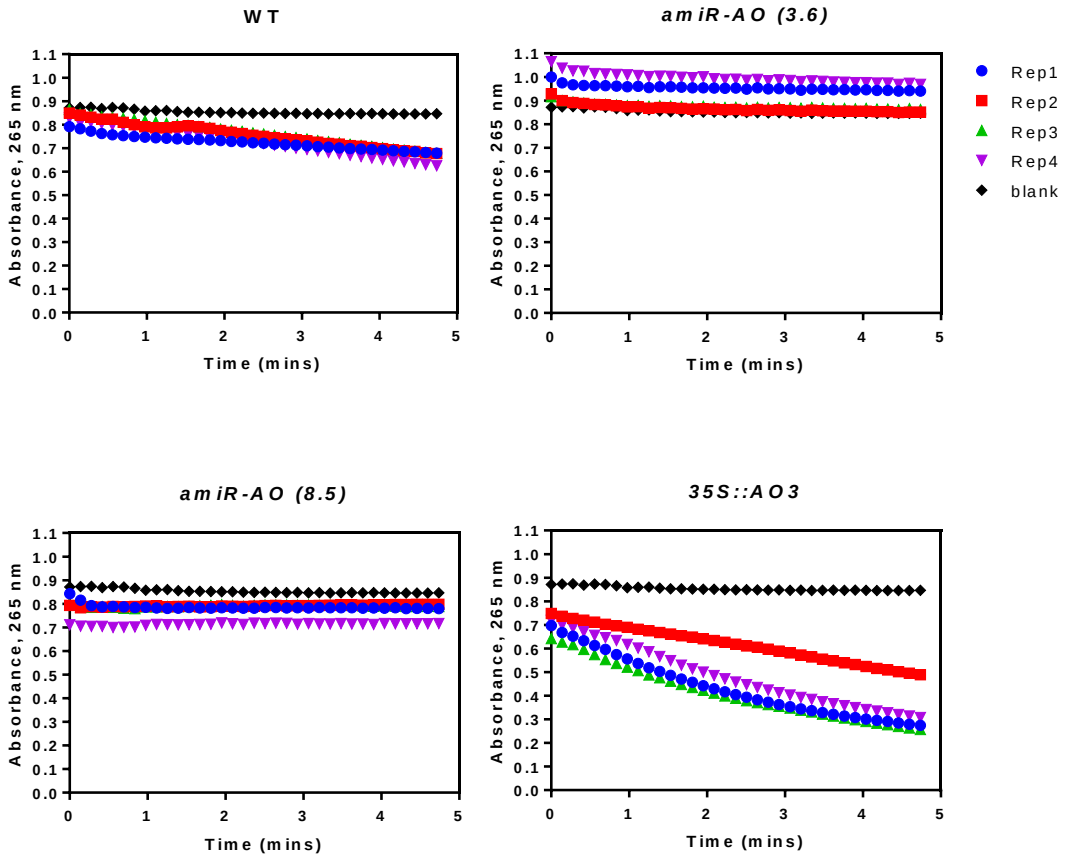

Figure 5-19: Representative spectrophotometer traces of absorbance versus time in the ionically-bound cell wall AO activity assay. Ionically-bound cell wall AO was extracted from 6-week-old WT, *amiR-AO (3.6)*, *amiR-AO (8.5)* and *35S::AO3* plants grown under short day condition (8 hrs light, 16 hrs dark). The AO activity was determined from 1.5 mins to 4 mins. Absorbance readings from four biological replicates of each line are shown. Assay buffer without plant extract was used as a blank.

AO activity is detected in the soluble extract of wild watermelon, tobacco and pea (Sanmartin *et al.*, 2003; de Pinto and De Gara, 2004; Nanasato *et al.*, 2005). Intriguingly, another study showed that soluble AO was undetectable in tobacco (Pignocchi *et al.*, 2003). To assess whether AO activity is present in the soluble extract of *A. thaliana*, AO in the ionically-bound cell wall and soluble fractions was extracted (described in section 2.9.2.) from fully expanded leaves of 6-week-old WT, *amiR-AO* (lines 3.6 and 8.5) and *35S::AO3* plants. When AO activity was expressed on a FW basis, an equal amount of AO activity was observed in the soluble and ionically-bound cell wall fractions of WT (Figure 5-20A). When AO activity expressed on a protein basis (Figure 5-20B), the ionically-bound fraction of WT had higher AO activity than the soluble fraction. This was due to higher total protein content in the soluble fraction. No AO activity (either expressed on a FW or protein basis) was found in both soluble and ionically-bound cell wall fractions of *amiR-AO (3.6)* and *amiR-AO (8.5)*, which suggests that AO activity is completely abolished in the leaves of these lines (Figure 5-20A and B). Compared to WT, *35S::AO3* had higher soluble and ionically-bound cell wall AO activities either expressed on a FW or protein basis (Figure 5-20A and B), with higher AO activity found in the ionically-bound cell wall fraction. Higher total protein content was found in the soluble fraction than the ionically-bound cell wall fraction in all lines (Figure 5-20C).

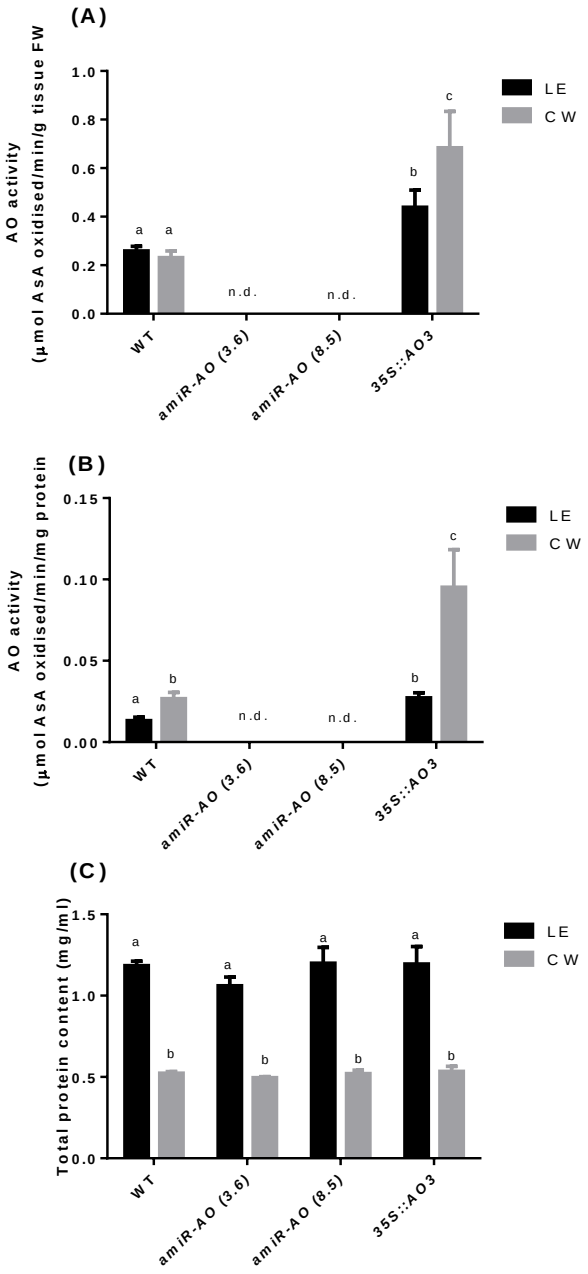

Figure 5-20: Soluble and ionically-bound cell wall AO activities of *amiR-AO* and *35S:AO3* transgenic plants. The AO activity was expressed on a fresh weight **(A)** and protein **(B)** basis, respectively. **(C)** Protein concentration in tissue extracts (mg ml^{-1}). Due to varying amount of tissue extracted these values cannot be directly compared to enzyme activity data in A and B. Values are mean ± SEM, n = 3. Different letters above the bars denote the values are significantly different using one way ANOVA and Tukey tests ($p<0.05$). Values bearing the same letter are not significantly different from each other. LE: soluble fraction, CW: ionically-bound cell wall fraction, n.d.: AO activity not detected.

5.2.12. *AO* gene expression in *amiR-AO* and *35S::AO3* transgenic lines

The *AO* gene expression of *amiR-AO (3.6)* and *35S::AO3* transgenic lines was assessed by RT-PCR from fully expanded leaves of a pool of 4 plants. The primers and PCR conditions are detailed in section 2.5.5.2. The PCR products were subjected to agarose gel electrophoresis and visualised after ethidium bromide staining. All three *AO* genes were detected in WT plants. Reduced expression of all three *AO* genes was detected in the *amiR-AO (3.6)* line that showed undetectable AO activity in leaves, suggesting the amiRNA transgenic plant had effectively knocked down the expression of all *AO* genes in *A. thaliana*. The *35S::AO3* overexpressor had higher expression in all three *AO* genes, in which the strongest expression was found for the *AO3* gene (Figure 5-21). The *AO* gene expression for another *amiR-AO* (line 8.5) was not assessed because this line was isolated at a very late stage compared to *amiR-AO* (*3.6)*. Therefore other experiments were prioritised (i.e. stress and growth responses of this line). However, a reduced or abolished expression for all three *AO* genes should be expected for *amiR-AO* (line 8.5) because AO activity was undetectable in this line.

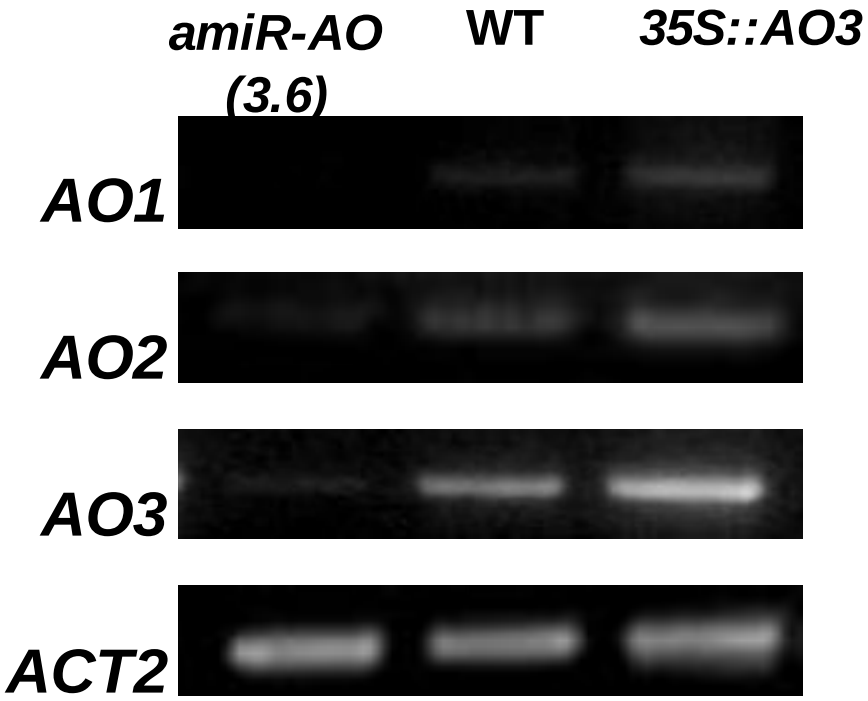

Figure 5-21: Transcript levels of *AO* genes in leaves of WT, *amiR-AO (3.6)* and *35S::AO3* plants. Leaves were pooled from four independent 6-week-old plants. Transcript levels were determined by semi-quantitative RT-PCR. Actin (*ACT2*) was used as the internal control.

5.2.13. The phenotype of *amiR-AO* and *35S::AO3* transgenic lines

Under unstressed normal growth conditions, two *amiR-AO* lines had bigger rosette size than WT. *35S::AO3* had similar rosette size to WT but with shorter petiole and larger leaf blade (Figure 5-22A). *amiR-AO (3.6)* and *amiR-AO (8.5)* lines had more rosette leaves than WT. By contrast, *35S::AO3* line had fewer rosette leaves. The flowering time (inflorescence emergence and flower initiation) of WT and two *amiR-AO* lines were similar but *35S::AO3* exhibited earlier flowering than WT and the two *amiR-AO* lines (Table 5-3). The flower morphology of WT and *amiR-AO* lines appeared to be similar but *35S::AO3* showed distinct flower morphology, where a cluster of tiny buds was observed in the middle of the flowers (Figure 5-22B).

Growth kinetics of these transgenic lines and WT were compared to determine the basis of the large rosette size in *amiR-AO* lines. The absolute leaf expansion rate (AER) and total absolute leaf area (ATLA) were quantified in plants grown at short day light (8 hrs light, 16 hrs dark) from 16 DAS to 44 DAS. The AER (Figure 5-23A) and ATLA (Figure 5-23B) of *amiR-AO* line 3.6 and line 8.5 were significantly greater than WT from 18 DAS onwards. There was no significant difference in the AER and ATLA between *amiR-AO (3.6)* and *amiR-AO (8.5)* lines. The AER and ATLA of *35S::AO* were similar to WT (Figure 5-23).

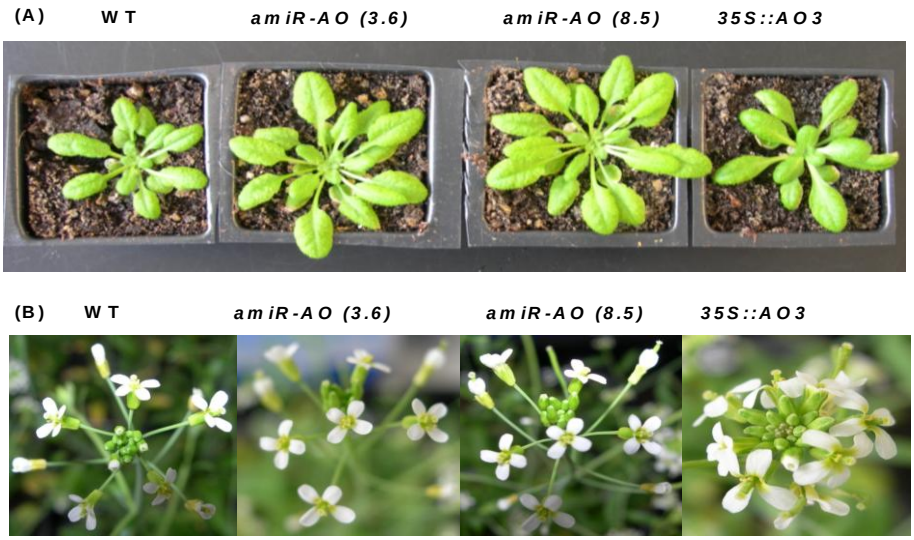

Figure 5-22: Phenotype of WT, *amiR-AO (3.6), amiR-AO (8.5) and 35S::AO3* transgenic plants. 5-week-old plants during the vegetative stage under a short day light regime (8 hrs light, 16 hrs dark) **(A)** and flowers of 6-week-old plants during the reproductive stage under a long day light regime (16 hrs light, 8 hrs dark) **(B)**.

Table 5-3: Growth parameters of WT, *amiR-AO* and *35S::AO3* transgenic plants. Values are mean ± SEM (n = 12). Asterisks denote significant differences compared to WT: **p<0.01 and ***p<0.001 (one way ANOVA and Tukey test). ns denotes the values are not significantly different from WT. DAS, days after sowing.

[1]**Phenotype**	**WT**	***amiR-AO (3.6)***	***amiR-AO (8.5)***	***35S::AO3***
Total number of rosette leaves / plant	18 ± 0.73	24 ± 0.56 ***	23 ± 0.71 ***	15 ± 0.26 **
Inflorescence emergence (DAS)	35.40 ± 1.03	33.83 ± 1.45 ^{ns}	32.38 ± 0.80 ^{ns}	28.13 ± 0.55 ***
Flower initiation (DAS)	38.88 ± 1.06	37.11 ± 1.23 ^{ns}	35.73 ± 1.11 ^{ns}	30.33 ± 0.22 ***

[1] Total number of rosette leaves was observed on 6-week-old plants grown in a short day light regime (photoperiod: 8 hrs light, 16 hrs dark). Inflorescence emergence and flower initiation were observed on plants grown in a long day light regime (photoperiod: 16 hrs light, 8 hrs dark).

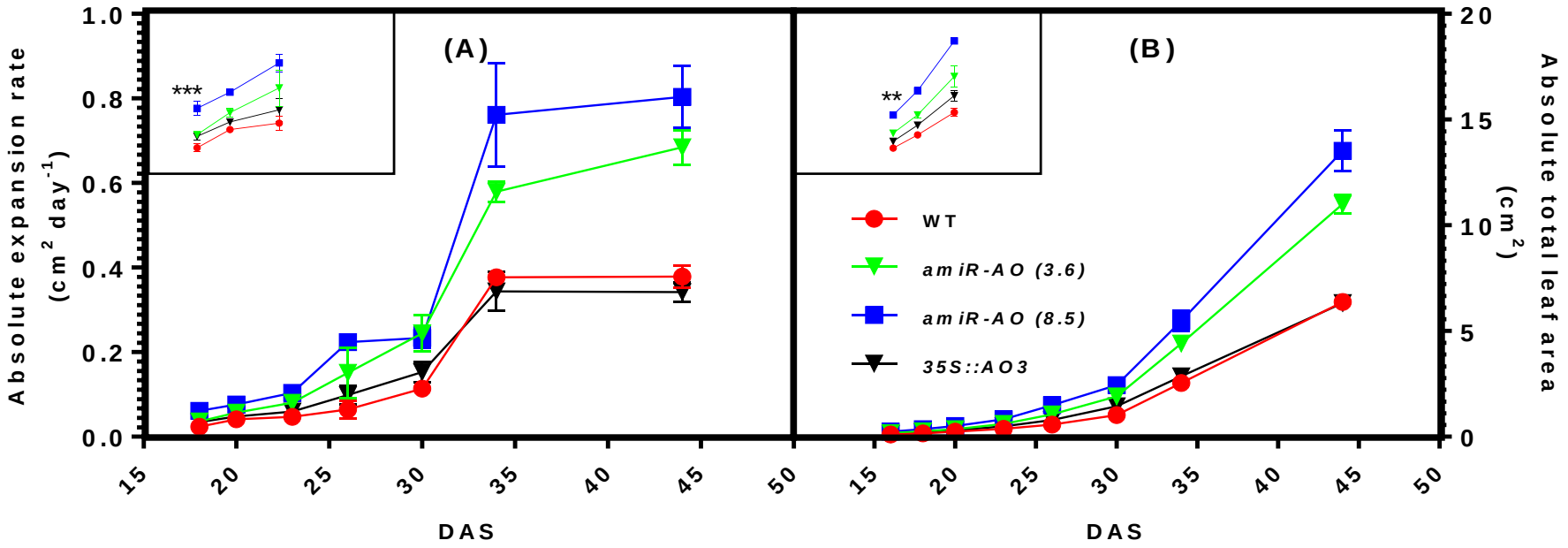

Figure 5-23: Leaf growth of WT, *amiR-AO (3.6)*, *amiR-AO (8.5) and 35S::AO3* transgenic lines under SD conditions (8 hrs light, 16 hrs dark). Absolute leaf expansion rate **(A)** and absolute total leaf area **(B)** were measured from 16 to 44 DAS. Insets are corresponding leaf growth from 18 DAS to 23 DAS. Values are means ± SEM, N = 4, n = 6, where N = number of independent experiments, n = number of biological replicates for each line per independent experiment. Asterisks denote significant differences compared to WT: **p<0.01 and ***p<0.001 (one way ANOVA and Tukey test) at the relevant time point, and only labelled where significant differences were first appeared. SD, short day; DAS, days after sowing.

5.2.14. AsA concentrations in *amiR-AO* and *35S::AO3* transgenic lines

As in the case of *AO* T-DNA insertion mutants, the whole leaf reduced AsA, DHA and AsA pool (AsA + DHA) of *amiR-AO* and *35S::AO3* transgenic lines were not significantly different from the WT (Figure 5-24A). The AsA redox state, defined as the ratio (%) of reduced AsA to total AsA, between WT and these transgenic lines were not significantly different under unstressed normal growth conditions (Figure 5-24B).

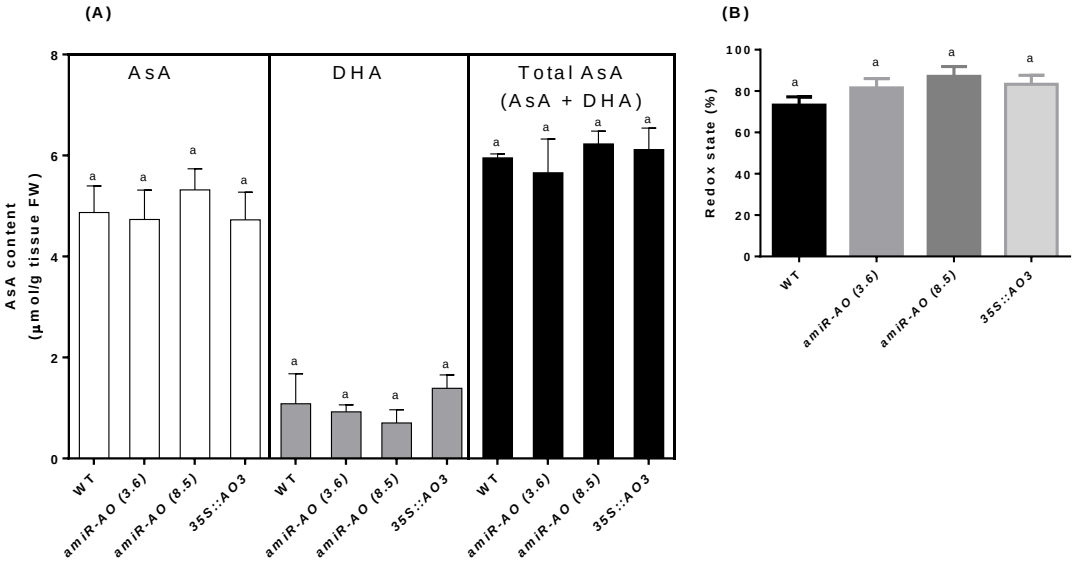

Figure 5-24: Whole leaf AsA concentrations in WT, *amiR-AO (3.6)*, *amiR-AO (8.5)* and *35S::AO3* transgenic lines. Fully expanded leaves from 6-week-old plants were used. **(A)** Reduced AsA, DHA and total AsA pool of WT, *amiR-AO (3.6)*, *amiR-AO (8.5)* and *35S::AO3*. **(B)** Percent redox state (ratio of reduced to total AsA). Values are mean ± SEM, n = 4. Different letters above the bars denote the values are significantly different using one way ANOVA and Tukey tests ($p<0.05$). Values bearing the same letter are not significantly different from each other. Statistical analyses for reduced AsA, DHA and total AsA data were performed separately.

In the apoplastic fraction, the reduced AsA level was higher in both *amiR-AO* lines compared to WT. *amiR-AO (8.5)* had the highest level of reduced AsA, followed by *amiR-AO (3.6)* and then WT. Reduced AsA was not detected in *35S::AO3* (Figure 5-25A). DHA and total AsA pool were similar across all lines (Figure 5-25A). The AsA redox state is defined as the ratio (%) of reduced AsA to total AsA. Both *amiR-AO* lines had higher AsA redox state (80% from line 8.5 and 40% from line 3.6) than WT (20%), whereas the total AsA pool for the *35S::AO3* line was completely oxidised (Figure 5-25B). The yield of apoplastic fluids for all lines were similar, indicated that all lines had similar extraction efficiency (Figure 5-25C).

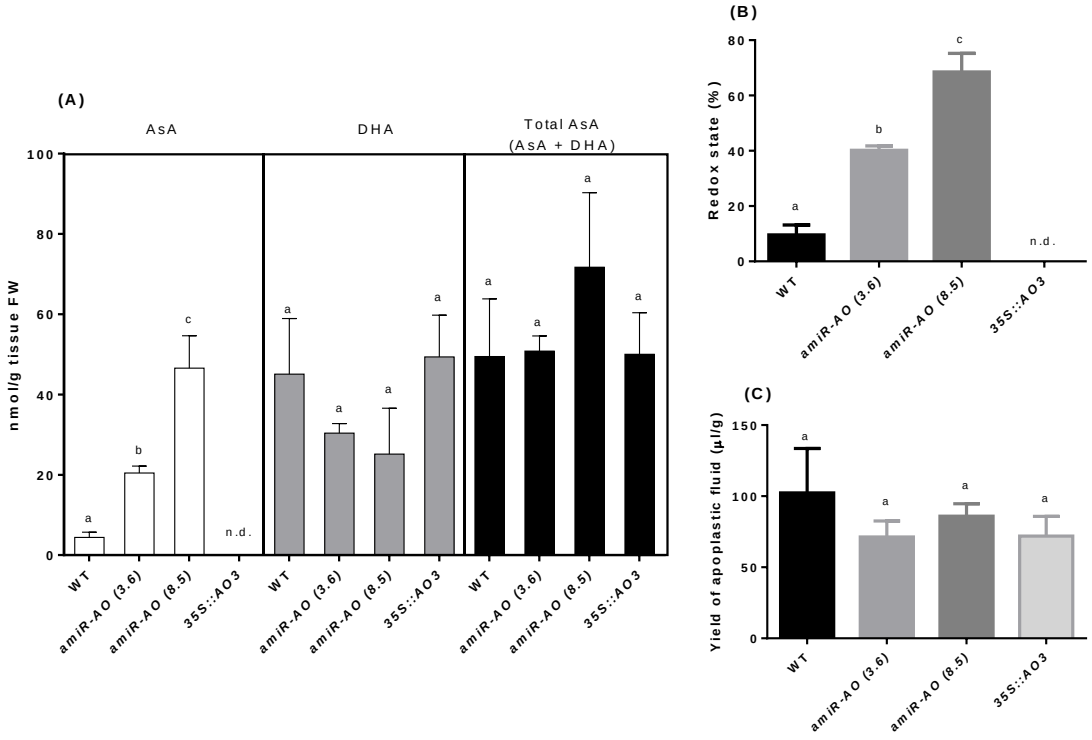

Figure 5-25: Apoplastic AsA concentrations in WT, *amiR-AO (3.6)*, *amiR-AO (8.5)* and *35S::AO3* transgenic lines. All rosette leaves from 6-week-old plants were used. **(A)** Reduced AsA, DHA and total AsA pool of WT and transgenic plants. **(B)** Percent redox state (ratio of reduced to total AsA). **(C)** Yield of apoplastic fluid after vacuum infiltration. Values are mean ± SEM, N = 2, n = 2, where N = number of biological replicate; n = pool of plants per biological replicate. Different letters above the bars denote the values are significantly different using one way ANOVA and Tukey tests ($p<0.05$). Values bearing the same letter are not significantly different from each other. Statistical analyses for reduced AsA, DHA and total AsA data were performed separately. N.d.: not detected.

5.2.15. Histological analyses of *amiR-AO* and *35S::AO3* transgenic lines

Characterisation of palisade mesophyll cells was performed to examine the basis of large leaf size in the amiRNA lines: *amiR-AO (3.6)*, *amiR-AO (8.5)* and the overexpressor, *35S::AO3*. The representative images of palisade mesophyll cells obtained from fully expanded leaves at the middle rosette of 30 DAS plants are shown in Figure 5-26, and the cell morphology was similar between WT and the transgenic lines. The cell area, cell width and cell length of these transgenic lines were not significantly different from the WT, but both *amiR-AO* and *35S::AO3* transgenic lines had a greater number of cells per leaf than the WT (Table 5-4).

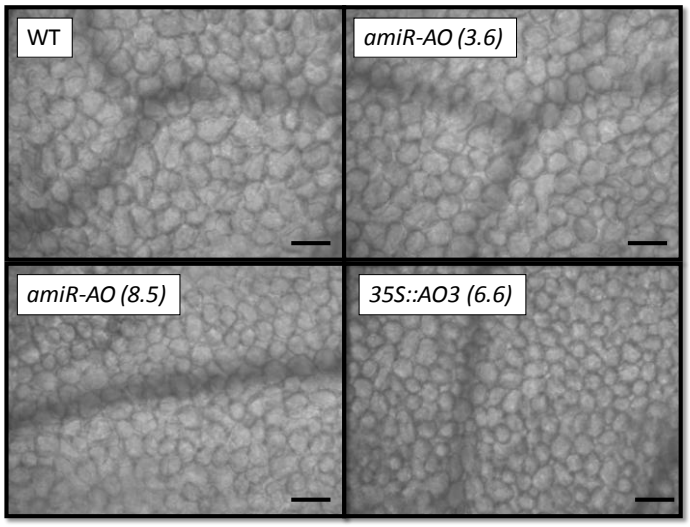

Figure 5-26: Adaxial palisade mesophyll cells from the middle lamina of WT, *amiR-AO (3.6)*, *amiR-AO (8.5)* and *35S::AO3* leaves. Fully expanded leaves of 30 DAS plants grown under long day light regime (16 hrs light, 8 hrs dark) were used. Scale bars = 50 µm.

Table 5-4: Dimensions of adaxial palisade mesophyll cells in WT, *amiR-AO (3.6)*, *amiR-AO (8.5)* and *35S::AO3* lines. Fully expanded leaves of the 30 DAS plants grown under long day light regime (16 hrs light, 8 hrs dark) were used. 6 biological replicates were used for each genotype, 40 cells at the middle lamina from a leaf of each replicate were measured and averaged. Values are mean ± SEM, asterisk (*) denotes the values are significantly different from WT using one way ANOVA and Tukey tests ($p<0.001$), ns indicates the values are not significantly different from WT.

Genotype	Cell area (μm^2)	Cell width (µm)	Cell length (µm)	[1]Cell number /unit area (0.09 mm^2)	[2]Estimated cell density (cells/mm^2)	Leaf area (mm^2)	[3]Estimated total number of cells/leaf
WT	1297 ± 35.77	30.75 ± 0.81	45 ± 0.75	69 ± 5	765 ± 51	76.64 ± 3.03	58618 ± 3942
amiR-AO (3.6)	1204 ± 43.30 ^{ns}	28.35 ± 0.76 ^{ns}	42 ± 0.67 ^{ns}	67 ± 3 ^{ns}	739 ± 32 ^{ns}	230.10 ± 15.59 *	170027 ± 7373 *
amiR-AO (8.5)	1192 ± 45.30 ^{ns}	28.47 ± 1.20 ^{ns}	42 ± 1.50 ^{ns}	79 ± 5 ^{ns}	872 ± 58 ^{ns}	221.60 ± 8.07 *	193263 ± 12820 *
35S::AO3	1244 ± 30.59 ^{ns}	30.84 ± 0.59 ^{ns}	43 ± 0.56 ^{ns}	76 ± 2 ^{ns}	839 ± 22 ^{ns}	207.30 ± 12.76 *	173888 ± 4480 *

[1] Cell number was counted on 300 µm × 300 µm sections (equivalent to 0.09 mm^2) within the microscopic images.
[2] Cell density was estimated by dividing the cell number by 0.09 mm^2.
[3] The total number of cells in a leaf was estimated by multiplying the estimated cell density to the leaf area.

5.2.16. Ionically-bound cell wall peroxidase activity of *amiR-AO* and *35S::AO3* transgenic lines

Ionically-bound cell wall peroxidase activity was measured to assess effects of altered leaf morphology and AO activity, as observed in these transgenic lines on peroxidase. In *amiR-AO* lines, the peroxidase activity appeared to be lower than WT but was not statistically significant. *35S::AO3* had higher peroxidase activity than WT and *amiR-AO* lines when the activity expressed on a FW or protein basis (Figure 5-27A and B). Total protein content were similar in all lines examined (Figure 5-27C).

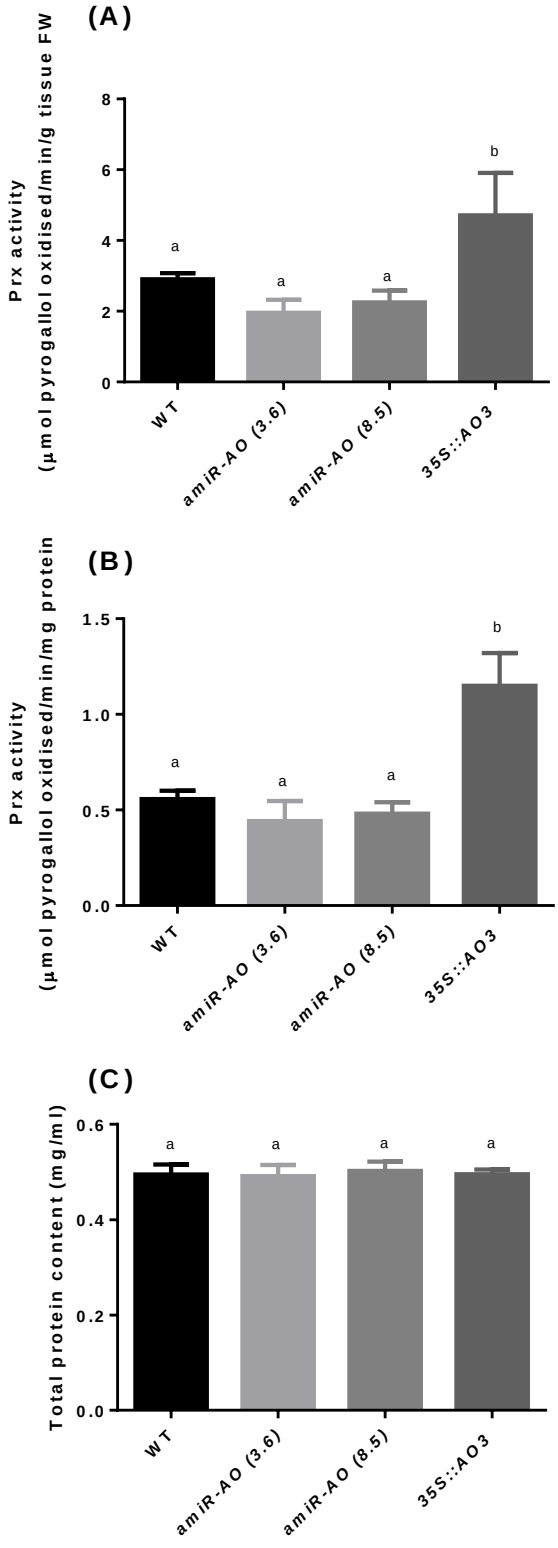

Figure 5-27: Ionically-bound cell wall peroxidase activity in the fully expanded leaves of six-week-old *A. thaliana* WT, *amiR-AO (3.6)*, *amiR-AO (8.5)* and *35S::AO3* transgenic lines, expressed on a fresh weight **(A)** and protein **(B)** basis, respectively.

(C) Protein concentration in tissue extracts (mg ml^{-1}). Due to varying amount of tissue extracted these values cannot be directly compared to enzyme activity data in A and B. Values are mean ± SEM, n = 3. Different letters above the bars denote the values are significantly different using one way ANOVA and Tukey tests ($p<0.05$). Values bearing the same letter are not significantly different from each other.

5.3. Discussion

5.3.1. AO activity and gene expression in various tissues of *A. thaliana* during vegetative and reproductive growth stages

In this study, AO activity of *A. thaliana* was determined in various tissues during vegetative and reproductive growth stages. During vegetative growth stage, the youngest leaf had the highest AO activity and the AO activity was then decreased with maturity, in which oldest leaves at the bottom layer showed the lowest activity. Since leaf expansion actively occurs at the leaf base rather than at the mid leaf and leaf tip (Poethig and Sussex, 1985), AO activity in different parts of a same leaf was assessed. The result showed that AO activity was progressively decreased from leaf base to leaf tip which is in associate with the pattern of leaf expansion. During the reproductive growth stage, high AO activity was found in flowers. Transition of flower buds to open flowers involved rapid growth and so higher AO activity was found in the flower buds than open flowers. These findings described above suggest that high AO activity is present in actively expanding tissue in *A. thaliana*, and is in agreement with studies reported in other plant species, collectively in zucchini leaves (Lin and Varner, 1991), melon fruit (Kato and Esaka, 1996), pumpkin (Esaka *et al.*, 1992), tobacco (Yamamoto *et al.*, 2005), pea (Matamoros *et al.*, 2010) and tomato (Garchery *et al.*, 2012). In addition, similar results were obtained for *Thellungiella halophila*, a close relative of *A. thaliana*, where higher AO activity also was found in younger leaves compared to mature leaves (Appendix D2). The possible mechanism of AO involvement in cell growth could be due to the oxidation of the apoplastic AsA pool *via* the production of DHA and the MDHA radical (detailed in Chapter 1). DHA is proposed to be involved in cell wall loosening through preventing cell wall protein cross-linking with wall

polysaccharides (Lin and Varner, 1991), while MDHA radical-mediated plasma membrane depolarisation and vacuolisation is proposed to induce cell elongation (Hidalgo *et al.*, 1989; González-Reyes *et al.*, 1995). Altogether, the results obtained here coupled with findings in published literature support the hypothesis that high AO activity in actively growing tissue is conserved across plant species.

The expressions of *AO* genes in various tissues during vegetative and reproductive growth stages were monitored using RT-PCR. There are three *AO* genes encoding AO in *A. thaliana*. Each *AO* gene in *A. thaliana* showed a distinct expression pattern and not all gene expression positively correlated with AO activity in *A. thaliana* during vegetative and reproductive growth stages. By contrast, in squash and tobacco cell culture, a positive correlation between *AO* gene expression and AO activity was reported (Lin and Varner, 1991; Kato and Esaka, 1999). However, it should be noted that there is only one gene predicted to have AO function in squash and tobacco, unlike melon (Sanmartin *et al.*, 2007) and *A. thaliana* where *AO* is encoded by a multigene family. This is because enzyme activity is a collective reaction contributed by isoforms in a gene family therefore it is possible that each gene contributes to total AO activity differently. Sanmartin *et al.* (2007) showed that out of four melon (*Cucumis melo*) *AO* genes, only two genes: *CmAO1* and *CmAO4* were expressed in a tissue- and developmental-specific manner and are associated with the AO activity. Transcriptional control and post-translational modifications could affect gene expression and there is evidence that AO is tightly regulated by its prosthetic metal, copper. Esaka *et al.* (1992) demonstrated that treatment with copper increased AO activity but not mRNA level in pumpkin, whereas

copper treatment is reported to enhance AO transcript level in melon (Sanmartin *et al.*, 2007). These differences between enzyme activity and transcript level have also been observed in other metabolic enzymes (Keurentjes *et al.*, 2008; Garchery *et al.*, 2012).

To address the discrepancy between *AO* gene expression and AO activity in *A. thaliana*, it would be interesting to examine the abundance of all three AO proteins in various tissues using Western blots. This should tell us the basis of high AO activity in actively growing tissue, whether is due to new enzyme synthesis or activation of existing enzyme. *AO1* expression was negatively correlated with AO activity in both growth stages of *A. thaliana*, where low expression was observed in young leaf and flowers. The unique *AO1* expression pattern with information from microarray database and phylogenetic analysis (Chapter 4) suggest that this gene could be involved different functions than *AO2* and *AO3*. To address this question, *AO*-deficient mutants were isolated and characterised (discussed in section 5.3.3.).

Gene expression results from RT-PCR were compared with those sourced from the microarray database, eFP browser. *AO2* and *AO3* expression was high in flowers compared with *AO1*, in agreement with the information from eFP browser. However, a small discrepancy was observed between RT-PCR and the microarray database in the expression of *AO3* in cauline leaves. It should be noted that information obtained from microarray databases should be interpreted with care and ideally should be validated with PCR due to irreproducibility and unreliability of microarray results (Wang *et al.*, 2006).

5.3.2. AsA concentrations in various tissues of *A. thaliana* during vegetative and reproductive growth stages

AsA level from whole tissue was assessed in different tissues from vegetative and reproductive growth stages. In agreement with previous studies (Conklin *et al.*, 2000; Dowdle *et al.*, 2007), a high total AsA pool was found in the young leaves and flowers. However, it is unknown why high AsA is present in actively growing tissues. This could be explained by the relationship between vacuole size and leaf age. A study on the subcellular distribution of AsA showed that the AsA level is low in vacuoles and high in cytosol (Zechmann *et al.*, 2011). Young leaves tend to have a larger proportion of cytosol compared to mature leaves. As a result, this should give rise to a high AsA concentration in young leaves, assuming the AsA concentration is high in cytosol. Another possible explanation is actively growing tissues tend to have high metabolic rates as such would require more antioxidant (AsA) (Conklin *et al.*, 2000).

Despite of high AO activity in young leaves and flowers, there was no increase in the DHA (oxidised form of AsA) in these tissues. This observation is consistent with previous studies (Lin and Varner, 1991; Matamoros *et al.*, 2010) that showed lack of a correlation between AO activity and whole tissue DHA content. This is because AO is an apoplastic enzyme that only involved in the regulation of apoplastic AsA redox (ratio of reduced AsA to total AsA) state (Pignocchi and Foyer, 2003). Given that there is a low concentration of AsA (only 5-10% of total AsA concentration in plant cells) in the apoplast, it is not sensible to relate whole tissue AsA level with AO activity.

5.3.3. Characterisation of *AO* T-DNA insertion mutants under unstressed normal growth conditions

AO T-DNA insertion mutants were isolated to study the effects of AO-deficiency in the development of *A. thaliana*. T-DNA mutants for all three *AO* genes (*AO1*, *AO2* and *AO3*) were backcrossed twice to WT, genotyped and homozygous lines were isolated as described in Chapter 3. RT-PCR was performed to confirm the genotyping result and to assess the *AO* gene expression level in these mutants. To the best of my knowledge, this is the first study that examined the gene expression of *AO* T-DNA insertion mutants because gene expression analysis was not reported for *AO* mutants in *A. thaliana* previously (Yamamoto *et al.*, 2005; Lee *et al.*, 2011). RT-PCR revealed that both *ao1* and *ao3* are knockout mutants. Surprisingly, the *ao2* mutant showed similar *AO2* expression pattern to the WT, which implied the T-DNA insertion did not affect *AO2* expression. The predicted T-DNA insertion site for the *ao2* mutant is located near the stop codon (see Figure 3-4). In fact, sequencing result showed that T-DNA insertion for *ao2* is situated 194 bp upstream of the stop codon (Appendix A). There is evidence that T-DNA insertion closer to the stop codon is least effective to knockout or knockdown the target gene (Lee *et al.*, 2004; Hurtado *et al.*, 2006; Wang, 2008). Since no other independent T-DNA line, the *ao2* mutant was not included in further experiments. Recently, a study by Fojtová *et al.* (2011) on different T-DNA insertion lines of a *TERT* gene (TElomerase Reverse Transcriptase) in *A. thaliana* revealed that expression of the target gene is affected by the position of T-DNA insertion. Fojtová *et al.* showed that T-DNA lines with insertion closer to the 3' end of the *TERT* gene did not affect the expression of *TERT* gene upstream of the T-DNA insertion. In fact in my study, the primers used to amplify *AO2* gene was located upstream of

the T-DNA insertion (Appendix A), therefore it is possible to amplify the *AO2* gene. Consequently, the gene expression of *ao2* mutant should be re-examined with a new set of primers that amplify *AO2* gene downstream of the T-DNA insertion in future. Also, the AO activity in the *ao2* mutant should be measured despite of the same transcript level to WT.

The *ao3* and the *ao1ao3* double mutant had only 10-20% AO activity to that of WT, whereas *ao1* showed similar AO activity to the WT. This result supports the findings obtained by Yamamoto *et al.* (2005), which suggesting that *AO3* is the major contributor in leaf and flower AO activity. No altered level of AO activity was observed in *ao1*, which suggests that *AO1* may play a distinct function in *A. thaliana*. Information from microarray database (Chapter 4) showed that *AO1* expression is predominant in roots, so root AO activity could be assessed in future. In addition, recombinant protein expression of *AO1* could be performed to study the substrate specificity of the AO1 enzyme.

The whole leaf reduced AsA, DHA and total AsA was not affected by AO-deficiency. In the apoplast, the total AsA level was similar for WT and *ao* mutants. However, AO perturbation shifted the redox state (ratio of reduced AsA to total AsA in percentage) of the apoplastic AsA pool. Low apoplastic AsA redox state (10%) was observed in WT and *ao1*, which had similar AO activity, whereas higher apoplastic AsA redox state (30%) was found in the *ao3* and *ao1ao3* mutants, which had only 10-20% AO activity. This result is in agreement with previous studies (Pignocchi *et al.*, 2003; Sanmartin *et al.*, 2003; Yamamoto *et al.*, 2005; Garchery *et al.*, 2012) that showed *AO* downregulation mainly affected apoplastic redox state in transgenic tobacco and tomato but did not perturb whole leaf AsA status of these plants. The effects of AO perturbation

being restricted to the apoplast support the predicted localisation of AO in the apoplast. AO only affected the apoplastic AsA redox state and more DHA is present in the apoplast than reduced AsA. This may be explained by two different locations between AO (apoplast) and whole leaf AsA (cytosol), and the transport of apoplastic DHA to cytosol for regeneration is too slow to overcome the oxidised environment in the apoplast (Pignocchi *et al.*, 2003).

In contrast to my result, Yamamoto *et al.* (2005) and Lee *et al.* (2011) showed that *ao3* and *ao1ao2* mutants, respectively, exhibited higher AsA redox state in the whole leaf fractions. The possible reasons are due to different growth conditions and different T-DNA insertion lines of the same genes were used in their studies. It should be noted that the mutants used in their studies were not backcrossed to WT (based on information in the literature), therefore any underlying extraneous mutation could have contributed to differences in the AsA level.

In comparison with WT, *ao* mutants did not show any morphology difference during vegetative and reproductive growth stages, suggesting that AO-deficiency observed in *ao3* and *ao1ao3* is insufficient to cause any phenotypic differences under unstressed normal growth conditions. Although high AO activity is found in expanding tissue of WT plants, no difference was observed in the leaf expansion rate of *ao* mutants. Histological analysis was performed to assess if any subtle phenotype occurred in the cellular level, but no difference found between WT and *ao* mutants. As AO in *A. thaliana* is encoded by a small family of three genes, it is possible that the lack of phenotype in *ao3* and *ao1ao3* was caused by functional redundancy (Krysan *et al.*, 1999). Alternatively it can be explained that hidden phenotype of *ao* mutants was not

triggered under unstressed normal growth conditions. *ao3* and *ao1ao2* mutants reported by Yamamoto *et al.* (2005) and Lee *et al.* (2011) respectively, showed altered phenotypes such as late flowering in *ao3*; smaller rosette size and late flowering in *ao1ao2* under unstressed normal growth conditions. These phenotypes were not reproducible in my studies, probably due to different growth conditions and different accessions used in their studies compared to mine. However, it should be noted that *ao* mutants used in Yamamoto *et al.* (2005) and Lee *et al.* (2011) studies were not backcrossed to WT so phenotypic differences could be due to extraneous mutations. Intriguingly, *ao2* single mutant used by Lee *et al.* (2011) to develop *ao1ao2* double mutant was not a knockdown or knockout mutant (verified by RT-PCR in my study). Also given that a*o1* showed similar AO activity to the WT, it is unclear what factors contributed to the altered morphology in *ao1ao2* mutant reported by Lee *et al.* (as there was no information on the apoplastic AsA concentration, *AO* gene expression and AO activity of the *ao1ao2* mutant) (Lee *et al.*, 2011). A similar level of peroxidase activity was found between WT and *ao* mutants, showing that altered AsA redox state in the apoplast is insufficient to affect peroxidases.

5.3.4. Characterisation of *amiR-AO* and *35S::AO3* transgenic lines under unstressed normal growth conditions

The lack of phenotypes observed in *AO* T-DNA insertion mutants during development (reported in this chapter) and stress (Chapter 6) prompted me to develop amiRNA lines with an attempt to knock out all three *AO* genes and an overexpressor to complement the knockout studies (detailed in Chapter 3). The characterisation of T-DNA insertion *ao* mutants was conducted in the first two years of this project, and the *amiR-AO (3.6)*, *amiR-AO (8.5)* and *35S::AO3* transgenic lines were developed rather recently (3-4 months before completing this project). Consequently, the results and discussion for these transgenic lines are presented separately from *AO* T-DNA insertion mutants.

The isolation of two independent *amiR-AO* lines with undetectable soluble and ionically-bound cell wall AO activities is surprising and fascinating. To the best of my knowledge, these are the first transgenic plants with undetectable AO activity ever developed. Gene expression analysis showed that *amiR-AO (3.6)* line is a knockdown for all three *AO* genes. This result together with an elevated level of AO activity and increased *AO3* transcript abundance observed in the *35S::AO3*, suggests that transgenic plants with altered AO activity were developed successfully. Only one *35S::AO3* plant with high AO activity was isolated, probably because of overexpression-induced post-transcriptional gene silencing. The isolation of *amiR-AO* lines with undetectable AO activity also suggests that the lack of AO is not lethal to plants. Previous study showed that AO inhibitors such as phenylthiourea and thioproline did not affect root elongation in pea seedlings (Suzuki and Ogiso, 1973) and the absence of AO

did not affect growth in a non-photosynthetic parasitic plant, *Cuscuta reflexa* (Tommasi *et al.*, 1990).

AO activity was detected in the soluble and ionically-bound cell wall fractions of WT and *35S::AO3* plants, consistent with previous findings on tobacco, pea and wild watermelon (Sanmartin *et al.*, 2003; de Pinto and De Gara, 2004; Nanasato *et al.*, 2005). Here, AO activity was contributed equally by soluble and ionically-bound cell wall fractions when the AO activity was expressed on a FW basis. When the AO activity was expressed on a protein basis, the specific AO activity in ionically-bound cell wall fraction was much higher than the soluble fraction. This was due to the low abundance of protein content in ionically-bound cell wall fraction. The presence of AO activity in the soluble fraction may be explained by the presence of AO in endoplasmic reticulum (ER) and Golgi vesicles *en route* for export to the cell wall (de Pinto and De Gara, 2004).

Although 35SCaMV promoter is a constitutive promoter (Odell *et al.*, 1985), it is not always expressed in all types of tissues in plants (Williamson *et al.*, 1989; Sunilkumar *et al.*, 2002; Hraška *et al.*, 2008). Williamson *et al.* (1989) showed that the expression of 35SCaMV constructs were higher in younger, actively growing leaf, stem, root, and flower than older, more quiescent tissues. Therefore, AO activity in various plant parts of *amiR-AO* and *35S::AO3* lines should be measured in future.

Whole leaf AsA and apoplastic AsA concentrations were determined in *amiR-AO* and *35S::AO3* plants. In whole leaf fraction, these plants shared similar reduced AsA, DHA and total AsA pool. Perturbation of AO did not affect the redox state of whole leaf AsA, while in the apoplast, *amiR-AO* lines had greater

level of reduced AsA, resulting in a higher redox state in these lines. The apoplastic AsA in *35S::AO3* was nearly completely oxidised compared to WT, which is in consistent with previous studies (Pignocchi *et al.*, 2003; Sanmartin *et al.*, 2003; Yamamoto *et al.*, 2005). The findings on the whole leaf, the apoplastic AsA and the AO activity in *amiR-AO* and *35S::AO3* lines, coupled with those observed in the T-DNA insertion *ao* mutant further reinforced the hypothesis that AO is indeed an apoplastic enzyme and its role in the regulation of apoplastic AsA redox is certain.

Early flowering time observed in the *35S::AO3* plant is in agreement with the tobacco sense line overexpressing *AO* (Yamamoto *et al.*, 2005). Additionally, the *35S::AO3* also showed altered morphology such as short petiole, large leaf blade and clustered flowers. It is unclear if these phenotypic differences were caused by overexpression of the *AO* gene or by other mutations caused by transformation. Another independent line with high AO activity would resolve this question in future. Histological analysis was performed to assess the basis of enhanced leaf size in *amiR-AO* and *35S::AO3*. Both *amiR-AO* and *35S::AO3* transgenic lines had greater number of cells per leaf, suggesting an increase rate of cell division occurred in these plants. It has been shown that AsA is involved in cell division (Smirnoff, 1996, 2011). Studies with cell cultures and root quiescent centres showed that cell division is inhibited by low reduced AsA or high DHA concentrations (Kerk and Feldman, 1995; Kato and Esaka, 1999; Kerk *et al.*, 2000; Horemans *et al.*, 2003; Liso *et al.*, 2004; Potters *et al.*, 2010). Exogenous AsA increased the progression of onion root cells from G1 to S phase of the cell cycle (Liso *et al.*, 1988; Innocenti *et al.*, 1990). Further evidence showed that high AO activity and gene expression are detected in the

quiescent centre of maize root tip compared to surrounding meristematic cells (Kerk and Feldman, 1995). However, findings from previous studies described above do not explain the result obtained in my study, because *amiR-AO* and *35S::AO3* lines had distinct level of AO activity as well as apoplastic AsA redox state, yet these two lines had similar number of cells. It is possible that the influence of apoplastic AsA in cell division is small, as supported by small phenotypic difference in other *AO* transgenic plants under unstressed normal growth conditions (Sanmartin *et al.*, 2003; Yamamoto *et al.*, 2005; Garchery *et al.*, 2012).

An increase in the peroxidase activity was found in the *35S::AO3* plant. This high peroxidase activity could be due to the low amount of reduced AsA present in the apoplast. It is possible that low apoplastic reduced AsA concentration is compensated by high peroxidase activity in H_2O_2 scavenging. The H_2O_2 level in the *35S::AO3* line should be measured to prove this hypothesis. Also, the peroxidase activity should be measured in independent *35S::AO3* lines and overexpressor from other species.

Large rosette size was observed in the *amiR-AO* lines. This observation is in opposition to the hypothesis that MDHA/DHA, generated *via* AO is needed for cell expansion (Hidalgo *et al.*, 1989; Lin and Varner, 1991; González-Reyes *et al.*, 1994). Bigger leaf size in the *amiR-AO* lines could be explained by the presence of another mechanism known as $^{\cdot}OH$-mediated non-enzymic cell wall scission (see section 1.5.), which involves AsA, H_2O_2 and Cu^{2+} (Fry, 1998; Fry *et al.*, 2001; Tabbì *et al.*, 2001; Fry *et al.*, 2002; Dumville and Fry, 2003). In this mechanism, enhanced leaf growth in the *amiR-AO* lines compared to WT, presumably involves: First, higher apoplastic reduced AsA concentration that

could increase the action of non-enzymatic AsA oxidation, producing more H_2O_2. Second, the absence of AO might result in more Cu^{2+} in the apoplast, which could increase the oxidation of AsA by Cu^{2+}, producing more Cu^{+}. Third, an increase in the level of H_2O_2 and Cu^{+} could produce more $^{\cdot}OH$ *via* the Fenton reaction. However, more studies are required to validate this claim. For example, the H_2O_2 and Cu^{2+} levels in the apoplast of *amiR-AO* plants should be measured.

Chapter 6. The function of ascorbate oxidase during stress

6.1. General introduction

Abiotic stresses such as extreme temperature, high light, drought and salinity significantly affect growth and reproduction of plants. The formation of reactive oxygen species (ROS) is a consequence of these environmental perturbations and overproduction of ROS is lethal to plant cells (Apel and Hirt, 2004; Suzuki *et al.*, 2012). Plants are equipped with a battery of antioxidants to overcome oxidative damage caused by ROS. As a major antioxidant in plant cells, AsA plays a crucial role in the scavenging of ROS (described in the following sections).

Evidence shows that AO is involved in response to various stresses, in particular ozone, water deficit, salt and biotic stress (see Chapter 1). In general, these studies showed that AO up-regulation increased plant sensitivity to stress, while AO down-regulation increased plant resistant to stress (Sanmartin *et al.*, 2003; Yamamoto *et al.*, 2005; Fotopoulos *et al.*, 2006; Pignocchi *et al.*, 2006; Garchery *et al.*, 2012). However, studies on the role of AO in *A. thaliana* during stress are small and incomplete. To date, only one publication has reported on the effect of salt stress in *A. thaliana ao3* T-DNA insertion mutant (Yamamoto *et al.*, 2005). Hence, more studies are needed to fill the knowledge gap in this area.

6.1.1. The generation of ROS in plants

ROS are mainly generated from active metabolic processes in the chloroplasts, the mitochondria and the peroxisomes in plants. ROS have dual roles in plant cells. ROS can act as signalling molecules in regulating development and pathogenic defence responses. On the contrary, overproduction of ROS tends to oxidise DNA, proteins and lipids, causing cellular damage. There are four types of ROS: singlet oxygen ($^1O_2$), superoxide radical (O_2^-), hydrogen peroxide (H_2O_2) and hydroxyl radical ($^{\cdot}OH$) (Apel and Hirt, 2004; Miller *et al.*, 2008).

In the mitochondria, complexes I and III of the mitochondrial electron transport chain are believed to be the site for ROS production, where O_2^- is formed from O_2. Photorespiration produces glycolate that is transported from chloroplasts to peroxisomes, H_2O_2 is generated from the reaction of glycolate oxidase in the peroxisome (Cruz de Carvalho, 2008). The photosystem I and II in the chloroplast thylakoids are the major site for ROS production. During photosynthesis, light energy is captured, resulting in O_2 release by water splitting and a series of redox reactions in the photosynthetic electron transport chain. The entire process generates ROS at various points and therefore an effective ROS scavenging system is required. O_2^- is produced from the photoreduction of oxygen, which is then rapidly disproportionated to H_2O_2 and O_2 in a reaction catalysed by superoxide dismutase (SOD). H_2O_2 is reduced to water by APX (ascorbate peroxidase, see section 1.3.). This process is known as the water-water cycle (see Asada, 1999). The water-water cycle in association with the chloroplastic AsA-GSH cycle (see section 1.3.) is important to maintain the proper function of the photosynthetic apparatus in plants (Asada, 2006; Foyer and Shigeoka, 2011).

6.1.2. The response of plants to high light – an overview

During HL, photooxidative stress will occur when light energy absorbed is far beyond the capacity of photosynthesis. In the early stage, plants employ several physiological adaptations to prevent light absorption. For example, changing leaf angle to the sun (heliotropism), losing chlorophyll and losing turgor in wilting leaves (Chaves *et al.*, 2003). If plants could not cope with HL stress with physiological adaptations, they can thermally dissipate excess excitation energy (non photochemical quenching, NPQ) (Niyogi, 1999). Prolonged HL stress causes an increase in ROS production and antioxidants in chloroplasts (Galvez-Valdivieso and Mullineaux, 2010; Foyer and Noctor, 2011; Murchie and Niyogi, 2011). These antioxidants include metabolites and enzymes of the AsA-GSH cycle (section 1.3.), water-water cycle (Section 6.1.1.) and flavonoids (Gould *et al.*, 2002).

AsA has a number of roles in photosynthesis and photoprotection (Smirnoff, 2000b, 2011). First, AsA is the key metabolite in the AsA-GSH cycle that participates in ROS detoxification (Foyer and Noctor, 2011). For example, AsA is the substrate for APX in scavenging H_2O_2. AsA can also scavenge $^1O_2$, O_2^- and $^{\cdot}OH$ directly. Second, AsA regenerates tocopheroxyl radicals that produced when tocopherol (vitamin E) scavenges lipid peroxyl radicals. Third, lumenal AsA can donate electrons to photosystem II. Under photooxidative stress, AsA can donate electrons to photosystem II to support electron flow in the photosynthetic electron transport chain (Tóth *et al.*, 2009). Fourth, AsA is a cofactor for violaxanthin de-epoxidase (VDE), an enzyme that is involved in the catalysis of violaxanthin to zeaxanthin in the xanthophyll cycle (Eskling *et al.*,

1997), which is required for thermal dissiption of excess excitation energy in NPQ.

6.1.3. The response of plants to drought – an overview

Drought can be defined as a condition where normal precipitation is decreased to an extent that limits plant growth and productivity in a natural environment (Boyer, 1982). A decrease in the availability of soil water is the key factor to induce drought stress and plants have adapted several strategies to cope with this water deficit stress, namely escape, avoidance and tolerance strategies (Chaves *et al.*, 2003; Verslues and Juenger, 2011). A summary of these strategies is illustrated in Figure 6-1.

Drought escape strategy refers to plants ability to complete their life cycle before the onset of drought stress. Such plants are equipped with short life cycles and high metabolic rates that adjusted for rapid growth and early flowering. These adaptations are essential to ensure reproductive success while soil water is still available. Besides, plants adapted for escape are believed to have better partitioning of assimilate to developing fruits (Chaves *et al.*, 2003; Verslues *et al.*, 2006). Dehydration avoidance strategy refers to the plant's capacity to maintain water status by reducing water loss and/or maximising water uptake. Water loss is reduced by closing stomata, decreasing light absorbance through curled leaves and shedding of older leaves. Water uptake is increased by enhancing root/shoot ratio, through the development of a large and deep root system to maximise water uptake (Luo, 2010). Besides, dehydration avoidance also is achieved through the accumulation of compatible

solutes, up-regulation of ROS scavenging system and cell wall hardening (Smirnoff, 1998; Verslues and Juenger, 2011). Finally, a dehydration tolerance strategy is employed to protect cellular structures of plants from severe dehydration. This is achieved *via* the accumulation of protective proteins like dehydrins and late-embryogenesis-abundant (LEA) proteins (Verslues *et al.*, 2006). Compatible solutes can also protect protein and membrane structures as well as to scavenge $^{\cdot}OH$ (Smirnoff and Cumbes, 1989). Additionally, antioxidants (e.g. AsA) are produced to overcome oxidative damage caused by ROS (Smirnoff, 1998; Bartels and Sunkar, 2005). In some plants (e.g. evergreen legume, *Retama raetam*), dehydration tolerance can be achieved by entering into a semi-dormant state. During dormancy, genes encoding photosynthetic proteins are repressed and activated within 6 to 24 hrs when water is available. Additionally, some “desiccation-tolerant” plants can undergo a metabolically dormant state when they encounter near complete dehydration, and are still able to recover their physiological and metabolic activities upon rehydration (Chaves *et al.*, 2003).

A meta-analysis on metabolites involved in plant drought responses based on a literature survey (from 1995 to 2010) showed that a high level of relatedness is found between drought, ROS, ABA, photosynthesis and sugar (Pinheiro and Chaves, 2011). As illustrated in Figure 6-2, the drought response in plant is a complicated process that involves cross-talk between different pathways and intermediates (Chaves *et al.*, 2003; Bartels and Sunkar, 2005; Miller *et al.*, 2010; Suzuki *et al.*, 2012). Drought stress is closely linked to HL stress. During drought stress, root is the first organ to sense water deficit; an ABA signal is triggered from root to shoot, resulting in stomatal closure to prevent water loss.

The entrance of CO_2 is limited by stomatal closure so the rate of carbon assimilation is reduced. Consequently, light energy absorbed is far beyond the capacity of photosynthesis. Essentially the ROS scavenging system during drought stress is similar to that in HL stress.

Figure 6-1: Three strategies (escape, avoidance and tolerance) adapted by plants in response to drought. Figure reproduced from Verslues and Juenger (2011).

Figure 6-2: Biological network generated for drought and metabolites interactions and as well as pathways involved. Figure modified from Pinheiro and Chaves (2011).

6.1.4. Chapter aim

In this project, characterisation of *ao3* and *ao1ao3* T-DNA mutants under unstressed normal growth conditions did not show any phenotypic differences although these mutants had only 10% AO activity compared to the WT (see Chapter 5). It is possible that the underlying phenotype of these mutants will be displayed only under stress conditions. Further evidence showed that all three *AO* genes have a substantial number of promoter elements that are predicted to be involved in stress responses (see Chapter 4). Consequently, the effect of high light and drought stress in T-DNA insertion mutants, *amiR-AO* and *35S::AO3* lines were studied and the findings are described in this chapter.

6.2. Results

6.2.1. The effects of HL acclimation on *AO* T-DNA insertion mutants

6-week-old plants, which correspond to stage 1.14 (14 rosette leaves > 1 mm in length, Boyes *et al.*, 2011) were subjected to high light (HL, 550-650 µmol m^{-2} s^{-1}) and low light (LL, 100 µmol m^{-2} s^{-1}) treatments for a period of 7 days or until anthocyanin accumulation was apparent.

ao mutants did not show any phenotypic difference compared with WT plants under LL and HL conditions. During HL acclimation, the accumulation of anthocyanin was more intense in the mature leaves compared to the young leaves. WT and *ao* mutants did not show visible anthocyanin accumulation during LL (control) treatment (Figure 6-3).

Figure 6-3: Phenotype of *AO* T-DNA insertion mutants during HL acclimation. 6-week-old plants (n = 4) were subjected to high light (HL, PPFD = 550-650 µmol m^{-2} s^{-1}) or low light (LL, PPFD = 100 µmol m^{-2} s^{-1}) treatments for 7 days. Picture was taken after high light treatment and representative plants are shown.

6.2.2. Determination of foliar anthocyanin, chlorophyll and carotenoid contents in *AO* T-DNA insertion mutants acclimated to LL or HL for 7 days

Foliar anthocyanin content of WT and *ao* mutants under LL or HL treatment for 7 days was measured. In agreement with the plant phenotype observed, HL acclimated plants had substantially increased the foliar anthocyanin content compared to the LL acclimated plants. The anthocyanin content between WT and the *ao* mutants, however, did not vary significantly either in LL or HL conditions (Figure 6-4).

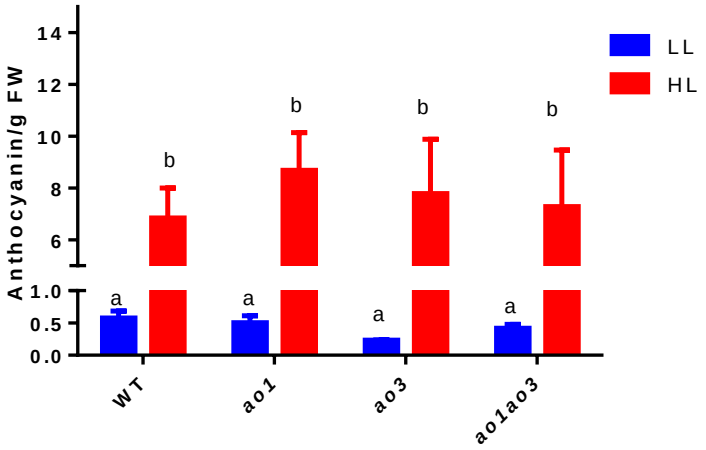

Figure 6-4: Foliar anthocyanin content of *AO* T-DNA insertion mutants acclimated to LL or HL for 7 days. Values are mean ± SEM, n = 4. Different letters above the bars denote the values are significantly different using one way ANOVA and Tukey tests ($p<0.05$). Values bearing the same letter are not significantly different from each other. LL, low light (PPFD = 100 µmol m^{-2} s^{-1}); HL, high light (PPFD = 550-650 µmol m^{-2} s^{-1}).

Quantitative determination of foliar chlorophyll and carotenoid contents were performed to assess if these pigments were affected by anthocyanin accumulation during HL. The chlorophyll a, chlorophyll b and total chlorophyll contents of WT and *ao* mutants grown at HL were not statistically different from the control plants at LL, although a general decrease in chlorophyll content under HL was observed (Figure 6-5A). Similarly, the carotenoid content of WT and *ao* mutants was not significantly different either grown at LL or HL conditions although the HL-treated plants appeared to have slightly higher carotenoid levels (Figure 6-5B).

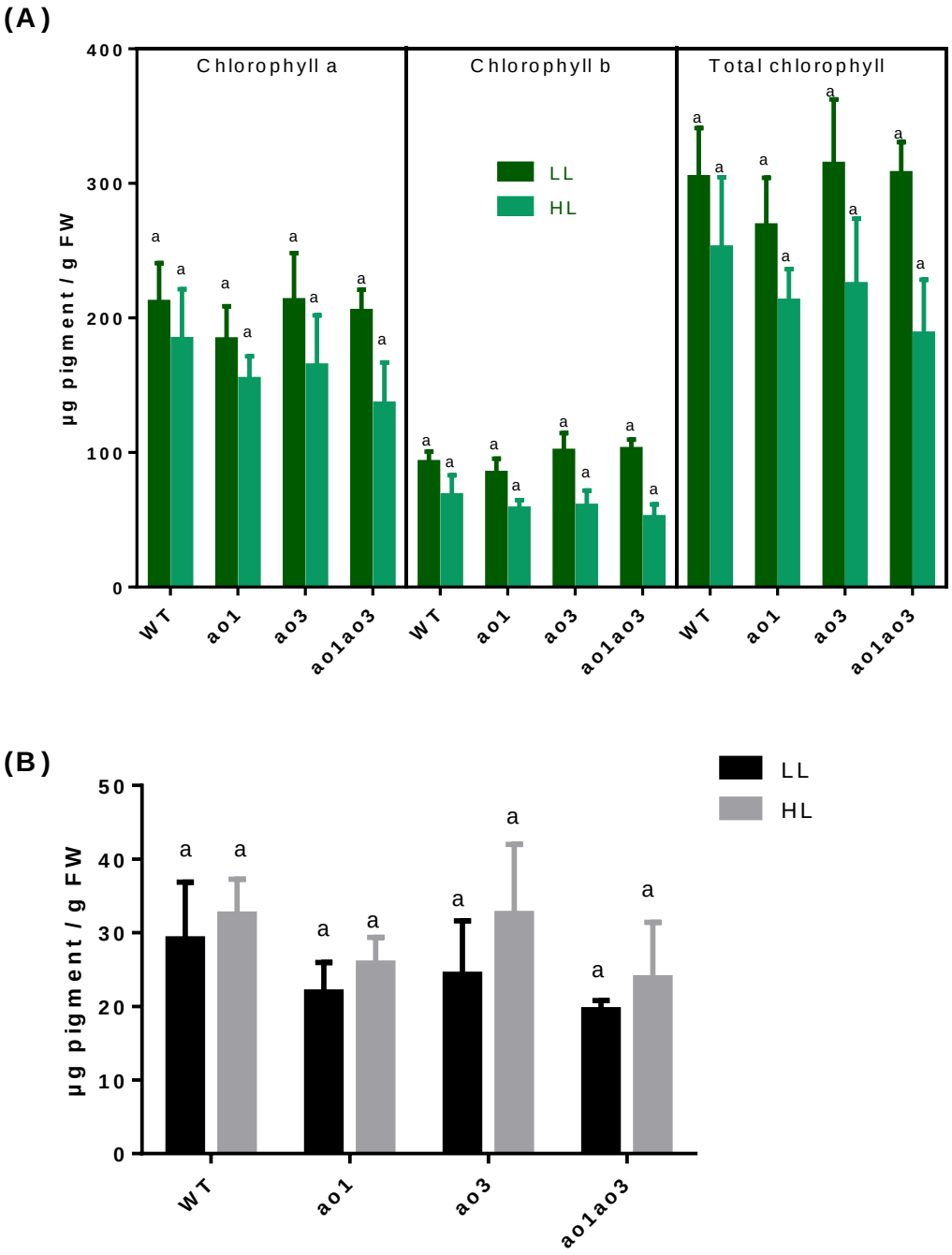

Figure 6-5: Chlorophyll **(A)** and carotenoid **(B)** contents in leaves of *AO* T-DNA insertion mutants acclimated to LL or HL for 7 days. Values are mean ± SEM, n = 4. Different letters above the bars denote the values are significantly different using one way ANOVA and Tukey tests ($p<0.05$). Values bearing the same letter are not significantly different from each other. Statistical analyses for chlorophyll a, chlorophyll b and total chlorophyll data were performed separately. LL, low light (PPFD = 100 µmol m^{-2} s^{-1}); HL, high light (PPFD = 550-650 µmol m^{-2} s^{-1}).

6.2.3. Ionically-bound cell wall AO activity of *AO* T-DNA insertion mutants during HL acclimation

Fully expanded leaves of 6-week-old plants after 7 days of HL and LL treatments were assayed for AO activity (Figure 6-6). AO activity, when expressed on a tissue FW or protein basis, was increased in WT and *ao1* plants acclimated to HL compared to WT and *ao1* plants in LL. However the increase between WT and *ao1* plants did not differ under HL. HL acclimation did not alter AO activity in *ao3* and *ao1ao3* plants. The total protein contents of WT and *ao* mutants were similar under LL and HL conditions.

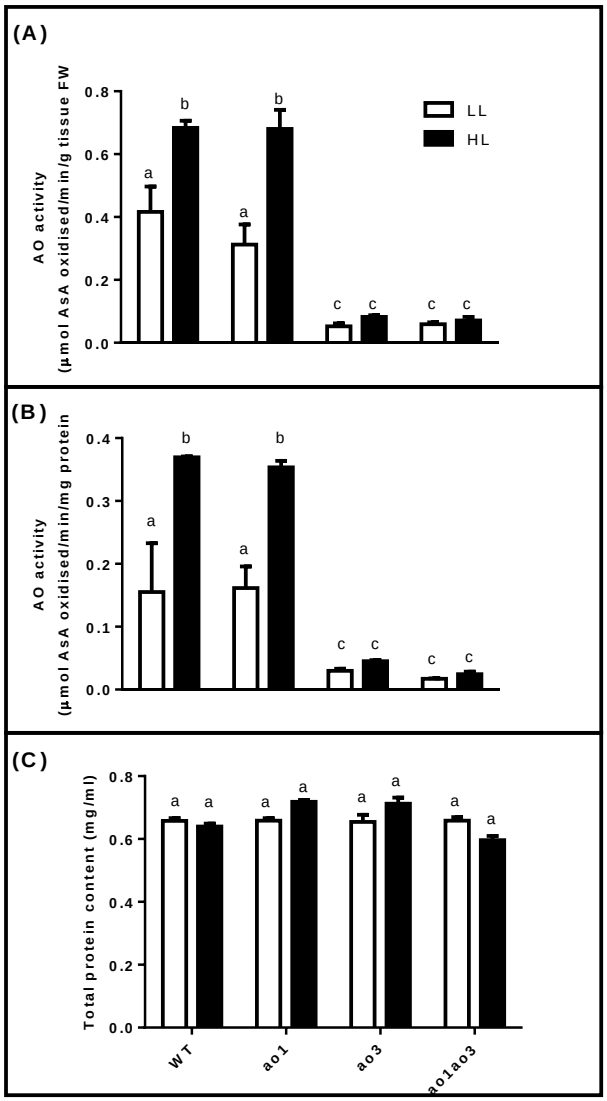

Figure 6-6: Ionically-bound cell wall AO activity of *AO* T-DNA insertion mutants after 7 days acclimation to LL or HL. The AO activity of plants subjected to low light (LL) and high light (HL) conditions was expressed on a fresh weight **(A)** and protein **(B)** basis, respectively. **(C)** Protein concentration in tissue extracts (mg ml^{-1}). Due to varying amount of tissue extracted these values cannot be directly compared to enzyme activity data in A and B. Values are mean ± SEM, n = 4 to 6. Different letters above the bars denote the values are significantly different using one way ANOVA and Tukey tests ($p<0.05$). Values bearing the same letter are not significantly different from each other.

6.2.4. The effect of HL acclimation on *AO* gene expression of *AO* T-DNA insertion mutants

Semi-quantitative RT-PCR analysis was used to determine whether HL acclimation affected the expression levels of *AO* genes (Figure 6-7). Under LL or HL conditions, *AO1* gene expression was undetectable in *ao1* and *ao1ao3* mutants whereas *AO3* gene expression was undetectable in *ao3* and *ao1ao3* mutants. In WT plants, HL acclimation decreased the expression of all three *AO* genes. A small decrease in *AO2* gene expression was observed in *ao1* and *ao1ao3* mutants except *ao3* mutant. HL acclimation also tended to decrease the gene expression of *AO1* and *AO3* in *ao3* and *ao1* mutants respectively.

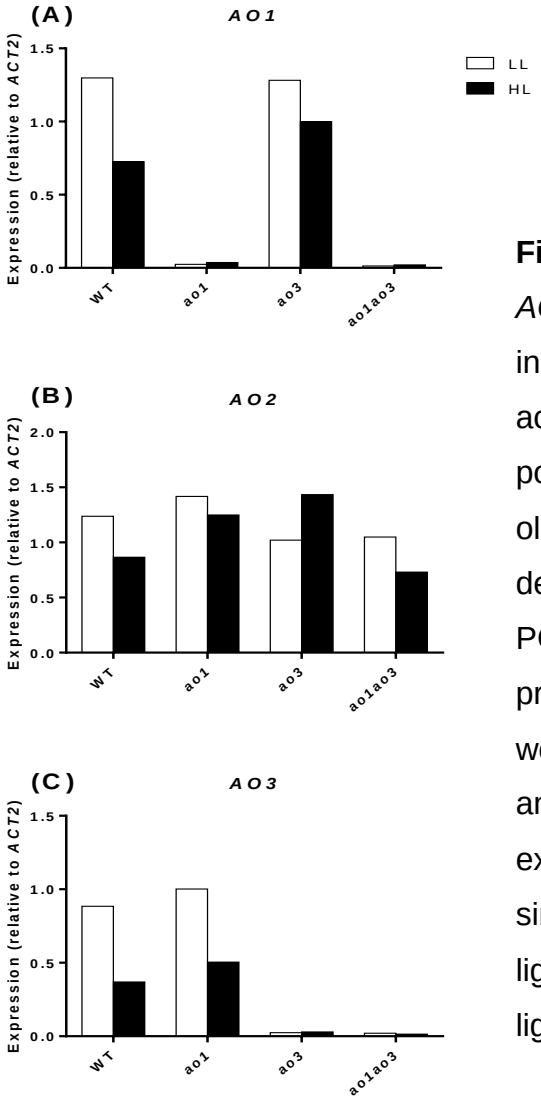

Figure 6-7: Relative transcript levels of *AO* genes in leaves of *AO* T-DNA insertion mutants after 7 days acclimation to LL or HL. Leaves were pooled from four independent 6-week-old plants. The transcript levels were determined by semi-quantitative RT-PCR, where staining intensities of PCR products: *AO1*, *AO2* and *AO3* (**A−C**) were quantified using Image J software and normalised against *ACT2*. This experiment was repeated two times and similar results were obtained. LL, low light (PPFD = 100 µmol m^{-2} s^{-1}); HL, high light (PPFD = 550-650 µmol m^{-2} s^{-1}).

6.2.5. AsA concentrations of *AO* T-DNA insertion mutants during HL acclimation

The whole leaf AsA and the apoplastic AsA concentrations of WT and *ao* mutants after 7 days of HL and LL treatments were assessed. Fully expanded leaves of WT and *ao* mutants were used for whole leaf AsA analyses. Under LL, the reduced AsA (known as AsA here) were significantly higher than the DHA in all lines (Figure 6-8A). When plants acclimated to HL, the AsA level was increased in the WT and *ao* mutants compared to their counterparts under LL treatment, thus contributed to a higher total AsA pool (AsA + DHA) in the HL plants than the LL plants. Meanwhile DHA was not significantly different between LL and HL plants. The concentrations of AsA, DHA and total AsA across genotypes were not significantly different under HL acclimation. Likewise, the levels of AsA, DHA and total AsA across genotypes were not significantly different under LL treatment (Figure 6-8A). No significant differences were found in the AsA redox state of LL and HL plants for all lines (Figure 6-8B).

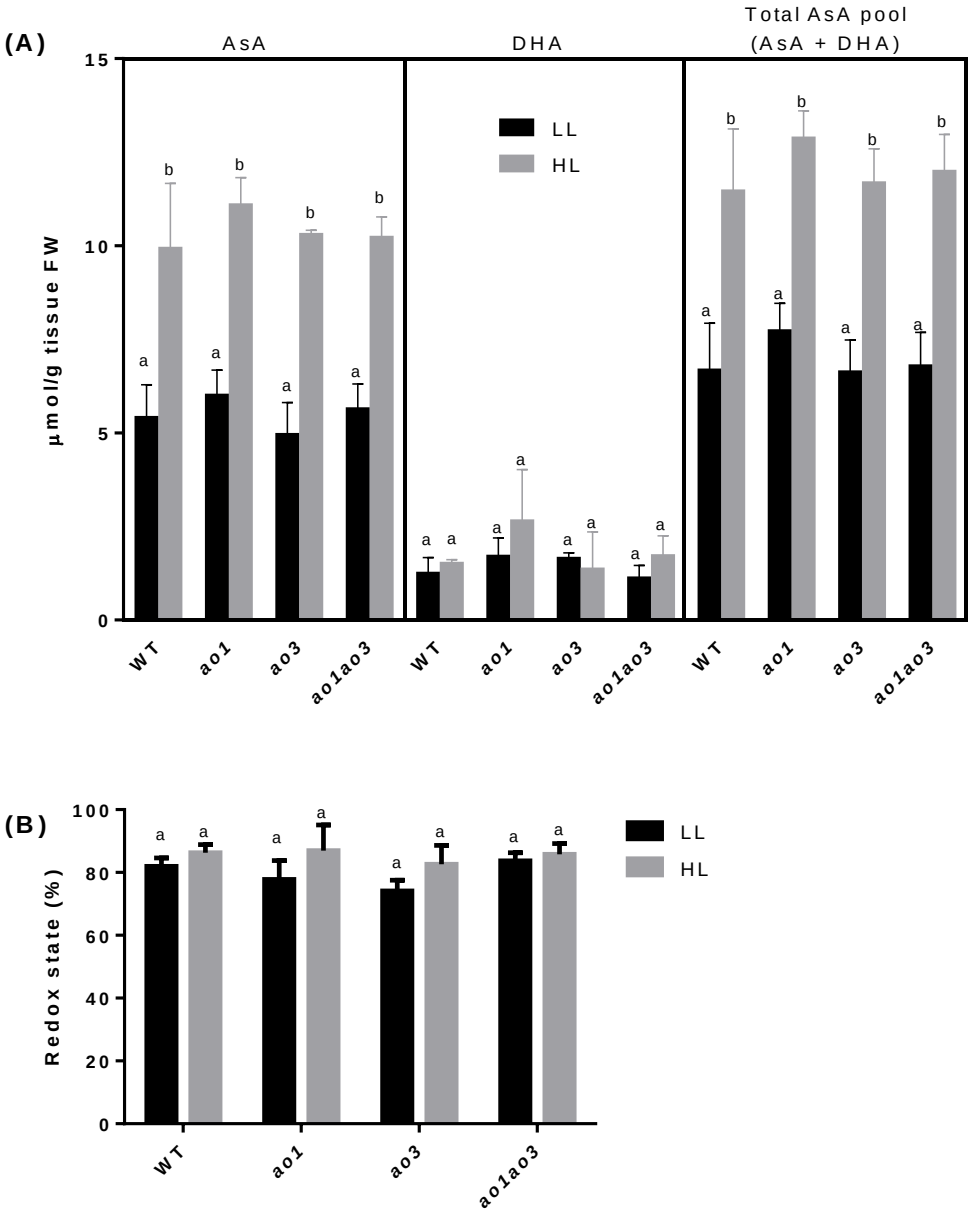

Figure 6-8: Whole leaf AsA concentrations of *AO* T-DNA insertion mutants acclimated to LL or HL for 7 days. **(A)** The concentrations of reduced AsA, DHA and total AsA pool in WT and *ao* mutants. **(B)** The percent AsA redox state (ratio of reduced AsA to total AsA) of WT and *ao* mutants. Values are mean ± SEM, n = 4. Different letters above the bars denote the values are significantly different using one way ANOVA and Tukey tests ($p<0.05$). Values bearing the same letter are not significantly different from each other. Statistical analyses for reduced AsA, DHA and total AsA data were performed separately. LL, low light (PPFD = 100 µmol m^{-2} s^{-1}); HL, high light (PPFD = 550-650 µmol m^{-2} s^{-1}).

Apoplastic AsA was extracted from all rosette leaves of the same plants as used for whole leaf AsA analysis. The yield of apoplastic fluid was not statistically different between LL and HL plants for all lines, although WT plants acclimated to HL appeared to have a lower yield of apoplastic fluid (Figure 6-9C). Unlike in whole leaf extracts, the apoplastic AsA was generally lower than the apoplastic DHA under both LL and HL conditions for all genotypes. *ao3* and *ao1ao3* mutants had significantly higher apoplastic AsA than the WT and the *ao1* mutant under LL and HL conditions (Figure 6-9A). In contrast to whole leaf AsA, the apoplastic AsA was not statistically different under LL or HL conditions, although AsA for *ao3* and *ao1ao3* declined under HL. The apoplastic DHA was not statistically different across genotype either acclimated to LL or HL (Figure 6-9A). The total apoplastic AsA pool (AsA + DHA) was similar across genotype and treatments (LL and HL acclimation). For all genotypes, the level of apoplastic total AsA (~100 nmol/g FW for both LL and HL plants, Figure 6-9A) was substantially lower than the respective whole leaf total AsA (~5 µmol/g FW for LL plants and ~12 µmol/g FW for HL plants, Figure 6-8A). In LL condition, *ao3* and *ao1ao3* plants had higher AsA redox state than WT and *ao1*. In HL condition, the AsA redox of *ao3* and *ao1ao3* were lower than the LL counterparts (Figure 6-9C).

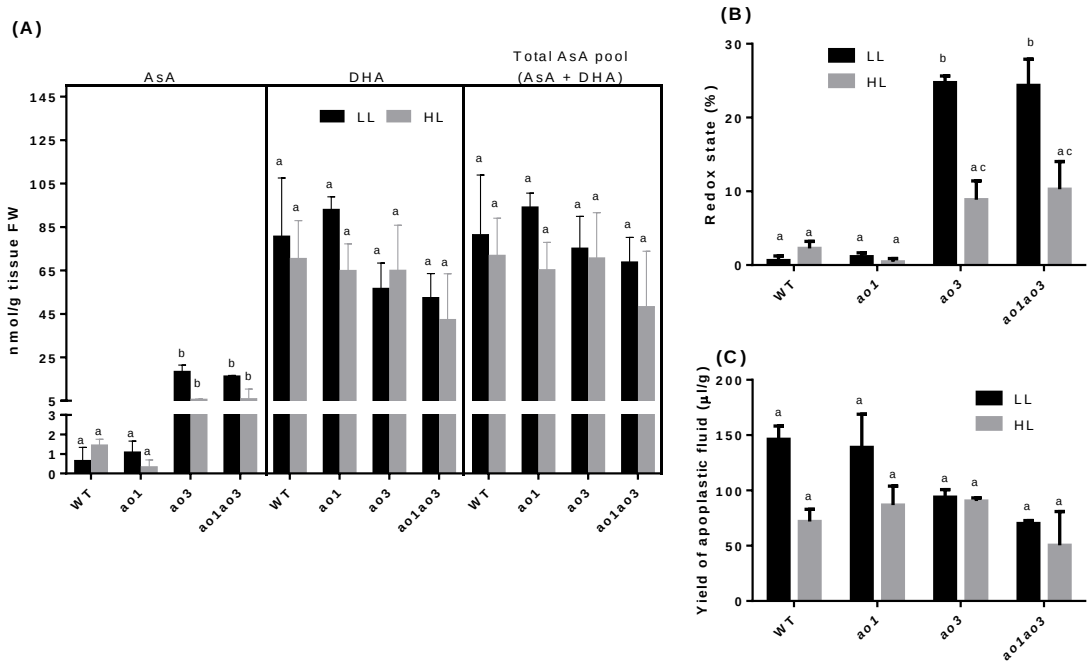

Figure 6-9: Apoplastic AsA concentrations of *AO* T-DNA insertion mutants acclimated to LL or HL for 7 days. **(A)** Apoplastic reduced AsA, DHA and total AsA pool from whole rosette leaves of WT and *ao* mutants. **(B)** The percent AsA redox state (ratio of reduced AsA to total AsA) of WT and *ao* mutants. **(C)** The yield of apoplastic fluid after vacuum infiltration. Values are mean ± SEM, n (pool of plants per replicate) = 2, N (number of replicate) = 2. Different letters above the bars denote the values are significantly different using one way ANOVA and Tukey tests ($p<0.05$). Values bearing the same letter are not significantly different from each other. Statistical analyses for reduced AsA, DHA and total AsA data were performed separately. LL, low light (PPFD = 100 µmol m^{-2} s^{-1}); HL, high light (PPFD = 550-650 µmol m^{-2} s^{-1}).

6.2.6. Ionically-bound cell wall peroxidase activity of *AO* T-DNA insertion mutants during HL acclimation

The effect of HL in the ionically-bound cell wall peroxidase activity of *ao* mutants was examined to assess whether ionically-bound cell wall peroxidase activity is affected by AO-deficiency. HL acclimation increased the peroxidase activity of *ao* mutants except WT when expressed on a tissue FW basis (Figure 6-10A). When the peroxidase activity expressed on a protein basis, all lines had higher peroxidase activity under HL than their LL counterparts (Figure 6-10B). The level of peroxidase activity between WT and *ao* mutants was not significantly different under LL or HL (Figure 6-10B). WT and *ao* mutants had similar level of total protein content under LL or HL conditions (Figure 6-10C).

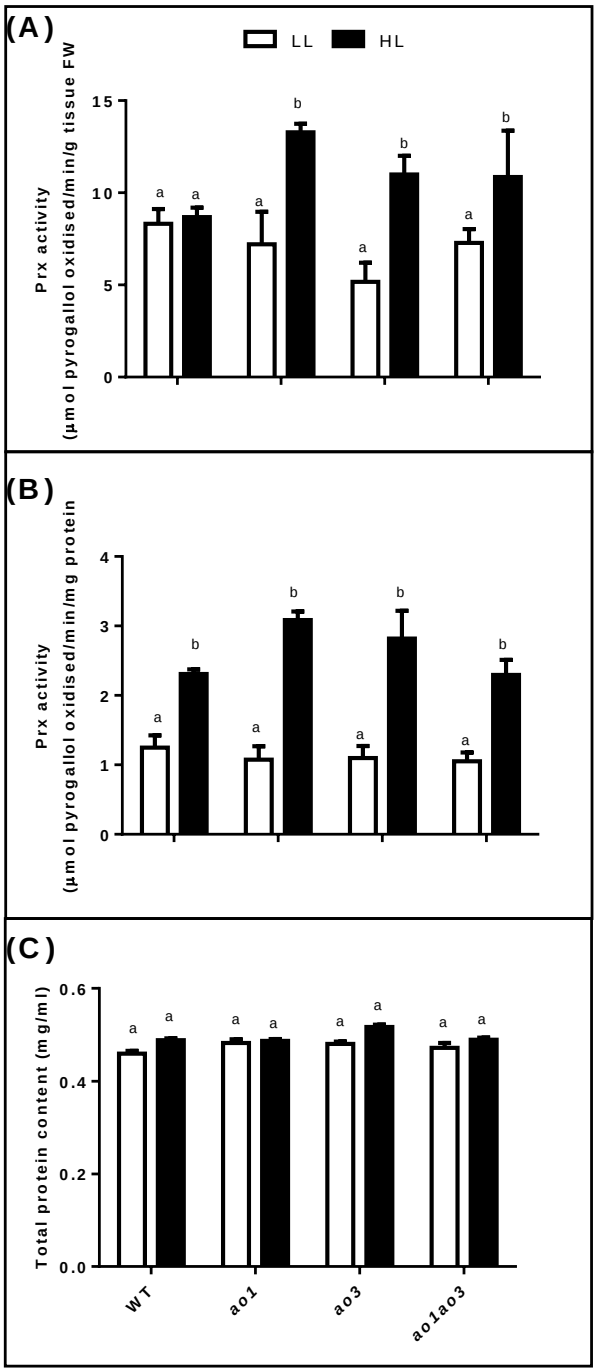

Figure 6-10: Ionically-bound cell wall peroxidase activity of *AO* T-DNA insertion mutants acclimated to LL or HL for 7 days. The peroxidase activity of plants subjected to low light (LL) and high light (HL) conditions was expressed on a fresh weight **(A)** and protein **(B)** basis, respectively. **(C)** Protein concentration in tissue extracts (mg ml^{-1}). Due to varying amount of tissue extracted these values cannot be directly compared to enzyme activity data in A and B. Values are mean ± SEM, n = 4 to 6. Different letters above the bars denote the values are significantly different using one way ANOVA and Tukey tests ($p<0.05$). Values bearing the same letter are not significantly different from each other.

6.2.7. The effect of drought on *AO* T-DNA insertion mutants

6-week-old plants, which correspond to stage 1.14 (14 rosette leaves > 1 mm in length, Boyes *et al.*, 2011) were subjected to progressive drought treatment, in which watering was withheld for a period of 14 days until wilting symptoms were observed. After 14 days of dehydration, WT and *ao* mutants showed leaf wilting symptoms and older leaves at the bottom of rosette exhibited early leaf senescence. The *ao* mutants had no obvious difference in drought sensitivity compared with the WT (Figure 6-11).

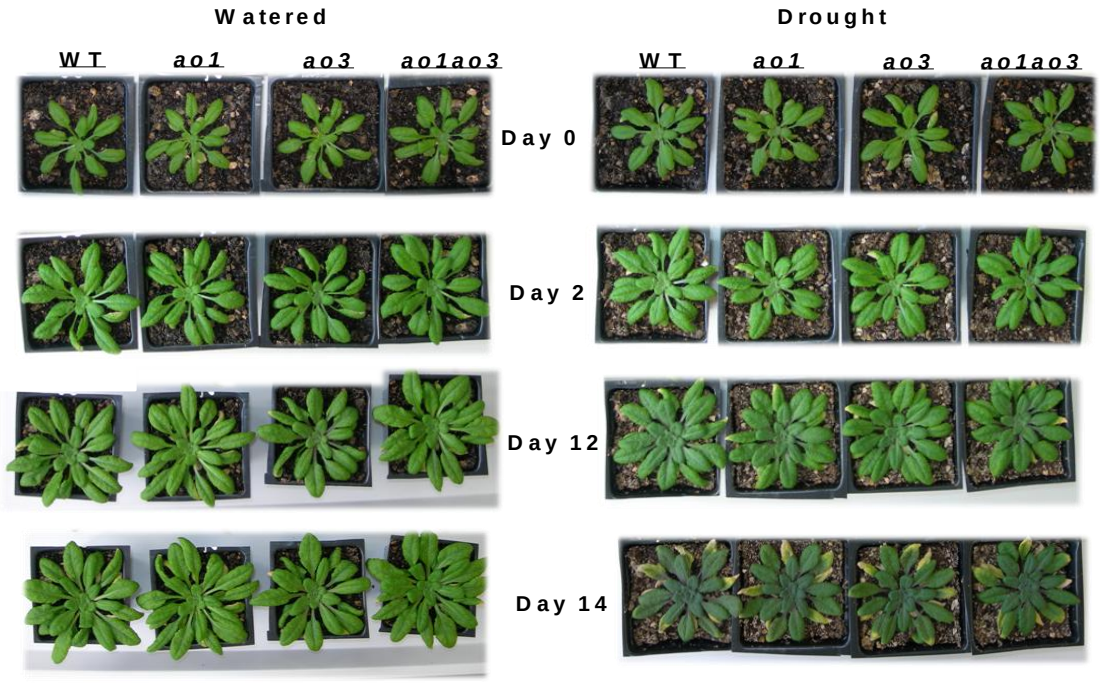

Figure 6-11: Phenotype of *AO* T-DNA insertion mutants during drought. Pictures of WT and *ao* mutants under control ("watered") and drought treatments were taken at the indicated days and representative plants are shown. Control: 6-week-old plants were watered every 3 days for 14 days. Drought stress: 6-week-old plants were withheld from watering for 14 days.

6.2.8. Leaf growth of *AO* T-DNA insertion mutants during drought

Throughout the drought experiment, pots plus plants were weighed and the reduction in pot weight relative to the initial weight was used to reflect soil water content, assuming that pot weight is negligible. The soil water content decreased over time in drought treated plants compared to the watered plants. However, the soil water content in drought treated WT and *ao* mutants was not significantly different from each other (Figure 6-12A), suggesting WT and *ao* mutants were exposed to a similar dehydration rate during drought. As plant growth is affected by drought stress, the absolute total leaf area (ATLA), the absolute expansion rate (AER) and the FW of watered and drought leaves were assessed.

The ATLA of watered plants increased over time but the expansion was not significantly different between WT and *ao* mutants. Drought treated plants only showed an increase in ATLA for the first 10 days of the treatment, then showed growth arrest followed by reduction in ATLA on day 14. A decrease in ATLA indicated the cessation of plant growth followed by the loss of turgor pressure in drought treated leaves (Figure 6-12B). No significant differences observed in the ATLA in any of the lines during drought.

The AER of leaves in WT and *ao* mutants under watered treatment varied but not significantly differ throughout 14 days of the experiment. In drought treated plants, a dynamic but not significantly differ AER was observed between WT and *ao* mutants in the first 10 days, then decreased dramatically on day 14 of the drought treatment (Figure 6-12C). It should be noted that the negative AER observed in day 14 of the drought treatment was due to the cessation of plant growth followed by the loss of turgor pressure in drought treated leaves.

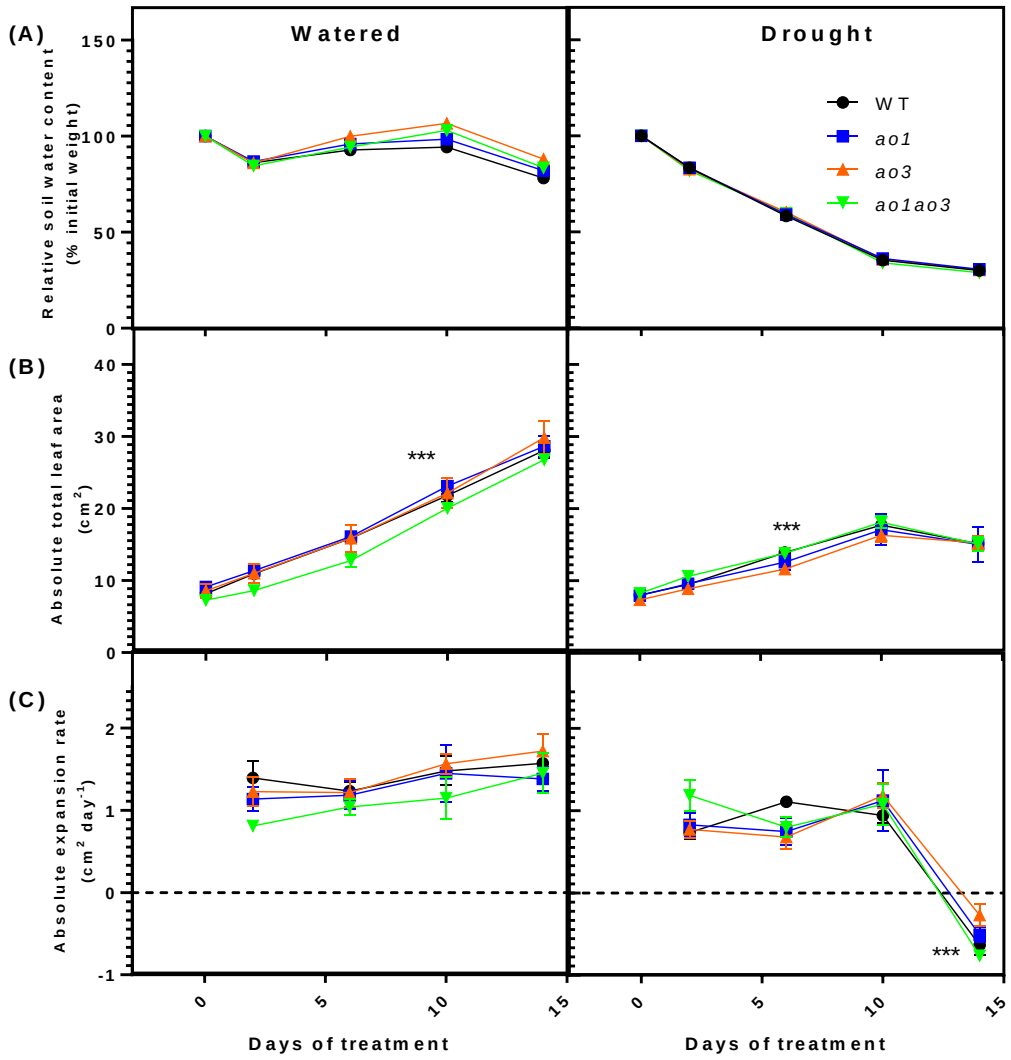

Figure 6-12: Leaf growth of *AO* T-DNA insertion mutants during drought. Observations were made in the 14 days of watered (left panels) and drought (right panels) treatments. **(A)** Soil water content, assessed by measuring reduction of pot + plant weight and plotted as percentage relative to initial weight. **(B)** Absolute total leaf area, the decrease of leaf area indicated the cessation of plant growth followed by the loss of turgor pressure in drought treated leaves. **(C)** Absolute expansion rate of leaves, the negative growth rates indicated the cessation of plant growth followed by the loss of turgor pressure in drought treated leaves. Values are mean ± SEM, n = 4. Asterisk (***) denotes the values are significantly different from the first time point at $p<0.001$. Control: 6-week-old plants were watered every 3 days for 14 days. Drought stress: 6-week-old plants were withheld from watering for 14 days.

6.2.9. Fresh weight and dry weight of *AO* T-DNA insertion mutants during drought

The FW of *ao* mutants and WT were not significantly different under watered conditions. In comparison with watered plants, drought stress markedly reduced the FW of WT and *ao* mutants, with no significant differences were found in any of the lines (Figure 6-13A). The difference in FW between watered and drought tissues could affect data interpretation (due to different water content), if FW is used as a reference. Therefore, FW of drought and watered tissues were calculated for DW (see section 2.9.1.). A typical result of calculated DW is given in Figure 6-13B, the corrected DW was not significantly different between the *ao* mutants and WT under watered and drought conditions. Calculated DW was used to express a number of results in this chapter (indicated in text or figure legends for the relevant experiments).

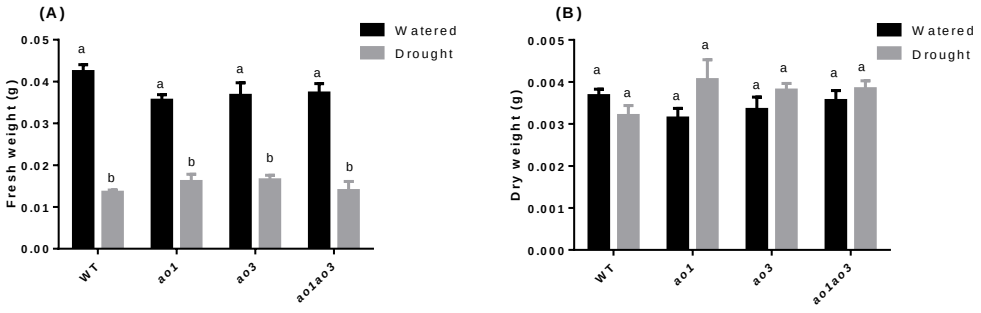

Figure 6-13: The effect of drought in leaves weight of WT and *AO* T-DNA insertion mutants. **(A)** Fresh weight of leaves after 14 days of watered or drought treatments. **(B)** Representative corrected dry weight that used as a reference system for several assays (indicated in text or figure legends for the relevant experiments). Values are mean ± SEM, n = 4. Different letters above the bars denote the values are significantly different using one way ANOVA and Tukey tests ($p<0.05$). Values bearing the same letter are not significantly different from each other.

6.2.10. Determination of foliar anthocyanin, chlorophyll and carotenoid contents in *AO* T-DNA insertion mutants subjected to watered or drought treatments

Anthocyanin has a protective role in plant response to abiotic stress. The foliar anthocyanin content in WT and *ao* mutants was determined to assess the relationship between anthocyanin accumulations and AO-deficiency during HL. Drought stress significantly increased the foliar anthocyanin content of WT and *ao* mutants than the watered plants. The anthocyanin content between WT and the *ao* mutants, however, did not significantly varied either in watered or drought conditions (Figure 6-14).

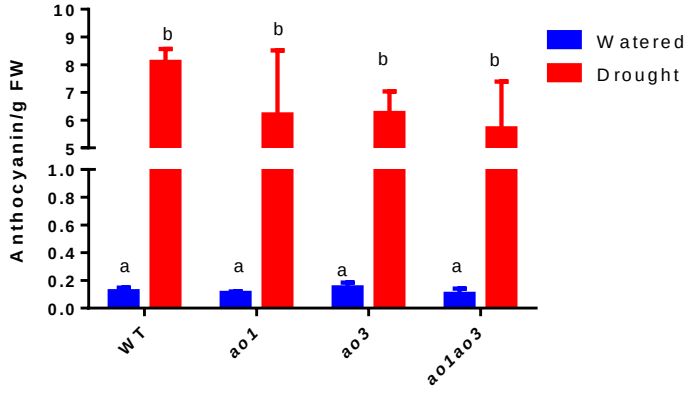

Figure 6-14: Foliar anthocyanin content of *AO* T-DNA insertion mutants after 14 days of watered or drought treatments. Values are mean ± SEM, n = 4. Different letters above the bars denote the values are significantly different using one way ANOVA and Tukey tests ($p<0.05$). Values bearing the same letter are not significantly different from each other. Control: 6-week-old plants were watered every 3 days for 14 days. Drought stress: 6-week-old plants were withheld from watering for 14 days.

The effect of drought in photosynthetic pigments (chlorophylls a, b, and carotenoid) of WT and *ao* mutants was assessed. Drought stress significantly decreased the concentrations of chlorophyll a, chlorophyll b, total chlorophyll (Figure 6-15A) and carotenoid (Figure 6-15B) in leaves of *ao* mutants and WT. No significant differences were found between WT and *ao* mutants either in watered or drought conditions.

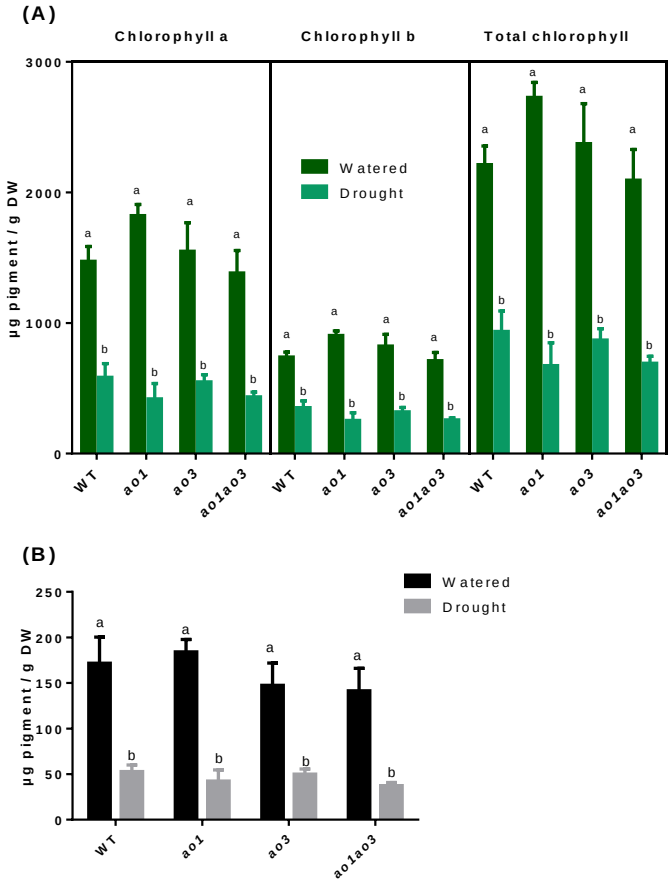

Figure 6-15: Chlorophyll **(A)** and carotenoid **(B)** contents in leaves of *AO* T-DNA insertion mutants after 14 days of watered or drought treatments. Values are mean ± SEM, n = 4. Different letters above the bars denote the values are significantly different using one way ANOVA and Tukey tests ($p<0.05$). Values bearing the same letter are not significantly different from each other. Statistical analyses for chlorophyll a, chlorophyll b and total chlorophyll data were performed separately.

6.2.11. Ionically-bound cell wall AO activity of *AO* T-DNA insertion mutants during drought

For drought studies, AO activity was expressed based on tissue DW rather than tissue FW due to a big variation in FW between watered tissue and drought tissue. Drought stress had little effect on the AO activity, where not significant differences were found between watered plants and drought treated plants when expressed on a tissue DW (Figure 6-16A) or protein basis (Figure 6-16B) for all lines. As in previous results, the AO activities of *ao3* and *ao1ao3* were lower than WT and *ao1*. The total protein content was similar in both watered and drought conditions across all genotypes studied (Figure 6-16C).

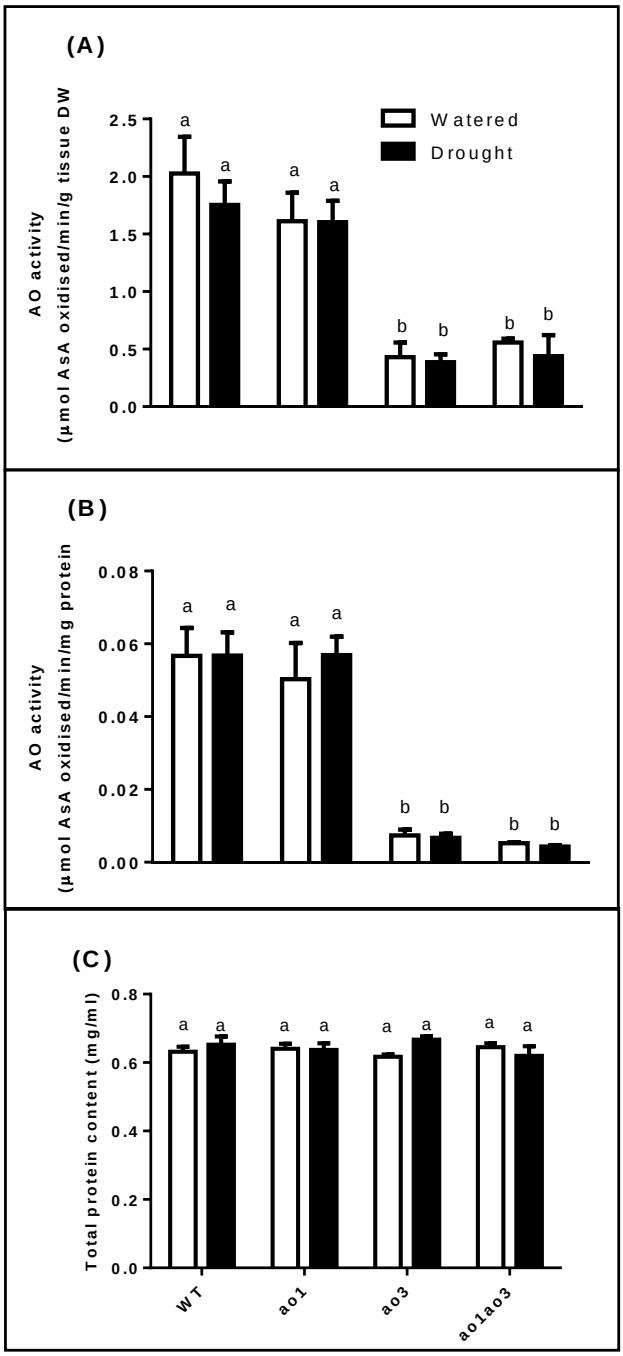

Figure 6-16: Ionically-bound cell wall AO activity of *AO* T-DNA insertion mutants after 14 days of watered or drought treatments. The AO activity was expressed on a dry weight **(A)** and protein **(B)** basis, respectively. **(C)** Protein concentration in tissue extracts (mg ml^{-1}). Due to varying amount of tissue extracted these values cannot be directly compared to enzyme activity data in A and B. Values are mean ± SEM, n = 4. Different letters above the bars denote the values are significantly different using one way ANOVA and Tukey tests ($p<0.05$). Values bearing the same letter are not significantly different from each other.

6.2.12. The effect of drought on *AO* gene expression of *AO* T-DNA insertion mutants

Semi-quantitative RT-PCR analysis was used to determine whether drought stress affected the expression levels of *AO* genes. Under watered or drought conditions, *AO1* gene expression was undetectable in *ao1* and *ao1ao3* mutants whereas *AO3* gene expression was undetectable in *ao3* and *ao1ao3* mutants. In WT plants, drought stress decreased the expression of all three *AO* genes. A small decrease in *AO2* gene expression was observed in all lines. Drought stress also tended to decrease the gene expression of *AO1* and *AO3* in *ao3* and *ao1* mutants respectively (Figure 6-17).

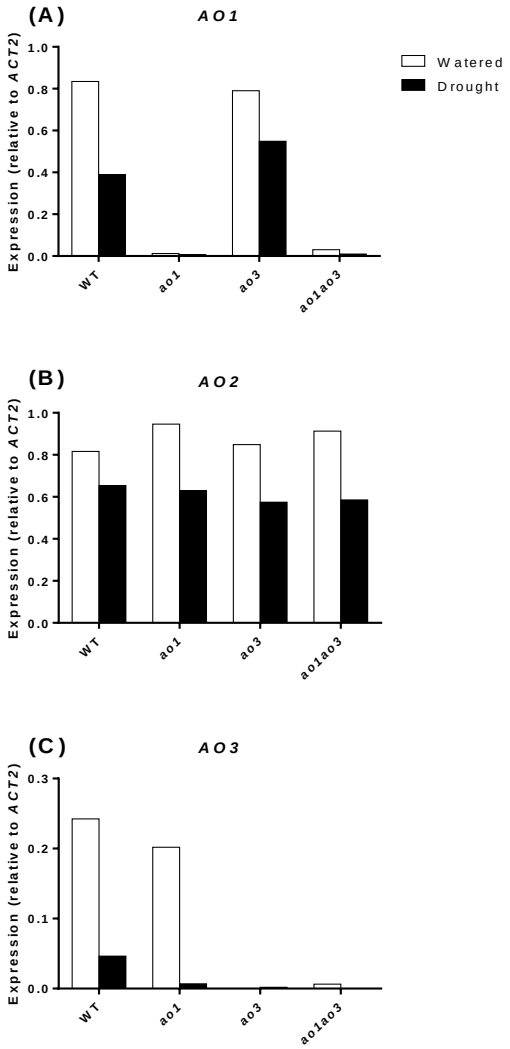

Figure 6-17: Relative transcript levels of *AO* genes in leaves of *AO* T-DNA insertion mutants after 14 days of watered or drought treatments. Leaves were pooled from four independent 6-week-old plants. The transcript levels were determined by semi-quantitative RT-PCR, where staining intensities of PCR products: *AO1*, *AO2* and *AO3* (**A−C**) were quantified using Image J software and normalised against *ACT2*. This experiment was repeated two times and similar results were obtained.

6.2.13. AsA concentrations of *AO* T-DNA insertion mutants during drought

14 days of drought treatment had little effect on the whole leaf AsA concentrations of WT and *ao* mutants. AsA concentration was expressed based on tissue DW rather than tissue FW due to a big variation in FW between watered tissue and drought tissue. The concentrations of reduced AsA, DHA and total AsA were similar between watered and drought treated plants across all genotypes studied (Figure 6-18A). The AsA redox state for all lines under watered and drought treatments were not significantly different (~ 80%) (Figure 6-18B).

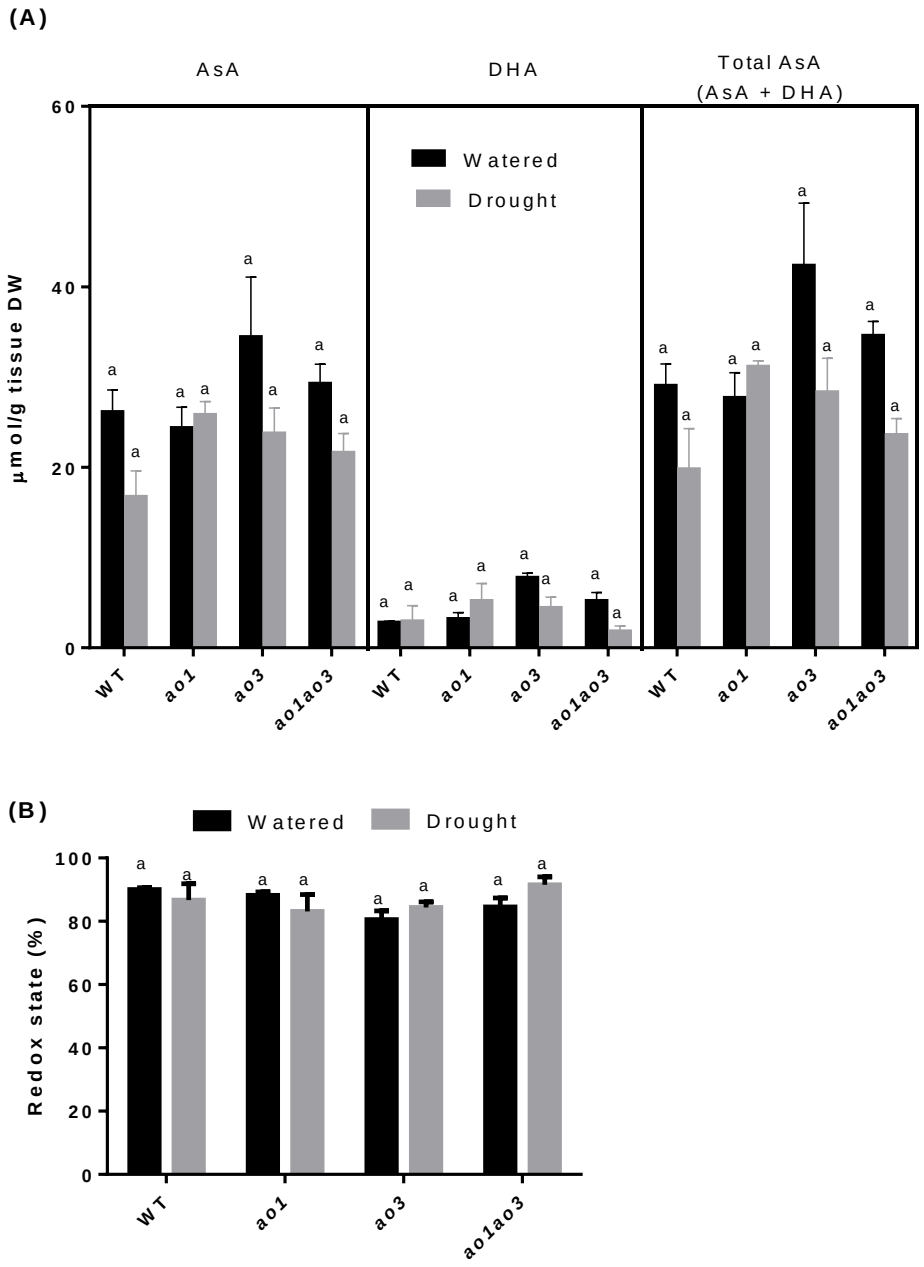

Figure 6-18: Whole leaf AsA concentrations of *AO* T-DNA insertion mutants after 14 days of watered or drought treatments. **(A)** The concentrations of reduced AsA, DHA and total AsA pool in WT and *ao* mutants. **(B)** The percent AsA redox state (ratio of reduced AsA to total AsA) of WT and *ao* mutants. Values are mean ± SEM, n = 4. Values bearing the same letter are not significantly different from each other using one way ANOVA and Tukey tests ($p<0.05$). Statistical analyses for reduced AsA, DHA and total AsA data were performed separately.

The concentrations of apoplastic AsA in WT and *ao* mutants after 14 days of drought treatment were examined. Apoplastic AsA was extracted from all rosette leaves of the same plants as used for whole leaf AsA analysis. Due to a big variation in tissue FW between watered and drought tissues, the apoplastic AsA concentrations were expressed on the basis of apoplastic fluid recovered (mM as the unit) rather than tissue FW. The concentrations of apoplastic reduced AsA in *ao3* and *ao1ao3* under watered and drought conditions were significantly higher than WT and *ao1*, although treatments (watered or drought) had little effect on the concentrations of apoplastic reduced AsA for all lines (Figure 6-19A). The apoplastic DHA concentrations in drought treated tissues for all lines were lower than the watered counterparts. No significant differences were found in the concentrations of apoplastic DHA between WT and *ao* mutants under drought or watered conditions (Figure 6-19A). The total AsA pool (reduced AsA + DHA) for drought treated plants were significantly lower than the watered counterparts for all lines, although no significant differences were found across genotypes under watered or drought conditions (Figure 6-19A). The AsA redox state appeared to be higher in drought treated plants than the watered plants (Figure 6-19B). It should be noted that the apoplastic fluid recovered in drought tissues were significantly lower than watered tissues (Figure 6-19C), because 3 mins infiltration period was insufficient to fill up the apoplastic space of drought tissues, a result of low stomatal conductance in drought tissues. This could be the reason contributed to low total AsA pool and high AsA redox state found in drought treated plants.

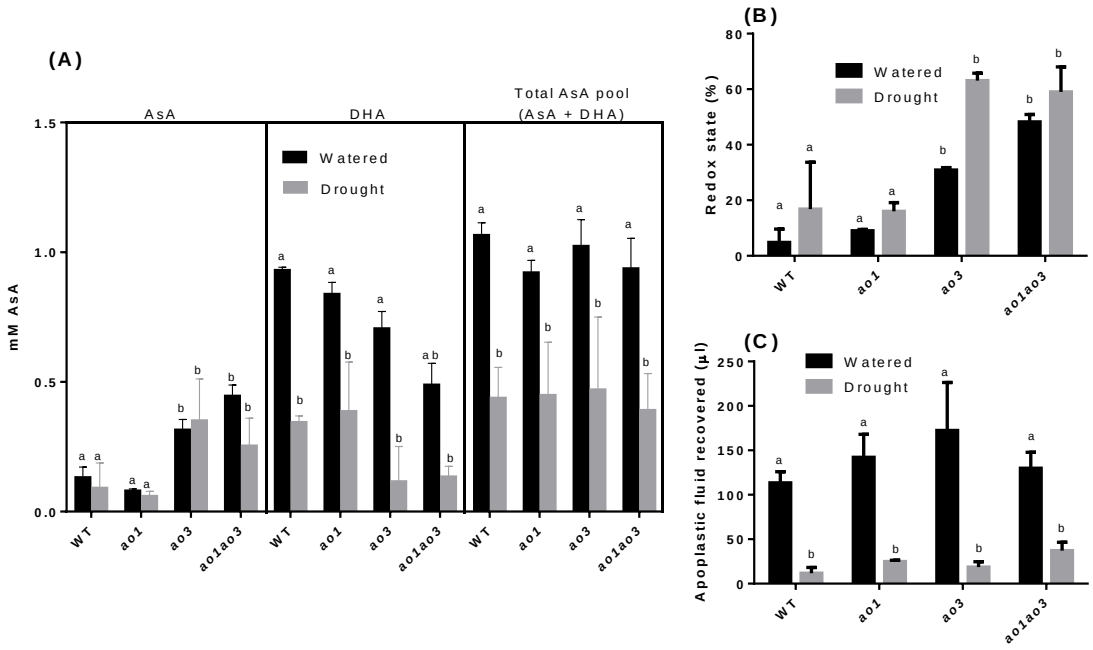

Figure 6-19: Apoplastic AsA concentrations of *AO* T-DNA insertion mutants after 14 days of watered or drought treatments. **(A)** Apoplastic reduced AsA, DHA and total AsA pool from whole rosette leaves of WT and *ao* mutants. **(B)** The percent AsA redox state (ratio of reduced AsA to total AsA) of WT and *ao* mutants. **(C)** The yield of apoplastic fluid after vacuum infiltration. Values are mean ± SEM, n (pool of plants per replicate) = 2, N (number of replicate) = 3. Different letters above the bars denote the values are significantly different using one way ANOVA and Tukey tests ($p<0.05$). Values bearing the same letter are not significantly different from each other. Statistical analyses for reduced AsA, DHA and total AsA data were performed separately.

6.2.14. The effect of drought on leaf water loss, relative water content and photosynthetic capacity of *AO* T-DNA insertion mutants

Analyses on leaf water loss, relative water content and photosynthetic capacity were performed to determine the physiological status and to understand stress tolerance between WT and *ao* mutants.

The leaf water loss, expressed as percent reduction of initial FW following leaf detachment from watered plants, was similar between WT and *ao* mutants. The percent initial FW for all lines steadily decreased over a period of 90 mins, but did not differ between WT and *ao* mutants (Figure 6-20A). Drought stressed plants showed significantly reduced in relative water content (RWC) than that of control, well watered plants after 14 days of dehydration. Within each treatment (watered and drought), the RWC between WT and *ao* mutants was not significantly different (Figure 6-20B). The dark adapted maximum quantum yield of photosystem II (F_v/F_m) was assessed to evaluate the effect of drought on the photosynthetic capacity of WT and *ao* mutants. F_v/F_m values (~0.80) did not vary for plants under watered condition, and only a small decline (~0.70 to 0.76) was observed in the drought treated plants. The F_v/F_m values between WT and *ao* mutants were not significantly different either in watered or drought conditions (Figure 6-20C).

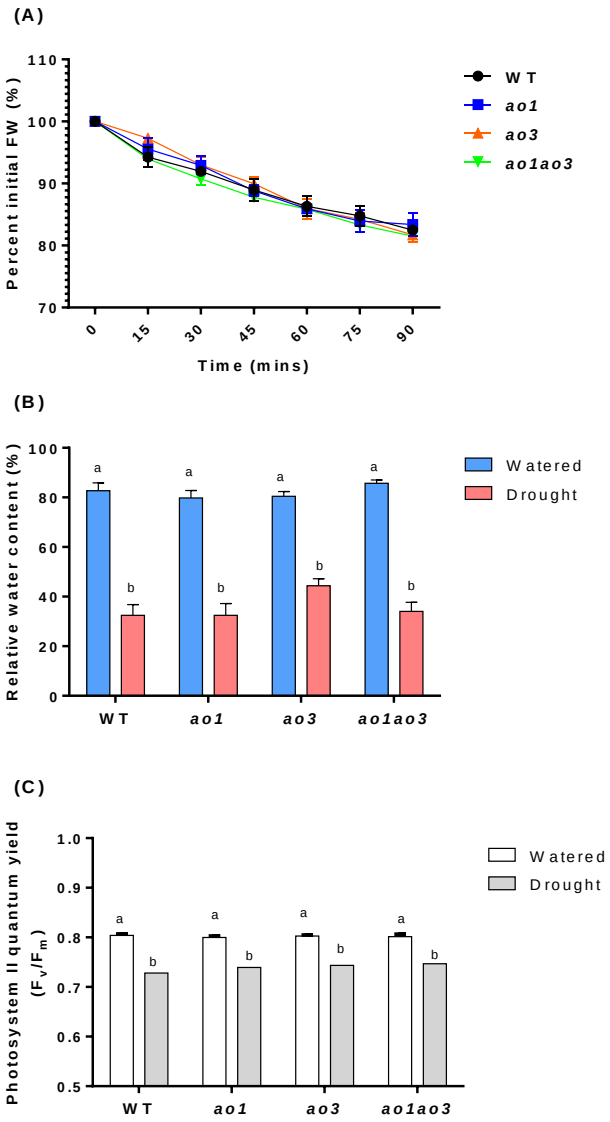

Figure 6-20: Analyses of the leaf water loss, relative water content and photosystem II quantum yield in *AO* T-DNA insertion mutants after 14 days of watered or drought treatments. **(A)** Leaf water loss assay. Fully expanded leaves were detached from watered plants. **(B)** Relative water content of detached leaves from watered or drought plants. **(C)** Photosystem II quantum yield of dark adapted watered or drought plants. Values are mean ± SEM, n = 4. Different letters above the bars denote the values are significantly different using one way ANOVA and Tukey tests ($p<0.05$). Values bearing the same letter are not significantly different from each other.

6.2.15. Ionically-bound cell wall peroxidase activity of *AO* T-DNA insertion mutants during drought

For drought studies, ionically-bound cell wall peroxidase activity was expressed based on tissue DW rather than tissue FW due to a big variation in FW between watered tissue and drought tissue. Drought stress had increased the peroxidase activity of WT and *ao* mutants compared to the watered counterparts, when expressed on a DW (Figure 6-21A) or protein (Figure 6-21B) basis. However, the difference between watered and drought treatments for all lines was not statistically significant, except *ao1ao3*. Also, the peroxidase activity between WT and *ao* mutants under watered and drought treatment was not significantly different. WT and *ao* mutants had similar level of total protein content under watered or drought conditions (Figure 6-21C).

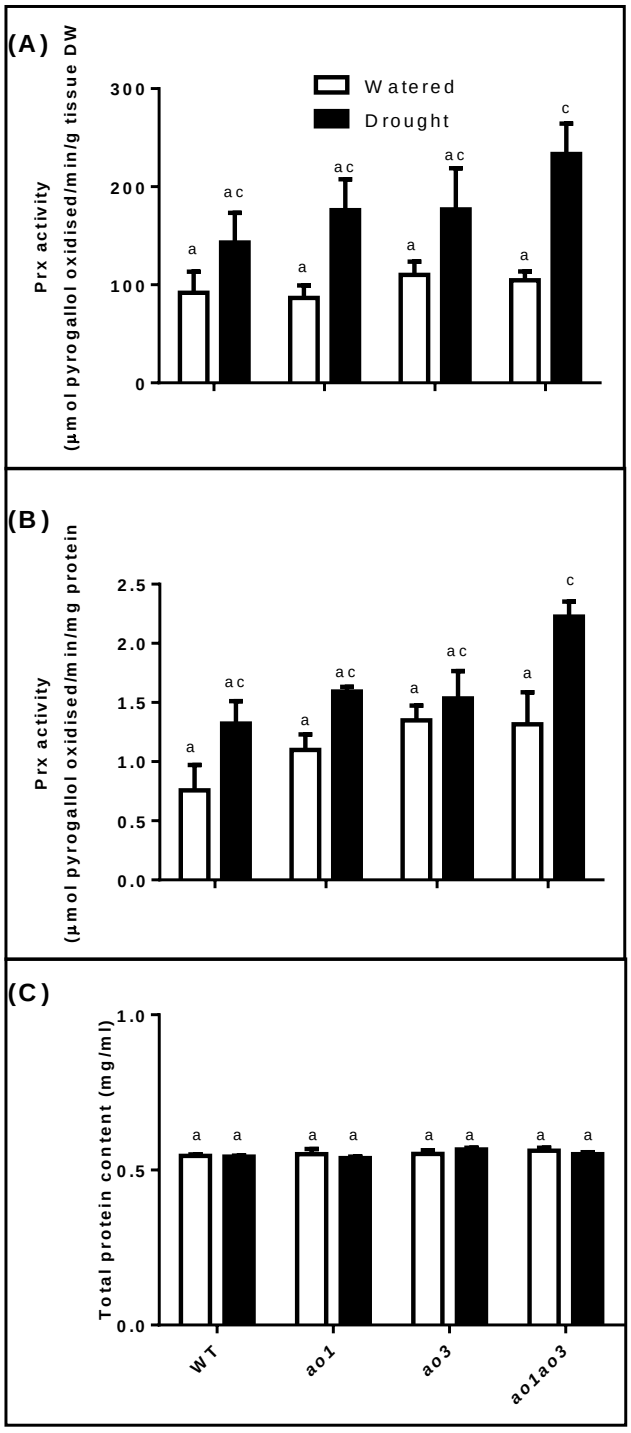

Figure 6-21: Ionically-bound cell wall peroxidase activity of *AO* T-DNA insertion mutants after 14 days of watered or drought treatments. The peroxidase activity was expressed on a dry weight **(A)** and protein **(B)** basis, respectively. **(C)** Protein concentration in tissue extracts (mg ml^{-1}). Due to varying amount of tissue extracted these values cannot be directly compared to enzyme activity data in A and B. Values are mean ± SEM, n = 4. Different letters above the bars denote the values are significantly different using one way ANOVA and Tukey tests ($p<0.05$). Values bearing the same letter are not significantly different from each other.

6.2.16. The effect of HL acclimation on *amiR-AO* and *35S::AO3* transgenic lines

In previous section, I have described the effect of HL acclimation in *AO* T-DNA insertion mutants. Although the ionically-bound cell wall AO activity of *ao3* and *ao1ao3* mutants was about 10% of the WT, these mutants did not show any phenotypic differences compared with WT under HL acclimation. Here, 6-week-old *amiR-AO* and *35S::AO3* transgenic lines were acclimated to HL for 7 days to assess the effect of abolished foliar AO activity (in *amiR-AO* lines) and elevated foliar AO activity (in *35S::AO3*) in anthocyanin accumulation of *A. thaliana*. After 7 days of HL treatment, two independent *amiR-AO* lines (line 3.6 and line 8.5) accumulated more anthocyanin than the WT and *35S::AO3* plants. No apparent difference in term of anthocyanin accumulation between WT and *35S::AO3*. Anthocyanin accumulation was more extensive in fully expanded leaves than in young leaves for all lines (Figure 6-22A). Anthocyanin initially accumulated in the lower epidermis where it was apparent in all lines (Figure 6-22C), then spread to upper epidermis where it was visible only in *amiR-AO (3.6)* and *amiR-AO (8.5)* (Figure 6-22B). Meanwhile, WT and transgenic lines did not show visible anthocyanin accumulation during LL treatment (Figure 6-22A).

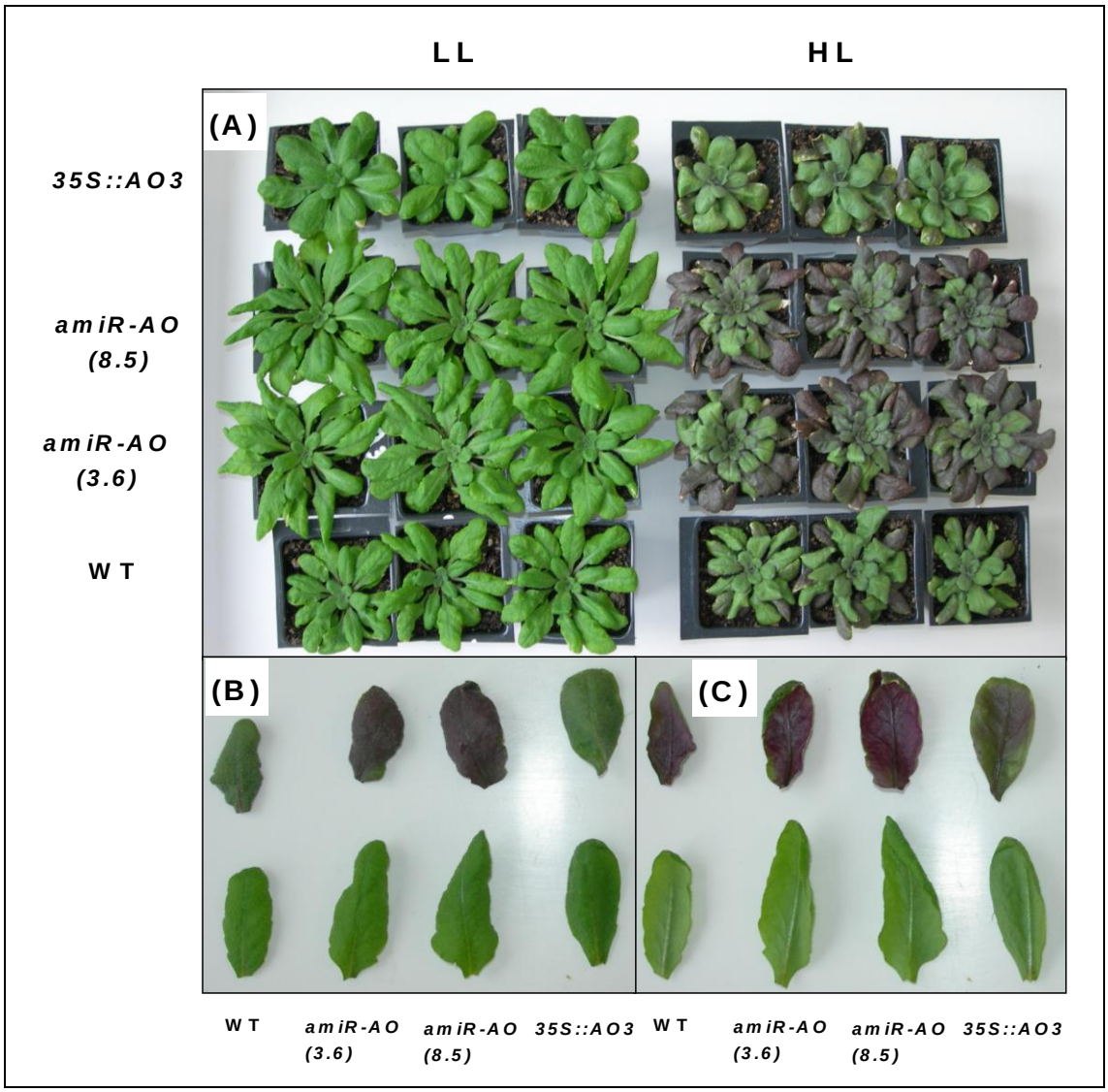

Figure 6-22: Phenotype of *amiR-AO* and *35S::AO3* transgenic lines during high light acclimation. 6-week-old plants (n = 3) were subjected to high light (HL, PPFD = 550-650 µmol m^{-2} s^{-1}) or low light (LL, PPFD = 100 µmol m^{-2} s^{-1}) treatments for 7 days. **(A)** Picture was taken after LL and HL treatments. **(B)** Representative leaves (upper epidermis) of WT and transgenic lines after acclimated to LL (bottom) or HL (top) for 7 days. **(C)** Representative leaves (lower epidermis) of WT and transgenic lines after acclimated to LL (bottom) or HL (top) for 7 days.

6.2.17. Determination of foliar anthocyanin, chlorophyll and carotenoid contents in *amiR-AO* and *35S::AO3* transgenic lines acclimated to LL or HL for 7 days

Fully expanded leaves of WT and transgenic lines were used to measure anthocyanin content after 7 days of LL or HL treatments. In agreement with the plant phenotype observed, HL acclimated plants had substantially increased the foliar anthocyanin content compared to the LL acclimated plants in all lines. Under HL acclimation, both *amiR-AO* lines had significantly higher anthocyanin content than WT and *35S::AO3*. WT had intermediate level of anthocyanin while *35S::AO3* had the lowest anthocyanin content among all lines acclimated to HL. Under LL, the anthocyanin content between WT and transgenic lines were not significantly different (Figure 6-23).

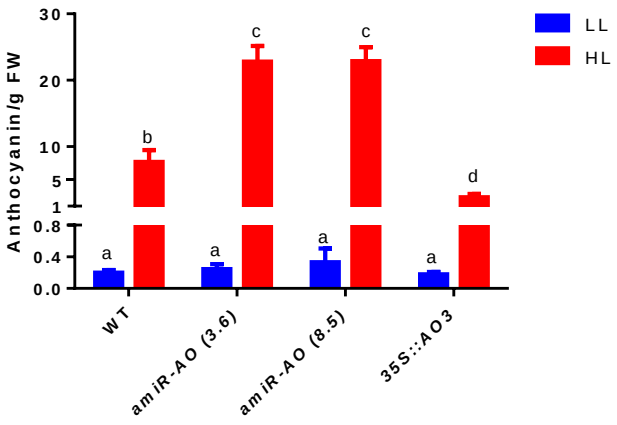

Figure 6-23: Foliar anthocyanin content of *amiR-AO* and *35S::AO3* transgenic lines acclimated to LL or HL for 7 days. Values are mean ± SEM, n = 4. Different letters above the bars denote the values are significantly different using one way ANOVA and Tukey tests ($p<0.05$). Values bearing the same letter are not significantly different from each other. LL, low light (PPFD = 100 µmol m^{-2} s^{-1}); HL, high light (PPFD = 550-650 µmol m^{-2} s^{-1}).

Foliar chlorophyll and carotenoid measurements were performed to assess if these pigments were affected by anthocyanin accumulation during HL. Chlorophyll a content appeared to be lower for all lines under HL acclimation but the differences were not statistically significant except *amiR-AO (8.5)*. No significance difference was found across genotype in terms of chlorophyll a content (Figure 6-24A). HL acclimation increased the chlorophyll b content of WT and *amiR-AO (3.6)* but decreased in *amiR-AO (8.5)* and *35S::AO3* lines, resulting higher total chlorophyll contents in WT and *amiR-AO (3.6)* compared with *amiR-AO (8.5)* and *35S::AO3*. However, the differences in total chlorophyll contents were not statistically significant except *amiR-AO (8.5)* that had significantly lower total chlorophyll contents under HL acclimation (Figure 6-24A). The carotenoid content of HL treated plants appeared to be lower than the LL plants for all lines, but the differences were not statistically significant except *amiR-AO (8.5)* (Figure 6-24B).

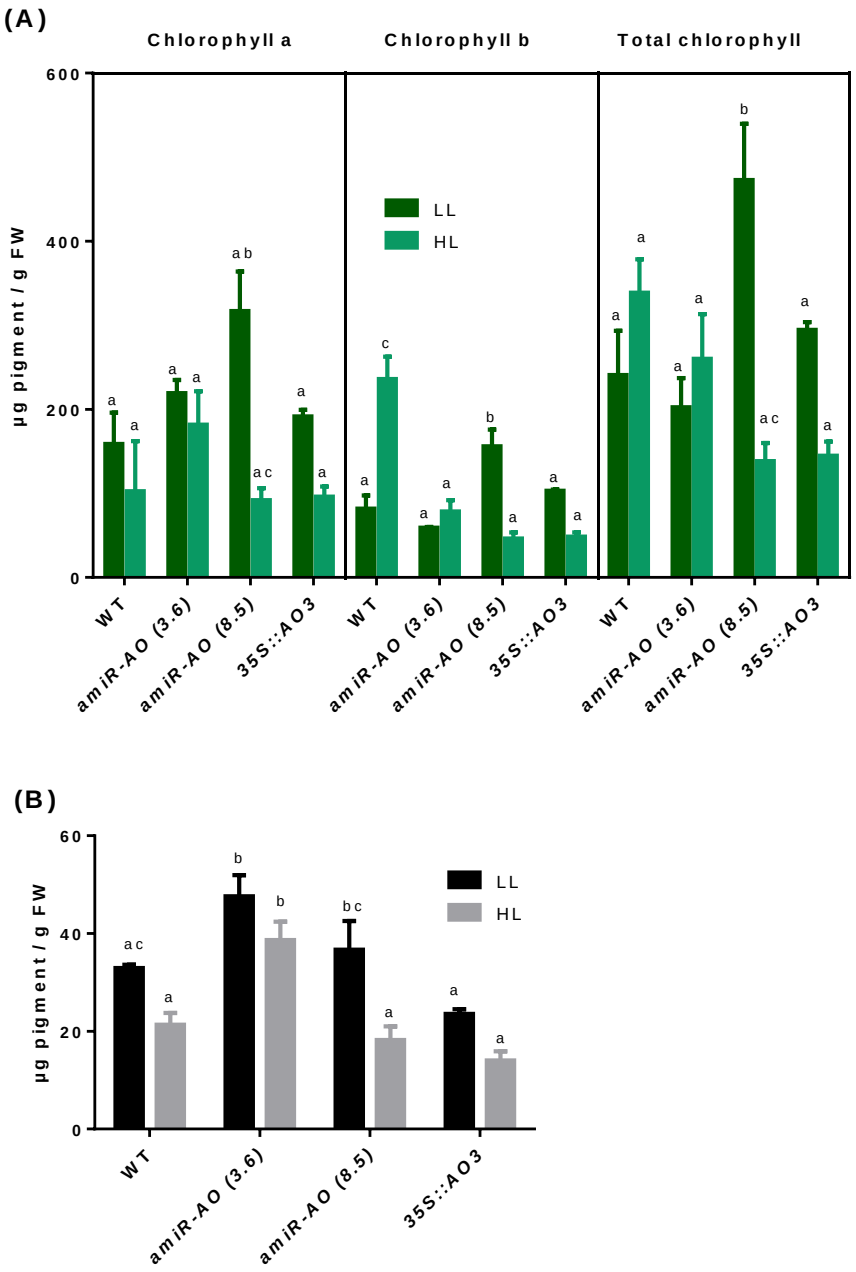

Figure 6-24: Chlorophyll **(A)** and carotenoid **(B)** contents in leaves of *amiR-AO* and *35S::AO3* transgenic lines acclimated to LL or HL for 7 days. Values are mean ± SEM, n = 4. Different letters above the bars denote the values are significantly different using one way ANOVA and Tukey tests ($p<0.05$). Values bearing the same letter are not significantly different from each other. Statistical analyses for chlorophyll a, chlorophyll b and total chlorophyll data were performed separately. LL, low light (PPFD = 100 µmol m^{-2} s^{-1}); HL, high light (PPFD = 550-650 µmol m^{-2} s^{-1}).

6.2.18. Ionically-bound cell wall AO activity of *amiR-AO* and *35S::AO3* transgenic lines acclimated to LL or HL for 7 days

HL acclimation significantly increased the ionically-bound cell wall AO activity of WT and *35S::AO3* compared to their counterparts under LL, when expressed on a tissue FW or protein basis, where the highest AO activity was found in *35S::AO3*. AO activity was undetectable in two *amiR-AO* lines under LL or HL (Figure 6-25A and B). No significant differences were found in the total protein content of all lines under LL or HL conditions (Figure 6-25C).

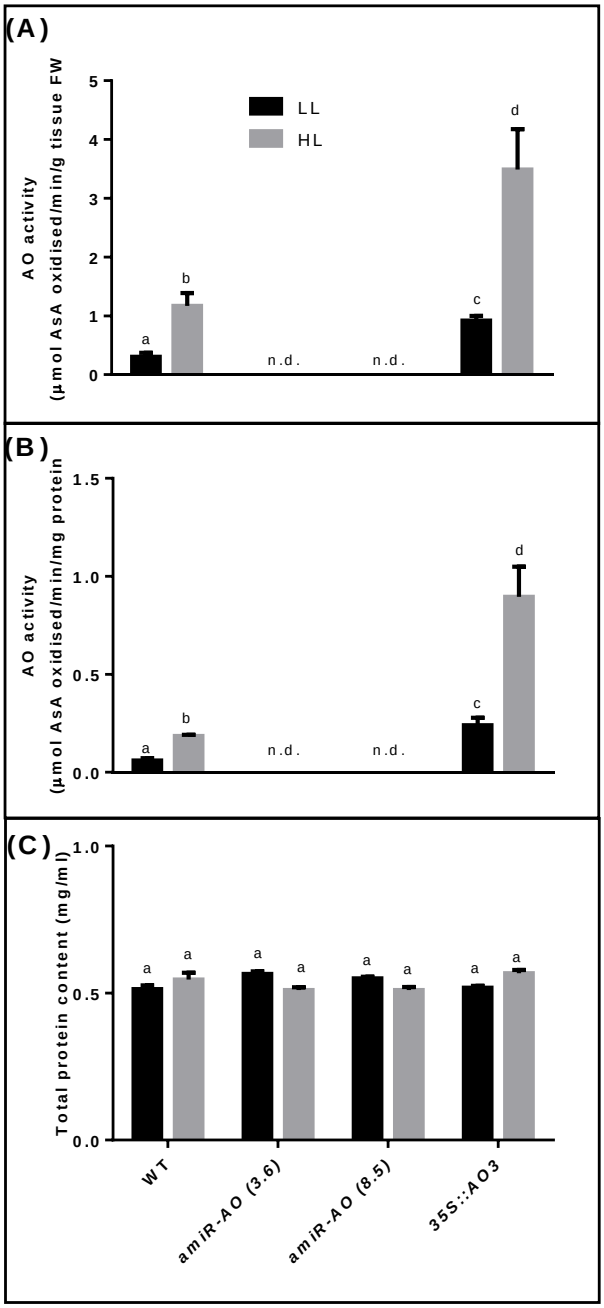

Figure 6-25: Ionically-bound cell wall AO activity of *amiR-AO* and *35S::AO3* transgenic lines acclimated to LL or HL for 7 days. The AO activity of plants subjected to low light (LL) and high light (HL) conditions was expressed on a fresh weight **(A)** and protein **(B)** basis, respectively. **(C)** Protein concentration in tissue extracts (mg ml^{-1}). Due to varying amount of tissue extracted these values cannot be directly compared to enzyme activity data in A and B. Values are mean ± SEM, n = 3. Different letters above the bars denote the values are significantly different using one way ANOVA and Tukey tests ($p<0.05$). Values bearing the same letter are not significantly different from each other. N.d. = AO activity not detected.

6.2.19. AsA concentrations of *amiR-AO* and *35S::AO3* transgenic lines during HL acclimation

HL acclimation had significantly increased the concentration of whole leaf reduced AsA in all lines, in which two *amiR-AO* lines (3.6 and 8.5) had significantly higher reduced AsA than WT and *35S::AO3*. The reduced AsA concentration of *35S::AO3* was similar to the WT under HL. No significant differences were found in the whole leaf reduced AsA concentration for all lines under LL (Figure 6-26A). The whole leaf DHA concentrations for WT and two *amiR-AO* lines were not statistically different under LL or HL conditions, except the *35S::AO3* line that had higher DHA concentration under HL (Figure 6-26A). No significant differences were found in the total AsA pool for all lines under LL. Meanwhile, two *amiR-AO* lines (3.6 and 8.5) had higher total AsA pool than WT and *35S::AO3* (Figure 6-26A) under HL. The total AsA pool in *35S::AO3* was not significantly different from WT under HL. The AsA redox state between WT and these transgenic lines were not significantly different under LL or HL conditions (Figure 6-26B).

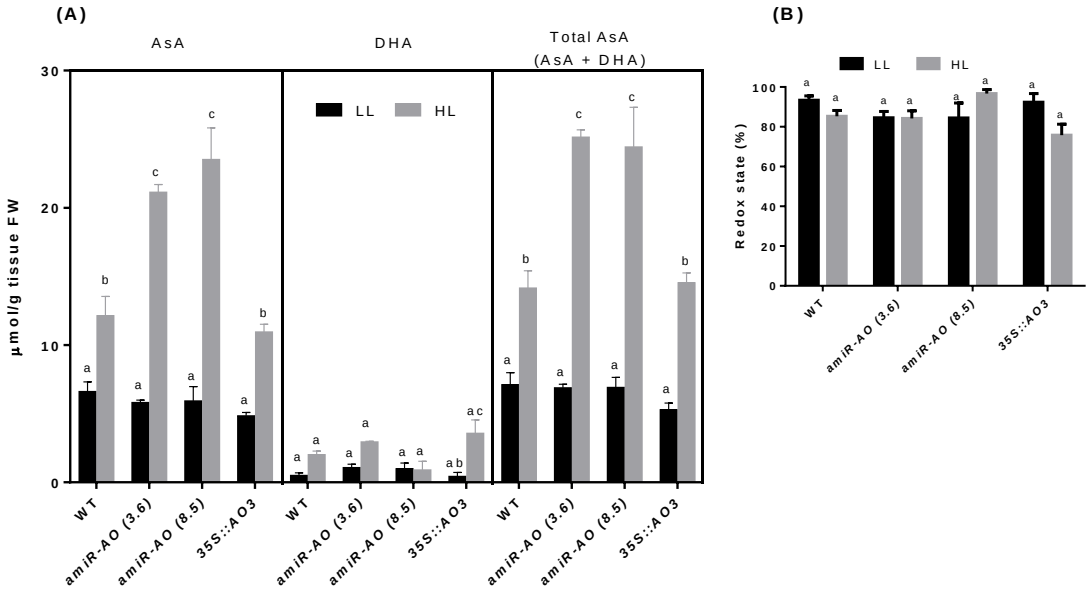

Figure 6-26: Whole leaf AsA concentrations of *amiR-AO* and *35S::AO3* transgenic lines acclimated to LL or HL for 7 days. **(A)** Reduced AsA, DHA and total AsA pool of plants acclimated to LL or HL for 7 days. **(B)** The percent redox state (ratio of reduced to total AsA) of WT and transgenic lines. Values are mean ± SEM, n = 3. Different letters above the bars denote the values are significantly different using one way ANOVA and Tukey tests ($p<0.05$). Values bearing the same letter are not significantly different from each other. Statistical analyses for reduced AsA, DHA and total AsA data were performed separately. LL, low light (PPFD = 100 µmol m^{-2} s^{-1}); HL, high light (PPFD = 550-650 µmol m^{-2} s^{-1}).

The apoplastic AsA concentration was determined to assess the relationship between apoplastic AsA and anthocyanin accumulation in these transgenic lines. Apoplastic AsA was extracted from all rosette leaves of the same plants as used for whole leaf AsA analysis. The yield of apoplastic fluid was not statistically different between LL and HL plants for all lines, although *amiR-AO (3.6)* plants under LL appeared to have higher yield of apoplastic fluid (Figure 6-27C). Under LL, *amiR-AO (3.6)* and a*miR-AO (8.5)* had significantly higher reduced AsA concentration in the apoplast than WT and *35S::AO3*, with the highest concentration was detected in the *amiR-AO (8.5)* line. The reduced AsA concentration in the apoplast of *35S::AO3* was nearly abolished compared to WT under LL (Figure 6-27A). In contrast to whole leaf reduced AsA, the apoplastic reduced AsA concentration for all lines was not significantly affected by HL acclimation (Figure 6-27A). The apoplastic DHA concentration for two *amiR-AO* lines were lower than WT and *35S::AO3* under LL. Under HL, all transgenic lines (*amiR-AO* and *35S::AO3*) had lower apoplastic DHA concentration than WT (Figure 6-27A). Despite of the variations observed in the apoplastic reduced AsA and DHA concentrations, no significance differences were found in the total AsA pool for all lines under LL or HL conditions (Figure 6-27A). The apoplastic AsA redox state for *amiR-AO* lines was significantly higher than WT and *35S::AO3* under LL or HL, in which *amiR-AO (8.5)* line had the highest AsA redox state. The apoplastic AsA redox state in all lines was not affected by HL acclimation (Figure 6-27B).

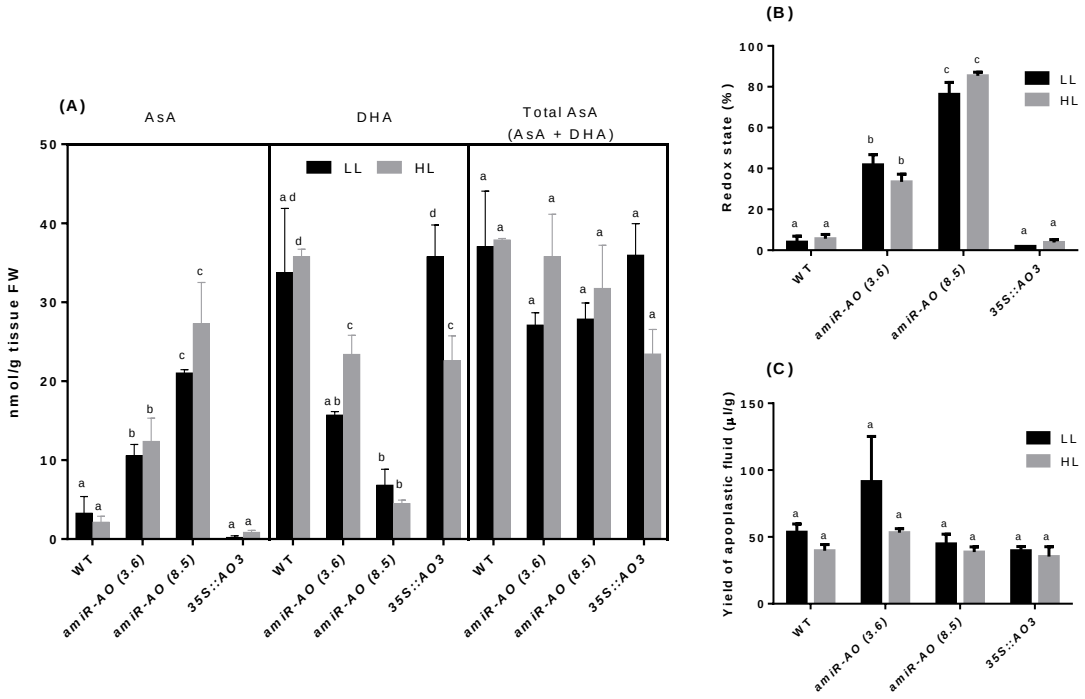

Figure 6-27: Apoplastic AsA concentrations of *amiR-AO* and *35S::AO3* transgenic lines acclimated to LL or HL for 7 days. **(A)** Apoplastic reduced AsA, DHA and total AsA pool from whole rosette leaves of WT and transgenic lines. **(B)** The percent AsA redox state (ratio of reduced AsA to total AsA) of WT and transgenic lines. **(C)** The yield of apoplastic fluid after vacuum infiltration. Values are mean ± SEM, n = 3. Different letters above the bars denote the values are significantly different using one way ANOVA and Tukey tests ($p<0.05$). Values bearing the same letter are not significantly different from each other. Statistical analyses for reduced AsA, DHA and total AsA data were performed separately. LL, low light (PPFD = 100 µmol m^{-2} s^{-1}); HL, high light (PPFD = 550-650 µmol m^{-2} s^{-1}).

6.2.20. Ionically-bound cell wall peroxidase activity of *amiR-AO* and *35S::AO3* transgenic lines during HL acclimation

When ionincally-bound cell wall peroxidase activity expressed on FW basis, HL acclimation increased the peroxidase activity in all lines, but the levels of peroxidase activity across all strains were not significantly different. Under LL, both *amiR-AO* lines (3.6 and 8.5) had lower peroxidase activity than WT and *35S::AO3*, where the highest peroxidase activity was found in *35S::AO3* (Figure 6-28A). Similar pattern was observed when peroxidase activity expressed on protein basis, but the differences became small compared to those expressed on FW basis (Figure 6-28B). WT, *amiR-AO* and *35S::AO3* lines had similar level of total protein content under LL or HL conditions (Figure 6-28C).

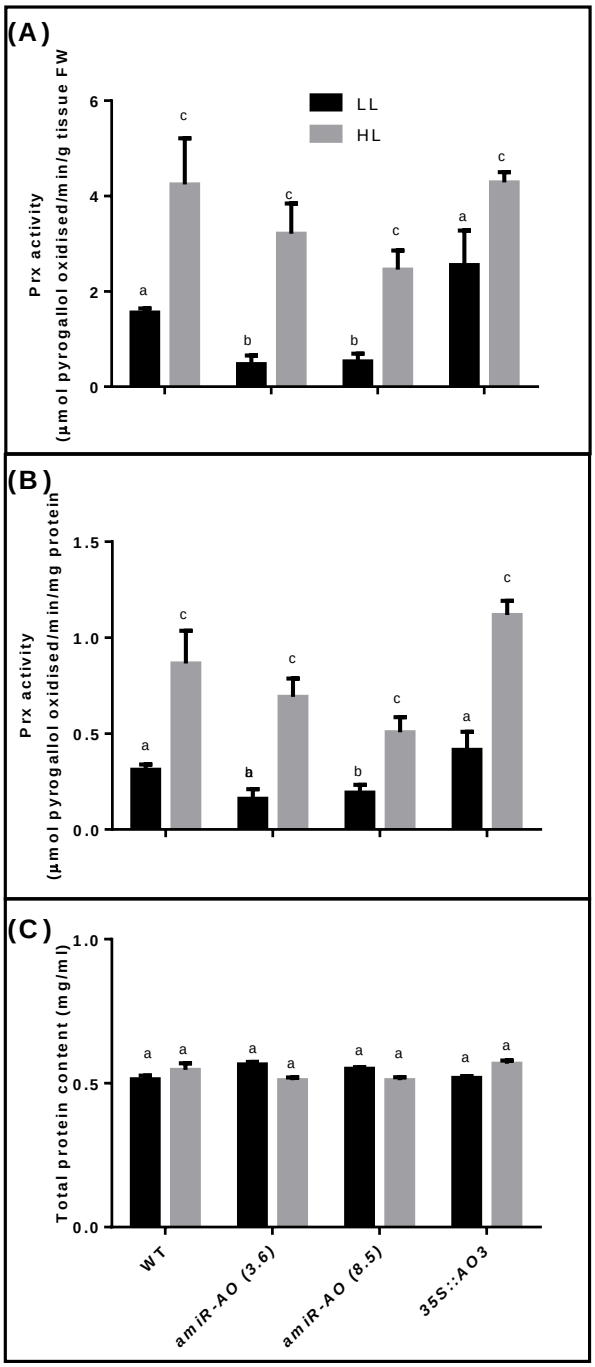

Figure 6-28: Ionically-bound cell wall peroxidase activity of *amiR-AO* and *35S::AO3* transgenic lines during HL acclimation. The peroxidase activity of plants subjected to low light (LL) and high light (HL) conditions was expressed on a fresh weight **(A)** and protein **(B)** basis, respectively. **(C)** Protein concentration in tissue extracts (mg ml^{-1}). Due to varying amount of tissue extracted these values cannot be directly compared to enzyme activity data in A and B. Values are mean ± SEM, n = 3. Different letters above the bars denote the values are significantly different using one way ANOVA and Tukey tests ($p<0.05$). Values bearing the same letter are not significantly different from each other.

6.2.21. The effect of drought on *amiR-AO* and *35S::AO3* transgenic lines

After 14 days of dehydration, all lines showed leaf wilting symptoms and older leaves at the bottom of rosette exhibited early senescence. The *amiR-AO* and *35S::AO3* transgenic lines had no obvious difference in drought sensitivity compared with the WT (Figure 6-29). A few spare plants were drought treated until day 18. After 18 days of drought treatment, the *35S::AO3* showed increased sensitivity to drought compared with WT and *amiR-AO* lines. No phenotypic differences were found between WT and *amiR-AO* lines after 18 days of drought (Figure 6-30). Other independent experiments performed before the *amiR-AO* lines were isolated showed that *35S::AO3* plants were more sensitive to drought (Appendix E). Leaves from plants subjected to 14 days drought treatment were harvested for experiments.

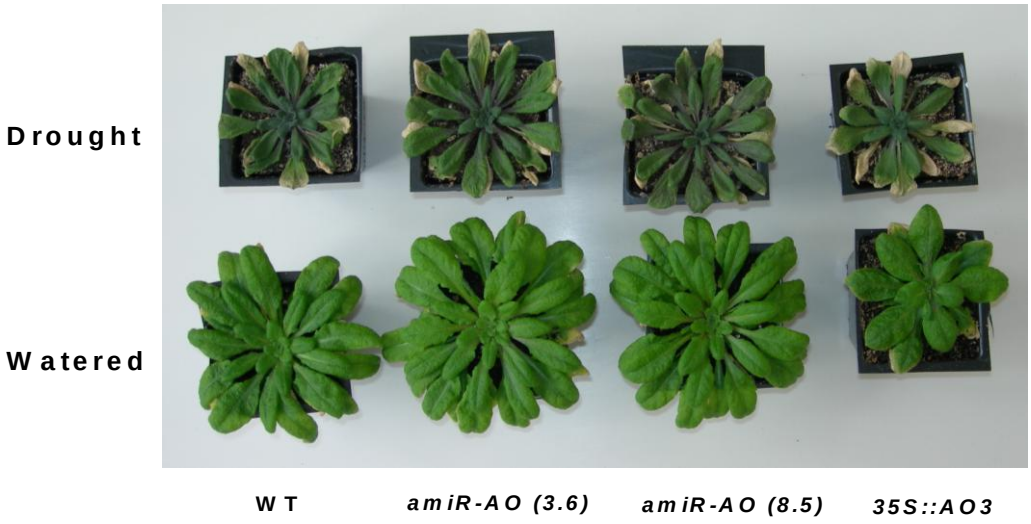

Figure 6-29: Phenotype of *amiR-AO* and *35S::AO3* transgenic lines after 14 days of watered or drought treatments. Pictures of WT and transgenic lines were taken on day 14 and representative plants are shown. Watered: 6-week-old plants were watered every 3 days for 14 days. Drought stress: 6-week-old plants were withheld from watering for 14 days.

Figure 6-30: Phenotype of *amiR-AO* and *35S::AO3* transgenic lines after 18 days of drought. Pictures of WT and transgenic lines were taken on day 18. Two plants per genotype are shown.

The soil water content decreased over time in drought treated plants compared to the watered plants. However, the soil water content in drought treated WT and transgenic lines were not significantly different from each other (Figure 6-31A), suggesting WT and these transgenic lines were exposed to a similar dehydration rate during drought. The absolute total leaf area (ATLA) and the absolute expansion rates (AER) in WT and transgenic lines were determined to assess the effect of drought on leaf growth of these transgenic lines. The ATLA of watered plants increased over time for all lines, in which two independent *amiR-AO* lines (3.6 and 8.5) had greater ATLA than WT and *35S::AO3*. The ATLA of WT and *35S::AO3* was not significantly different under watered condition (Figure 6-31B). Drought treated plants only showed an increase in

ATLA for the first 8 days of the treatment, then showed growth arrest followed by reduction in ATLA on day 11. Compared with WT and *35S::AO3*, *amiR-AO* lines had greater ATLA in the first 8 days of drought followed by a big reduction in ATLA from day 11 onwards (15.7% for line 3.6 and 11.7% for line 8.5), whereas the reduction observed in WT and *35S::AO3* was smaller (6.3% for WT and 7.8% for *35S::AO3*). A decrease in ATLA indicated the cessation of plant growth followed by the loss of turgor pressure in drought treated leaves (Figure 6-31B).

The AER of leaves in WT and transgenic lines under watered treatment varied throughout 14 days of the experiment, in which the *amiR-AO* lines showed greater AER than WT and *35S::AO3* in general. In drought treated plants, a dynamic but not significantly differ AER was observed between WT and transgenic lines in the first 8 days and then decreased dramatically from day 11 onwards (Figure 6-31C). It should be noted that the negative AER observed from day 11 of the drought treatment was due to the cessation of plant growth followed by the loss of turgor pressure in drought treated leaves.

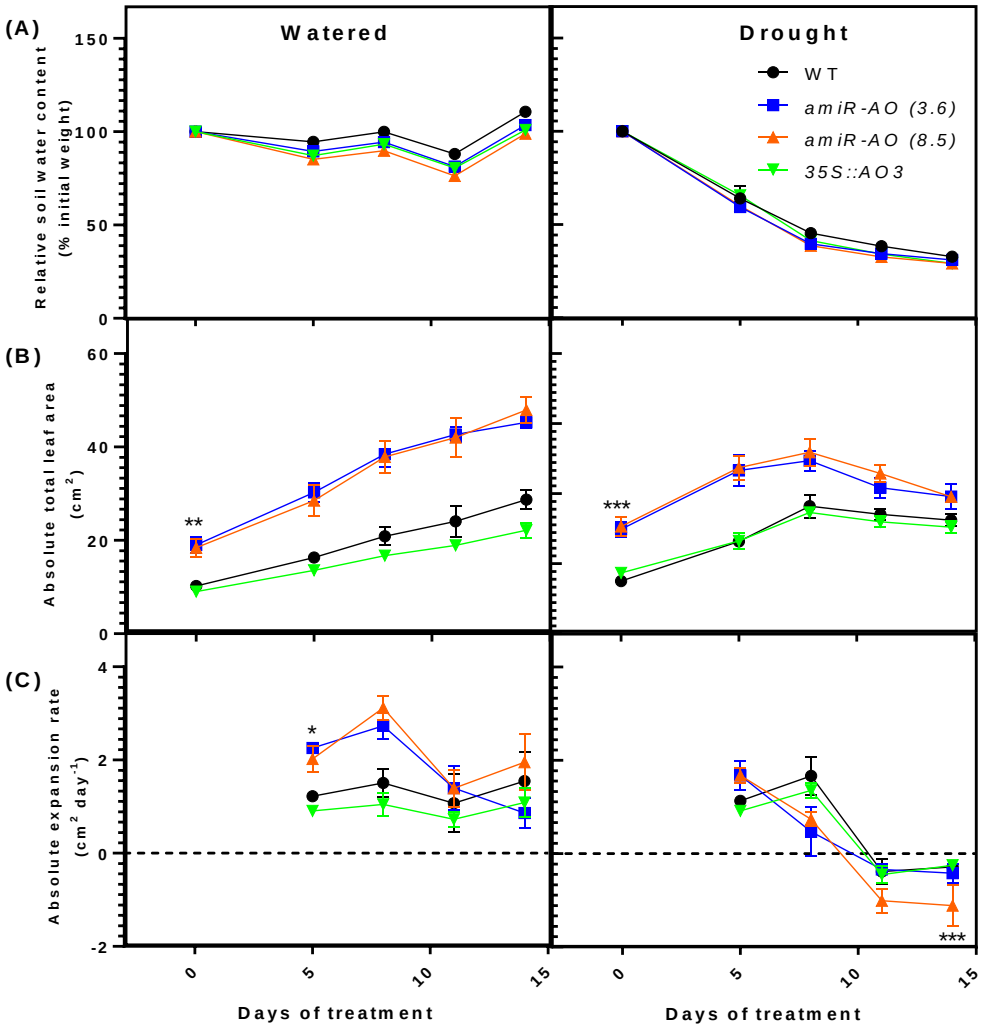

Figure 6-31: Leaf growth of *amiR-AO* and *35S::AO3* transgenic lines during drought. Observations were made in the 14 days of watered (left panels) and drought (right panels) treatments. **(A)** Soil water content, assessed by measuring reduction of pot + plant weight and plotted as percentage relative to initial weight. **(B)** Absolute total leaf area, the decrease of leaf area indicated the cessation of plant growth followed by the loss of turgor pressure in drought treated leaves. **(C)** Absolute expansion rate of leaves, the negative growth rates indicated the cessation of plant growth followed by the loss of turgor pressure in drought treated leaves. Values are mean ± SEM, n = 4. Asterisks denote the values are significantly different from the WT at *p<0.05, **p<0.01 and ***p<0.001. Control: 6-week-old plants were watered every 3 days for 14 days. Drought stress: 6-week-old plants were withheld from watering for 14 days.

6.2.22. Determination of foliar anthocyanin, chlorophyll and carotenoid contents in *amiR-AO* and *35S::AO3* transgenic lines subjected to drought

Drought stress significantly increased the foliar anthocyanin content of WT and transgenic lines compared with the watered plants. The anthocyanin content between WT and these transgenic lines, however, did not significantly varied either in watered or drought conditions (Figure 6-32). The chlorophylls (chlorophyll a, b and total chlorophyll) and carotenoid contents were significantly decreased in drought treated plants compared with the watered counterparts. However, there were no significant differences across all strains either under watered or drought conditions (Figure 6-33).

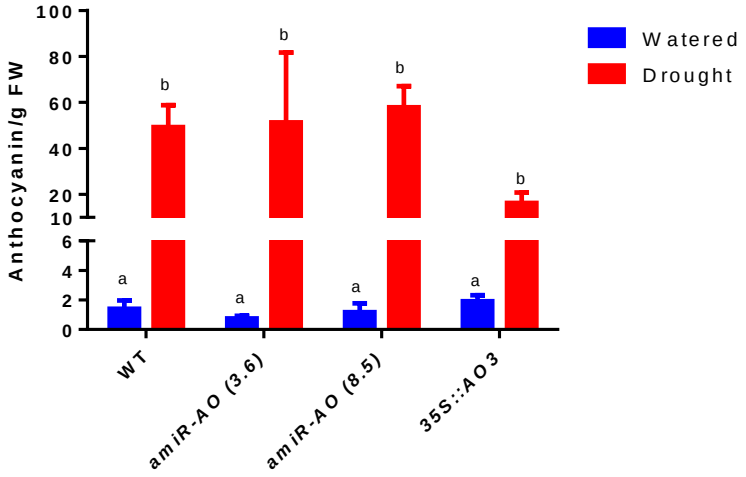

Figure 6-32: Foliar anthocyanin content of *amiR-AO* and *35S::AO3* transgenic lines after 14 days of watered or drought treatments. Values are mean ± SEM, n = 4. Different letters above the bars denote the values are significantly different using one way ANOVA and Tukey tests ($p<0.05$). Values bearing the same letter are not significantly different from each other. Control: 6-week-old plants were watered every 3 days for 14 days. Drought stress: 6-week-old plants were withheld from watering for 14 days.

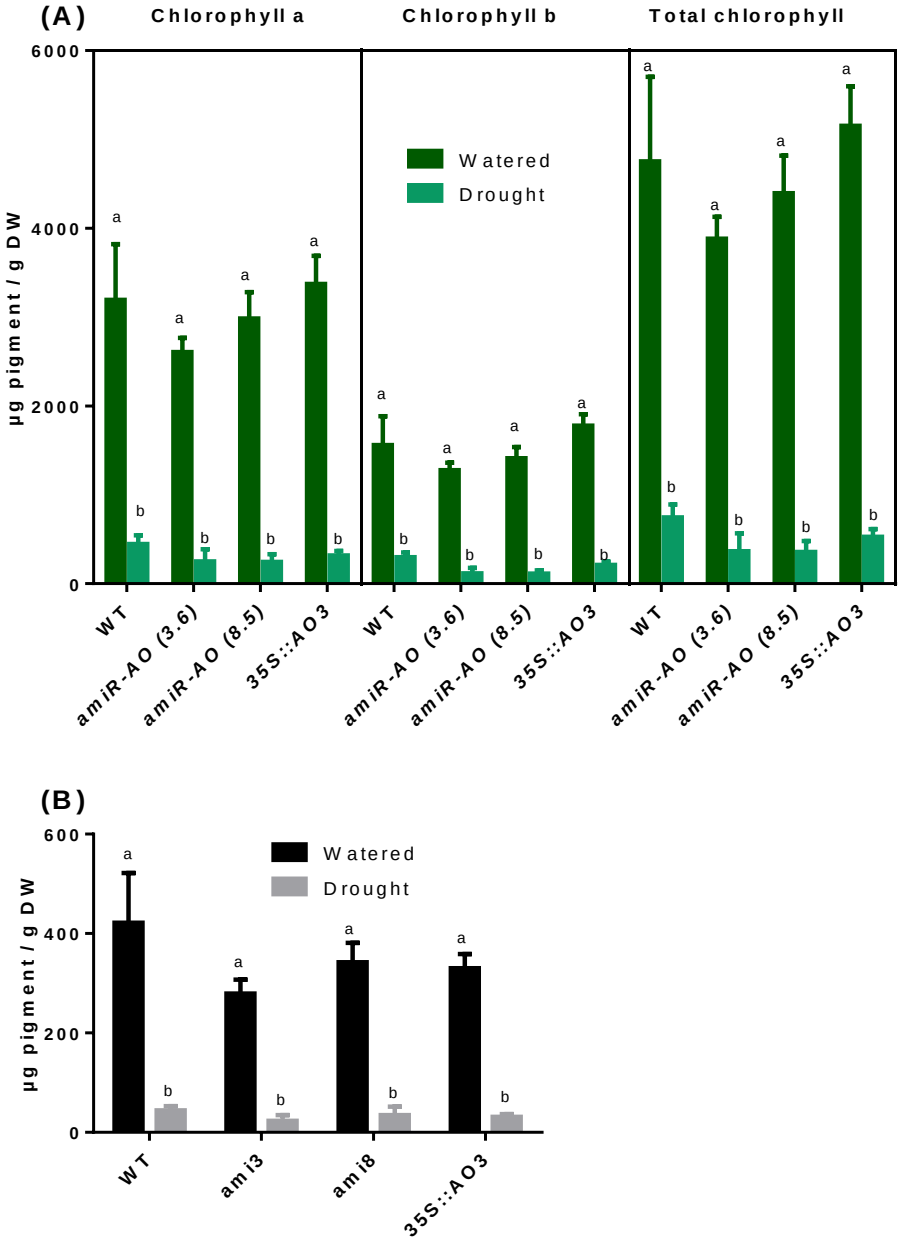

Figure 6-33: Chlorophyll **(A)** and carotenoid **(B)** contents in leaves of *amiR-AO* and *35S::AO3* transgenic lines after 14 days of watered or drought treatments. Values are mean ± SEM, n = 4. Different letters above the bars denote the values are significantly different using one way ANOVA and Tukey tests ($p<0.05$). Values bearing the same letter are not significantly different from each other. Statistical analyses for chlorophyll a, chlorophyll b and total chlorophyll data were performed separately.

6.2.23. Ionically-bound cell wall AO activity of *amiR-AO* and *35S::AO3* transgenic lines during drought

As in *ao* mutants, the ionically-bound cell wall AO activity was expressed based on tissue DW rather than tissue FW due to a big variation in FW between watered tissue and drought tissue. Similar observations were obtained when AO activity expressed on the basis of tissue DW or protein. AO activity was not detected in the *amiR-AO* lines under watered or drought conditions. While in WT, the level of AO activity was not affected by drought. *35S::AO3* had higher AO activity than WT under watered condition. The AO activity in drought-stressed *35S::AO3* line was not statistically different from the watered or drought treated WT plants because of high error bars present in the datasets (Figure 6-34A and B). The total protein content was similar in both watered and drought conditions across all genotypes studied (Figure 6-34C).

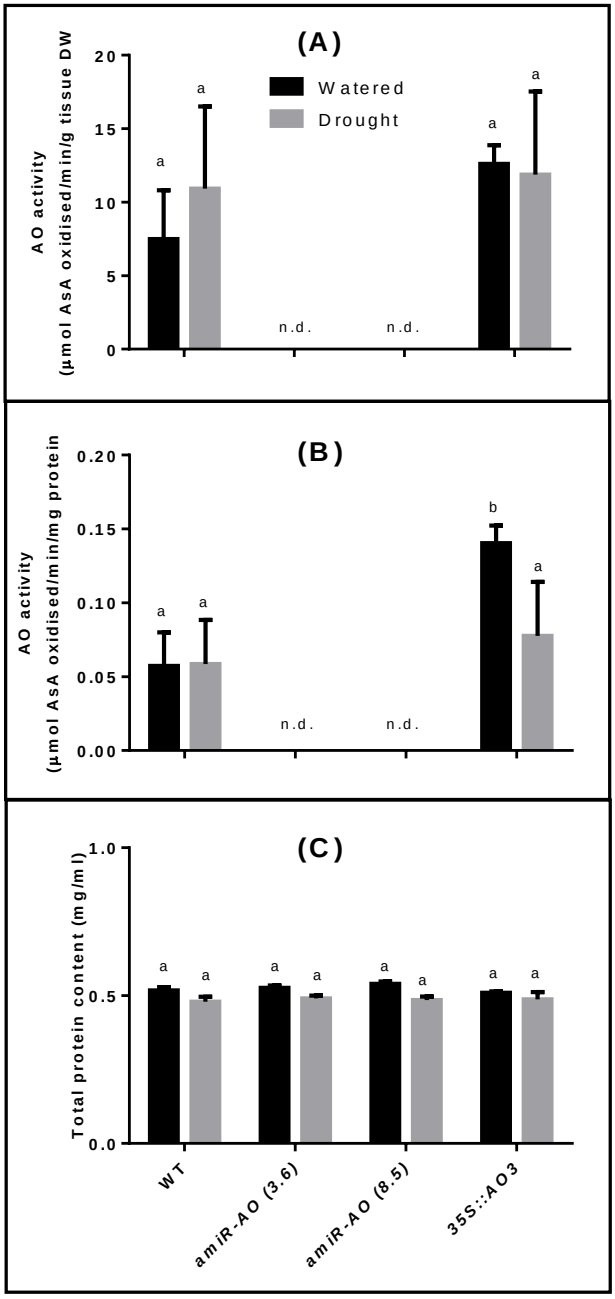

Figure 6-34: Ionically-bound cell wall AO activity of *amiR-AO* and *35S::AO3* transgenic lines after 14 days of watered or drought treatments. The AO activity was expressed on a dry weight **(A)** and protein **(B)** basis, respectively. **(C)** Protein concentration in tissue extracts (mg ml^{-1}). Due to varying amount of tissue extracted these values cannot be directly compared to enzyme activity data in A and B. Values are mean ± SEM, n = 3. Different letters above the bars denote the values are significantly different using one way ANOVA and Tukey tests ($p<0.05$). Values bearing the same letter are not significantly different from each other. N.d. = not detected

6.2.24. AsA concentrations of *amiR-AO* and *35S::AO3* transgenic lines during drought

As in the *AO* T-DNA insertion mutants, 14 days of drought treatment had little effect on the whole leaf AsA concentrations of *amiR-AO* and *35S::AO3* transgenic lines. AsA concentration was expressed based on tissue DW rather than tissue FW due to a big variation in FW between watered tissue and drought tissue. The concentrations of reduced AsA, DHA and total AsA were similar between watered and drought treated plants across all strains studied (Figure 6-35A). The AsA redox state for all lines under watered and drought treatments were not significantly different (~ 80%) (Figure 6-35B).

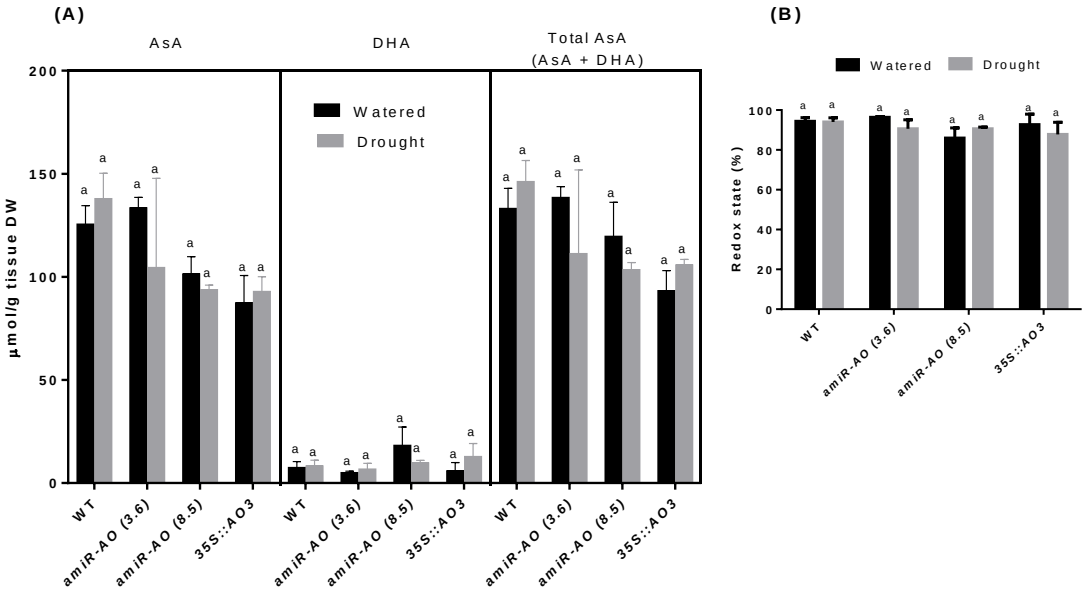

Figure 6-35: Whole leaf AsA concentrations of *amiR-AO* and *35S::AO3* transgenic lines after 14 days of watered or drought treatments. **(A)** The concentrations of reduced AsA, DHA and total AsA pool in WT and transgenic lines. **(B)** The percent AsA redox state (ratio of reduced AsA to total AsA) of WT and transgenic lines. Values are mean ± SEM, n = 4. Values bearing the same letter are not significantly different from each other using one way ANOVA and Tukey tests ($p<0.05$). Statistical analyses for reduced AsA, DHA and total AsA data were performed separately.

Apoplastic AsA was extracted from all rosette leaves of the same plants as used for whole leaf AsA analysis. Due to a big variation in tissue FW between watered and drought tissues, the apoplastic AsA concentrations were expressed on the basis of apoplastic fluid recovered (mM as the unit) rather than tissue FW. Under watered condition, *amiR-AO (3.6)* and a*miR-AO (8.5)* had a significantly higher reduced AsA concentration in the apoplast than WT and *35S::AO3*, with the highest concentration was detected in the *amiR-AO (8.5)* line. The reduced AsA concentration in the apoplast of *35S::AO3* was nearly completely abolished compared to WT under watered condition (Figure 6-36A). In response to drought, WT and two *amiR-AO* lines had similar levels of apoplastic reduced AsA, whereas apoplastic reduced AsA was not detected in *35S::AO3* (Figure 6-36A). Under watered or drought conditions, the apoplastic DHA concentration and total AsA pool in all lines were not statistically different. This was due to great variability in data obtained (Figure 6-36A). The AsA redox state is defined as the ratio (%) of reduced AsA to total AsA. Under watered condition, the AsA redox state in *amiR-AO* lines was higher than WT and *35S::AO3*. The lowest AsA redox state was found in the *35S::AO3* line. In response to drought, the AsA redox in WT appeared to be higher than the watered counterparts. Drought did not affect the AsA redox state in *amiR-AO* lines. In drought stressed *35S::AO3*, the total AsA pool was completely oxidised (Figure 6-36B). It should be noted that the apoplastic fluid recovered in drought tissues were significantly lower than watered tissues (Figure 6-36C). This could be the reason contributed to low total AsA pool and high AsA redox state found in drought treated plants.

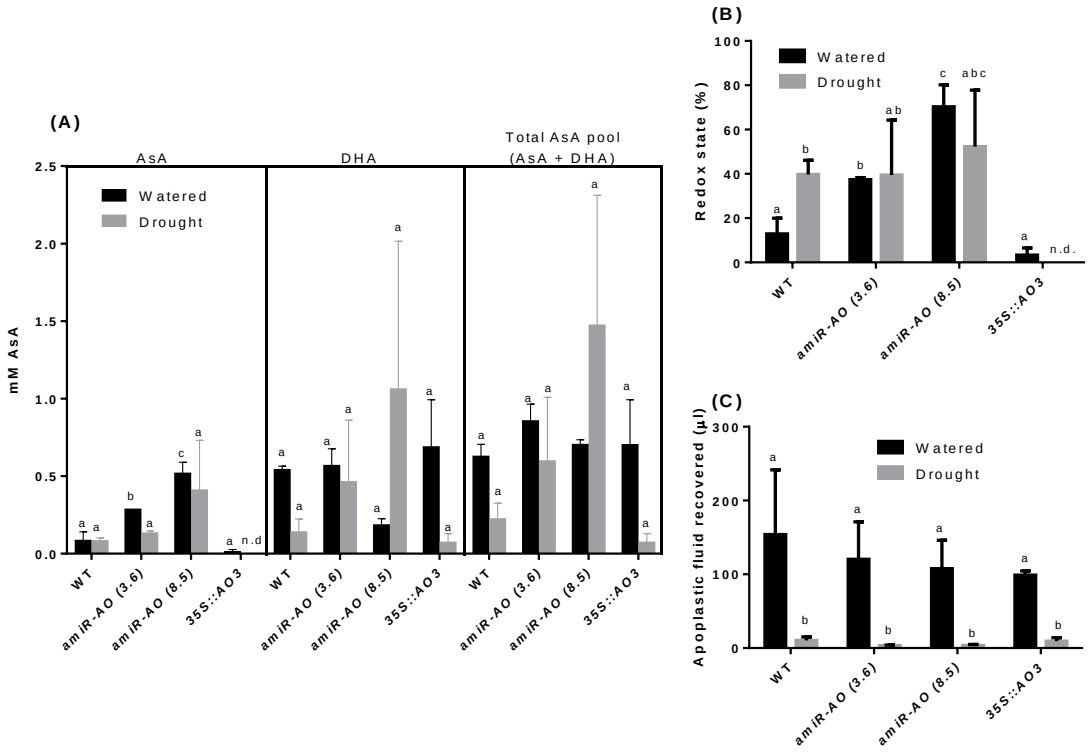

Figure 6-36: Apoplastic AsA concentrations of *amiR-AO* and *35S::AO3* transgenic lines after 14 days of watered or drought treatments. **(A)** Apoplastic reduced AsA, DHA and total AsA pool from whole rosette leaves of WT and transgenic lines. **(B)** The percent AsA redox state (ratio of reduced AsA to total AsA) of WT and transgenic lines. **(C)** The yield of apoplastic fluid after vacuum infiltration. Values are mean ± SEM, n = 2, N = 2 for watered plants and n = 2, N = 3 for drought stressed plants. N = number of replicate, n = pool of plants per replicate. Different letters above the bars denote the values are significantly different using one way ANOVA and Tukey tests ($p<0.05$). Values bearing the same letter are not significantly different from each other. Statistical analyses for reduced AsA, DHA and total AsA data were performed separately. N.d. = not detected.

6.2.25. The effect of drought on leaf water loss, relative water content and photosynthetic capacity of *amiR-AO* and *35S::AO3* transgenic lines

The rate of leaf water loss was similar between WT and *amiR-AO* lines. There was a steady decrease in the percent initial FW over a period of 105 mins, but did not differ between WT and *amiR-AO* lines (Figure 6-37A). *35S::AO3* line had greatly decreased percent initial FW over 75 to 105 mins compared with WT and *amiR-AO* lines, suggesting that the *35S::AO3* line had more rapid leaf water loss than the other lines.

Drought stressed plants showed significantly reduced in RWC than that of control, well watered plants after 14 days of dehydration. Of which, the *amiR-AO* lines appeared to have lower RWC than WT and *35S::AO3* under drought treatment, although the difference was not statistically significant. The RWC in watered plants was not significantly different across all strains (Figure 6-37B).

The dark adapted maximum quantum yield of photosystem II (F_v/F_m) in WT and transgenic lines did not vary under watered condition (F_v/F_m = ~0.80). A small decline (F_v/F_m = ~0.74 to 0.76) was observed in the drought treated plants, but the differences between WT and transgenic lines were not significant (Figure 6-37C).

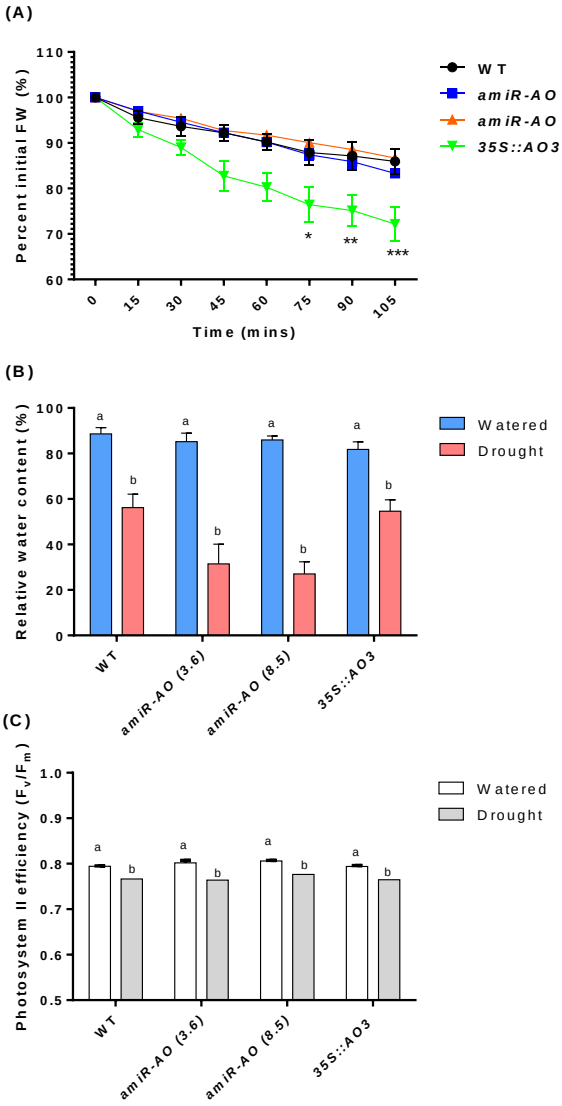

Figure 6-37: Analyses of the leaf water loss, relative water content and photosystem II quantum yield in *amiR-AO* and *35S::AO3* transgenic lines after 14 days watered or drought treatments. **(A)** Leaf water loss assay. Fully expanded leaves were detached from watered plants. **(B)** Relative water content of detached leaves from watered or drought plants. **(C)** Photosystem II quantum yield of dark adapted watered or drought plants. Values are mean ± SEM, n = 3. Different letters above the bars denote the values are significantly different using one way ANOVA and Tukey tests ($p<0.05$). Values bearing the same letter are not significantly different from each other. Asteriks denote significant differences compared to WT: *$p<0.05$, **$p<0.01$ and ***$p<0.001$ (one way ANOVA and Tukey tests) at the relevant time point.

6.2.26. Ionically-bound cell wall peroxidase activity of *amiR-AO* and *35S::AO3* transgenic lines during drought

As in *AO* T-DNA insertion mutants, the ionically-bound cell wall peroxidase activity was expressed based on tissue DW rather than tissue FW due to a big variation in FW between watered tissue and drought tissue. There were discrepancies in the peroxidase activities expressed on DW basis and on protein basis. The ionically-bound cell wall peroxidase activity, either expressed on a DW or protein basis, did not statistically differ between WT and transgenic lines under watered or drought conditions (Figure 6-38A and B). There was a considerable variations in data obtained that made data interpretations difficult. When peroxidase activity expressed on a DW basis, drought treated *amiR-AO* and *35S::AO3* transgenic lines had higher peroxidase activity than the watered counterparts, while peroxidase activity in the WT did not differ under drought or watered conditions (Figure 6-38A). When peroxidase activity expressed on a protein basis, higher peroxidase activity was only found in the drought treated *amiR-AO (3.6)*, whereas WT, *amiR-AO (8.5)* and *35S:AO3* had lower peroxidase activity during drought (Figure 6-38B). The total protein content was similar in both watered and drought conditions across all genotypes studied (Figure 6-38C).

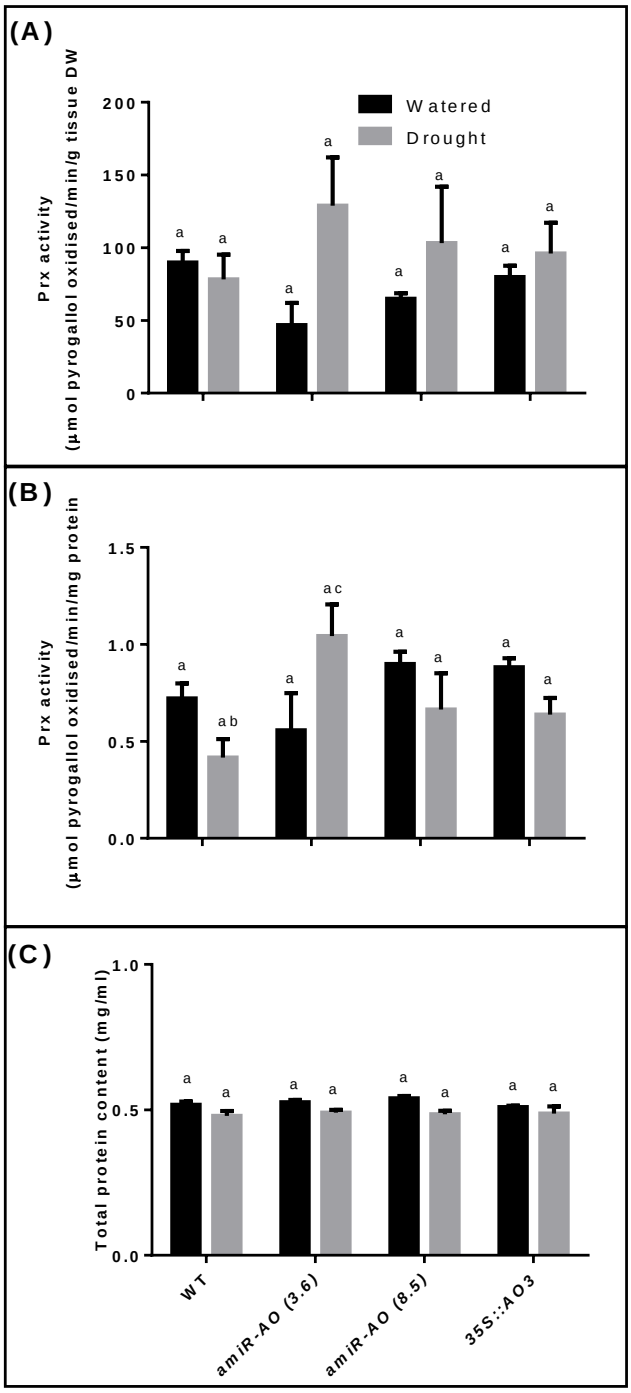

Figure 6-38: Ionically-bound cell wall peroxidase activity of *amiR-AO* and *35S::AO3* transgenic lines after 14 days of watered or drought treatments. The peroxidase activity was expressed on a dry weight **(A)** and protein **(B)** basis, respectively. **(C)** Protein concentration in tissue extracts (mg ml^{-1}). Due to varying amount of tissue extracted these values cannot be directly compared to enzyme activity data in A and B. Values are mean ± SEM, n = 3. Different letters above the bars denote the values are significantly different using one way ANOVA and Tukey tests ($p<0.05$). Values bearing the same letter are not significantly different from each other.

6.3. Discussion

6.3.1. The effect of high light in *AO* T-DNA insertion mutants, *amiR-AO* and *35S::AO3* transgenic lines

As described in Chapter 5, *AO* T-DNA insertion mutants did not show phenotypic differences to WT, although *ao3* and *ao1ao3* mutants had only 10-20% of the WT AO activity. As a result, two different stress treatments, high light and drought were applied in this project to assess whether AO perturbations affect *A. thaliana* stress response. High light was selected in this project for two reasons. First, the protocol for this stress experiment was established in my lab. Second, previous studies showed that AsA concentration is increased under high light and is positively correlated with anthocyanin content. Further evidence suggests that AsA-deficient *vtc* mutants failed to accumulate anthocyanin (Giacomelli *et al.*, 2006; Giacomelli *et al.*, 2007; Page *et al.*, 2012). Therefore, it is interesting to find out whether changes in apoplastic AsA redox state caused by AO could affect anthocyanin accumulation.

In response to HL, all lines (WT and *AO* T-DNA insertion mutants) showed an increase accumulation of anthocyanin, although no difference observed between WT and *AO* T-DNA insertion mutants. This is in agreement with previous studies, showing that anthocyanin production is needed for photoprotection in plants during HL (Gould *et al.*, 2002; Zhang *et al.*, 2011; Page *et al.*, 2012). Anthocyanin and other flavonoids are proposed to have two functions during HL, it can acts as a sunscreen that can effectively absorb UV-B and prevent it from penetrating into the mesophyll cells (Landry *et al.*, 1995; Ormrod *et al.*, 1995). Another function is that anthocyanin and other flavonoids

can also function as an ROS scavenger (Yamasaki *et al.*, 1997; Gould *et al.*, 2002; Zhang *et al.*, 2011). *A. thaliana* mutant (*tt3tt4*) that is deficient in anthocyanin biosynthesis accumulated more O_2^- and H_2O_2 than the WT during HL (Zhang *et al.*, 2011). HL acclimated plants appeared to have lower, but not significantly different, chlorophyll contents. This is because HL stress tends to inhibit chloroplasts biosynthesis and increases its degradation (Hidema *et al.*, 1992; Zhang *et al.*, 2011).

HL increased AO activity in *A. thaliana* WT and *ao1* but the AO activity in *ao3* and *ao1ao3* mutants remained low. High AO activity observed in WT plant upon HL induction is in consistent with wild watermelon (*Citrullus lanatus*) subjected to HL (Nanasato *et al.*, 2005). A positive correlation was found between AO activity and the gene expression of *CLb561A* in the leaves of *C. lanatus* during HL and drought. *CLb561A* is one of the genes that encodes for plasma membrane cytochrome b_{561} protein and it shared 68% amino acid sequence identity to a cytochrome b_{561} protein (At4g25570) in *A. thaliana*. Cytochrome b_{561} is believed to regenerate apoplastic MDHA using electron from cytosolic AsA (see section 1.3.). AO activity is increased during HL, because up regulation of the *CLb561A* gene is believed to regenerate more apoplastic AsA that can be used as a substrate for AO. Additionally, during HL stress, reducing equivalents in chloroplasts could be transported to the cytosol *via* malate-oxaloacetate shuttle, and then transport to the apoplast via plasma membrane bound MDHAR or cytochrome b_{561}. These reducing equivalents can be used by AO for the reduction of oxygen to water. This proposed "cytochrome b_{561}–AO" redox chain is believed to dissipate excess light energy in chloroplasts, indirectly alleviating photooxidative stress (Nanasato *et al.*, 2005). However, this

hypothesis has not been experimentally validated. Besides, Pignocchi *et al*. (2006) showed that the expression of genes involved in photorespiration (e.g. glycolate oxidase) is affected by AO perturbation. In addition, high AO activity is needed for O_2 management, where apoplastic O_2 is reduced to water by AO, creating a steep O_2 concentration gradient thereby increasing O_2 diffusion from chloroplasts to the apoplast (De Tullio *et al.*, 2004). These findings showed that the potential role of AO in photosynthesis or photoprotection merits future investigation.

Intriguingly, the transcript levels for all three *AO* genes in WT as well as remaining *AO* gene(s) for T-DNA mutants were repressed despite of high AO activity in HL treated plants, suggesting a post-transcriptional control involved. It is unknown whether post-transcriptional control in *AO* genes during stress is common for other species. This is because the expression of *AO* genes during stress was not reported in previous studies (Sanmartin *et al.*, 2003; Yamamoto *et al.*, 2005; Fotopoulos *et al.*, 2006; Pignocchi *et al.*, 2006; Garchery *et al.*, 2012). It has been shown that AO treated with its prosthetic metal, copper tended to increase the enzyme activity but not the mRNA level in pumpkin fruit tissue. This suggests a translational control could be involved in *AO* expression (Esaka *et al.*, 1992).

In this study, high light increased reduced AsA concentrations and total AsA pool in the whole leaf extract, although no difference observed between genotypes. A correlation between AsA and HL in present study is in consistent with previous studies (Smirnoff, 2000b; Bartoli *et al.*, 2006; Golan *et al.*, 2006; Dowdle *et al.*, 2007; Page *et al.*, 2012). Additionally, a positive correlation between whole leaf AsA concentrations and anthocyanin content was found in

this study. Previous study showed that AsA-deficient *vtc* mutants failed to accumulate anthocyanin in response to HL acclimation (Giacomelli *et al.*, 2006; Giacomelli *et al.*, 2007; Page *et al.*, 2012). Further evidence showed that the gene expression of anthocyanin biosynthesis enzymes as well as transcription factors (*PAP1*, *GL3* and *EGL3*) that activate the pathway were impaired in *vtc1* and *vtc2* mutants upon HL induction. The correlation between AsA and anthocyanin is also reinforced by the same results obtained for six different *A. thaliana* ecotypes (Page *et al.*, 2012).

The apoplastic AsA concentration was determined in WT and *AO* T-DNA insertion mutants subjected to LL or HL conditions. In contrast to whole leaf AsA, HL acclimation did not appear to affect apoplastic AsA in *A. thaliana*. It is possible that the apoplastic AsA concentration is too low to give any changes compared with whole leaf AsA. This result also suggests that altered AsA redox state alone with no changes in the total AsA pool, as observed in the *ao3* and *ao1ao3* mutants, is insufficient to give any phenotypic difference such as anthocyanin accumulation. In support of this, *vtc* mutants that failed to accumulate anthocyanin have lower total AsA pool in whole leaf and the apoplast (Veljovic-Jovanovic *et al.*, 2001; Sultana, 2011). Also, it is possible that the apoplastic reduced AsA was oxidised during extraction procedure because the apoplast is a sensitive and highly oxidised compartment (Pignocchi and Foyer, 2003). It is difficult to draw a conclusion from the result obtained because a big biological variation was observed across independent experiments.

As described in the Results, *AO* T-DNA insertion mutants did not show any differences in term of phenotype, whole leaf AsA concentration, chlorophyll and anthocyanin contents despite of low AO activity and high apoplastic AsA

concentration. This suggests that AO-deficiency in *ao3* and *ao1ao3* had little effect in HL response of *A. thaliana*. A possible explanation is due to functional redundancy compensated by another *AO* gene.

The effect of HL on *amiR-AO* and *35::AO3* was studied. During HL, the *amiR-AO* had higher anthocyanin content and greater concentrations of reduced AsA and total AsA pool in whole leaf. Intriguingly, the apoplastic AsA concentration and total AsA pool was not significantly increased by HL. It is not clear if the contribution of apoplastic AsA in HL stress is small or otherwise the apoplastic extraction method in present study need to be critically revised. Apoplast AsA redox state could be a frontier to sense HL stress and trigger following signalling events or cytosolic antioxidant system (Pignocchi and Foyer, 2003). This would have to relate with the AsA transport system across the plasma membrane. The transport of AsA, preferentially with DHA, from the apoplast to cytosol was described previously (Horemans *et al.*, 2000b), so the activity of AsA transporters can be examined in future. It is unclear whether AO perturbation in T-DNA insertion mutants and transgenic lines has affected the enzyme activity and expression of genes involved in AsA recycling (e.g. MDHAR and DHAR). HL stress encountered by the *amiR-AO* presumably could have increased the activity of enzymes involved in AsA regeneration.

6.3.2. The effect of drought in *AO* T-DNA insertion mutants, *amiR-AO* and *35S::AO3* transgenic lines

Drought stress was selected in this study, because previous evidence suggests that AO could be involved in drought response. Garchery *et al.* (2012) showed that *AO* RNAi tomato plants give better fruit yield under water-deficit treatment. Altered stomatal dynamic, leaf water loss and RWC were shown in tobacco plants overexpressing *AO* (Fotopoulos *et al., 2008*). Yamamoto *et al.* (2005) showed that tobacco overexpressing *AO* had increased sensitivity to salt stress, while tobacco underexpressing *AO* showed enhanced tolerance to salt stress. The stress mechanism of salt and drought is similar, because both stresses also affect plant water status (Verslues *et al.*, 2006). These observations suggest a role of AO in drought.

The present study has included a number of assays to measure plant response to drought such as chlorophyll content, anthocyanin content, AsA content, leaf water loss and peroxidase activity, etc (Verslues *et al.*, 2006; Luo, 2010). As described in the Results section, *AO* T-DNA insertion mutants did not exhibit any differences from WT, suggesting AO-deficiency had little effect on drought response of *A. thaliana*. Drought treated WT and *AO* T-DNA insertion mutants showed typical drought stress signs such as reduced growth rate, decreased chlorophyll and carotenoid contents, decreased photosynthetic efficiency, decreased relative water content and increased peroxidase activity, etc (Smirnoff, 1993; Bartels and Sunkar, 2005; Jubany-Marí *et al.*, 2010a).

In contrary to HL acclimation, AO activity was not induced by drought stress. A similar observation was reported in drought treated watermelon (Nanasato *et al.*, 2005). AO activity also was not significantly affected by salt stress in *A. thaliana*

(Yamamoto *et al.*, 2005). The level of AO activity in leaves challenged with a pathogen (*P. syringae* DC300) was similar to the control plants (Appendix C). This suggests that not all stresses tend to increase AO activity. The abundance of AO protein was not assessed in this study; it is possible that the level of AO protein was decreased in drought, because protein synthesis is generally inhibited by drought (Smirnoff and Colombé, 1988). As in HL response, transcript levels for all three *AO* genes were repressed during drought, further reinforce the hypothesis that a post-transcriptional control mechanism is involved in *AO* expression during stress. However, this should be examined in a wide variety of species in response to different stresses.

Only a small reduction in the dark adapted quantum yield of photosystem II (F_v/F_m) was observed after 14 days of dehydration. Although F_v/F_m is the straightforward and most commonly used parameter in stress studies (Baker, 2008), it is relatively insensitive to drought stress compared to other assays such as growth rate, chlorophyll content etc. (Munns *et al.*, 2010). Indeed, F_v/F_m is the most effective parameter to assess survival rate of plants undergoing severe drought stress (Woo *et al.*, 2008). It should be noted that in this experiment only moderate drought was applied, where RWC for drought plants was maintained at ~ 40%, so that viable tissues could be obtained for experiments. As a rule of thumb, the drought stressed plants should have at least 30% RWC over a 12-day period of drought experiment (Smirnoff, 1993; Verslues *et al.*, 2006).

The ionically-bound cell wall peroxidase activity increased with drought stress, in consistent with previous studies (see Jubany-Marí *et al.*, 2010a), supporting the role of peroxidase in H_2O_2 detoxification. However, the increase, in general

was not statistically significant. This could be due to the severity of drought stress applied in present study is different from other studies. Alternatively, the peroxidase assay used in this study only gives little information about H_2O_2 scavenging capacity of drought stressed plants. It has been shown that the measurement of ascorbate peroxidase activity could provide a better estimate of plant tolerance to drought (Smirnoff, 1993).

The whole leaf AsA levels were not affected by drought stress. This could be caused by different growth conditions or different degree of drought stress employed in the present study. Hu *et al.* (2005) did not observe significant changes in the reduced AsA concentrations and total AsA pool in drought stressed maize seedlings. A number of studies have measured the AsA concentrations of plants subjected to drought stress and variously found no effect, increases or decreases in AsA concentrations (see Jubany-Marí *et al.*, 2010a). Previous study showed that *A. thaliana* subjected to 11 days drought stress, in comparison with watered plants, had similar level of DHA, higher levels of reduced AsA and total AsA pool. This contributed to higher AsA redox state in drought stressed plant, although the variation is small (Jubany-Marí *et al.*, 2010b). It should be noted that different experimental conditions were employed by Jubany-Marí *et al.*, in which 3-week-old *A. thaliana* were used and the drought stress was performed in a glasshouse. The effect of drought stress on the apoplastic AsA concentrations was assessed. A decrease in the total AsA pool was observed, owing to a decrease in apoplastic DHA concentrations. This resulted in a higher AsA redox state because AsA redox state was determined by the ratio of reduced AsA to total AsA. However, the result obtained should be interpreted carefully, because low total AsA pool may have

been a result of low apoplastic fluid recovered. Drought stressed plants have lower stomatal conductance, which means less extraction buffer was infiltrated under vacuum. Hu *et al.* (2005) showed that drought stress significantly decreased the apoplastic reduced AsA concentration and significantly increased the apoplastic DHA concentration in maize seedlings. Hu *et al.* (2005) proposed that a decrease in apoplastic AsA during drought is required for ABA accumulation.

Two independent *amiR-AO* lines with undetectable AO activity did not show increased sensitivity or susceptibility to drought, in comparison with WT. Indeed, these lines had slightly lower RWC compared to WT. Despite of the low RWC observed, it is very difficult to determine the severity of stress encountered by these plants. This is because the *amiR-AO*, which had bigger rosette size, tended to deplete soil water rapidly compared with the WT that had smaller rosette size. Two solutions could use to overcome these difficulties (Verslues *et al.*, 2006). First is by quantification of soil water potential throughout the experimental period but this method is difficult for *A. thaliana*. Alternatively, WT and mutants can be grown in the same pot; this will ensure both genotypes had the same water potential, i.e. the same degree of drought stress. The *35S::AO3* had greater rate of leaf water loss, suggesting that the overexpressor had higher stomatal conductance and enhanced sensitivity to drought. Stomatal conductance is largely affected by ABA concentration (Verslues *et al.*, 2006), so the ABA concentration in the *35S::AO3* can be measured in future. In opposition to the present study, Fotopoulos *et al.* (2008) found the *AO* overexpressing tobacco had higher RWC, lower stomatal conductance and reduced rate of leaf water loss, which suggests that the *AO* overexpressing tobacco could have

better resistance drought, although drought experiment was not conducted for this overexpressor. In support of this, tobacco plants overexpressing *DHAR*, an enzyme of AsA-GSH cycle which involved in the recycling of AsA, showed higher level of AsA redox state and reduced level of H_2O_2 in guard cells. This resulted more open stomata, greater rate of leaf water loss, higher stomatal conductance and transpiration thus increased sensitivity to drought stress (Chen and Gallie, 2004). On the contrary, antisense suppression of the same gene had decreased AsA redox, accumulated more H_2O_2 in guard cells, enhanced stomatal closure and improve plant growth during drought (Chen and Gallie, 2004). The *DHAR* transgenic plants had equally affected the AsA redox state in whole leaf and the apoplast, so it is unknown if the altered stomatal dynamics exhibited by *DHAR* mutants was contributed solely by apoplastic AsA, whole leaf AsA or both. Drought experiments with *AO* mutants that only had altered AsA redox state in the apoplast should shed some light in this gap. Indeed, an *AO* RNAi tomato that had higher apoplast AsA redox state tended to have better fruit yield under water deficit stress (Garchery *et al.*, 2012).

Chapter 7. General discussion

The research on AO has started since 1930's when it was first isolated from the cabbage leaf by Szent-Györgyi (1931). Yet, today, the exact function of AO remains to be determined although many hypotheses were proposed but there is no conclusive evidence about its function. By making use of the model plant, *A. thaliana* and *in silico* resources available, a comprehensive study of AO was performed.

A phylogenetic study showed that AO was already present even before the evolution of higher plants. However, there is a significant sequence divergence between AO in higher plants and AO in green alga, pteridophytes and mosses, suggesting an alternative function in these species.

The following plant lines were established to study the function of AO in *A. thaliana*: 1) *AO* T-DNA insertion mutants, 2) *amiR-AO* lines with targeted knockdown of three *AO* genes and 3) an overexpressor that constitutively expressed the *AO3* gene. Under unstressed normal growth conditions, the AO activity decreased in the following order: *35S::AO3* > WT and *ao1* > *ao3* and *ao1ao3* > *amiR-AO*. Whereas, the apoplastic AsA redox state (%) increased in the following order: *35S::AO3* (~0-5%) < WT and *ao1* (~5-10%) < *ao3* and *ao1ao3* (~25%) < *amiR-AO* line 3.6 (~40%) < *amiR-AO* line 8.5 (~80%).

Similar to other studies, high AO activity was found in actively growing tissues of WT *A. thaliana*. Attempts were made by previous studies *via* genetic manipulation of AO, as well as present study using T-DNA mutants (see Chapter 1 and Chapter 5) showed that AO perturbations at best only give subtle phenotype under unstressed normal growth conditions. This suggests that high

AO activity could be a general response of high metabolic activity in growing tissues. In fact, plant growth and development is tightly regulated, the role of AO could not simply resolved by genetic manipulation. Also, if AO has a role in cell expansion, then the interaction of DHA (oxidised product of AO) with cell wall components need to be elucidated experimentally. The metabolites of AsA/DHA degradation in the apoplast should be characterised in the mutant.

Under unstressed and stressed conditions, *AO* T-DNA mutants did not show any phenotypic differences compared to WT, although *ao3* and *ao1ao3* had only 10-20% of WT AO activity. This observation is reinforced by the fact that many stresses such as cold, salt, wound, high temperature, low nutrient (Appendix B) and pathogenic infection (Appendix B) were attempted on *ao3* and *ao1ao3* T-DNA insertion mutants, but no phenotypic differences were observed. Furthermore, untargeted metabolomic analyses using liquid chromatography-quadrupole time of flight mass spectrometry (LC-QToF MS) showed that metabolites in WT and *ao1ao3* subjected to drought were rather similar (data not shown). This suggests that AO might play an insignificant role in growth and stress response of *A. thaliana* or a complete suppression of AO activity is required. The AO activity in *ao2* is remains to be determined. Since knockout of *AO3* gene resulted in 10-20% of WT AO activity, it is uncertain whether *AO2* contributed to the remaining AO activity or higher, considering high sequence identity between *AO2* and *AO3*.

Interesting phenotypes were observed in *amiR-AO* and *35S::AO3* lines. Currently the basis of large rosette size in *amiR-AO* is unknown. A few hypotheses are proposed for the phenotype observed in the *amiR-AO* lines. It could be contributed by $^{\cdot}OH$ mediated non-enzymic scission of polysaccharides,

assuming more apoplastic AsA and free copper ions available for the formation of ˙OH (see section 1.5.). However, histological analysis showed that the cell size of the *amiR-AO* lines was similar to WT and *35S::AO3*, suggesting that the effect of AO perturbation in cell expansion is small. Alternatively, an increase in foliar auxin concentration is a possible explanation for large rosette size observed in the *amiR-AO*. Evidence showed that AO is involved in the oxidative decarboxylation of auxin, in which high AO activity is associated with a decrease level of auxin in maize roots (Kerk *et al.*, 2000). Additionally, transgenic tobacco seedlings overexpressing *AO* have a decrease growth response to auxin treatment (Pignocchi *et al.*, 2006). This suggests that the absence of AO in the *amiR-AO* lines could have increased the concentration of auxin, resulting in an increase rate of cell division (Campanoni and Nick, 2005; Perrot-Rechenmann, 2010). In support of this, the *amiR-AO* lines in present study had a greater number of cells and more rosette leaves, a consequence of increased cell division. In future, the auxin concentration in the *amiR-AO* lines should be measured to support this hypothesis. Also, it is possible that the *amiR-AO* lines had caused the up-regulation of cell wall components such as sugars, peroxidases, expansins and etc., in order to compensate for the loss of AO, thus resulting bigger rosette. “Omics” could be employed to assess the metabolome and cell wall proteome of *amiR-AO* and *35S::AO3* lines, as a consequence of AO perturbation.

Massive accumulation of anthocyanin and whole leaf AsA concentrations exhibited by *amiR-AO* lines is surprising. Whether this response is a result of sensitivity or resistance to HL is remains to be determined. If taken the role of AsA as a photoprotectant into consideration, high concentration of apoplastic

reduced AsA could act as a first barrier to scavenge ROS (Smirnoff, 2000b; Foyer and Shigeoka, 2011) and function as an external signal that activates the intracellular plant antioxidant system. Based on data from previous reports coupled with result in this study, a model is proposed to describe the role of AO during HL acclimation in controlling intracellular AsA pool size (Figure 7-1). During HL acclimation, an increase in AO activity tends to increase the apoplastic DHA concentration. DHA in the apoplast can either proceed to an irreversible AsA degradation pathway to produce threonate and oxalate (Green and Fry, 2005; Parsons *et al.*, 2011; Parsons and Fry, 2012), or transport into intracellular for AsA regeneration (Horemans *et al.*, 2000b). The rate/fluxes of DHA to AsA degradation pathway or transport into cytosol for regeneration are unknown. *In planta* evidence showed that *AO* overexpression in tobacco could increase the rate of AsA degradation (Parsons, 2008), suggesting that AO and apoplastic AsA redox state might influence the fluxes of this pathway. High light acclimation presumably could have increased the transport of DHA into cytosol for regeneration using enzymes and metabolites of the AsA-GSH cycle, thereby producing more intracellular AsA, which in turn increase the accumulation of anthocyanin. In present study, the *amiR-AO* lines had higher level of intracellular AsA and anthocyanin compared to WT. The possible explanation is because the lack of AO activity could have decreased the rate of AsA degradation, and therefore more DHA are transported into cytosol for regeneration. As a result, the concentration of intracellular AsA is enhanced, thus increasing anthocyanin accumulation (Figure 7-1).

These observations suggest that AO could play a role in AsA turnover or breakdown during HL stress. A detailed study is required to prove or disprove

this hypothesis. It is essential to compare the transporter activity in the *amiR-AO* lines and WT during HL, notably the cytochrome b_{561} (Nanasato *et al.*, 2005) and AsA/DHA exchange systems (Horemans *et al.*, 2000a) at the plasma membrane. Also, the products of AsA degradation in the apoplast of *amiR-AO* and WT after HL acclimation should be examined.

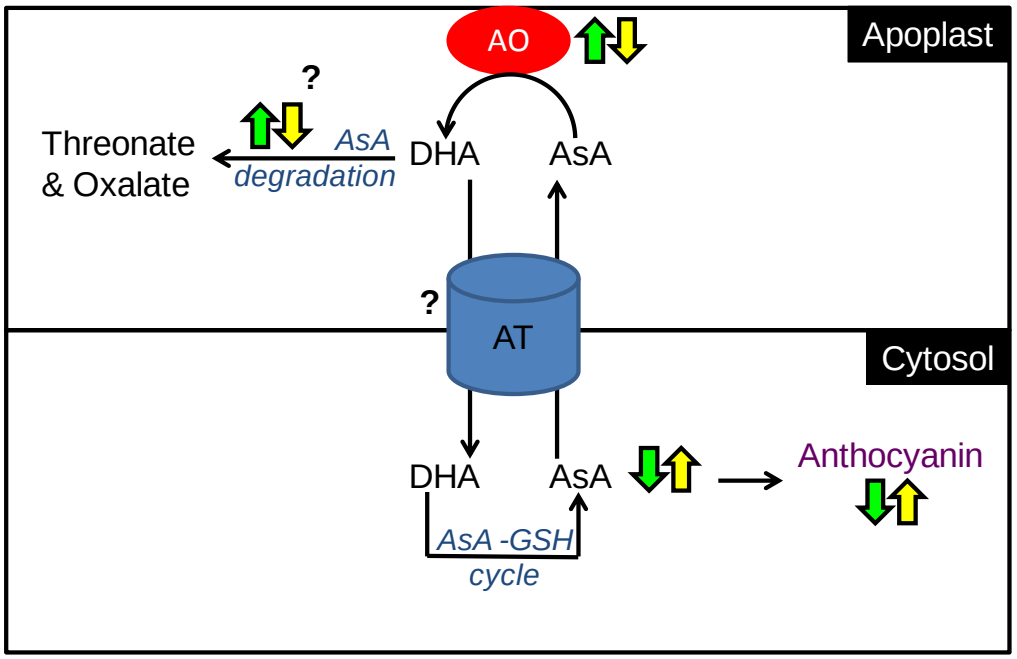

Figure 7-1: A model of the proposed role of AO during HL acclimation. See text for descriptions. Green block arrows are possible reaction following up-regulation of AO activity (e.g. WT plants); yellow block arrows are possible reaction following down-regulation/absence of AO activity (e.g. *amiR-AO* plants). AO = ascorbate oxidase, AsA = ascorbate, DHA = dehydroascorbate, AT = plasma membrane AsA/DHA transporter. Up arrows denote high AO activity, increase AsA degradation rate, more intracellular AsA and more anthocyanin accumulation. Down arrows denote low AO activity, decrease AsA degradation rate, less intracellular AsA and less anthocyanin accumulation. Question marks indicate unconfirmed fluxes of DHA to degradation or transport to cytosol for regeneration.

On the contrary, it has been proposed that high AO activity is essential to control O_2 concentration in chloroplasts (De Tullio *et al.*, 2004) and reducing equivalents in the photosynthetic electron transport chain (Nanasato *et al.*, 2005). In this case, lack of AO activity would be harmful to plants, so early accumulation of anthocyanin and high reduced AsA concentrations in whole leaves could be a consequence of stress injuries rather than adaptation. To resolve this, photosynthetic capacity of the *amiR-AO* should be assessed using gas exchange and chlorophyll fluorescence imaging device.

The *35S::AO3* line appeared to be sensitive to drought and is supported by a greater rate of leaf water loss observed in this overexpressor. It is crucial to isolate more independent lines to prove this observation, and the concentrations of proline and ABA should be assessed to determine the basis of stress sensitivity. Based on the translatome analysis, AO could play a role in hypoxia stress, and the idea that AO could be involved in O_2 management, suggesting that a study on AO mutants in response to hypoxic could be worthwhile. It is also remains to be determined if high AO activity is essential for stress adaptation. Wild watermelon that can adapt to severe growth conditions had higher AO activity than the domesticated watermelon (Nanasato *et al.*, 2005). Additionally, a pilot study performed also showed that the “extremophile” *Thellungiella halophila*, a close relative of *A. thaliana* tended to have higher AO activity than *A. thaliana* under unstressed normal growth conditions (Appendix D1).

A negative correlation between gene expression and AO activity during stress suggests that a post-transcriptional control is involved. A Dof (DNA-binding with one finger) protein, known as the ascorbate oxidase gene binding protein

(AOBP) was characterised previously. DNA binding activity of this AOBP transcription factor was inhibited by a number of metals such as Co(II), Ni(II), Cd(II), Cu(II), Hg(II), Fe(II), and Fe(III) (Umemura *et al.*, 2004). In future, it would be interesting to examine the effect of stress on the expression of AOBP transcription factor.

In coclusion, this study showed that:

- AO is highly conserved in higher plants. AO2 and AO3 of *A. thaliana* showed greater sequence identity than AO1.
- Bioinformatic resources showed that three *AO* genes in *A. thaliana* (*AO1*, *AO2* and *AO3*) are predicted to be present in the apoplast. Each *AO* gene has a distinct expression pattern during development, drought and high light stress.
- High AO activity is found to be present in actively growing tissues of WT *A.thaliana* during vegetative and reproductive growth stages, supporting the hypothesis that AO is involved in cell expansion.
- Negative correlation between AO activity and *AO* gene expression is observed during high light and drought stress, suggesting a post-transcriptional control involved.
- *AO* T-DNA insertion mutants were isolated and characterised, in which *ao3* and *ao1ao3* mutants had only 10 to 20% of WT AO activity. However, no phenotypic differences were observed in these mutants during development and stress, suggesting that the effect of AO perturbation in plant growth and development is small.

- By using amiRNA approach, transgenic plants (*amiR-AO*) without AO activity were developed successfully. In addition, an overexpressor (*35S::AO3*) with high AO activity was developed. The isolation of *amiR-AO* plants showed that the lack of AO activity is not lethal to plants.

- The *amiR-AO* plants exhibited greater leaf growth compared with WT and *35S::AO3*. This finding is in opposition to the hypothesis that high AO activity is correlated with tissue expansion. Three hypotheses are proposed, which merit for future investigation: 1) the lack of AO could enhance the rate of ˙OH-mediated non-enzymic cell wall scission, 2) the lack of AO could increase auxin concentration in plants and 3) the lack of AO could cause the up-regulation of cell wall components in order to compensate the abolition of AO.

- The *amiR-AO* plants had higher level of intracellular AsA and anthocyanin compared to WT during high light, suggesting the lack of AO could affect the rate of AsA degradation in the apoplast and the turnover of intracellular AsA.

Appendices

Appendix A: Sequenced T-DNA insertion site of *ao2* mutant

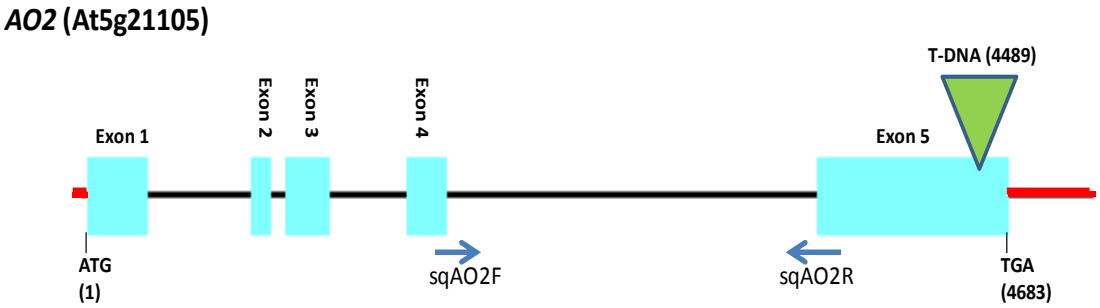

Figure A: Schematic representation of sequenced T-DNA insertion site in the *ao2* T-DNA insertion mutant (SALK_039183C). The T-DNA insertion site was verified *via* DNA sequencing of *ao2* gDNA, which amplified using LBb forward primer and ao2R reverse primer (see 2.5.5.1.). The red line indicates untranslated region, dark line indicates intron. The numbers (1), (4489) and (4683) denote the position of the "A" of the "ATG" start codon, the T-DNA insertion site and the "A" of the "TGA" stop codon, respectively, in the *AO2* gene. sqAO2F and sqAO2R are primers used in semi quantitative RT-PCR.

Appendix B: Stresses have been performed in *AO* T-DNA insertion mutants

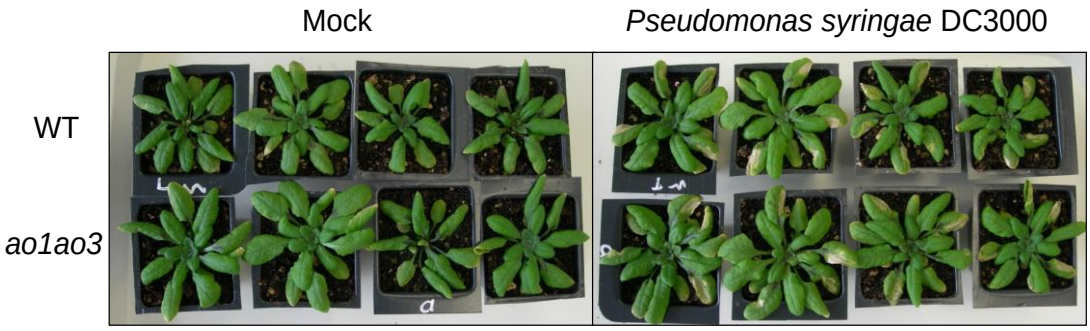

Figure B: Phenotype of 5-week-old WT and *ao1ao3* plants in response to *P. syringae* DC3000 infection. Leaves were syringe infiltrated with 10 mM $MgCl_2$ (mock, left panel) or with 1×10^5 cfu/ml *P. syringae* DC3000 and grown under a short day light regime (8 hrs light, 16 hrs dark). Picture was taken 4 days after inoculation.

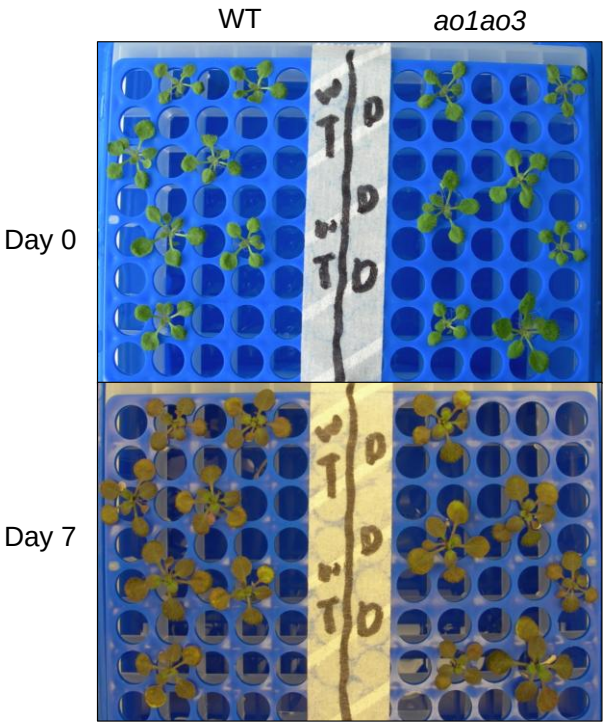

Figure C: Phenotype of 2-week-old WT and *ao1ao3* hydroponically grown (long day light regime: 16 hrs light, 8 hrs dark) seedlings in response to low nutrient treatment. 20-fold dilution of half-strength MS media was prepared and defined as low nutrient solution. Picture was taken at day 0 and day 7 of the treatment.

Appendix C: The effect of *P. syringae* infection on ionically-bound cell wall AO activity of WT and *ao1ao3* T-DNA insertion mutant

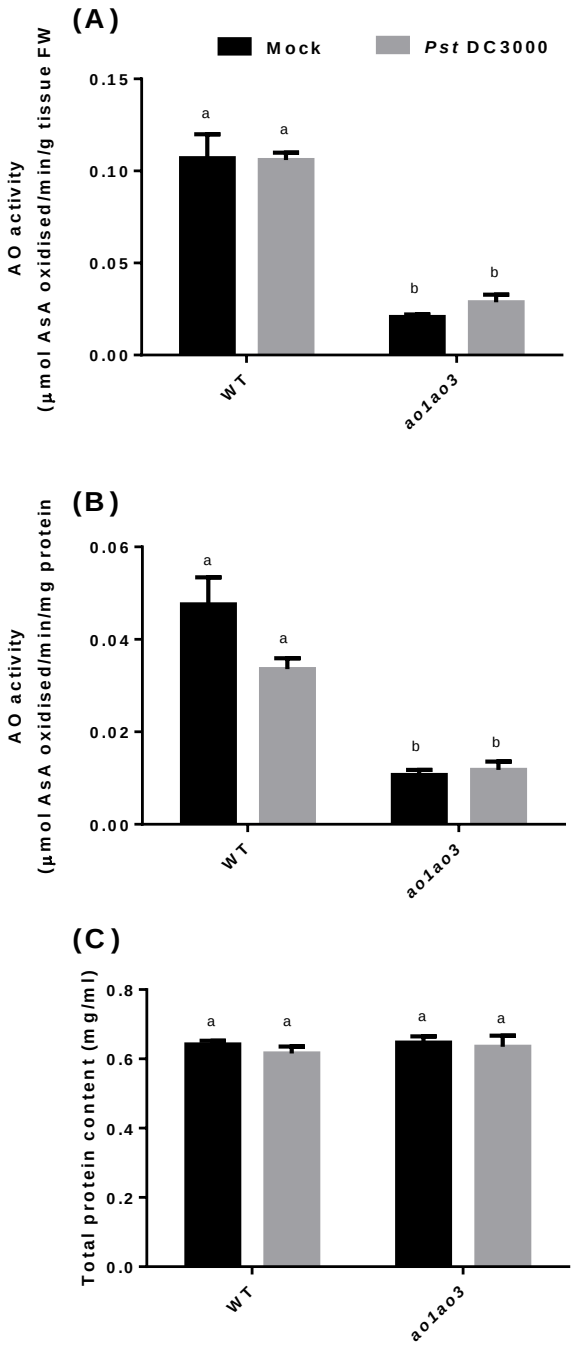

Figure D: Ionically-bound cell wall AO activity of WT and *ao1ao3* T-DNA insertion mutant after four days inoculation with *P. syringae* DC3000 (*Pst* DC3000). 5-week-old plants were used. The AO activity was expressed on a fresh weight **(A)** and protein **(B)** basis, respectively. **(C)** The total protein content in WT and *ao1ao3* mutant. Values are mean ± SEM, n = 3. Different letters above the bars denote the values are significantly different using one way ANOVA and Tukey tests ($p<0.05$). Values bearing the same letter are not significantly different from each other.

Appendix D: The AO activity of *Thellungiella halophila*

Appendix D1: Comparison between ionically-bound cell wall AO activity in *A. thaliana* and *T. halophila* under unstressed normal growth conditions

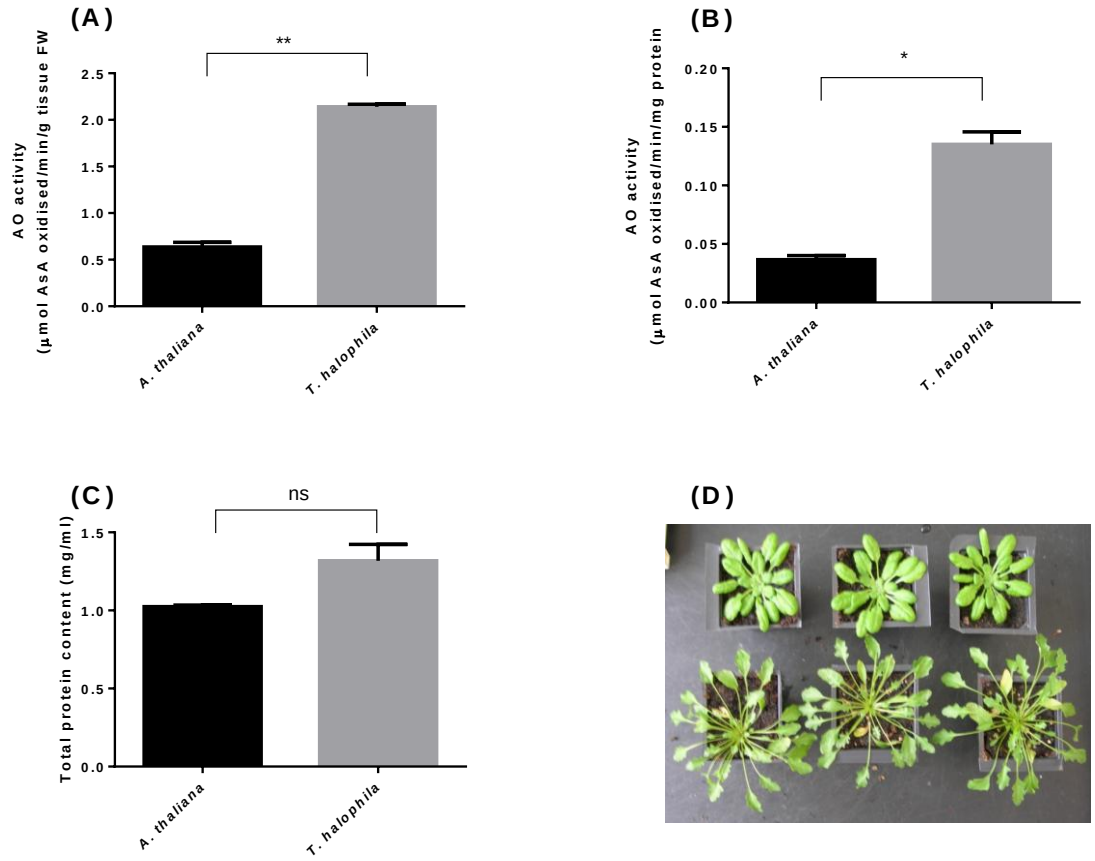

Figure E: Ionically-bound cell wall AO activity of WT *A. thaliana* and WT *T. halophila*. Fully expanded leaves from 5-week-old *A. thaliana* and 7-week-old *T. halophila* were used. The AO activity was expressed on a fresh weight **(A)** and protein **(B)** basis, respectively. **(C)** The total protein content in *A. thaliana* and *T. halophila*. **(D)** Representative plants used in this assay, *A. thaliana* (top) and *T. halophila* (bottom). Values are mean ± SEM, n = 2. Asterisks denote the values are significantly different at $p<0.05$ (*) and $p<0.01$ (**) using a two-tailed *t*-test. N.s. denotes the values are not significantly different from each other.

Appendix D2: Ionically-bound cell wall AO activity in vegetative tissues of WT *T. halophila*

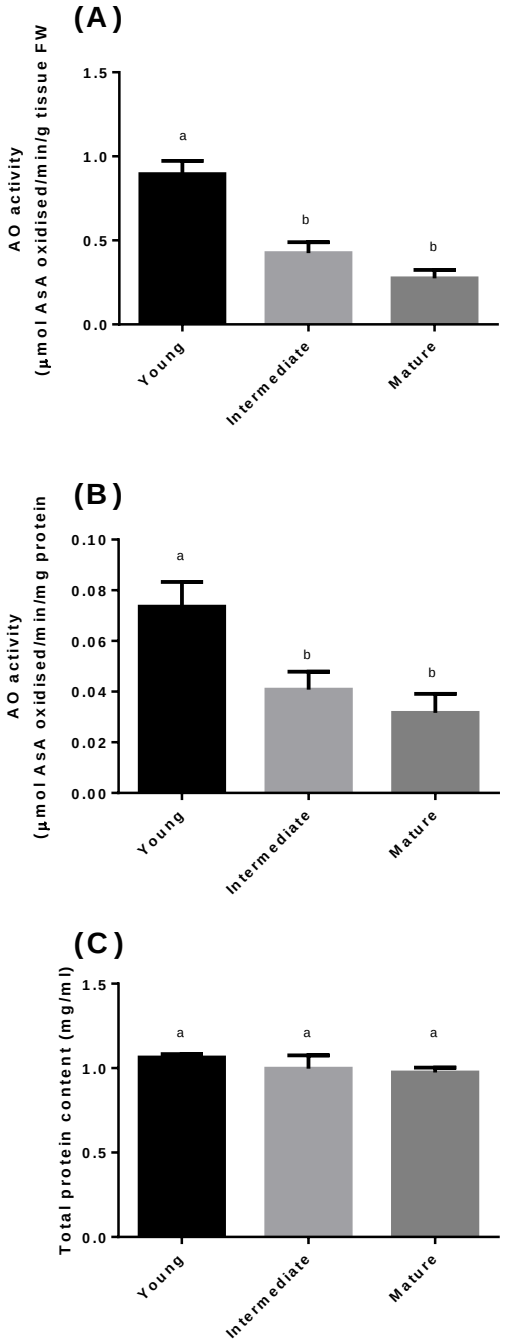

Figure F: Ionically-bound cell wall AO activity in vegetative tissues of 7-week-old WT *T. halophila*. The AO activity was expressed on a fresh weight **(A)** and protein **(B)** basis, respectively. **(C)** The total protein content in vegetative tissues. Values are mean ± SEM, n = 4. Different letters above the bars denote the values are significantly different using one way ANOVA and Tukey tests ($p<0.05$). Values bearing the same letter are not significantly different from one another.

Appendix D3: Soluble and ionically-bound cell wall AO activities of WT *T. halophila* under unstressed normal growth conditions

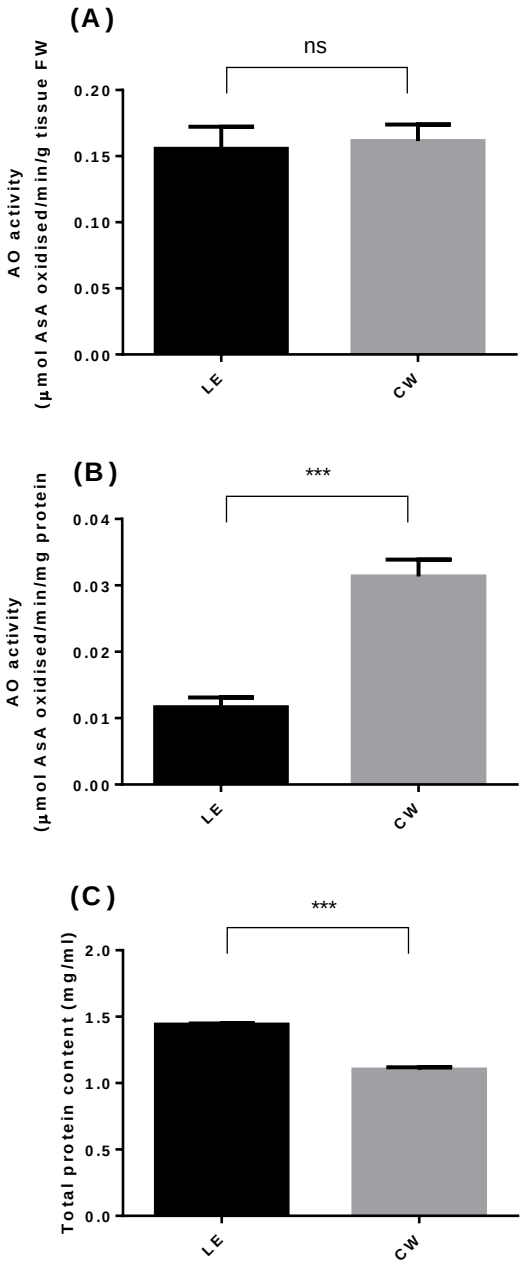

Figure G: Soluble and ionically-bound cell wall AO activities of WT *T. halophila*. Fully expanded leaves from 7-week-old *T. halophila* were used. The AO activity was expressed on a fresh weight **(A)** and protein **(B)** basis, respectively. **(C)** The total protein content in *A. thaliana* and *T. halophila*. Values are mean ± SEM, n = 4. Asterisk denotes the values are significantly different at $p<0.001$ (***) using a two-tailed *t*-test. N.s. denotes the values are not significantly different from each other.

Appendix D4: The effect of salt stress on ionically-bound cell wall AO activity of WT *T. halophila*

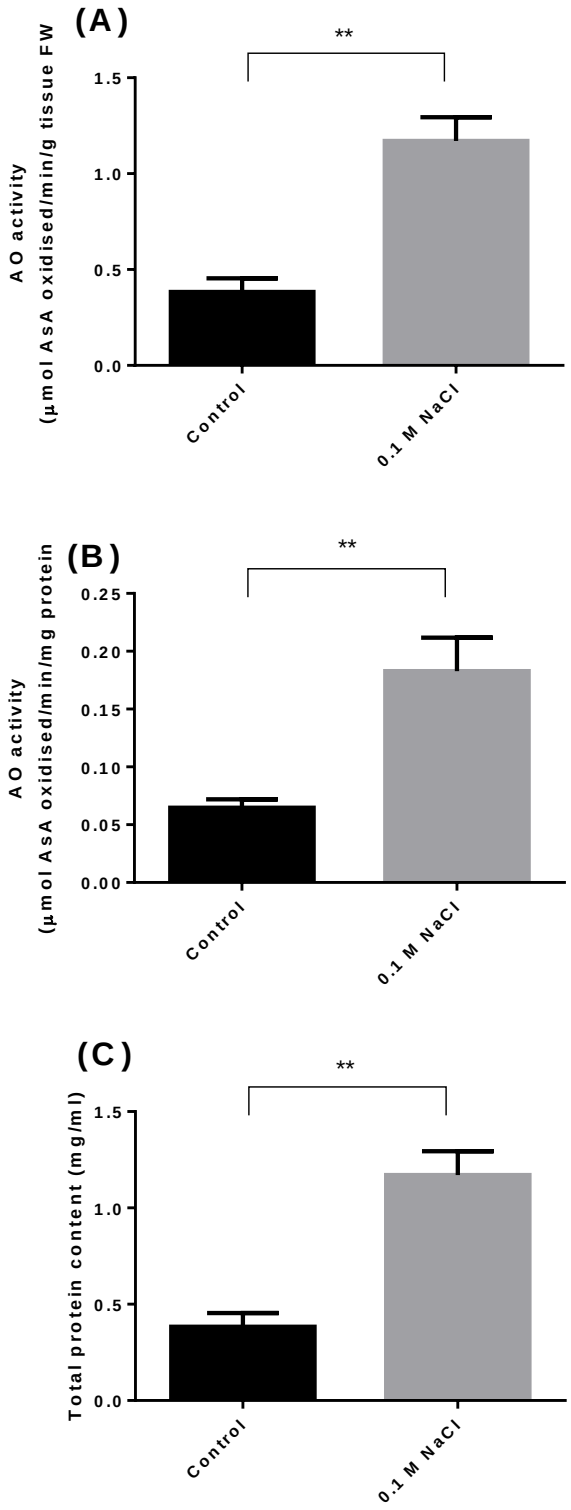

Figure H: Ionically-bound cell wall AO activity of WT *T. halophila* after 14 days of salt treatment with 0.1 M NaCl. Fully expanded leaves from 7-week-old *T. halophila* were used. The AO activity was expressed on a fresh weight **(A)** and protein **(B)** basis, respectively. **(C)** The total protein content in control and salt stressed plants. Values are mean ± SEM, n = 4. Asterisk denotes the values are significantly different at $p<0.01$ (**) using a two-tailed *t*-test.

Appendix E: The effect of drought on *35S::AO3*

Appendix E1: Phenotype of *35S::AO3* in response to drought

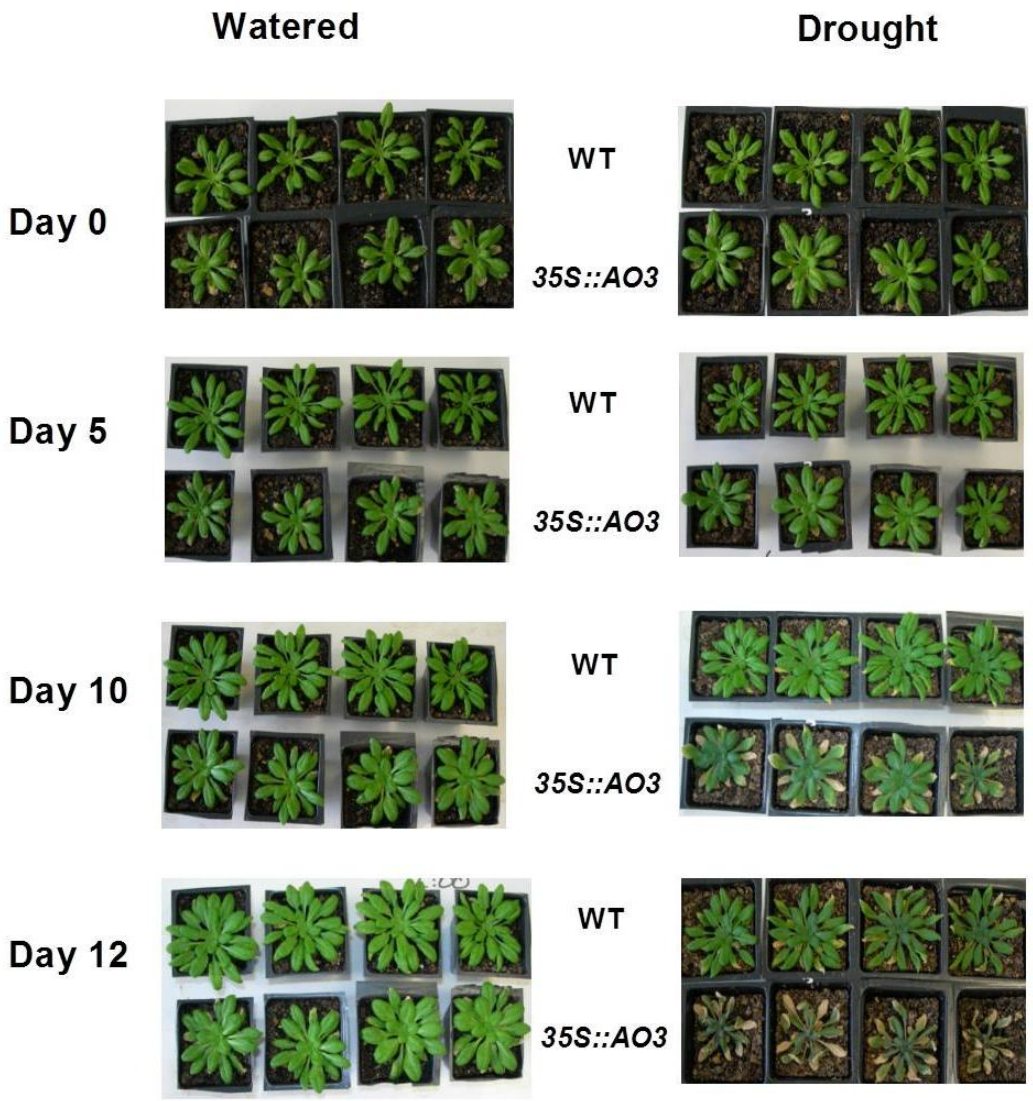

Figure I: The effect of drought on WT and *35S::AO3* transgenic plants. Pictures of WT and *35S::AO3* under control ("watered") and drought treatments were taken at the indicated days and representative plants are shown. Control: 7-week-old plants were watered every 3 days for 12 days. Drought stress: 7-week-old plants were withheld from watering for 12 days.

Appendix E2: The effect of drought on photosynthetic capacity of *35S::AO3*

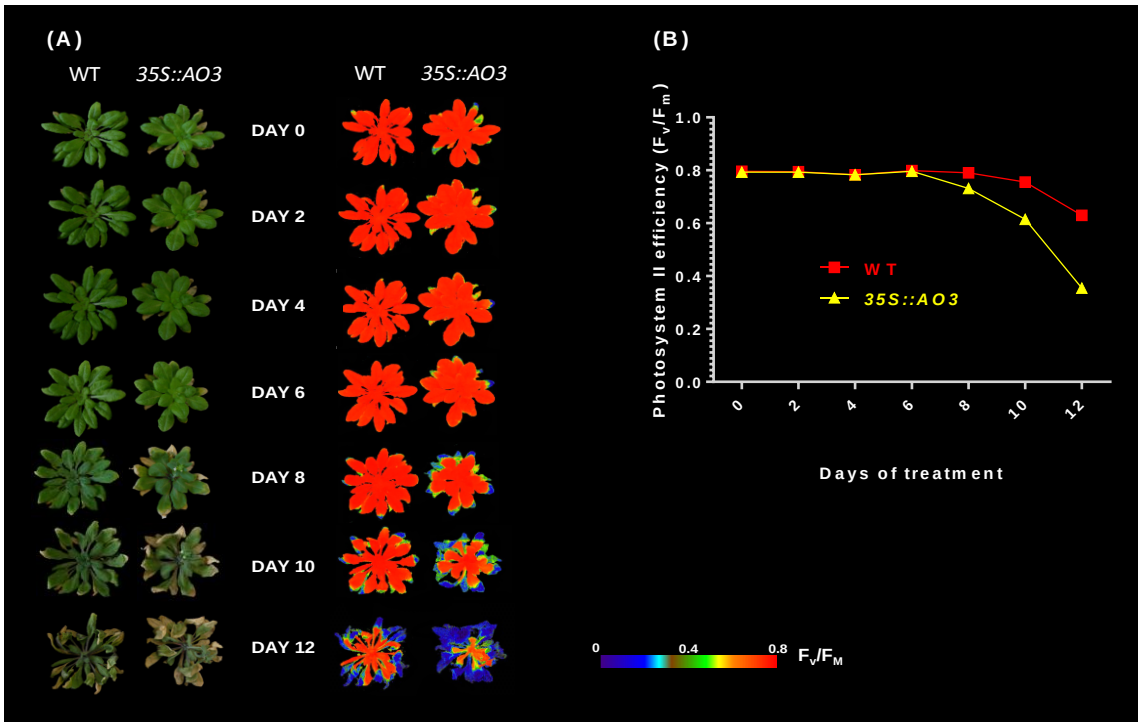

Figure J: Time-course photosystem II quantum yield (F_v/F_m) in WT and *35S::AO3* during 12 days of drought treatment. **(A)** Representative plants subjected to drought treatment (left) and the corresponding fluorescence images (right) to illustrate changes in F_v/F_m, indicated by the false colour code. **(B)** Changes in the F_v/F_m in WT and *35S::AO3* subjected to 12 days of drought treatment.

References

The Arabidopsis Genome Initiative. (2000). Analysis of the genome sequence of the flowering plant *Arabidopsis thaliana*. Nature **408,** 796-815.

Alonso, J.M., Stepanova, A.N., Leisse, T.J., Kim, C.J., Chen, H., Shinn, P., Stevenson, D.K., Zimmerman, J., Barajas, P., Cheuk, R., Gadrinab, C., Heller, C., Jeske, A., Koesema, E., Meyers, C.C., Parker, H., Prednis, L., Ansari, Y., Choy, N., Deen, H., Geralt, M., Hazari, N., Hom, E., Karnes, M., Mulholland, C., Ndubaku, R., Schmidt, I., Guzman, P., Aguilar-Henonin, L., Schmid, M., Weigel, D., Carter, D.E., Marchand, T., Risseeuw, E., Brogden, D., Zeko, A., Crosby, W.L., Berry, C.C., and Ecker, J.R. (2003). Genome-Wide Insertional Mutagenesis of *Arabidopsis thaliana*. Science **301,** 653-657.

Altschul, S.F., Gish, W., Miller, W., Myers, E.W., and Lipman, D.J. (1990). Basic local alignment search tool. Journal of Molecular Biology **215,** 403-410.

Alvarez, J.P., Pekker, I., Goldshmidt, A., Blum, E., Amsellem, Z., and Eshed, Y. (2006). Endogenous and synthetic microRNAs stimulate simultaneous, efficient, and localized regulation of multiple targets in diverse species. The Plant Cell **18,** 1134-1151.

Apel, K., and Hirt, H. (2004). Reactive oxygen species: metabolism, oxidative stress, and signal transduction. Annual Review of Plant Biology **55,** 373-399.

Arrigoni, O. (1994). Ascorbate system in plant development. Journal of Bioenergetics and Biomembranes **26,** 407-419.

Arrigoni, O., Chinni, E., Ciraci, S., and De Tullio, M.C. (2003). *In vivo* elicitation of ascorbate oxidase activity by dioxygen and its possible role in photosynthesizing leaves. Rend. Fis. Acc. Lincei **14,** 127-134.

Asada, K. (1999). The water-water cycle in chloroplasts: scavenging of active oxygens and dissipation of excess photons. Annual Review of Plant Physiology and Plant Molecular Biology **50,** 601-639.

Asada, K. (2006). Production and scavenging of reactive oxygen species in chloroplasts and their functions. Plant Physiology **141,** 391-396.

Azpiroz-Leehan, R., and Feldmann, K.A. (1997). T-DNA insertion mutagenesis in *Arabidopsis*: going back and forth. Trends in Genetics **13,** 152-156.

Baker, N.R. (2008). Chlorophyll fluorescence: a probe of photosynthesis *in vivo*. Annual Review of Plant Biology **59,** 89-113.

Balestrini, R., Ott, T., Güther, M., Bonfante, P., Udvardi, M.K., and De Tullio, M.C. (2012). Ascorbate oxidase: the unexpected involvement of a 'wasteful enzyme' in the symbioses with nitrogen-fixing bacteria and arbuscular mycorrhizal fungi. Plant Physiology and Biochemistry **59,** 71-79.

Bartel, D.P. (2004). MicroRNAs: genomics, biogenesis, mechanism, and function. Cell **116,** 281-297.

Bartels, D., and Sunkar, R. (2005). Drought and salt tolerance in plants. Critical Reviews in Plant Sciences **24,** 23-58.

Bartoli, C.G., Yu, J., Gómez, F., Fernández, L., McIntosh, L., and Foyer, C.H. (2006). Inter-relationships between light and respiration in the control of ascorbic acid synthesis and accumulation in *Arabidopsis thaliana* leaves. Journal of Experimental Botany **57,** 1621-1631.

Baulcombe, D. (2004). RNA silencing in plants. Nature **431,** 356-363.

Bindschedler, L.V., Dewdney, J., Blee, K.A., Stone, J.M., Asai, T., Plotnikov, J., Denoux, C., Hayes, T., Gerrish, C., Davies, D.R., Ausubel, F.M., and Paul Bolwell, G. (2006). Peroxidase-dependent apoplastic oxidative burst in *Arabidopsis* required for pathogen resistance. The Plant Journal **47,** 851-863.

Blokhina, O., and Fagerstedt, K.V. (2010). Oxidative metabolism, ROS and NO under oxygen deprivation. Plant Physiology and Biochemistry **48,** 359-373.

Blom, N., Gammeltoft, S., and Brunak, S. (1999). Sequence and structure-based prediction of eukaryotic protein phosphorylation sites. Journal of Molecular Biology **294,** 1351-1362.

Blom, N., Sicheritz-Pontén, T., Gupta, R., Gammeltoft, S., and Brunak, S. (2004). Prediction of post-translational glycosylation and phosphorylation of proteins from the amino acid sequence. Proteomics **4,** 1633-1649.

Bolwell, G.P., and Wojtaszek, P. (1997). Mechanisms for the generation of reactive oxygen species in plant defence – a broad perspective. Physiological and Molecular Plant Pathology **51,** 347-366.

Boyer, J.S. (1982). Plant Productivity and Environment. Science **218,** 443-448.

Boyes, D.C., Zayed, A.M., Ascenzi, R., McCaskill, A.J., Hoffman, N.E., Davis, K.R., and Görlach, J. (2001). Growth stage based phenotypic analysis of *Arabidopsis*: a model for high throughput functional genomics in plants. The Plant Cell **13,** 1499-1510.

Bradford, M.M. (1976). A rapid and sensitive method for the quantitation of microgram quantities of protein utilizing the principle of protein-dye binding. Analytical Biochemistry **72,** 248-254.

Campanoni, P., and Nick, P. (2005). Auxin-dependent cell division and cell elongation. 1-naphthaleneacetic acid and 2,4-dichlorophenoxyacetic acid activate different pathways. Plant Physiology **137,** 939-948.

Caputo, E., Ceglie, V., Lippolis, M., La Rocca, N., and De Tullio, M.C. (2010). Identification of a NaCl-induced ascorbate oxidase activity in *Chaetomorpha linum* suggests a novel mechanism of adaptation to increased salinity. Environmental and Experimental Botany **69,** 63-67.

Chaves, M.M., Maroco, J.P., and Pereira, J.S. (2003). Understanding plant responses to drought — from genes to the whole plant. Functional Plant Biology **30,** 239-264.

Chen, Z., and Gallie, D.R. (2004). The ascorbic acid redox state controls guard cell signaling and stomatal movement. The Plant Cell **16,** 1143-1162.

Chichiricco, G., Ceru, M.P., D'Allessandro, A., Oratore, A., and Avigliano, L. (1989). Immunohistochemical localization of ascorbate oxidase in *Cucurbita pepo* medullosa. Plant Science **64,** 61-66.

Clough, S.J., and Bent, A.F. (1998). Floral dip: a simplified method for *Agrobacterium*-mediated transformation of *Arabidopsis thaliana*. The Plant Journal **16,** 735-743.

Colville, L., and Smirnoff, N. (2008). Antioxidant status, peroxidase activity, and PR protein transcript levels in ascorbate-deficient *Arabidopsis thaliana vtc* mutants. Journal of Experimental Botany **59,** 3857-3868.

Conklin, P.L., Saracco, S.A., Norris, S.R., and Last, R.L. (2000). Identification of ascorbic acid-deficient *Arabidopsis thaliana* mutants. Genetics **154,** 847-856.

Conklin, P.L., Norris, S.R., Wheeler, G.L., Williams, E.H., Smirnoff, N., and Last, R.L. (1999). Genetic evidence for the role of GDP-mannose in plant ascorbic acid (vitamin C) biosynthesis. Proceedings of the National Academy of Sciences **96,** 4198-4203.

Cosio, C., and Dunand, C. (2009). Specific functions of individual class III peroxidase genes. Journal of Experimental Botany **60,** 391-408.

Cruz de Carvalho, M.H. (2008). Drought stress and reactive oxygen species: production, scavenging and signaling. Plant Signaling & Behavior **3,** 156-165.

D'Haese, D., Vandermeiren, K., Asard, H.A.N., and Horemans, N. (2005). Other factors than apoplastic ascorbate contribute to the differential ozone tolerance of two clones of *Trifolium repens* L. Plant, Cell & Environment **28,** 623-632.

Daudi, A., Cheng, Z., O'Brien, J.A., Mammarella, N., Khan, S., Ausubel, F.M., and Bolwell, G.P. (2012). The apoplastic oxidative burst peroxidase in *Arabidopsis* is a major component of Pattern-Triggered Immunity. The Plant Cell **24,** 275-287.

Dawson, C.R., Strothkamp, K.G., and Krul, K.G. (1975). Ascorbate oxidase and related copper proteins. Annals of the New York Academy of Sciences **258,** 209-220.

de Felippes, F.F., Wang, J.-w., and Weigel, D. (2012). MIGS: miRNA-induced gene silencing. The Plant Journal **70,** 541-547.

De Gara, L. (2004). Class III peroxidases and ascorbate metabolism in plants. Phytochemistry Reviews **3,** 195-205.

de Pinto, M.C., and De Gara, L. (2004). Changes in the ascorbate metabolism of apoplastic and symplastic spaces are associated with cell differentiation. Journal of Experimental Botany **55,** 2559-2569.

De Tullio, M., Ciraci, S., Liso, R., and Arrigoni, O. (2007). Ascorbic acid oxidase is dynamically regulated by light and oxygen. A tool for oxygen management in plants? Journal of Plant Physiology **164,** 39-46.

De Tullio, M.C., Liso, R., and Arrigoni, O. (2004). Ascorbic acid oxidase: an enzyme in search of a role. Biologia Plantarum **48,** 161-166.

Diallinas, G., Pateraki, I., Sanmartin, M., Scossa, A., Stilianou, E., Panopoulos, N.J., and Kanellis, A.K. (1997). Melon ascorbate oxidase: cloning of a multigene family, induction during fruit development and repression by wounding. Plant Molecular Biology **34,** 759-770.

Dowdle, J., Ishikawa, T., Gatzek, S., Rolinski, S., and Smirnoff, N. (2007). Two genes in *Arabidopsis thaliana* encoding GDP-$_L$-galactose phosphorylase are required for ascorbate biosynthesis and seedling viability. The Plant Journal **52,** 673-689.

Dumville, J.C., and Fry, S.C. (2003). Solubilisation of tomato fruit pectins by ascorbate: a possible non-enzymic mechanism of fruit softening. Planta **217,** 951-961.

Dyrløv Bendtsen, J., Nielsen, H., von Heijne, G., and Brunak, S. (2004). Improved prediction of signal peptides: SignalP 3.0. Journal of Molecular Biology **340,** 783-795.

Edwards, K., Johnstone, C., and Thompson, C. (1991). A simple and rapid method for the preparation of plant genomic DNA for PCR analysis. Nucleic Acids Research **19,** 1349.

Eisen, J.A. (1998). Phylogenomics: improving functional predictions for uncharacterized genes by evolutionary analysis. Genome Research **8,** 163-167.

Emanuelsson, O., Nielsen, H., Brunak, S., and von Heijne, G. (2000). Predicting subcellular localization of proteins based on their N-terminal amino acid sequence. Journal of Molecular Biology **300,** 1005-1016.

Emanuelsson, O., Brunak, S., von Heijne, G., and Nielsen, H. (2007). Locating proteins in the cell using TargetP, SignalP and related tools. Nat. Protocols **2,** 953-971.

Esaka, M., Fujisawa, K., Goto, M., and Kisu, Y. (1992). Regulation of ascorbate oxidase expression in pumpkin by auxin and copper. Plant Physiology **100,** 231-237.

Esaka, M., Hattori, T., Fujisawa, K., Sakajo, S., and Asahi, T. (1990). Molecular cloning and nucleotide sequence of full-length cDNA for ascorbate oxidase from cultured pumpkin cells. European Journal of Biochemistry **191,** 537-541.

Eskling, M., Arvidsson, P.-O., and Åkerlund, H.-E. (1997). The xanthophyll cycle, its regulation and components. Physiologia Plantarum **100,** 806-816.

Farley, A.R., and Link, A.J. (2009). Chapter 40 Identification and quantification of protein posttranslational modifications. In Methods in Enzymology, R.B. Richard and P.D. Murray, eds (Academic Press), pp. 725-763.

Fojtová, M., Peška, V., Dobšáková, Z., Mozgová, I., Fajkus, J., and Sýkorová, E. (2011). Molecular analysis of T-DNA insertion mutants identified putative regulatory elements in the *AtTERT* gene. Journal of Experimental Botany **62,** 5531-5545.

Fotopoulos, V., Sanmartin, M., and Kanellis, A.K. (2006). Effect of ascorbate oxidase over-expression on ascorbate recycling gene expression in response to agents imposing oxidative stress. Journal of Experimental Botany **57,** 3933-3943.

Fotopoulos, V., De Tullio, M.C., Barnes, J., and Kanellis, A.K. (2008). Altered stomatal dynamics in ascorbate oxidase over-expressing tobacco plants suggest a role for dehydroascorbate signalling. Journal of Experimental Botany **59,** 729-737.

Foyer, C.H., and Lelandais, M. (1996). A comparison of the relative rates of transport of ascorbate and glucose across the thylakoid, chloroplast and plasmalemma membranes of pea leaf mesophyll cells. Journal of Plant Physiology **148,** 391-398.

Foyer, C.H., and Shigeoka, S. (2011). Understanding oxidative stress and antioxidant functions to enhance photosynthesis. Plant Physiology **155,** 93-100.

Foyer, C.H., and Noctor, G. (2011). Ascorbate and glutathione: the heart of the redox hub. Plant Physiology **155,** 2-18.

Fry, S.C. (1998). Oxidative scission of plant cell wall polysaccharides by ascorbate-induced hydroxyl radicals. Biochem. J. **332,** 507-515.

Fry, S.C., Dumville, J.C., and Miller, J.G. (2001). Fingerprinting of polysaccharides attacked by hydroxyl radicals *in vitro* and in the cell walls of ripening pear fruit. Biochem. J. **357,** 729-737.

Fry, S.C., Miller, J.G., and Dumville, J.C. (2002). A proposed role for copper ions in cell wall loosening. Plant and Soil **247,** 57-67.

Galvez-Valdivieso, G., and Mullineaux, P.M. (2010). The role of reactive oxygen species in signalling from chloroplasts to the nucleus. Physiologia Plantarum **138,** 430-439.

Garchery, C., Gest, N., Do, P.T., Alhagdow, M., Baldet, P., Rothan, C., Massot, C., Gautier, H., Aarrouf, J., Fernie, A.R., and Stevens, R. (2012). A diminution in ascorbate oxidase activity affects carbon allocation and improves yield in tomato under water-deficit. Plant, Cell & Environment **Early view article**.

García-Pineda, E., Castro-Mercado, E., and Lozoya-Gloria, E. (2004). Gene expression and enzyme activity of pepper (*Capsicum annuum* L.) ascorbate oxidase during elicitor and wounding stress. Plant Science **166,** 237-243.

Gatzek, S., Wheeler, G.L., and Smirnoff, N. (2002). Antisense suppression of $_L$-galactose dehydrogenase in *Arabidopsis thaliana* provides evidence for its role in ascorbate synthesis and reveals light modulated $_L$-galactose synthesis. The Plant Journal **30,** 541-553.

Ge, W., Song, Y., Zhang, C., Zhang, Y., Burlingame, A.L., and Guo, Y. (2011). Proteomic analyses of apoplastic proteins from germinating *Arabidopsis thaliana* pollen. Biochimica et Biophysica Acta (BBA) - Proteins & Proteomics **1814,** 1964-1973.

Giacomelli, L., Rudella, A., and van Wijk, K.J. (2006). High light response of the thylakoid proteome in *Arabidopsis* wild type and the ascorbate-deficient mutant *vtc2-2*. A comparative proteomics study. Plant Physiology **141,** 685-701.

Giacomelli, L., Masi, A., Ripoll, D., Lee, M., and van Wijk, K. (2007). *Arabidopsis thaliana* deficient in two chloroplast ascorbate peroxidases shows accelerated light-induced necrosis when levels of cellular ascorbate are low. Plant Molecular Biology **65,** 627-644.

Goh, H.H., Sloan, J., Dorca-Fornell, C., and Fleming, A.J. (2012). Inducible repression of multiple expansin genes leads to growth suppression during leaf development. Plant Physiology **159,** 1759-1770.

Golan, T., MüLler-Moulé, P., and Niyogi, K.K. (2006). Photoprotection mutants of *Arabidopsis thaliana* acclimate to high light by increasing photosynthesis and specific antioxidants. Plant, Cell & Environment **29,** 879-887.

González-Reyes, J.A., Hidalgo, A., Caler, J.A., Palos, R., and Navas, P. (1994). Nutrient uptake changes in ascorbate free radical-stimulated onion roots. Plant Physiology **104,** 271-276.

González-Reyes, J.A., Alcaín, F.J., Caler, J.A., Serrano, A., Córdoba, F., and Navas, P. (1995). Stimulation of onion root elongation by ascorbate and ascorbate free radical in *Allium cepa* L. Protoplasma **184,** 31-35.

Gould, K.S., McKelvie, J., and Markham, K.R. (2002). Do anthocyanins function as antioxidants in leaves? Imaging of H_2O_2 in red and green leaves after mechanical injury. Plant, Cell & Environment **25,** 1261-1269.

Green, M.A., and Fry, S.C. (2005). Vitamin C degradation in plant cells *via* enzymatic hydrolysis of 4-*O*-oxalyl-$_L$-threonate. Nature **433,** 83-87.

Gupta, R., Jung, E., Gooley, A.A., Williams, K.L., Brunak, S., and Hansen, J. (1999). Scanning the available *Dictyostelium discoideum* proteome for *O*-

linked GlcNAc glycosylation sites using neural networks. Glycobiology **9,** 1009-1022.

Hall, T.A. (1999). BioEdit: a user-friendly biological sequence alignment editor and analysis program for Windows 95/98/NT. Nucl. Acids. Symp. Ser. **41,** 95-98.

Harrison, S., Mott, E., Parsley, K., Aspinall, S., Gray, J., and Cottage, A. (2006). A rapid and robust method of identifying transformed *Arabidopsis thaliana* seedlings following floral dip transformation. Plant Methods **2,** 19.

Hartley, J.L., Temple, G.F., and Brasch, M.A. (2000). DNA cloning using *in vitro* site-specific recombination. Genome Res **10,** 1788-1795.

Hayashi, R., and Morohashi, Y. (1993). Phytochrome control of the development of ascorbate oxidase activity in mustard (*Sinapis alba* L.) cotyledons. Plant Physiology **102,** 1237-1241.

Heazlewood, J.L., Tonti-Filippini, J., Verboom, R.E., and Millar, A.H. (2005). Combining experimental and predicted datasets for determination of the subcellular location of proteins in *Arabidopsis*. Plant Physiology **139,** 598-609.

Heazlewood, J.L., Verboom, R.E., Tonti-Filippini, J., Small, I., and Millar, A.H. (2007). SUBA: the *Arabidopsis* Subcellular Database. Nucleic Acids Research **35,** D213-D218.

Hidalgo, A., González-Reyes, J.A., and Navas, P. (1989). Ascorbate free radical enhances vacuolization in onion root meristems. Plant, Cell & Environment **12,** 455-460.

Hidema, J., Makino, A., Kurita, Y., Mae, T., and Ojima, K. (1992). Changes in the levels of chlorophyll and light-harvesting chlorophyll a/b protein of PS II in rice leaves aged under different irradiances from full expansion through senescence. Plant and Cell Physiology **33,** 1209-1214.

Higo, K., Ugawa, Y., Iwamoto, M., and Korenaga, T. (1999). Plant *cis*-acting regulatory DNA elements (PLACE) database: 1999. Nucleic Acids Research **27,** 297-300.

Hilson, P., Allemeersch, J., Altmann, T., Aubourg, S., Avon, A., Beynon, J., Bhalerao, R.P., Bitton, F., Caboche, M., Cannoot, B., Chardakov, V., Cognet-Holliger, C., Colot, V., Crowe, M., Darimont, C., Durinck, S., Eickhoff, H., de Longevialle, A.F., Farmer, E.E., Grant, M., Kuiper, M.T.R., Lehrach, H., Léon, C., Leyva, A., Lundeberg, J., Lurin, C., Moreau, Y., Nietfeld, W., Paz-Ares, J., Reymond, P., Rouzé, P., Sandberg, G., Segura, M.D., Serizet, C., Tabrett, A., Taconnat, L., Thareau, V., Van Hummelen, P., Vercruysse, S., Vuylsteke, M., Weingartner, M., Weisbeek, P.J., Wirta, V., Wittink, F.R.A., Zabeau, M., and Small, I. (2004). Versatile gene-specific sequence tags for *Arabidopsis* functional genomics: transcript profiling and reverse genetics applications. Genome Research **14,** 2176-2189.

Horemans, N., Foyer, C.H., and Asard, H. (2000a). Transport and action of ascorbate at the plant plasma membrane. Trends in Plant Science **5,** 263-267.

Horemans, N., H. Foyer, C., Potters, G., and Asard, H. (2000b). Ascorbate function and associated transport systems in plants. Plant Physiology and Biochemistry **38,** 531-540.

Horemans, N., Potters, G., De Wilde, L., and Caubergs, R.J. (2003). Dehydroascorbate uptake activity correlates with cell growth and cell

division of tobacco Bright Yellow-2 cell cultures. Plant Physiology **133,** 361-367.

Hraška, M., Rakouský, S., and Čurn, V. (2008). Tracking of the CaMV-35S promoter performance in GFP transgenic tobacco, with a special emphasis on flowers and reproductive organs, confirmed its predominant activity in vascular tissues. Plant Cell, Tissue and Organ Culture **94,** 239-251.

Hu, J.-F., Li, G.-F., Gao, Z.-H., Chen, L., Ren, H.-B., and Jia, W.-S. (2005). Regulation of water deficit-induced abscisic acid accumulation by apoplastic ascorbic acid in maize seedlings. Journal of Integrative Plant Biology **47,** 1335-1344.

Hurtado, L., Farrona, S., and Reyes, J. (2006). The putative SWI/SNF complex subunit BRAHMA activates flower homeotic genes in *Arabidopsis thaliana*. Plant Molecular Biology **62,** 291-304.

Innocenti, A.M., Bitonti, M.B., Arrigoni, O., and Liso, R. (1990). The size of quiescent centre in roots of *Allium cepa* L. grown with ascorbic acid. New Phytologist **114,** 507-509.

Ioannidi, E., Kalamaki, M.S., Engineer, C., Pateraki, I., Alexandrou, D., Mellidou, I., Giovannonni, J., and Kanellis, A.K. (2009). Expression profiling of ascorbic acid-related genes during tomato fruit development and ripening and in response to stress conditions. Journal of Experimental Botany **60,** 663-678.

Jamet, E., Albenne, C., Boudart, G., Irshad, M., Canut, H., and Pont-Lezica, R. (2008). Recent advances in plant cell wall proteomics. Proteomics **8,** 893-908.

Jiang, K., Meng, Y.L., and Feldman, L.J. (2003). Quiescent center formation in maize roots is associated with an auxin-regulated oxidizing environment. Development **130,** 1429-1438.

Jimenez, A., Hernandez, J.A., del Rio, L.A., and Sevilla, F. (1997). Evidence for the presence of the Ascorbate-Glutathione cycle in mitochondria and peroxisomes of pea leaves. Plant Physiology **114,** 275-284.

Jubany-Marí, T., Munné-Bosch, S., and Alegre, L. (2010a). Redox regulation of water stress responses in field-grown plants. Role of hydrogen peroxide and ascorbate. Plant Physiology and Biochemistry **48,** 351-358.

Jubany-Marí, T., Alegre-Batlle, L., Jiang, K., and Feldman, L.J. (2010b). Use of a redox-sensing GFP (c-roGFP1) for real-time monitoring of cytosol redox status in *Arabidopsis thaliana* water-stressed plants. FEBS Letters **584,** 889-897.

Kanna, M., Tamaoki, M., Kubo, A., Nakajima, N., Rakwal, R., Agrawal, G.K., Tamogami, S., Ioki, M., Ogawa, D., Saji, H., and Aono, M. (2003). Isolation of an ozone-sensitive and jasmonate-semi-insensitive *Arabidopsis* mutant (*oji1*). Plant and Cell Physiology **44,** 1301-1310.

Karimi, M., Depicker, A., and Hilson, P. (2007). Recombinational cloning with plant Gateway vectors. Plant Physiology **145,** 1144-1154.

Kärkönen, A., and Fry, S.C. (2006). Effect of ascorbate and its oxidation products on H_2O_2 production in cell-suspension cultures of *Picea abies* and in the absence of cells. Journal of Experimental Botany **57,** 1633-1644.

Kato, N., and Esaka, M. (1996). cDNA cloning and gene expression of ascorbate oxidase in tobacco. Plant Molecular Biology **30,** 833-837.

Kato, N., and Esaka, M. (1999). Changes in ascorbate oxidase gene expression and ascorbate levels in cell division and cell elongation in tobacco cells. Physiologia Plantarum **105,** 321-329.

Kato, N., and Esaka, M. (2000). Expansion of transgenic tobacco protoplasts expressing pumpkin ascorbate oxidase is more rapid than that of wild-type protoplasts. Planta **210,** 1018-1022.

Kerk, N.M., and Feldman, N.J. (1995). A biochemical model for the initiation and maintenance of the quiescent center: implications for organization of root meristems. Development **121,** 2825-2833.

Kerk, N.M., Jiang, K., and Feldman, L.J. (2000). Auxin metabolism in the root apical meristem. Plant Physiology **122,** 925-932.

Keurentjes, J., Sulpice, R., Gibon, Y., Steinhauser, M.-C., Fu, J., Koornneef, M., Stitt, M., and Vreugdenhil, D. (2008). Integrative analyses of genetic variation in enzyme activities of primary carbohydrate metabolism reveal distinct modes of regulation in *Arabidopsis thaliana*. Genome Biology **9,** R129.

Kilian, J., Whitehead, D., Horak, J., Wanke, D., Weinl, S., Batistic, O., D'Angelo, C., Bornberg-Bauer, E., Kudla, J., and Harter, K. (2007). The AtGenExpress global stress expression data set: protocols, evaluation and model data analysis of UV-B light, drought and cold stress responses. The Plant Journal **50,** 347-363.

Kisu, Y., Harada, Y., Goto, M., and Esaka, M. (1997). Cloning of the pumpkin ascorbate oxidase gene and analysis of a *cis*-acting region involved in induction by auxin. Plant and Cell Physiology **38,** 631-637.

Krysan, P.J., Young, J.C., and Sussman, M.R. (1999). T-DNA as an insertional mutagen in *Arabidopsis*. The Plant Cell **11,** 2283-2290.

Kumar, S., Nei, M., Dudley, J., and Tamura, K. (2008). MEGA: A biologist-centric software for evolutionary analysis of DNA and protein sequences. Briefings in Bioinformatics **9,** 299-306.

Landry, L.G., Chapple, C., and Last, R.L. (1995). *Arabidopsis* mutants lacking phenolic sunscreens exhibit enhanced ultraviolet-B injury and oxidative damage. Plant Physiology **109,** 1159-1166.

Lee, L.-Y., and Gelvin, S.B. (2008). T-DNA binary vectors and systems. Plant Physiology **146,** 325-332.

Lee, S., Lee, E.J., Yang, E.J., Lee, J.E., Park, A.R., Song, W.H., and Park, O.K. (2004). Proteomic identification of Annexins, calcium-dependent membrane binding proteins that mediate osmotic stress and abscisic acid signal transduction in *Arabidopsis*. The Plant Cell **16,** 1378-1391.

Lee, Y., Park, C.H., Ram Kim, A., Chang, S.C., Kim, S.-H., Lee, W.S., and Kim, S.-K. (2011). The effect of ascorbic acid and dehydroascorbic acid on the root gravitropic response in *Arabidopsis thaliana*. Plant Physiology and Biochemistry **49,** 909-916.

Lescot, M., Déhais, P., Thijs, G., Marchal, K., Moreau, Y., Van de Peer, Y., Rouzé, P., and Rombauts, S. (2002). PlantCARE, a database of plant *cis*-acting regulatory elements and a portal to tools for *in silico* analysis of promoter sequences. Nucleic Acids Research **30,** 325-327.

Lichtenthaler, H.K., and Buschmann, C. (2001). Chlorophylls and carotenoids: measurement and characterization by UV-VIS spectroscopy. In Current Protocols in Food Analytical Chemistry (John Wiley & Sons, Inc.)), pp. F4.3.1-F4.3.8.

Lin, L.-S., and Varner, J.E. (1991). Expression of ascorbic acid oxidase in Zucchini Squash (*Cucurbita pepo* L.). Plant Physiology **96,** 159-165.

Liso, R., Innocenti, A.M., Bitonti, M.B., and Arrigoni, O. (1988). Ascorbic acid-induced progression of quiescent centre cells from G1 to S phase. New Phytologist **110,** 469-471.

Liso, R., De Tullio, M.C., Ciraci, S., Balestrini, R., La Rocca, N., Bruno, L., Chiappetta, A., Bitonti, M.B., Bonfante, P., and Arrigoni, O. (2004). Localization of ascorbic acid, ascorbic acid oxidase, and glutathione in roots of *Cucurbita maxima* L. Journal of Experimental Botany **55,** 2589-2597.

Loewus, F.A. (1999). Biosynthesis and metabolism of ascorbic acid in plants and of analogs of ascorbic acid in fungi. Phytochemistry **52,** 193-210.

Loscos, J., Matamoros, M.A., and Becana, M. (2008). Ascorbate and homoglutathione metabolism in common bean nodules under stress conditions and during natural senescence. Plant Physiology **146,** 1282-1292.

Lu, Y., and Last, R.L. (2008). Web-based *Arabidopsis* functional and structural genomics resources. The Arabidopsis Book **6,** e0118.

Luo, L.J. (2010). Breeding for water-saving and drought-resistance rice (WDR) in China. Journal of Experimental Botany **61,** 3509-3517.

Marchler-Bauer, A., Lu, S., Anderson, J.B., Chitsaz, F., Derbyshire, M.K., DeWeese-Scott, C., Fong, J.H., Geer, L.Y., Geer, R.C., Gonzales, N.R., Gwadz, M., Hurwitz, D.I., Jackson, J.D., Ke, Z., Lanczycki, C.J., Lu, F., Marchler, G.H., Mullokandov, M., Omelchenko, M.V., Robertson, C.L., Song, J.S., Thanki, N., Yamashita, R.A., Zhang, D., Zhang, N., Zheng, C., and Bryant, S.H. (2011). CDD: a Conserved Domain Database for the functional annotation of proteins. Nucleic Acids Research **39,** D225-D229.

Matamoros, M.A., Loscos, J., Dietz, K.-J., Aparicio-Tejo, P.M., and Becana, M. (2010). Function of antioxidant enzymes and metabolites during maturation of pea fruits. Journal of Experimental Botany **61,** 87-97.

Mertz, D. (1961). Distribution and cellular localization of ascorbic acid oxidase in the maize root tip. American Journal of Botany **48,** 405-413.

Messerschmidt, A., and Huber, R. (1990). The blue oxidases, ascorbate oxidase, laccase and ceruloplasmin. Modelling and structural relationships. European Journal of Biochemistry **187,** 341-352.

Miller, G., Shulaev, V., and Mittler, R. (2008). Reactive oxygen signaling and abiotic stress. Physiologia Plantarum **133,** 481-489.

Miller, G., Suzuki, N., Ciftci-Yilmaz, S., and Mittler, R. (2010). Reactive oxygen species homeostasis and signalling during drought and salinity stresses. Plant, Cell & Environment **33,** 453-467.

Munns, R., James, R.A., Sirault, X.R.R., Furbank, R.T., and Jones, H.G. (2010). New phenotyping methods for screening wheat and barley for beneficial responses to water deficit. Journal of Experimental Botany **61,** 3499-3507.

Murchie, E.H., and Niyogi, K.K. (2011). Manipulation of photoprotection to improve plant photosynthesis. Plant Physiology **155,** 86-92.

Mustroph, A., Zanetti, M.E., Jang, C.J.H., Holtan, H.E., Repetti, P.P., Galbraith, D.W., Girke, T., and Bailey-Serres, J. (2009). Profiling translatomes of discrete cell populations resolves altered cellular

priorities during hypoxia in *Arabidopsis*. Proceedings of the National Academy of Sciences **106,** 18843-18848.

Nakagawa, T., Kurose, T., Hino, T., Tanaka, K., Kawamukai, M., Niwa, Y., Toyooka, K., Matsuoka, K., Jinbo, T., and Kimura, T. (2007). Development of series of Gateway Binary Vectors, pGWBs, for realizing efficient construction of fusion genes for plant transformation. Journal for Bioscience & Bioengineering **104,** 34-41.

Nanasato, Y., Akashi, K., and Yokota, A. (2005). Co-expression of cytochrome b_{561} and ascorbate oxidase in leaves of wild watermelon under drought and high light conditions. Plant and Cell Physiology **46,** 1515-1524.

Nei, M. (1996). Phylogenetic analysis in molecular evolutionary genetics. Annual Review of Genetics **30,** 371-403.

Nishikawa, F., Kato, M., Hyodo, H., Ikoma, Y., Sugiura, M., and Yano, M. (2003). Ascorbate metabolism in harvested broccoli. Journal of Experimental Botany **54,** 2439-2448.

Niyogi, K.K. (1999). Photoprotection revisited: genetic and molecular approaches. Annual Review of Plant Physiology and Plant Molecular Biology **50,** 333-359.

Noctor, G., and Foyer, C.H. (1998). Ascorbate and glutathione: keeping active oxygen under control. Annual Review of Plant Physiology and Plant Molecular Biology **49,** 249-279.

O'Brien, J.A., Daudi, A., Finch, P., Butt, V.S., Whitelegge, J.P., Souda, P., Ausubel, F.M., and Bolwell, G.P. (2012). A peroxidase-dependent apoplastic oxidative burst in cultured *Arabidopsis* cells functions in MAMP-elicited defence. Plant Physiology **158,** 2013-2027.

O'Malley, R.C., Alonso, J.M., Kim, C.J., Leisse, T.J., and Ecker, J.R. (2007). An adapter ligation-mediated PCR method for high-throughput mapping of T-DNA inserts in the *Arabidopsis* genome. Nat. Protocols **2,** 2910-2917.

Oberbacher, M.F., and Vines, H.M. (1963). Spectrophotometric assay of ascorbic acid oxidase. Nature **197,** 1203-1204.

Odell, J.T., Nagy, F., and Chua, N.-H. (1985). Identification of DNA sequences required for activity of the cauliflower mosaic virus 35S promoter. Nature **313,** 810-812.

Ohkawa, J., Okada, N., Shinmyo, A., and Takano, M. (1989). Primary structure of cucumber (*Cucumis sativus*) ascorbate oxidase deduced from cDNA sequence: homology with blue copper proteins and tissue-specific expression. Proceedings of the National Academy of Sciences **86,** 1239-1243.

Ormrod, D.P., Landry, L.G., and Conklin, P.L. (1995). Short-term UV-B radiation and ozone exposure effects on aromatic secondary metabolite accumulation and shoot growth of flavonoid-deficient *Arabidopsis* mutants. Physiologia Plantarum **93,** 602-610.

Ossowski, S., Schwab, R., and Weigel, D. (2008). Gene silencing in plants using artificial microRNAs and other small RNAs. The Plant Journal **53,** 674-690.

Paciolla, C., and Tommasi, F. (2003). The ascorbate system in two bryophytes: *Brachythecium velutinum* and *Marchantia polymorpha*. Biologia Plantarum **47,** 387-393.

Page, M., Sultana, N., Paszkiewicz, K., Florance, H., and Smirnoff, N. (2012). The influence of ascorbate on anthocyanin accumulation during high light acclimation in *Arabidopsis thaliana*: further evidence for redox control of anthocyanin synthesis. Plant, Cell & Environment **35,** 388-404.

Pallanca, J.E., and Smirnoff, N. (1999). Ascorbic acid metabolism in pea seedlings. A comparison of $_{D}$-glucosone, $_{L}$-sorbosone, and $_{L}$-galactono-1,4-lactone as ascorbate precursors. Plant Physiology **120,** 453-462.

Parizotto, E.A., Dunoyer, P., Rahm, N., Himber, C., and Voinnet, O. (2004). *In vivo* investigation of the transcription, processing, endonucleolytic activity, and functional relevance of the spatial distribution of a plant miRNA. Genes & Development **18,** 2237-2242.

Parsons, H.T. (2008). Transport and metabolism of symplastic and apoplastic ascorbate during oxidative stress. Ph.D. Thesis. In The Edingburgh Cell Wall Group, Institute of Molecular Plant Sciences. (Edinburgh: University of Edinburgh).

Parsons, H.T., and Fry, S.C. (2012). Oxidation of dehydroascorbic acid and 2,3-diketogulonate under plant apoplastic conditions. Phytochemistry **75,** 41-49.

Parsons, H.T., Yasmin, T., and Fry, S.C. (2011). Alternative pathways of dehydroascorbic acid degradation *in vitro* and in plant cell cultures: novel insights into vitamin C catabolism. Biochem. J. **440,** 375-383.

Passardi, F., Penel, C., and Dunand, C. (2004). Performing the paradoxical: how plant peroxidases modify the cell wall. Trends in Plant Science **9,** 534-540.

Passardi, F., Cosio, C., Penel, C., and Dunand, C. (2005). Peroxidases have more functions than a Swiss army knife. Plant Cell Reports **24,** 255-265.

Passardi, F., Tognolli, M., De Meyer, M., Penel, C., and Dunand, C. (2006). Two cell wall associated peroxidases from *Arabidopsis* influence root elongation. Planta **223,** 965-974.

Pastori, G.M., Kiddle, G., Antoniw, J., Bernard, S., Veljovic-Jovanovic, S., Verrier, P.J., Noctor, G., and Foyer, C.H. (2003). Leaf vitamin C contents modulate plant defense transcripts and regulate genes that control development through hormone signaling. The Plant Cell **15,** 939-951.

Pavlopoulos, G., Soldatos, T., Barbosa-Silva, A., and Schneider, R. (2010). A reference guide for tree analysis and visualization. BioData Mining **3,** 1.

Pedreira, J., Herrera, M.T., Zarra, I., and Revilla, G. (2011). The overexpression of *AtPrx37*, an apoplastic peroxidase, reduces growth in *Arabidopsis*. Physiologia Plantarum **141,** 177-187.

Perrot-Rechenmann, C. (2010). Cellular responses to auxin: division versus expansion. Cold Spring Harbor Perspectives in Biology **2,** 1-15.

Pignocchi, C., and Foyer, C.H. (2003). Apoplastic ascorbate metabolism and its role in the regulation of cell signalling. Current Opinion in Plant Biology **6,** 379-389.

Pignocchi, C., Fletcher, J.M., Wilkinson, J.E., Barnes, J.D., and Foyer, C.H. (2003). The function of ascorbate oxidase in tobacco. Plant Physiology **132,** 1631-1641.

Pignocchi, C., Kiddle, G., Hernández, I., Foster, S.J., Asensi, A., Taybi, T., Barnes, J., and Foyer, C.H. (2006). Ascorbate oxidase-dependent changes in the redox state of the apoplast modulate gene transcript

accumulation leading to modified hormone signaling and orchestration of defense processes in tobacco. Plant Physiology **141,** 423-435.

Pinheiro, C., and Chaves, M.M. (2011). Photosynthesis and drought: can we make metabolic connections from available data? Journal of Experimental Botany **62,** 869-882.

Poethig, R.S., and Sussex, I.M. (1985). The developmental morphology and growth dynamics of the tobacco leaf. Planta **165,** 158-169.

Potters, G., Jansen, M., Horemans, N., Guisez, Y., and Pasternak, T. (2010). Dehydroascorbate and glutathione regulate the cellular development of *Nicotiana tabacum* L. SR-1 protoplasts. In Vitro Cellular & Developmental Biology - Plant **46,** 289-297.

Ranieri, A., Castagna, A., Padu, E., Moldau, H., Rahi, M., and Soldatini, G.F. (1999). The decay of O_3 through direct reaction with cell wall ascorbate is not sufficient to explain the different degrees of O_3-sensitivity in two Poplar clones. Journal of Plant Physiology **154,** 250-255.

Rautenkranz, A., Li, L., Mächler, F., Märtinoia, E., and Oertli, J.J. (1994). Transport of ascorbic and dehydroascorbic acids across protoplast and vacuole membranes isolated from barley (*Hordeum vulgare* L. cv Gerbel) leaves. Plant Physiology **106,** 187-193.

Rhee, S.Y., Beavis, W., Berardini, T.Z., Chen, G., Dixon, D., Doyle, A., Garcia-Hernandez, M., Huala, E., Lander, G., Montoya, M., Miller, N., Mueller, L.A., Mundodi, S., Reiser, L., Tacklind, J., Weems, D.C., Wu, Y., Xu, I., Yoo, D., Yoon, J., and Zhang, P. (2003). The *Arabidopsis* Information Resource (TAIR): a model organism database providing a centralized, curated gateway to *Arabidopsis* biology, research materials and community. Nucleic Acids Research **31,** 224-228.

Rombauts, S., Déhais, P., Van Montagu, M., and Rouzé, P. (1999). PlantCARE, a plant *cis*-acting regulatory element database. Nucleic Acids Research **27,** 295-296.

Rombauts, S., Florquin, K., Lescot, M., Marchal, K., Rouzé, P., and Van de Peer, Y. (2003). Computational approaches to identify promoters and *cis*-regulatory elements in plant genomes. Plant Physiology **132,** 1162-1176.

Sakurai, N. (1998). Dynamic function and regulation of apoplast in the plant body. Journal of Plant Research **111,** 133-148.

Sanmartin, M., Pateraki, I., Chatzopoulou, F., and Kanellis, A. (2007). Differential expression of the ascorbate oxidase multigene family during fruit development and in response to stress. Planta **225,** 873-885.

Sanmartin, M., Drogoudi, P., Lyons, T., Pateraki, I., Barnes, J., and Kanellis, A. (2003). Over-expression of ascorbate oxidase in the apoplast of transgenic tobacco results in altered ascorbate and glutathione redox states and increased sensitivity to ozone. Planta **216,** 918-928.

Sattelmacher, B. (2001). The apoplast and its significance for plant mineral nutrition. New Phytologist **149,** 167-192.

Schmid, M., Davison, T.S., Henz, S.R., Pape, U.J., Demar, M., Vingron, M., Scholkopf, B., Weigel, D., and Lohmann, J.U. (2005). A gene expression map of *Arabidopsis thaliana* development. Nat. Genet. **37,** 501-506.

Schwab, R., Ossowski, S., Riester, M., Warthmann, N., and Weigel, D. (2006). Highly specific gene silencing by artificial microRNAs in *Arabidopsis*. The Plant Cell **18,** 1121-1133.

Smirnoff, N. (1993). The role of active oxygen in the response of plants to water deficit and desiccation. New Phytologist **125,** 27-58.

Smirnoff, N. (1996). Botanical briefing: The function and metabolism of ascorbic acid in plants. Annals of Botany **78,** 661-669.

Smirnoff, N. (1998). Plant resistance to environmental stress. Current Opinion in Biotechnology **9,** 214-219.

Smirnoff, N. (2000a). Ascorbic acid: metabolism and functions of a multi-facetted molecule. Current Opinion in Plant Biology **3,** 229-235.

Smirnoff, N. (2000b). Ascorbate biosynthesis and function in photoprotection. Philosophical Transactions: Biological Sciences **355,** 1455-1464.

Smirnoff, N. (2011). Chapter 4 - Vitamin C: the metabolism and functions of ascorbic acid in plants. In Advances in Botanical Research, R. Fabrice and D. Roland, eds (Academic Press), pp. 107-177.

Smirnoff, N., and Colombé, S.V. (1988). Drought influences the activity of enzymes of the chloroplast hydrogen peroxide scavenging system. Journal of Experimental Botany **39,** 1097-1108.

Smirnoff, N., and Cumbes, Q.J. (1989). Hydroxyl radical scavenging activity of compatible solutes. Phytochemistry **28,** 1057-1060.

Spiro, R.G. (2002). Protein glycosylation: nature, distribution, enzymatic formation, and disease implications of glycopeptide bonds. Glycobiology **12,** 43R-56R.

Sultana, N. (2011). The biochemical consequences of ascorbate deficiency in *Arabidopsis thaliana*. Ph.D. Thesis. In College of Life and Environmental Sciences, School of Biosciences. (Exeter: University of Exeter).

Sunilkumar, G., Mohr, L., Lopata-Finch, E., Emani, C., and Rathore, K.S. (2002). Developmental and tissue-specific expression of CaMV 35S promoter in cotton as revealed by GFP. Plant Molecular Biology **50,** 463-479.

Suzuki, N., Koussevitzky, S., Mittler, R., and Miller, G. (2012). ROS and redox signalling in the response of plants to abiotic stress. Plant, Cell & Environment **35,** 259-270.

Suzuki, Y., and Ogiso, K. (1973). Development of ascorbate oxidase activity and its iso-enzyme pattern in the roots of pea seedlings. Physiologia Plantarum **29,** 169-172.

Szent-Györgyi, A. (1931). On the function of hexuronic acid in the respiration of the cabbage leaf. Journal of Biological Chemistry **90,** 385-393.

Tabbì, G., Fry, S.C., and Bonomo, R.P. (2001). ESR study of the non-enzymic scission of xyloglucan by an ascorbate–H_2O_2–copper system: the involvement of the hydroxyl radical and the degradation of ascorbate. Journal of Inorganic Biochemistry **84,** 179-187.

Takahama, U. (1996). Effects of fusicoccin and indole-3-acetic acid on the levels of ascorbic acid and dehydroascorbic acid in the apoplast during elongation of epicotyl segments of *Vigna angularis*. Physiologia Plantarum **98,** 731-736.

Takahama, U., and Oniki, T. (1994). The association of ascorbate and ascorbate oxidase in the apoplast with IAA-enhanced elongation of epicotyls from *Vigna angularis*. Plant and Cell Physiology **35,** 257-266.

Tamura, K., Peterson, D., Peterson, N., Stecher, G., Nei, M., and Kumar, S. (2011). MEGA5: Molecular Evolutionary Genetics Analysis using Maximum Likelihood, Evolutionary Distance, and Maximum Parsimony Methods. Molecular Biology and Evolution.

Thompson, J.D., Higgins, D.G., and Gibson, T.J. (1994). CLUSTAL W: improving the sensitivity of progressive multiple sequence alignment through sequence weighting, position-specific gap penalties and weight matrix choice. Nucleic Acids Research **22,** 4673-4680.

Thornton, J.W., and DeSalle, R. (2000). Gene family evolution and homology: Genomics Meets Phylogenetics. Annual Review of Genomics and Human Genetics **1,** 41-73.

Tognolli, M., Penel, C., Greppin, H., and Simon, P. (2002). Analysis and expression of the class III peroxidase large gene family in *Arabidopsis thaliana*. Gene **288,** 129-138.

Tommasi, F., De Gara, L., Liso, R., and Arrigoni, O. (1990). The Ascorbic Acid System in *Cuscuta reflexa* Roxb. Journal of Plant Physiology **135,** 766-768.

Tóth, S.Z., Puthur, J.T., Nagy, V., and Garab, G. (2009). Experimental evidence for ascorbate-dependent electron transport in leaves with inactive oxygen-evolving complexes. Plant Physiology **149,** 1568-1578.

Umemura, Y., Ishiduka, T., Yamamoto, R., and Esaka, M. (2004). The Dof domain, a zinc finger DNA-binding domain conserved only in higher plants, truly functions as a Cys2/Cys2 Zn finger domain. The Plant Journal **37,** 741-749.

Veljovic-Jovanovic, S.D., Pignocchi, C., Noctor, G., and Foyer, C.H. (2001). Low ascorbic acid in the *vtc-1* mutant of *Arabidopsis* is associated with decreased growth and intracellular redistribution of the antioxidant system. Plant Physiology **127,** 426-435.

Verslues, P.E., and Juenger, T.E. (2011). Drought, metabolites, and Arabidopsis natural variation: a promising combination for understanding adaptation to water-limited environments. Current Opinion in Plant Biology **14,** 240-245.

Verslues, P.E., Agarwal, M., Katiyar-Agarwal, S., Zhu, J., and Zhu, J.-K. (2006). Methods and concepts in quantifying resistance to drought, salt and freezing, abiotic stresses that affect plant water status. The Plant Journal **45,** 523-539.

Wang, Y., Barbacioru, C., Hyland, F., Xiao, W., Hunkapiller, K., Blake, J., Chan, F., Gonzalez, C., Zhang, L., and Samaha, R. (2006). Large scale real-time PCR validation on gene expression measurements from two commercial long-oligonucleotide microarrays. BMC Genomics **7,** 59.

Wang, Y.H. (2008). How effective is T-DNA insertional mutagenesis in *Arabidopsis*? J Biochem Tech **1,** 11-20.

Welinder, K.G. (1992). Superfamily of plant, fungal and bacterial peroxidases. Current Opinion in Structural Biology **2,** 388-393.

Wheeler, G.L., Jones, M.A., and Smirnoff, N. (1998). The biosynthetic pathway of vitamin C in higher plants. Nature **393,** 365-369.

Williamson, J.D., Hirsch-Wyncott, M.E., Larkins, B.A., and Gelvin, S.B. (1989). Differential accumulation of a transcript driven by the CaMV 35S promoter in transgenic tobacco. Plant Physiology **90,** 1570-1576.

Winter, D., Vinegar, B., Nahal, H., Ammar, R., Wilson, G.V., and Provart, N.J. (2007). An "Electronic Fluorescent Pictograph" browser for exploring and analyzing large-scale biological data sets. PLoS ONE **2,** e718.

Woo, N., Badger, M., and Pogson, B. (2008). A rapid, non-invasive procedure for quantitative assessment of drought survival using chlorophyll fluorescence. Plant Methods **4,** 27.

Yamamoto, A., Bhuiyan, M.N.H., Waditee, R., Tanaka, Y., Esaka, M., Oba, K., Jagendorf, A.T., and Takabe, T. (2005). Suppressed expression of the apoplastic ascorbate oxidase gene increases salt tolerance in tobacco and *Arabidopsis* plants. Journal of Experimental Botany **56,** 1785-1796.

Yamasaki, H., Sakihama, Y., and Ikehara, N. (1997). Flavonoid-peroxidase reaction as a detoxification mechanism of plant cells against H_2O_2. Plant Physiology **115,** 1405-1412.

Zechmann, B., Stumpe, M., and Mauch, F. (2011). Immunocytochemical determination of the subcellular distribution of ascorbate in plants. Planta **233,** 1-12.

Zhang, Q., Su, L., Chen, J., Zeng, X., Sun, B., and Peng, C. (2011). The antioxidative role of anthocyanins in *Arabidopsis* under high-irradiance. Biologia Plantarum**,** 1-8.